Electrically Polarised Electrodes in DMSO and DMF electrolytes of Pseudohalide Salts: In situ IR studies supported by EXAFS/XANES and other techniques

A thesis submitted in fulfilment
of the requirements for the degree
of
Doctor of Philosophy
In Chemistry
at
The University of Waikato
by

Kethsiri Alwis

THE UNIVERSITY OF
WAIKATO
Te Whare Wānanga o Waikato

2015

Abstract

This thesis presents, subtractively normalised interfacial Fourier transform infrared spectroscopic (SNIFTIRS) investigations of anodically polarised nickel, copper and gold electrodes in pseudohalide-containing (i.e. NCO^-, NCS^-, $NCSe^-$, CN^- and $TeCN^-$) dimethyl formamide (DMF) and dimethyl sulfoxide (DMSO) solutions, with a supporting electrolyte, tetrabutylammonium perchlorate (TBAP), is presented. Cyclic voltammograms, and current-potential data were recorded while the infrared spectral acquisition was in progress for nickel, copper and gold electrodes in a thin-layer cell. A thin layer electrochemical cell with CaF_2 IR windows was used to acquire data.

For the anodic dissolution of Ni, Cu and Au electrodes in DMF and DMSO media containing pseudohalide ions, it was found that all electrodes anodically dissolved generating Ni^{2+}, Cu^+/Cu^{2+} and Au^+ coordination complexes consisting of pseudohalide ions (i.e. NCO^-, NCS^-, $NCSe^-$) and solvent molecules. These conclusions were confirmed by demonstrating that the same complex ion species were formed in model solutions prepared by mixing Ni(II), Cu(I), Cu(II) and Au(III) salts with the corresponding pseudohalide salts (KOCN, NaSCN, KSeCN, KCN and KTeCN) in either DMSO or DMF solvent by comparison of their IR transmission spectra with the in situ IR spectra. Additionally the geometry of the nickel/copper-pseudohalide complex ions formed in particular during anodic dissolution experiments was probed using other techniques which involved X-ray absorption spectroscopy (XAS). Further electrospray ionisation mass spectrometry (ESI-MS) was also used to confirm the presence of such species and to characterize other by-products formed in the model solutions.

In general, the data showed that the nickel electrode undergoes irreversible anodic dissolution in all solutions studied at high applied potentials, greater than +500 mV (AgCl/Ag). Nickel predominantly speciated into Ni^{2+} complexes. Insoluble films and dissolved CO_2 were also detected, though mostly in the Ni/NCO^- systems studied.

In general, the Ni/NCO^- electrochemical system behaved differently relative to those of Ni/NCS^- and $Ni/NCSe^-$, as observed via the difference in colours in cell

solutions produced after SNIFTIRS experiments which was mirrored in the model solutions. Ni(II)-cyanate species had a different coordination geometry and gave a characteristic bright blue colour due possibly to the species $[Ni(NCO)_4]^{2-}$, while Ni(II) thiocyanate and selenocyanate complex ion species were proposed to have octahedral coordination geometry containing solvent and one coordinated pseudohalide ion, and formed green-yellow solutions.

X-ray absorption near edge spectroscopy (XANES) and extended X-ray absorption fine structure (EXAFS) were used to obtain direct information on the coordination state of electrogenerated products. From EXAFS/XANES data, the Ni(II)/NCS^- and $NCSe^-$ complexes were confirmed to be octahedral bearing at least one monopseudohalide-ligand with the balance of ligands being the coordinated DMSO solvent while the data for Ni/cyanate system suggested a "five-coordinate" Ni/pseudohalide-ion complex. In reality, this suggested species was regarded as the result of XAS being a sample averaging technique and that in this solution there is perceived to be a mixture of 4 coordinate (tetrahedral) $[Ni(NCO)_4]^{2-}$ and octahedral $[Ni(DMSO)_6]^{2+}$ species. These observations of the octahedral geometry for the Ni(II)/thiocyanate and Ni(II)/selenocyanate systems and 5-coordinate geometry in the Ni(II)/cyanate systems are supported by the differences in colour observed between the two samples.

An IR spectroelectrochemical and X-ray absorption spectroscopy (XAS) study of anodically polarized copper electrodes in polar aprotic solvents (DMSO and DMF) in the presence of pseudohalide ions and tetrabutylammonium perchlorate has been presented in Chapter 5. Cu dissolves in all 6 systems studied (i.e. DMF and DMSO, in the presence of NCO^-, NCS^- and $NCSe^-$) to produce stable Cu(I) pseudohalide complex ion species in addition to other species such as electrogenerated CO_2. Insoluble films were also observed to be deposited at higher anodic applied potentials. These films were thought to be CuSCN and $K(SeCN)_3$ depending on the solvent system used. The predominance of the Cu(I) oxidation state in these complexes was clearly proven from examining the single-scan spectra and was supported by model solution studies.
SNIFTIRS studies of Au electrodes under similar experimental conditions are presented in chapter 6. This work has demonstrated the significance of the Au(I) oxidation state which occurs after applied voltages of +500 mV(AgCl/Ag) in the

little characterised electrochemistry of this metal in polar aprotic solvents, DMSO and DMF. Generally, all studies conducted showed that Au electrodes dissolved to form the corresponding Au(I) pseudohalide complexes (i.e. $[Au(NCO)_2]^-$, $[Au(SCN)_2]^-$ and $[Au(SeCN)_2]^-$).

The Au(I) species observed electrochemically by SNIFTIRS were confirmed by independent preparation in DMSO/DMF containing mixtures of $KAuBr_4$ and the pseudohalide salt (KOCN/NaSCN/KSeCN) and exploiting fortuitous redox chemistry where Au(I) formed spontaneously. The model solutions examined by transmission FTIR and ESI-MS confirmed the existence of the Au(I) species posited in the SNIFTIRS experiments but additionally revealed other interesting side reactions occurring in the model solutions.

In situ IR studies are reported of the interaction of the little studied tellurocyanate ion with electrically polarised nickel, copper and gold electrodes in TBAP-supported DMSO and DMF-based electrolytes for the first time. SNIFTIRS combined with voltammetric methods (and model solution + DFT calculations) have revealed that the $TeCN^-$ ion is decomposed at anodic potentials at the metal electrodes. It was found that the speciation observed in the in situ IR spectra reflected more that of an interaction of a metal electrode with a CN^- ion species (a decomposition product of the $TeCN^-$ ion) rather than with the $TeCN^-$ ion itself. This ion was incapable of forming any discrete metal ion complexes. Fouling of the electrode by deposited elemental Te was also found to have influenced electrochemistry by blocking surface reactions. In general, the studies have confirmed the instability of $TeCN^-$ ion when subjected to electrical polarisation with the observed speciation being indicative of the difference in chemical reactivity of the “fouled” Ni, Cu and Au electrodes toward anodic polarization in the presence of CN^- ion.

Acknowledgements

I wish to convey my sincere thanks to my supervisor, Dr. Michael Mucalo for his guidance, encouragement, enthusiasm and most of all for placing confidence in me. I am grateful for his extraordinary kindness, understanding, patience and support and above all for imparting knowledge. I am indebted for the time he has spent advising me on job opportunities, scholarships, seminars and preparation of scientific publications.

My special thanks to Assoc. Prof. Merilyn Manley-Harris, who assisted me to come to New Zealand, without her help, I would not have been able to come to UOW. My sincere thanks to my second supervisor, Assoc. Prof. Graham Saunders and Prof. Brian Nicholson, Prof. Bill Henderson from Chemistry Department who contributed with their valuable comments and suggestions.

I am very grateful to Dr. Bridget Ingham for the opportunity to carry out portions of this research on the X-ray Absorption Spectroscopy (XAS) Beamline at the Australian Synchrotron, Victoria, Australia. Her expertise advice, comments and support in analysing results and preparation of scientific publications are also very much appreciated. My thanks to Dr. Peter Kappen and Dr. Chris Glover for their support when conducting experiments in Australian Synchroton. My thanks to New Zealand Synchrotron Group for travel funding to use facility.

My thanks to Dr. Joseph Lane and his student Else Hall for their contribution on Gaussian calculations for CN stretching frequencies in portions of this research.

I would like to express my sincere thanks to technical officers John Little, Wendy Jackson, Pat Gread, Jenny Stockdill and Annie Barker at the Department of Chemistry, for the support from the very beginning of the research.

A special thanks to Peter Jarman on instrument support and Steve Hardy for making electrode and electrochemical cell.

I am grateful to the University Scholarship Committee for financial support in the form of a Scholarship for the last three months. Also my sincere gratitude to

Dr. Michael Mucalo, Prof. David Lowe, Prof. Peter Kamp, Dr. Martin Danisik for understanding and supporting me in time of family crisis and arranging funds for emergency travel to my home country.

I would also like to thank the Science Librarian Cheryl Ward who has been very helpful in formatting and compiling my thesis.

Finally my sincere thanks to my brother, Nandasiri Alwis for sponsoring my tuition fees and helping me and family to comfortably settle in New Zealand. My thanks to my mother, siblings and in-laws for their love, support and prayers throughout the years.

To my dearest children Sanura and Hesara, thank you for your big smiles and words of affection that kept me cheerful throughout this work and my wife Thilini.

Table of Contents

List of Figures

List of Tables

Chapter 1

Theory and Methodology

This thesis focuses on in situ IR spectroelectrochemical studies of little- studied systems involving the anodic polarisation of nickel, copper and gold electrodes in the presence of pseudohalide ions in non-aqueous electrolytes. This study has also involved the application of other spectroscopic techniques such as U.V./Vis Spectrophotmetry and EXAFS/XANES to study the systems as well as electrospray ionization mass spectrometry. Chapter 1 serves to introduce the electrochemical and IR spectroscopic aspects of this field while Chapter 2 will provide a comprehensive literature review of work done in this area up to now and will describe the rationale for the current research.

1.1 Electrochemistry

Electrochemistry investigates the interrelation between electrical current and chemical reactions. When the electric current is passed through the electrode, the charge is carried through the electrolyte phase by the movement of ions. Many electrochemical techniques involve measurement of applied potential to the electrode and the resultant current (I) flowing through the electrochemical cell. Thus, at certain applied potentials, a change in the concentration of an electroactive species at an electrode surface can occur via reduction or oxidation. The chemical species in the solution can be represented at its simplest as two different oxidation states, i.e., an oxidized (Ox) form and a reduced (Red) form, and the overall transformation can be presented by equation 1-1

$$Ox + ne^- \rightarrow Red \qquad (1\text{-}1)$$

There are other elementary processes occurring in between the starting species and end products which provide the conditions for maintaining a continuous flow of electrons in the system. The solution species (e.g. Ox) travels from the bulk to the electrode surface, donates electrons via a charge transfer process forming a reaction product (Red) on the electrode surface. Once formed, the product molecule or ion leaves the electrode surface. Zanello [1] summarises the above in the following 3 elementary steps as given by Equations (1-2) to (1-4) below.

$$Ox_{(\text{in bulk solution})} \xrightarrow{\text{MASS TRANSPORT}} Ox_{(\text{electrode surface})} \quad (1\text{-}2)$$

$$Ox_{(\text{electrode surface})} \xrightarrow{\text{ELECTRON TRANSPORT}} Red_{(\text{electrode surface})} \quad (1\text{-}3)$$

$$Red_{(\text{electrode surface})} \xrightarrow{\text{MASS TRANSPORT}} Red_{(\text{in bulk solution})} \quad (1\text{-}4)$$

In addition to the above processes, other phenomena can give some degree of complexity to these electrode reactions such as coupled chemical reactions, adsorption and formation of phases. For example, the electrochemical reaction can form an unstable species which can subsequently decompose. Furthermore, it may react with other solution species as it diffuses into the bulk and these are called coupled chemical reactions. This can lead to further species which, in themselves could also become electroactive [1] and hence react again at the electrode surface to form new products.

The sequences shown in Equation (1-2) to (1-4) assume a charge transfer without any interaction of the species with the electrode surface. However, some charge transfer reactions involve adsorption of electroactive species before charge transfer occurs. Sometimes this might cause poisoning of the electrode surface. Further, some reactions can form new phases. The electrode itself could enter solution as ions via an anodic dissolution process. The formation of species by whatever means may be a multi-stage process.

There are two types of processes occurring at electrodes which are termed faradaic and non-faradaic processes. Reactions that involve charge transfer (oxidation or reduction) are governed by Faraday's law. The extent of the chemical reaction is proportional to the amount of electricity passed. However, some reactions involve only adsorption and desorption of species at the electrode due to the fact that many charge transfer reactions are either thermodynamically or kinetically very unfavourable. Such processes are called non-faradaic processes [2].

1.1.1 The Electrode/Solution interface and the Electrical double layer

An electrode reaction is a heterogeneous process [1] which involves the passage of an electron from an electrode to a species in solution or the reverse.

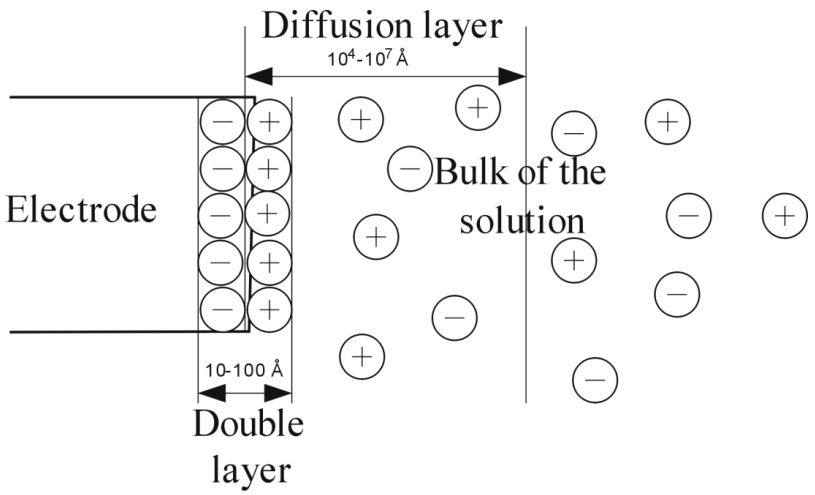

Figure 1.1: The charge distribution at the electrode/solution interface and the electrode is negatively charged. (Adapted from Zanello, 2003, p.11) [1]

Through the illustration in Figure 1.1 which functions as a model of an electrified interface, it can be shown that the electrode/solution system may be roughly divided into four categories. They are:

1) The electrode
2) The double layer
3) The diffuse layer
4) The bulk of the solution

A negatively charged electrode attracts positive species and repels negative charged species establishing an electrical potential gradient form the electrode to the bulk of the solution. The simplest model of this interface is presented as an electrical double layer, which is, for example, a sheet of negative charge at the surface of electrode and a nearby sheet of positive charge. The electric double layer acts like a two plate capacitor due to this electrostatic attraction, the diffusion layer has an unequal charge distribution of ions in it, with a net attraction and accumulation of oppositely charged species (to what charge exists on the electrode) in the diffusion layer.

There are three main electrical double layer models that describe the distribution of charge species at the electrode/solution interface: the Helmholtz model, the Gouy-Chapman model and the Stern model [3]. In the Helmholtz model, the electrical double layer is presented as made up of [2] an inner Helmholtz plane (IHP) which consists of charges within the electrode surface and the second consisting of a layer of solvated ions which is called the outer Helmholtz plane (OHP). The solvated ions interacting with the charged metal electrode involves only electrostatic forces. These ions are said to be non-specifically adsorbed ions. The Helmholtz model neglects, however, the influence of thermal gradients in solution which can disrupt the rigid solution layer comprising the double layer at the interface. In contrast, another model called the Gouy-Chapman model, envisages that there is a diffuse double layer of charges, near the electrode which is equivalent to a charged parallel plate capacitor. The potential between these two varies exponentially as opposed to linearly as a point charge is made to move through the double layer. However this model deemphasizes the ordering of the charged interface. The best compromise is when these two models are combined to give the Stern model (as illustrated in Figure 1.2) which has the electrical potential varying linearly through the electrode up to the OHP and then exponentially through the diffuse layer. This is the best model in terms of the ordering effect of the charging and the dynamics/chaos caused by the thermal fluctuations [4].

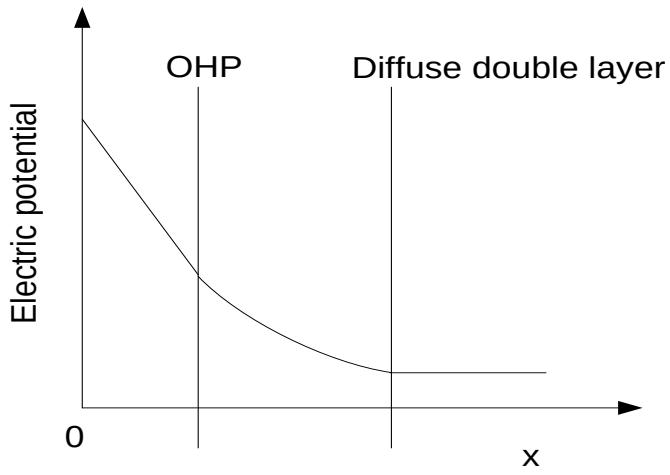

Figure 1.2: The Stern model of the electric field double layer showing the potential profile in the double layer formed at an electrode up to diffuse layer. (Adapted from Bockris and Drazic, 1972, p. 49) [4].

1.1.2 Measuring Electrode Potentials Essential components of an electrochemical cell: The two electrode and three electrode systems

An electrode, electrolyte and external part of circuit are the main parts of an electrochemical cell (see Figure 1.3). A chemical reaction in the cell always implies a transfer of electrons takes place. From equation-1-1 it can be easily determined that for each mole of species Ox, n mol of electrons must transfer from the electrode (A)

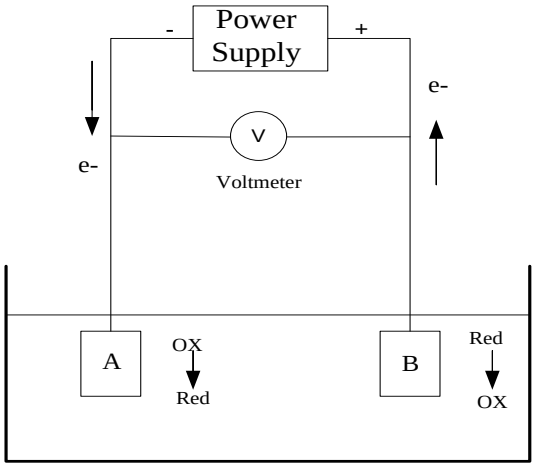

Figure 1.3: Schematic diagram of two electrode system. It represents the reduction reaction at the working electrode (electrode A) and oxidation reaction at the counter electrode (electrode B). The voltmeter connected between two electrodes is to measure the cell voltage.

As illustrated in Figure 1.3 these electrons are supplied through an external circuit, by an electrode reaction that occurs at a second electrode (electrode B) at the expense of any other redox-active species Red present in the same electrolytic solution. As discussed above, for an electrode reaction to take place one needs two electrodes, a working electrode, at which the electron transfer process of interest occurs and a counter electrode, that operates to maintain the electro-neutrality of the solution through a half-reaction of opposite sign. The difference of potential set up between the two electrodes is experimentally measured and is defined, as the cell voltage (V). However, as illustrated in Figure 1.4, this cell voltage is the sum of a series of differences of potential.

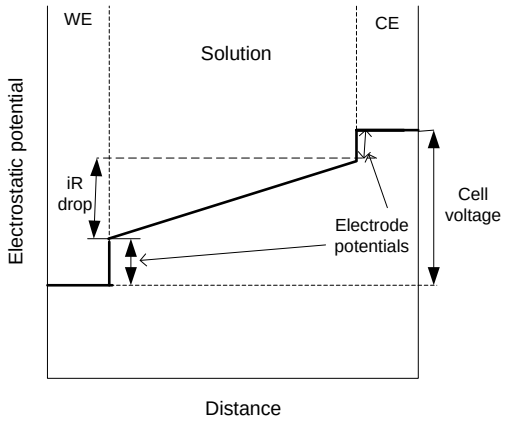

Figure 1.4: Potential profile along the path from the interior of the working electrode to the interior of the counter electrode in the electrochemical experiment illustrated in Figure 1.3. (Adapted from Zanello, 2003, p.21) [1]

1.1.2.1 Two electrode cells

At each of the two electrode/solution interfaces in a two electrode cell, where an electrical double layer is set up, there are sharp gradients in potential. This potential gradient controls the rate of the faradaic reactions that occur at the two electrodes. The gradient is constant only when there is a net zero current in the cell. When a net electrochemical reaction ensues, non-zero current is flowing through the cell, internal resistance drops the cell potential by the amount $I * R$, where I is cell current and R is the internal resistance. This drop is known as the ohmic or *IR* drop.

This implies that it is impossible to control accurately the potential of the working electrode unless one resorts to a cell in which: 1) the potential of the counter electrode is invariant and, 2) the *IR* drop is made negligible.

Generally, the use of a two-electrode cell (working and reference electrodes) must be considered only as a first attempt to control adequately the potential of the working electrode. In principle, that a reference electrode (RE) does function as a counter electrode in a two electrode cell has the disadvantage that the incoming current can cause instantaneous variations in the concentration of the cell solution species, therefore leading to a potential value that is different from the standard potential. A satisfactory solution to maintain the potential of the working electrode constant while allowing measurable reaction to occur, is found in the three electrode cell arrangement that will be discussed in the next section.

1.1.2.2 Three-electrode electrochemical cell

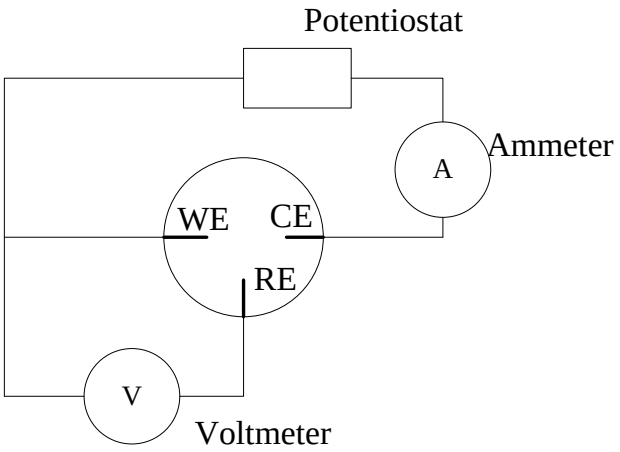

Figure 1.5: Schematic diagram of the three electrode system and potentiostat. An ammeter and a voltmeter is used to measure the current and potential in the circuit. (Adapted from Zanello, 2003, p.20) [1].

A schematic of the three-electrode cell is shown in Figure 1.5. Here, a third electrode, which is called the reference electrode, is introduced together with the counter electrode (CE) and working electrode (WE). The counter electrode must be positioned in such a way that the electroactive species generated by it does not reach the working electrode. In some techniques the counter electrode is placed in a compartment separated by a sintered glass membrane. In addition, the *IR* drop can be minimized by positioning the reference electrode close to the working electrode by use of a Luggin capillary (see later).

As deducible from Figure 1.5, to apply a precise 'potential' value to the working electrode means to apply a precise difference of potential between the working and the reference electrodes. Since the electronic circuit to monitor such potential difference, (V), is assembled to possess a high input resistance, only a small fraction of the current enters the reference electrode (thus not modifying its intrinsic potential) most current is channelled between the working and the counter electrodes.

Even with this experimental set-up, the *IR* drop is not completely eliminated. The situation can be improved if the reference electrode is placed very close to the working electrode by means of a Luggin capillary.

1.1.2.3 The basic potentiostat circuit

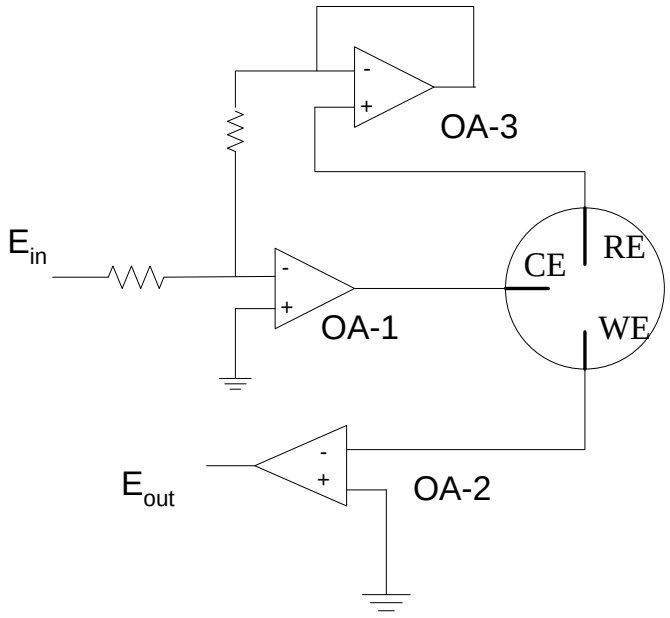

Figure 1.6: Schematic diagram of the basic potentiostat circuit with three electrode cell. Three operational amplifiers (OA-1= inverting amplifier, OA-2= current to voltage converter and OA-3= buffer amplifier) are used to connect counter electrode, working electrode and reference electrode respectively for control the current and potential in the three electrode system. (Adapted from Kounaves) [5]

A simple potentiostat circuit for a three-electrode cell with three operational amplifiers (OA) is shown in Figure 1.6. The output of OA-1 is connected to the counter electrode with feedback to its own inverting input through the reference electrode. This feedback decreases the difference between the inverting and non-inverting inputs of OA-1 and causes the reference electrode to assume the same potential as E_{in} of OA-1. Because the potential difference between the working electrode and the reference electrode is zero the working electrode is set to the same potential as applied to the OA-1 input. With the reference electrode connected to E_{in} through the high impedance of OA-3, the current must flow through the counter electrode. Current flow through the reference not only is undesirable because of its higher resistance but also would eventually cause its potential to become unreliable. An OA-2 acting as a current-to-voltage converter provides the output signal for the A/D converter.

1.2 Technique of cyclic voltammetry

When studying electrochemical processes, the technique of cyclic voltammetry (CV) is often the first analytical technique to be applied to the system to get fundamental information [1, 2, 6]. CV is generally performed using three electrode cell systems as described in section 1.1.2.2 where a potentiostat controls

the potential between the WE and RE while current flows through the solution between the WE and CE. A saturated calomel electrode (SCE) or a silver/silver chloride electrode (Ag/AgCl) are conventionally used as reference electrodes. The controlling potential that is applied across the WE is thus the "excitation signal" and can be varied linearly with time. The potential at the WE is adjusted from some initial cathodic (negative, reduction) or anodic (positive, oxidising) value of the potential to some other potential value and is then reversed back to the initial value. This represents hence the potential "cycle". Single or multiple cycles can be used on the same electrode interface system being studied. The manner by which it is ramped can be represented (linear sweep vs. time) as the triangular waveform as shown in Figure 1.7(a) and the forward and reverse scan. The potentiostat controls the sweep rate and records the current generated in the three electrode cell as a function of applied potential simultaneously. The plot of current vs. potential as shown in Figure 1.7(b) is known as a cyclic voltammogram. The convention of negative current being cathodic current (i_{pc}) and positive current being anodic current (i_{pa}) has been used for all cyclic voltammetry studies in this thesis.

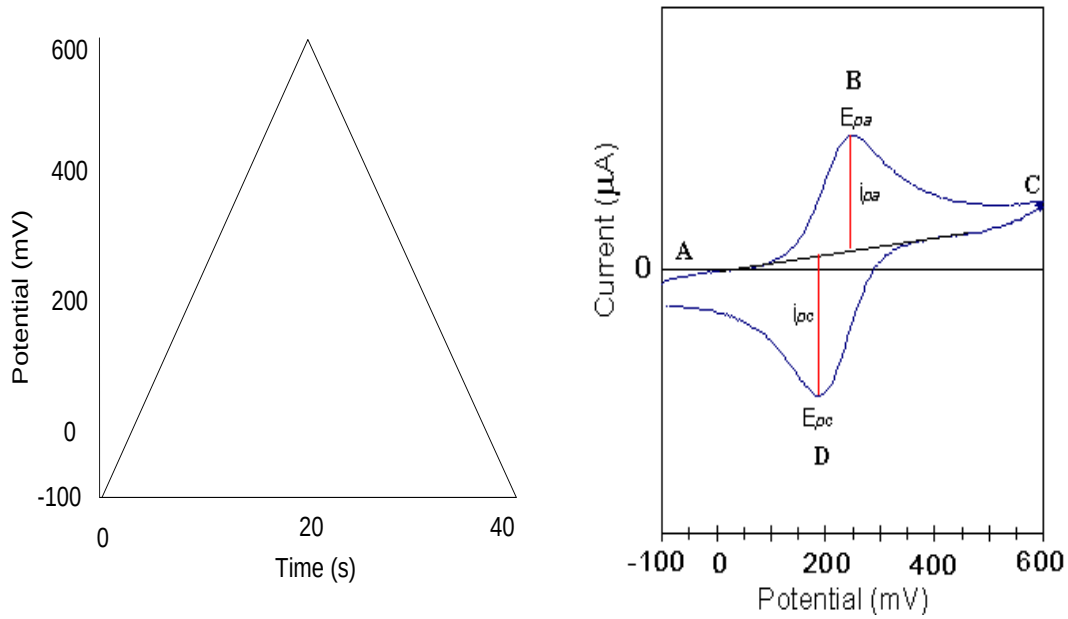

(a) (b)

Figure 1.7: (a) Illustrated potential vs. time, triangular waveform and forward and reverse scan as a linear sweep vs. time. (b) cyclic voltammogram trace with various parameters obtained from the experiment defined. B (E_{pa}) and D (E_{pc}) represent the peak potentials for oxidation and reduction processes in the ferri/ferrocyanide couple [6]. Working electrode and reference electrode is platimun and Ag/AgCl respectively.

CV experiments are usually conducted in unstirred solutions so that the measured current is limited by analyte diffusion at the electrode surface. The ferri/ferrocyanide redox coupled with a platinum electrodes is commonly used to teach CV as an electroanalytical technique. If the applied potential is scanned from an anodic to cathodic potential in an electrolyte solution of ferricyanide, it becomes sufficiently negative to reduce $[Fe(CN)_6]^{3-}$ to $[Fe(CN)_6]^{4-}$. The cathodic current (i_{pc}) generated is thus due to the electrode process,

$$[Fe(CN)_6]^{3-} + e \rightarrow [Fe(CN)_6]^{4-}$$

The current initially increases as the applied potential reaches the reduction potential of the ferricyanide but then falls off as the concentration of the ferricyanide ion is depleted close to the electrode surface due to concentration polarization effects [6]. As the applied potential is reversed back to its original value, the electrode will eventually reach a point when it becomes a sufficiently strong oxidant so that the $[Fe(CN)_6]^{4-}$ which has been forming adjacent to the electrode surface will be oxidised back to the ferricyanide ion by the electrode process,

$$[Fe(CN)_6]^{4-} \rightarrow [Fe(CN)_6]^{3-} + e$$

This results in an anodic current (i_{pa}) which peaks and then decays as the supply of $[Fe(CN)_6]^{4-}$ adjacent to the electrode surface is depleted.

Kunimatsu et. al. [7] discussed typical cyclic voltammograms generated from gold electrodes exposed to electrolytes containing 0.1 mol L^{-1} cyanide ion in 0.5 mol L^{-1} K_2SO_4 solution. In the experiment, the potential was cycled between -1.3 V(Ag/AgCl) to -0.7 V (Ag/AgCl) and the scan rate was 1 mV/s in the forward and reverse directions. When the potential was increased in the forward direction (anodic) in the CV the gold electrode entered the active dissolution region where current was observed to rise significantly and continuously until the voltage was reversed at -0.7 V(Ag/AgCl). In this region, Au was being oxidized to Au(I) and formed the $[Au(CN)_2]^-$ complex in solution. The equation for this electrochemical oxidation has reported as:

$$Au + 2CN^- \rightarrow [Au(CN)_2]^- + e^-$$

When the potential was returned to the starting voltage -1.3 V(Ag/AgCl) all the gold complex in the solution had reduced again to Au and cyanide ions, i.e. the reverse of the equation above:

$$Au + 2CN^- \leftarrow [Au(CN)_2]^- + e^-$$

The subsequent reverse scan shows a linear decrease in the anodic current and finally cathodic current peak at -0.9 V(Ag/AgCl), due to the reduction of the $[Au(CN)_2]^-$ complex.

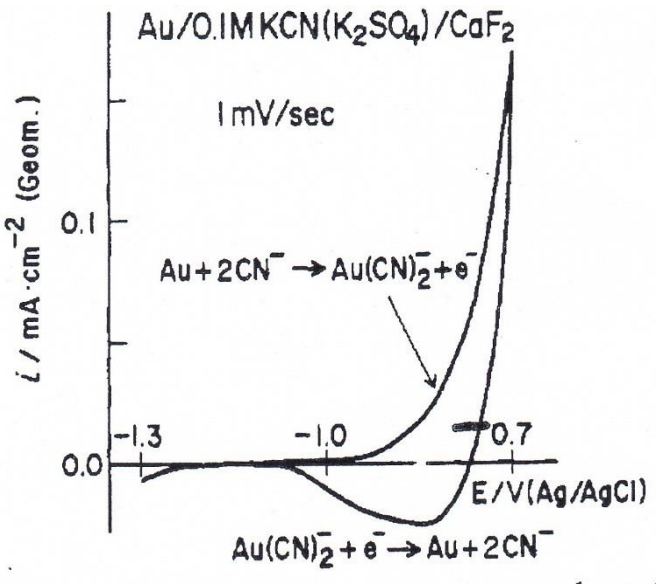

Figure 1.8: Cyclic voltammogram of gold in 0.5 mol L^{-1} K_2SO_4 solution containing 0.1 mol L^{-1} cyanide interface in the cell. (sweep rate=1 mV/s) (after Kunimatsu et.al.) [7]

1.3 IR spectroelectrochemical techniques

1.3.1 Introduction

Infrared spectroscopy has been used widely in electrochemistry for over 20 years [8-11]. IR spectra being a molecular spectroscopy technique in the identification of reactants, products, and long-lived intermediates, enables potential dependent changes in the interfacial solvent, electrode surface and electrolyte composition to be tracked such as the occurrence of surface adsorbed species and bulk solution species. Various kinds of spectral sampling, data collection methods and special electrochemical thin layer cells have been developed to approach this challenging area of in situ IR spectroelectrochemical study. The technique has found two broad areas of application: 1) *adsorption on electrodes*. In situ IR spectra can give

information about the identity and molecular structure of adsorbed species at these species to the electrode surface. 2) *electrode reactions*. In situ IR spectra can conveniently be used to identify reactants, products, and intermediates of electrode reactions, both on the electrode surface and in solution. Species on the electrode surface can be distinguished from species in solution by varying the polarization state of the incident light.

The special properties of reflection of electromagnetic radiation from metal surfaces in the infrared region make it possible to obtain information about the orientation of molecular species at the interface.

A beam of light incident on a plane surface (such as an electrode) can be considered to be made up of two components, s-polarized light, which has its electric field vector oriented perpendicular to the plane of incidence (and therefore parallel to the metal surface and undergoes a phase shift of nearly 180^0 at all angles of incidence). Therefore, the incident and reflected waves cancel at the surface, p-polarized light, whose electric field vector component is polarized parallel to the incidence plane, undergoes a phase shift that is a function of the angle of incidence. A phase shift of about 90^0 is attained at a glancing angle of incidence, and a standing wave that has measurable amplitude near the surface results from the interaction of incident and reflected light.

Since p-polarized light is the only component of infrared radiation with appreciable field strength at the electrode surface, it alone carries information on vibrations of interfacial adsorbed species. Greenler [12] was the first to propose that p-polarized infrared radiation carries all of the vibrational absorption information of species adsorbed at a metallic reflecting surface. He further showed that since the electric field intensity increases sharply with angle of incidence up to near grazing (for p-polarized light), the absorbance by an oscillator could be expected to increase as well. He showed that the absorption of radiation by an oscillator varies as the square of the cosine of the angle between the electric field vector of the radiation and the oscillating dipole. If the infrared beam is incident at very glancing angles, a sizable component of the electric field will lie in a direction perpendicular to the electrode surface. Oscillators with their dipole derivative component more parallel to the surface will have a smaller

probability of infrared absorption. In this way the relative intensities of infrared absorption bands can give information regarding molecular orientations on the electrode surface. This distinction between absorbances due to oscillators oriented parallel and perpendicular with respect to the surface is known as the surface selection rule.

1.3.2 Experimental problems

Two major problems in measuring the IR spectra of species at the electrode/electrolyte interface are: 1) absorption of most of the radiation by the bulk solvent, whenever IR radiation is passed through; it is a serious issue with solvents like water, which absorbs strongly throughout most of the mid-IR region, and 2) sensitivity of detection as electrogenerated species are typically at very low concentrations and hence undetectable by conventional room temperature-operating IR detectors. This usually means that total amount of radiation absorbed by the species of interest is small compared with the detector noise. In the following sections some of the experimental methods that are used to overcome the problems of sensitivity and absorption are presented.

1.3.2.1 Thin-layer electrochemical cells

The first problem of solvent absorption is minimized by using a thin-layer electrochemical cell in in situ IR spectroelectrochemical experiments. To achieve this, Bewick and co-workers[13, 14] suggested the electrode be set very close to the IR window, forming a very thin-layer (1-10 μm) of electrolyte solution between electrode and window. The working electrode can be positioned at a distance of few micrometres from the window in order to avoid a significant absorption of the IR beam by the solvent. When the infrared beam is passed through the window and the thin layer of electrolyte solution to the electrode, (at which point the IR beam is reflected off the specularly reflecting electrode surface and then back out again through the solution to the window) it is directed to the detector. This is thus a double pass experiment.

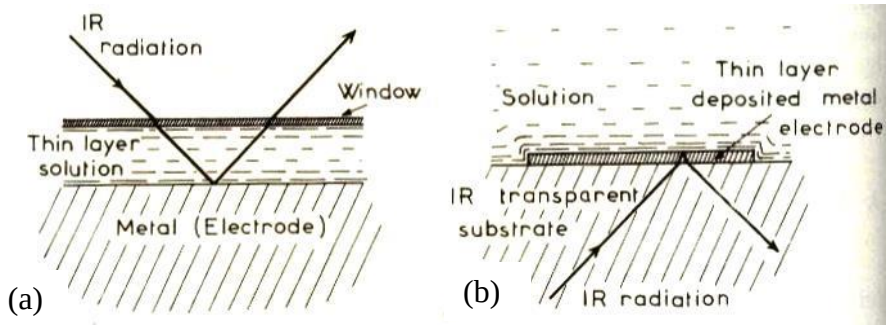

Figure 1.9: Two optical layouts as shown schematically and the difference between (a) external reflection and (b) internal reflection (after Beden, 1988 p206) [8]

To achieve this, two optical configurations have been discussed by Pons [15] i.e. external reflection and internal reflection as shown in Figure 1.9(a) and Figure 1.9(b) respectively.

1.3.2.1.1 External reflection method

The external reflection method is very commonly used in a thin- layer spectroelectrochemical cell. The cell is equipped with an IR transparent window which contains different geometry (flat or bevelled) for the in situ spectroelectrochemical cell. The working electrode is a disk sealed into the end of an insulating cylinder, which can be moved inside a cell perpendicular to the window. For the IR spectroscopic experiments the electrode is pushed forward until it makes contact with the window, forming a thin-layer cell with solution thickness of 1-50 μm. The IR window material chosen depends on the spectral region of interest and on the solvent. For mid-IR applications calcium fluoride, silicon, or zinc selenide windows are used most often, while polyethylene or Mylar window materials are used in the far-IR region [16].The cell housing can be comprised of inert materials such as glass or Teflon [16]. The electrode material has to be able to specularly reflect IR radiation. Polished disks of Pt, Au, Ag, Cu, Ni, Fe, and Pd have all been used as the working electrode. The electrode is mounted onto the end of a metal disk which is generally sheathed in glass or Teflon so that the connecting metal disk is insulated from solution. The exposed face is polished to a mirror finish with a slurry of alumina or diamond paste. A wire or metal rod is attached to the opposite face to allow electrical contact with a potentiostat. In situ IR spectroelectrochemical cell usually uses the potentiostated three-electrode arrangement as described above section 1.1.2.2. The secondary (counter) electrode is usually a platinum wire which is placed behind the working electrode in a configuration that minimizes the solution resistance. The geometry

of the counter electrode is circular, this gives a symmetric current distribution pattern to the working electrode. A Luggin capillary reference electrode is positioned near the edge of the working electrode for minimising the *IR* drop in the three electrode electrochemical cell.

1.3.2.1.2 Internal reflection method

Early efforts in electrochemical vibrational spectroscopy were based on the use of optically transparent electrodes [17]. These were typically infrared transparent germanium plate electrodes or thin metal films deposited on an infrared transparent substrate and were used as internal reflectance elements. In this method (Attenuated total reflection (ATR)), the light is passed through the cell at an angle such that it undergoes total internal reflection at the electrode-solution interface (see Figure 1.9b). The electric field of internally reflected light penetrates a short distance across the interface, its intensity falling off exponentially with distance into the solution. The depth of penetration of this "evanescent wave," which is a function of the wavelength of the radiation, is greatest at the light critical angles and decreases to about one-tenth of the wavelength of the light at angles well above the critical angle. This means that the internally reflected radiation can be absorbed by species on the solution side of the interface, but only by species either adsorbed on the electrode or in solution within a micrometer or so of the electrode. Thus the bulk of the solution does not contribute to the total absorbance. This type of experiment puts quite strict demands on the electrode material, which must both conduct electricity and transmit IR light.

1.3.3 Spectral acquisition

It consists in using ensemble averaging and signal processing by means of computers or sophisticated digital oscilloscopes. The data acquisition and signal processing techniques in in situ IR spectroelectrochemistry serve two purposes to remove the spectrum of the bulk solvent, which would otherwise block out the spectrum of adsorbed or electrogenerated species, and to enhance the very low signal to noise ratios encountered in in situ IR spectroelectrochemical experiments. Therefore, acquisition of in situ infrared spectra has been achieved by several methods as has been practised by previous workers in the field.

The most widely applied techniques are potential modulation. The electrode potential is changed from a value E_1 where the reflectance is R_1 to a value E_2 where the reflectance, R_2, is different. The quantity measured is a function of

$$\frac{\Delta R}{R}(\bar{\upsilon}) = \frac{R_2(\bar{\upsilon}) - R_1(\bar{\upsilon})}{R_1(\bar{\upsilon})}$$

And spectra are usually presented as plots of $\frac{\Delta R}{R}$ vs. wavenumber $\bar{\upsilon}$. Thus the spectrum is a difference spectrum, which shows only changes in reflectance caused by the change in potential. The spectra are plotted as transmittance or absorbance against wavenumber. A change in potential can cause a change in the reflectance for any of several reasons, including changes in the number and bonding of species adsorbed on the electrode, migration of ions into or out of the optical path, electron transfer reactions that form or destroy film on the electrode surface, and electron transfer reactions that form or consume species in solution.

Several approaches to increasing the S/N ratio are in use, depending particularly on whether a dispersive or a Fourier transform IR spectrometer is used. With a dispersive instrument the variation of reflectance with potential is measured at constant wavenumber, whereas with an FTIR instrument the variation of reflectance with wavenumber is measured at constant potential.

1.4 Electrochemically modulated infrared spectroscopy (EMIRS)

Electrochemically modulated infrared spectroscopy was the earliest in situ IR spectroelectrochemical technique used with an IR dispersive spectrometer to record the in situ IR spectra of molecules present at an electrode/solution interface. When using a dispersive instrument the most common method is to modulate the electrode potential between E_1 and E_2 with a square wave of about 10 Hz frequency. When the electrode is alternately fixed at one of the two fixed potentials defined by the square wave modulation, the signal can be observed in an EMIRS experiment which is proportional to the difference in the intensity of the radiation received by the detector. A differential spectrum is recorded by feeding the detector signal to a lock-in amplifier tuned to the potential modulation frequency. The first EMIRS experimentally performed and developed by Bewick et.al. used a standard infrared spectrometer with monochromator and large number of mirrors to the modified optical path [18].

The drawback of EMIRS is that phenomena under investigation must be electrochemically reversible processes. However, EMIRS has been especially useful for the study of the electrical double layer and diffuse layer structures. With the advent of FTIR spectrometers, this technique is no longer commonly used by researche.

1.5 Subtractively normalised interfacial Fourier Transform infrared spectroscopy/ single potential alteration infrared spectroscopy (SNIFTIRS/SPAIRS)

With FTIR spectrometers, there are two basic subtractive techniques in common use for spectroelectrochemistry. Single potential alteration infrared spectroscopy (SPAIRS) is the most general. It is one of the original subtractively normalized interfacial Fourier transform infrared spectroscopy (SNIFTIRS) data acquisition methods. With SPAIRS, a set of interferograms is collected while the electrode is held at constant potential. In a spectroelectrochemical experiment the working electrode in the electrochemical cell is held at a constant background potential (E_1), while a sequence of interferograms are collected, averaged and Fourier transformed to a single beam spectrum and electronically stored. The electrode is then stepped to a new potential (E_2), the data collection and processing are repeated and the resulting single beam spectrum is stored in a new file. The background potential is one where no electrolytes or untransformed electroactive species are detectable in the spectrum at the electrochemical cell. The single beam spectra encode the wavelength dependent reflectivity of the system as ΔR. The ratio of single beam spectra recorded at two different electrode potentials can then be used to compute a potential difference spectrum. Spectra are typically displayed with the y-axis in units of $\frac{\Delta R}{R}$ or $-\log\frac{R_2}{R_1}$, where the subscripts indicate the different electrode potentials. For small values of $\frac{\Delta R}{R}$, this quantity is proportional to absorbance and reported as such. Both positive and negative bands may be observed. Positive bands are due to absorbance peaks from species present at the new applied potential (E_2) relative to the background potential (E_1). The negative bands are due to species present in greater quantity at the background

potential. Hence the measured spectrum can show only changes in species caused by changes in potential at the working electrode.

This spectroscopic acquisition method has several advantages. One is that interferences from atmospheric absorbance due to water and carbon dioxide may be easily eliminated by cancellation in the ratioing of the spectra.

1.6 Polarisation-modulated infrared reflection-adsorption spectroscopy (PM-IRRAS)

When using the PM-IRRAS technique, Fourier transform spectroscopy is combined with polarisation modulation, especially with a ZnSe photoelastic modulator at 74 kHz. The polariser needs to be positioned to enable radiation with its electric field vector oriented parallel to the plane of incidence to strike the electrode surface. The light is switched between s-polarisation and p-polarisation states in polarisation modulation experiments. In these experiments, differential reflectance ($\Delta R/R$) spectra are computed as the ratio of $(I_s-I_p)/(I_s+I_p)$, where I_p is the intensity of reflected p-polarised radiation and I_s is the intensity of reflected s-polarised radiation. The sum (I_s+I_p) and difference (I_s-I_p) spectra are obtained by Fourier transformation of the interferogram signal before and after demodulation. In this method, recording of in situ infrared spectra of an electrode/electrolyte interface at a single potential is possible. According to the surface selection rule only adsorbed molecules with the dipole moment perpendicular to the surface will absorb IR energy. Thus, modulating the state of polarisation yields the IR spectra of the adsorbed species, due to contributions from the solution and the diffusion layers being eliminated by this technique.

1.7 X-ray absorption spectroscopy (XAS)

1.7.1 Introduction

XAS has been used in this thesis to investigate coordinative geometries in solutions of complex ions. The basis of measuring a sample using XAS is by scanning the X-ray energy across an absorption edge. X-ray absorption spectroscopy has the ability to probe short and medium range order in liquid and solid samples and oxidation states of atoms in a diverse range of samples, in

particular coordination environments around inorganic metal ion centres [19]. The X-ray absorption near-edge structure gives chemical information (especially oxidation state) and in simple terms, is often used for a "fingerprint" identification of chemical environments. The extended X-ray absorption fine structure gives structural or crystallographic information and is used to determine the distances, coordination number, and species of the neighbours of the absorbing atom.

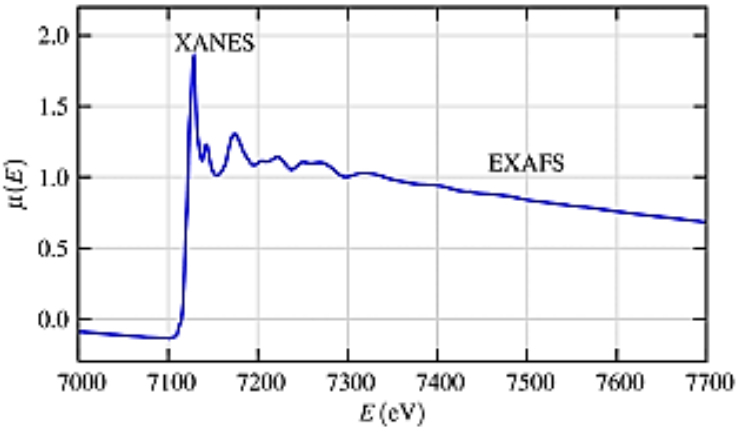

Figure 1.10: Schematic illustration of an X-ray absorption spectrum with the XANES and EXAFS regions identified. (After Newville, 2004 [20])

The absorption edge is a continuous increase in absorption, as suggested by Figure 1.10, but in fact shows significant structure both in the immediate surroundings of the edge jump and well above the edge. It is called the white line in the absorption spectra. The structure in the surroundings of the edge is sometimes referred to as X-ray absorption near-edge structure (XANES). The oscillations above the edge, which can extend for 1000 eV or more, are often referred to as extended X-ray absorption fine structure (EXAFS). They arise as the ejected photoelectron interacts with the atoms surrounding the excited atoms. Such information if analysed can then give information on the coordinative environment surrounding a central metal ion.

1.7.2 Simple theoretical description of XAS

In the discussion of X-ray absorption, the primary concern is the absorption coefficient, μ which gives the probability that the X-ray will be absorbed according to Lambert-Beer's Law:

$$I = I_0 e^{-\mu t}$$

Where I_0 is the X-ray intensity incident on a sample, t is the sample thickness, and I is the intensity transmitted through the sample. For the X-ray, as for all light, the X-ray intensity is proportional to the number of X-ray photons.

XAS can be measured either in transmission or fluorescence geometries. The energy dependence of the absorption coefficient $\mu(E)$ either in transmission is given by:

$$\mu(E) = \log\frac{I_0}{I}$$

or in X-ray fluorescence as:

$$\mu(E) \propto \frac{I_f}{I_0}$$

Where I_f is the monitored intensity of a fluorescence line which is associated with the absorption process.

For the EXAFS, the focus is on the oscillations above the absorption edge, and the EXAFS fine-structure function χ(E) can be defined as:

$$\chi(E) = \frac{\mu(E) - \mu_0(E)}{\Delta\mu_0(E)}$$

Where $\mu(E)$ is the measured absorption coefficient, $\mu_0(E)$ is a smooth background function representing the absorption of an isolated atom, and $\Delta\mu_0$ is the measured jump in the absorption $\mu(E)$ at the threshold energy E_0. (See Figure 1.11)

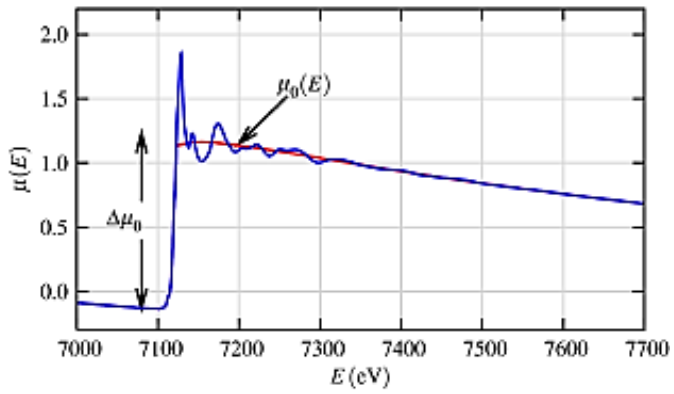

Figure 1.11: Schematic illustration of $\mu(E)$ with smooth background function $\mu 0(E)$ and the edge –step $\Delta\mu 0(E0)$ (After Newville, 2004) [20]

EXAFS is best understood in terms of the wave behaviour of the photo-electron created in the absorption process. Because of this, it is common to convert the X-ray energy to *k*, the wave number of the photo-electron and is defined as:

$$k = \sqrt{\frac{2m_e\left(E - E_0\right)}{\mathrm{h}^2}}$$

Where E_0 is the absorption edge energy and m_e is the electron mass.

The EXAFS signal contains the contributions of all of the coordination shells. Each contribution can be approximated to a damped sinusoidal function in k-space, whose frequency is proportional to the absorber-scatterer distance. The EXAFS signal is Fourier transformed to obtain a radial distribution function. Fourier transform (FT) is the standard tool used for frequency separation. In fact, this operation transforms each sinusoidal component in a FT modulus peak, going from k-space to R-space. The outcome of this operation is the χ(k) function related to absorber-scatterer pairs whose interatomic distances belong to that specific integration interval. The different frequencies apparent in the oscillations in χ(k) correspond to different near neighbour coordination shells which can be described and modelled according to the EXAFS equation,

$$\chi(k) = \sum_j \frac{N_j f_j\ (k) e^{-2k^2\sigma_j^2}}{kR_j^2} \sin[2kR_2 + \delta_j(k)]$$

Where *f(k)* and *δ(k)* are photo-electron scattering properties of the neighbouring atoms. *N* is the number of neighbouring atom, *R* is the distance to the neighbouring atom, and σ^2 is the disorder in the neighbour distance. Further, scattering amplitude *f(k)* and phase-shift *δ(k)* depends on atomic number Z of the scattering atom. If these properties are known, *N*, *R*, and σ^2 can be determined.

1.7.3 EXAFS data processing

Data processing is largely automatic using a programme known as Athena, to subtract the background, determine the edge position, and normalise the oscillations resulting in a plot in k-space,

$$k = \sqrt{\frac{2m_e\left(E - E_0\right)}{\eta^2}}.$$

Because the XANES region just above the edge consists of peaks with the photoelectron's energy is matched to unoccupied states, analysis of the EXAFS

region typically starts at k=2 as a convention. The maximum k depends on the signal-to-noise ratio of the data. For the example, NiO powder standard, the signal-to-noise is good out to very high k. For the solutions, the signal-to-noise means that k_{max} is limited to about k = 10. The final step in assessing a fit to EXAFS data is to vary the k-range being used, at both the high and low ends. If the values of the fitted parameters do not change significantly, it means the fit is stable.

1.7.3.1 k-weightings

The data are often weighted by integer powers of k, in both k-space and R-space (R-space is the Fourier transform of k-space, having both real and imaginary components). This enables different components of the EXAFS spectrum to be highlighted. Overall, the intensity of the oscillations decreases with energy above the absorption edge. However, interaction of the photoelectron with heavier elements (higher atomic number Z) persists to higher energy/higher k than interactions with lighter elements. Therefore, contributions from heavier elements will be more dominant in k^3-weighted spectra than k^1-weighted spectra. By fitting multiple k-weighted data simultaneously, additional constraints can be placed on the model.

1.7.4 EXAFS fitting

The EXAFS equation (discussed above), assumed that the X-ray excited photoelectron was scattered only by a single scattering atom before returning to the absorbing atom. In fact, the X-ray excited photoelectron can be scattered by two (or more) atoms prior to returning to the absorbing atom. Multiple scattering is particularly important at low *k* where the photoelectron has a very low energy and consequently a long mean-free path, allowing it to undergo extensive multiple scattering. Multiple scattering is particularly strong if the two scattering atoms are nearly collinear since the photoelectron is strongly scattered in the forward direction. In this case, the EXAFS oscillations due to the multiple scattering pathway (examples of Figure 1.12(b), multiple-scattering paths path T-4-2-T is co-linear while the path T-1-3-T) can be as much as one order of magnitude stronger than that due to the single scattering pathway (Figure 1.12(a) single-scattering paths from the target atom 'T' only, note that paths T-1-T and T-2-T are degenerate). The preferred method of fitting EXAFS spectra is to use a crystal

structure of the compound. This allows not only the single scattering paths, but also multiple scattering paths to be considered.

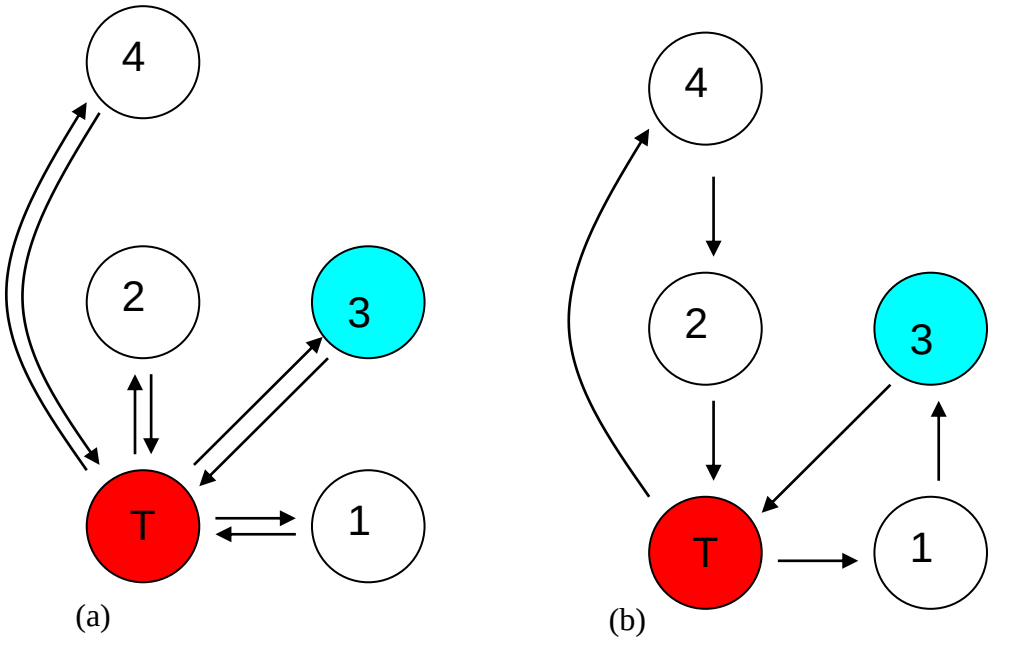

Figure 1.12: Schematic diagram of model structure and photoelectron scattering paths. Left: single-scattering paths from the target atom 'T' only. Note that paths T-1-T and T-2-T are degenerate. Right: examples of multiple-scattering paths. Note that the path T-4-2-T is co-linear while the path T-1-3-T is not. Co-linear paths can have significant contributions to the overall intensity.

1.8 Electrospray ionization mass spectrometry (ESI-MS)

ESI-MS has been used in this study to elucidate the complex ions species in some model solution systems prepared in this thesis project. Electrospray ionization is a technique used to produce gaseous ionized species from a liquid solution generated by creating a fine spray of charge molecules in the presence of a strong electric field. As with conventional mass spectrometry instruments, (such as Fast atom bombardment or Electron impact techniques) the ESI-MS instrument is able to ionise and separate molecules in space according to their mass to charge ratio (m/z), providing accurate molecular weight determinations and isotope patterns. The ions that are produced have little extra energy, and so have little fragmentation. The characteristic feature of the soft electrospray ionisation method is the relatively low fragmentation and ability to impart multiple charges to large molecular weight molecules which therefore places their m/z values into the range of the detectors [21].

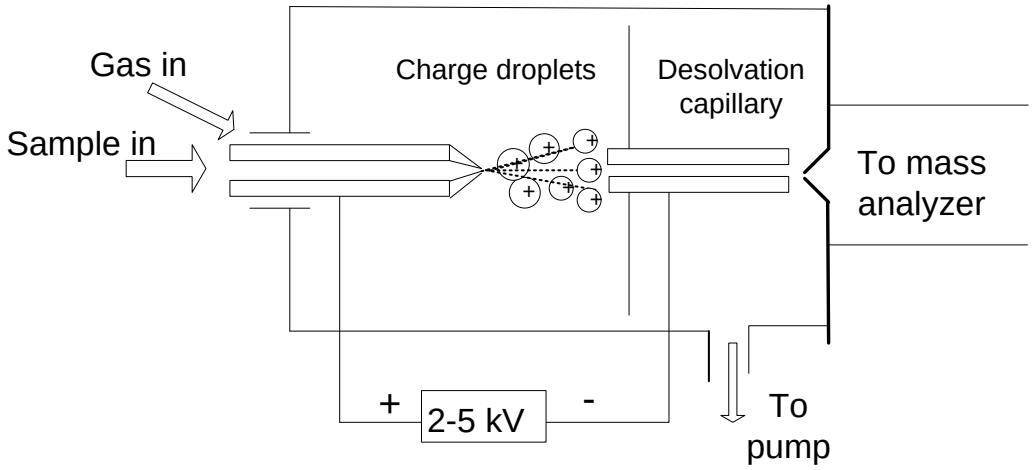

Figure 1.13: Schematic diagram of electrospray ion source (Adapted from Robinson, p 544) [22]

An electrospray ion source is illustrated in Figure 1.13.The electrospray ionisation process first involves the injected sample being pumped through a capillary tube to produce a fine aerosol of highly charged droplets in the presence of a strong electric field at the end of the capillary. These electrically charged droplets are formed from a solution flowing out of a hollow needle into an electric field of 5-10 kV. The droplets so produced have a charge to volume ratio close to the physical maximum for droplet stability, manifested by a 'coulomb explosion' caused by the surface charge density exceeding the surface tension of the solvent [21, 23]. The droplets move through a gas flow, which evaporates some of the solvent in a process called desolvation. The desolvation of the charged droplets is aided by their passage through a desolvation capillary, which consists of a glass capillary and a flow of dry, heated N_2. The skimmer cones transmit as many ions as possible to the mass spectrometer, while decreasing the pressure at each stage. Finally, the spectra are obtained often easily interpreted by comparing the mass/charge (m/z) ratio values and isotope patterns to calculated patterns of chemically sensible candidate molecules.

Chapter 2

Literature review

2.1 Introduction

In situ infrared spectroscopic techniques for the study of electrochemical phenomena in thin-layer electrochemical cells have provided a large amount of information on the various electrochemical systems investigated. The primary focus of these studies is the characterization of molecular species in the electrical double layer and species interacting with the electrode surface. Surface phenomena are obviously extremely important in electrochemical systems. Due to this a lot of focus was given to the characterization of electrode surfaces by IR techniques. These surface infrared studies have benefited experiments conducted in situ and also have provided additional advantageous information to other surface spectroscopic techniques such as surface-enhanced Raman scattering (SERS), optical-harmonic generation (SHG) and x-ray methods. IR spectroscopy when applied to electrode surfaces was found to be a very powerful probe of electrochemical surface processes.

Compared to surface adsorption studies, applications of IR spectroscopy to characterise electrochemical species occurring *in solution* only have been very few.In past studies of some thin layer electrochemical systems, solution composition information has been obtained as additional data in surface adsorption studies [11]. As the solvent strongly absorbs IR radiation which can compromise the detection of the weak absorption peaks by a low level of dissolved redox species, it is important to have a thin layer electrochemical cell to minimise solvent absorption. In addition, the electrochemical species that contain bound carbonyl (-CO) or cyano (-CN) moieties are favourable for study by IR spectroelectrochemical techniques as these are among the few functional groups that absorb IR radiation in the so-called “first infrared window of water” (2500-1800 cm^{-1}) where a usefully low background IR absorption by water occurs. This property allows IR spectra of species in this region to be easily acquired by spectral rationing where the background spectrum contains just the solvent. On the other hand the spectra of adsorbed species are much easier to obtain in non-aqueous media, as organic solvents generally absorb infrared radiation far less

than water [8]. The region where the main absorption peaks are DMSO/DMF only have weak peaks is the same region as the first infrared window of water therefore these can be ratioed out without causing any interferences or loss of information.

The use of spectroelectrochemical techniques has a long history and began in the 1960s via the use of UV-visible spectroscopy coupled with an electrochemical cell [11]. In the early days of spectroelectrochemical technique development, optically transparent electrodes were used to conduct electrochemical experiments [16, 24, 25]. The electrodes generally used were infrared transparent germanium plate electrodes or deposited thin metal films. They were deposited on an infrared transparent substrate and used as internal reflectance elements. The disadvantage was that these experiments lacked sensitivity and the choices of infrared transparent electrode materials were limited [16]. Raman spectra of electrochemical systems (Surface-enhanced Raman spectroscopy (SERS) were obtained conducting experiments which used external reflection cells [16, 26]. The successful adaptation of modulated UV-visible specular reflectance techniques to infrared studies were proved by Bewick, Kunimatsu, and Pons [14]. Electrochemically modulated infrared spectroscopy (EMIRS), a technique which uses the more old fashioned dispersive IR instrument, was used in the first infrared reflectance spectroelectrochemical experiments [18]. Pons et. al. [27] developed the subtractively normalized interfacial FTIR spectroscopy (SNIFTIRS) technique, which is suitable for the in situ detection of either electrogenerated intermediates in the double layer or species adsorbed at the electrode surface. Another method commonly used in this area of study is the technique of polarization modulated Fourier transform infrared reflection absorption spectroscopy (PM-FTIRRAS)[28].

In providing this literature review, the application of IR spectroscopy in metal/carbon monoxide system, metal/cyanide system and metal/pseudohalide systems have been discussed and the review will also deal with SNIFTIRS, PM-FTIRRAS and EMIRS as in situ IR techniques that have often been used to provide information on electrochemical systems.

2.2 Pt/CO electrochemical systems studied by IR spectroelectrochemical techniques

The Pt/CO system can be identified as one of the earliest systems to be studied by in situ infrared spectroscopic techniques, especially by PM-FTIRRAS. The Pt/CO (in 1 N H_2SO_4) was studied by PM-FTIRRAS techniques, by Golden et. al. [29], and exhibited generally the good sensitivity of these techniques. In this system, the presence of a band at 2070 – 2090 cm^{-1} in the PM-FTIRRAS spectra was detected over the potential range 0 to 0.55 V (NHE) which was attributed to adsorbed CO on the platinum electrode surface. The position of the band correlated with the $\nu(CO)_{ads}$ stretching frequency expected for CO adsorbed linearly on platinum metal. Lambert [30] proposed that the potential-dependent linear frequency shift of the ν(C-O) stretching mode was primarily due to the first-order Stark shift. The frequency of the band (due to adsorbed CO) increased linearly from 2070 to 2090 cm^{-1} as the potential was increased more anodically owing to the Stark shift. Golden et. al. [29] further reported that the intensity of the band due to adsorbed CO decreased sharply after 0.55 V (SHE) which was ascribed to the onset of CO oxidation to CO_2.

Kunimatsu et. al.[31] studied adsorption and oxidation of CO on a platinum electrode in 0.5 M H_2SO_4. The results were obtained by combining the technique of PM-FTIRRAS with an FTIR spectrometer for the in-situ study of the electrode/electrolyte interface. Adsorption of carbon monoxide on the electrode was carried out by bubbling CO gas through the solution. The potential of the platinum electrode during this process was held at either 0.05 V or 0.4 V which led to CO being adsorbed in the hydrogen region or in the double-layer region respectively. The in situ IR studies also revealed two different oxidation mechanisms for the transformation of CO to CO_2. The operation of either oxidation mechanism was found to depend on the potential at which the CO became adsorbed on the platinum electrode. For instance, when CO became adsorbed on the platinum electrode at 0.4 V, a linear increase in the frequency (with increasing anodic potential) of the band due to adsorbed CO was observed. In contrast, the band due to CO adsorbed at 0.05 V did not increase in frequency as the potential was increased anodically. In addition, for the 0.05 V situations CO_2 was observed in the PM-IRRAS spectrum at less anodic potentials. They

deduced that these phenomena were due to the formation of another surface species (besides adsorbed CO that had formed at 0.05 V) which was oxidised to CO_2 at less anodic potentials. It was reported that this surface species was assumed to be CO adsorbed on the platinum electrode surface in the two-fold bridging mode.

2.3 Metal/cyanide electrochemical systems

In the past, in situ FTIR studies of metal/CN^- electrochemical systems have been carried out for various reasons. Since, cyanide is isoelectronic with carbon monoxide, this was generally the purpose to carry out experiments to compare the metal/CN^- electrochemical systems with the metal/CO systems. Another important reason was the well-established vibrational spectroscopy knowledge of cyanide in metal-ion complexes [32]. One specific aim of the in situ infrared spectroscopic techniques was to study the adsorption of cyanide ions and its electrochemical behaviour on gold and silver. These studies aided in understanding the role of cyanide as an important component in the industry of mining extraction and plating baths of these metals. Studies have also been conducted at length using electrochemical methods on anodic oxidation of cyanide at platinum or graphite electrodes. Accordingly, the overall aim in carrying out SNIFTIRS and PM-FTIRRAS studies of cyanide at platinum electrodes is generally to obtain additional vibrational information on the electro-oxidation of cyanide to cyanate to supplement the information gained from pure electrochemical studies. Information from the studies of the oxidation mechanisms of cyanide to cyanate and CO_2 on various metals by IR have contributed to the development of electrolytic oxidation methods for processing of cyanide to more innocuous products. These methods have benefited disposal methods of the cyanide wastes that accumulate in the electroplating and mining industry.

So far, Ag/CN^-, Au/CN^-, Cu/CN^-, Pt/CN^- and Ni/CN^- are the transition metal/CN^- electrochemical systems on which in situ FTIR studies have been conducted on and bands due to cyanide adsorbed on the metal electrode, or electrogenerated solution species of these studies have been reported.

2.3.1 Silver/cyanide electrochemical studies

Kunimatsu et. al. [33] reported the spectra of cyanide adsorbed on a polycrystalline silver electrode from 1 N K_2SO_4 aqueous solutions obtained by in situ polarization-modulated Fourier transformed infrared reflection absorption spectroscopy. A thin-layer spectroelectrochemical cell was used with a CaF_2 prism window. They observed a band at ca. 2100 cm^{-1} in the p-polarised spectra recorded (in the potential range -1.3 to -0.6 V (SHE)) of a silver electrode immersed in 0.1 mol L^{-1} KCN and 1 mol L^{-1} K_2SO_4. The band at ca. 2100 cm^{-1} was assigned to cyanide adsorbed on the silver electrode on the basis of the linear increase in frequency from 2093 to 2111 cm^{-1} observed when the potential was gradually increased from -1.3 to -0.6 V (SHE). The results revealed that the linear shift of band centre with potential was similar to that observed for adsorbed CO in the Pt/CO electrochemical system. Thus, Kunimatsu et al. established two conclusions; 1) that the mechanism of the band centre shift with potential was the same as assumed for adsorbed CO, and 2) that the cyanide anion was linearly bonded to the silver surface atoms on the electrode. At more anodic potentials (-0.5 to -0.2 V (SHE)), the s-polarised and p-polarised IRRAS spectra displayed a relatively more intense band centred at 2136 cm^{-1}. This band at 2136 cm^{-1} was recognised to develop at the expense of the band at ca. 2100 cm^{-1} assigned to adsorbed cyanide. Since the position of the band centre did not shift with potential, Kunimatsu assigned the band at 2136 cm^{-1} to a solution species $[Ag(CN)_2]^-$. The presence of the band at 2136 cm^{-1} in both the p-polarised and s-polarised IRRAS spectra also supported the assignment of this band to a solution species. Lastly, a band appearing at 2167 cm^{-1} in the p-polarised spectrum recorded at 0.3 V(SHE), which was also insensitive to the potential, was assigned to the v(CN) stretching frequency of a film of AgCN.

2.3.2 Gold/cyanide electrochemical studies

Kunimatsu et al. [7, 31] also studied the gold/cyanide system by using polarization-modulated Fourier transform infrared reflection absorption spectroscopy. Similar to the Ag/CN^- electrochemical system, the gold electrode was immersed in 0.5 mol L^{-1} potassium sulphate solution containing either 10^{-2} or 10^{-1} mol L^{-1} KCN. The spectro-electrochemical cell used in this case was made from Kel-F with a CaF_2 prism window. A band at ca. 2100 cm^{-1} was revealed in

the p-polarised IRRAS spectra (recorded at -1.0 to -0.5 V (SHE)) of the Au/CN^- electrochemical system. As the potential was increased from -0.1 to -0.5 V(SHE), the band was observed to shift in frequency from 2097 to 2114 cm^{-1}. This was assigned to cyanide adsorbed on the gold electrode. The origin of the shift was most reasonably explained by the first-order Stark effect. Finally, a band appearing at 2146 cm^{-1} in the s- and p-polarised spectra from -0.7 V(SHE) onwards was assigned to $[Au(CN)_2]^-$ complex ions in solution which is generated by reaction of the electrodissolved Au(I) species with cyanide ion.

2.3.3 Copper/cyanide electrochemical studies

Polarization-modulated Fourier transform infrared reflection absorption spectroscopy (PM-FTIRRAS) studies were carried out by Lee at al.[34] on the Cu/CN^- electrochemical system. The cell was made from Kel-F with a prismatic CaF_2 window at the bottom of the cell and polycrystalline copper electrode was pushed up close to the window so that it behaved mostly as a thin layer cell. The electrolyte solutions were 0.5 mol L^{-1} K_2SO_4 and 10^{-3} mol L^{-1} KOH to which KCN as added to give the desired concentration of CN^-. The study revealed that the adsorbed cyanide species in the PM-FTIRRAS spectra was found to depend on the concentration of KCN used in spectroelectrochemical experiments.

When a concentration of KCN 0.1 mol L^{-1} was used, the PM-FTIRRAS spectra of the copper/cyanide solution interphase revealed only solution species. In other words, the s- and p-polarised spectra recorded in the potential range: -1.4 to -0.2 V(SHE) revealed bands at 2077, 2093 and 2126 cm^{-1} which were assigned to the solution species: $[Cu(CN)_4]^{3-}$, $[Cu(CN)_3]^{2-}$ and $[Cu(CN)_2]^-$ respectively. Although, the total amount of cyanide ion concentration is fixed throughout the experiment, the free copper ion concentration is completely determined by the electrode potential. Therefore, at more cathodic potentials, the free copper ion concentration is very low and the CN^-/Cu^+ concentration ratio is high and the dominant species is $[Cu(CN)_4]^{3-}$ while at more anodic potentials, this is higher Cu^+ content and so lower CN^-/Cu^+ ratio so that the dominant species is $[Cu(CN)_2]^-$. This trend was recognised and attributed by Lee at el. to an increase in the amount of Cu^+ generated as the potential at the copper electrode was made more anodic. This would lead to a reduction of the CN^-/Cu, ratio in the thin-layer. Further as seen

with the Ag/CN^- and the Au/CN^- systems, a band at 2172 cm^{-1} was detected at more anodic potentials (>-0.2V (Ag/AgCl)) in the p-polarised spectrum of the Cu/0.1 mol L^{-1} KCN system which was assigned to precipitated CuCN on the electrode surface. The explanation of Lee at al. for the absence of $(CN^-)_{ads}$ peaks at this concentration of CN^- (0.1 mol L^{-1}) because of the masking of the expectedly weak bands of adsorbed cyanide by the intense bands due to the peaks of solution species observed at 2077, 2093 and 2126 cm^{-1}.

On the other hand, it was revealed that when KCN concentration was reduced to $2x10^{-3}$ mol L^{-1} in this system, the p-polarised IRRAS spectra of the Cu/CN^- electrochemical system recorded in the potential range: -1.4 to -1.3 V(Ag/AgCl) featured a weak band at 2084 cm^{-1}. As the potential was increased from -1.4 to -1.2 V(Ag/AgCl), it was observed that the frequency in turn increased from 2084 cm^{-1} to 2094 cm^{-1} for this band. This was accordingly assigned to cyanide adsorbed on the copper electrode. The p-polarised IRRAS spectra of the Cu/CN^- electrochemical system at potentials: -1.1 to -0.8 V(Ag/AgCl) contained a band at 2094-2097 cm^{-1}. It was found that the band centre varied randomly with potential. The p-polarised IRRAS spectra contained a band at 2116-2121 cm^{-1} which also varied randomly with potential of -0.5 to -0.1 V(Ag/AgCl). The bands at 2094-2097 and 2116-2121 cm^{-1} were assigned respectively to $[Cu(CN)_3]^{2-}$ and $[Cu(CN)_2]^-$ adsorbed on the electrode surface. The very slight dependence of the ν(CN) stretching frequencies of these adsorbed species with potential were explained by the assignments of the bands at 2094-2097 and 2116-2121 cm^{-1} due to adsorbed copper-cyano complexes. The variation in potential affects the Cu^+ concentration in the thin-layer, which in turn would affect the chemical equilibria of these ($[Cu(CN)_3]^{2-}$, $[Cu(CN)_2]^-$, CN^-) ions and their adsorption. This may explain the random variation in ν(CN) of these adsorbed Cu(I)CN complexes.

2.3.4 Platinum/cyanide electrochemical studies

Kitamura et. al.[35] carried out a PM-FTIRRAS studied of the Pt/CN^- system. The working electrode was a polycrystalline platinum disk mounted on the end of a Teflon rod and immersed in 0.1 mol L^{-1} NaCN and 0.1 mol L^{-1} KCl aqueous solution.

The p-polarised spectra recorded at -0.7 V(Ag/AgCl) to +1.0 V(Ag/AgCl) and showed a band at 2080 cm^{-1} which was assigned to free solution CN^- close to the electrode surface.

A band appearing at ca. 2106 cm^{-1} which shifted to 2126 cm^{-1} as the potential was increased from -0.7 to 0.4 V (Ag/AgCl) while the intensity remains constant. This band was assigned to the C-N stretching vibration of adsorbed cyanide on the platinum electrode. The continuous band shift against the electrode potential indicates that the band was due to surface species.

The s- and p-polarised spectra at 0.4 V(Ag/AgCl) revealed the presence of a band at 2170 cm^{-1} which was assigned to solution cyanate, an oxidation product of the cyanide ion. This band cannot be attributed to adsorbed species because the band does not shift with potential and the intensities from p-and s-polarised incident light are almost the same. In addition, a sharp band at 2342 cm^{-1} and a weak band at 2260 cm^{-1} first appeared at 0.6 V(Ag/AgCl) and increased in intensity with further anodic excursion of the applied potential. They assigned these peaks to CO_2 and HNCO and suggested that HNCO was further oxidised to give CO_2. However, solution cyanate species are not observed in the IRRAS spectra of the Ag/CN^-, Au/CN^- and Cu/CN^- electrochemical systems reported previously [7, 31, 33, 34] because these systems used applied potentials which were not anodic enough to oxidise CN^- to CO_2 or may have formed solid films or insoluble complex species.

2.3.5 Nickel/cyanide electrochemical studies

Mucalo et al.[36] used a simple thin-layer spectroelectrochemical cell and in situ IR spectroscopic techniques such as SNIFTIRS for detecting corrosion of Ni electrodes in aqueous 0.1 mol L^{-1} KCN solutions. In this study only solution species could be detected in the setup used for acquisition of in situ IR spectra. They reported the formation of various species, for instance $[Ni(CN)_4]^{2-}$ (2124 cm^{-1}), NCO^- (2168 cm^{-1}) and other species. A band due to $[Ni(CN)_4]^{2-}$ (2124 cm^{-1}) appeared in the potential range -800 to 250 mV(SCE). However, a band at 2168 cm^{-1} was detected in spectra recorded at potentials more anodic than +250 mV(SCE). They found that Ni readily dissolved to form the

tetracyanonickelate(II) complex ion in solution but also observed oxidation of the cyanide ion at the Ni electrode to NCO^- and later to CO_2 as the applied potential at the working electrode was made more anodic. In addition other interesting species were observed, which were a reflection of the lowering of the pH in the thin layer (compared to the bulk solution pH of 11.4). Hence, HCN (2094 cm^{-1}) as well as possibly HNCO (2256 cm^{-1}) species were observed. Further, a band detected at 2218 cm^{-1} in the IR spectra of the thin-layer at high anodic potentials (>1000 mV (SCE)) was reasoned to be an unstable nickel(II) isocyanate complex ($[Ni(NCO)_x]^{(x-2)-}$) which was later observed in the study of Li and Mucalo [37] (see later).

2.4 In situ IR study of metal electrode /pseudohalide systems

2.4.1 Introduction

The cyanide, cyanate, thiocyanate, selenocyanate and tellurocyanate ions are called pseudohalides and also can be called chalcogenocyanates. More generally there have been identified in this thesis as NCX^- (where X is O, S, Se, Te).These ions can function as ambidentate ligands in that they can form a coordinate bond to a Lewis acid through either the N or X atom. Hence these ions may coordinate to a metal ion through either one of the end atoms. For example, Nakamoto summarized in his reference text that the following linkage isomers are possible [32]:

M-CN, cyano complex	M-NC, isocyano complex
M-OCN, cyanato complex	M-NCO, isocyanato complex
M-SCN, thiocyanato complex	M-NCS, isothiocyanato complex
M-SeCN, selenocyanato complex	M-NCSe, isoselenocyanato complex

In metal–cyanate complexes, the NCO^- ion may coordinate through the nitrogen (M-NCO) or through the oxygen (M-OCN) [32]. Most complexes reported have usually been N-bonded [32] (such as M= Si, Ge, Zn, Mn, Co, Ni, Fe, Pd, Sn, Zr, Mo, and Ln). However, O-bonded complexes have been suggested for $[M(OCN)_6]^{n-}$ [38] (M= Mo(III), Rh). In general, the CN stretching frequencies for N-bonded metal-cyanate (i.e. isocyanato) complexes occur in the range 2170-2290 cm^{-1} [32].

In the O-bound (i.e. cyanato) metal complexes, the CN stretching frequencies occur in the range 2200-2250 cm^{-1} with the ν(CO) stretching and δ(NCO) bending frequencies occurring in the ranges: 1000-1300 cm^{-1} and 590-630 cm^{-1} respectively. However, Norbury [39] claims that the use of infrared spectral data for the determination of the cyanate bonding mode in these complexes is difficult due to inconsistent trends.

Finally, it should be noted that the cyanato ion is isomeric with the fulminate ion (CNO^-). The CN stretching frequency of the fulminate ion CNO^- ion occurs at 2052 cm^{-1} with the NO stretching frequency and the CNO bending frequency occurring at 1057 and 471 cm^{-1} respectively [32]. Metal-fulminato complexes have been reported which exhibit ν(CN) and ν(NO) stretching and δ(CNO) frequencies in the ranges: 2110-2200 cm^{-1}, 1040-1180 cm^{-1} and 450-500 cm^{-1} respectively. Fulminate salts, however, are explosive (shock sensitive) compounds and hence not many studies exist involving these ions.

The thiocyanate ion have the ability to bond with either N- or S-bonded complexes are formed depending on the nature of the metal [32]. This formation can be modified by the presence of other ligands or by state of the complex-either solid state or solution state. While the chalcogenocyanates can be present in a variety of bridging modes, many different and conflicting examples and explanations have been put forward regarding the coordination behaviour of the thiocyanate ion. However, other factors which influence the mode of coordination are the oxidation state of the metal and the nature of other ligands in a complex. Yamagachi et. al [40] showed for the $[M(NCS)_4]^{2-}$ (M=Zn,Cd and Hg) series, aqueous Raman studies that all ligands are N-bonded in the Zn and S-bonded in the Hg complexes, but both types coexist in the Cd complex.

The $NCSe^-$ ion also coordinates to a metal through the nitrogen (M-NCSe) or the selenium (M-SeCN). However, the trends of SCN and SeCN complexes are very similar. The number of SeCN complexes studied are much lesser than that of SCN complexes [32] due to the instability of $SeCN^-$ ions.

Austad et. al[41] reported that aprotic solvents, and small alkali ions and other hard Lewis acids, associated to the nitrogen end of the thiocyanate ion and

selenocyanate ion. Further, they show in the case of the selenocyanate ion, this association can cause weakening of the carbon-selenium bond sufficient to make the selenium atom electrophilic. Tellurocyanate ion, on the other hand, is very unstable because the chemical evidence shows that the tellurium-carbon bond is very weak and decomposition in humid air is rapid. The use of "feebly polarizing" cations was necessary in the isolation of the salt because tellurocyanate ion cannot exist in a solid in the presence of strongly polarizing cations like potassium or even the larger cesium cation. Although the tellurocyanate ion ($TeCN^-$) is relatively stable in DMF or acetone, the addition of water will instantly lead to decomposition to elemental tellurium and cyanide ion.

However, for aqueous or non-aqueous solutions, the cyanate and thiocyanate ions are reasonably stable for lengthy periods. Pseudohalide ions and any CN^- containing electrolyte systems are particularly well suited to IR spectroelectrochemical studies because the CN stretching frequency occurs in a region of the IR spectrum where there is low background absorption from the solvent and also low interference from other fundamental vibrational frequency.

The electrochemical behaviour and bonding mode of different metals (i.e. Ag, Au, Cu, Pt and Ni) have been studied in electrolytes containing pseudohalide ions using in situ IR spectroscopy. These studies are summarised below:

2.4.2 Silver/pseudohalide electrochemical studies

Dennis et. al.[42] used potential-difference infrared spectroscopy (PDIRS) to examine the potential dependent adsorption of thiocyanate on a silver electrode surface. The PDIR technique involves the subtraction of spectra obtained at pairs of electrode potentials in order to cancel the bulk solvent interferences. PDIR and EMIRS techniques have been, which is explained in chapter 1.

The PDIR spectra were recorded in an electrolyte containing 0.005 mol L^{-1} NaSCN and 0.1 mol L^{-1} $NaClO_4$ in aqueous solution and a polycrystalline silver electrode in a thin-layer electrochemical cell. When the sample potential was adjusted from -450 mV to 0 V (vs. SCE) an increase in peak intensity observed at 2065 cm^{-1} was attributed to free thiocyanate ion in solution. Further, a smaller

negative going band of 2105 cm^{-1}- 2115 cm^{-1} was observed and the peak position was found to shift with changes of potential. This peak was assigned to the S-bonded thiocyanate ion adsorbed to the silver electrode. The shift of vibrational frequency with applied potential was evidence that this was a surface adsorbed species which is the Stark effect.

In another study which was a different approach for studying this electrochemical system, the attenuated total reflectance Fourier transform infrared spectroscopy (ATR-FTIR) technique was used to investigate the adsorption of thiocyanate on a silver surface by Parry et. al.[43]. The optically transparent silver coating on a silicon plate was used for the electrode and the electrolyte used was 0.025 mol L^{-1} NaSCN with 0.15 mol L^{-1} $NaClO_4$ in aqueous solution. They observed bands from 2124 to 2114 cm^{-1} when potentials were applied from 0.2 to -0.6 V(SCE), with these bands gaining in intensity at positive potentials and losing intensity at negative potentials compared to the 0 V(SCE) reference spectrum. The peak was assigned to the S-bonded thiocyanate species on the silver surface. A further, large positive peak at 2144 cm^{-1} was assigned to the occurrence of a AgSCN solid film on the electrode surface.

2.4.3 Gold/pseudohalide electrochemical studies

2.4.3.1 Gold/cyanate electrochemical studies

Dennis et al. [44] examined the electrooxidation of cyanate on gold by using PDIRS. However, they have referred to this approach as single-potential alteration infrared spectroscopy (SPAIRS). The SPAIRS spectra were obtained for gold electrodes immersed in aqueous electrolytes containing 0.01 mol L^{-1} NaOCN and 0.1 mol L^{-1} $NaClO_4$ in a thin-layer cell. The SPAIRS spectra were acquired from 0.6 V to 1.2 V (SCE) potential and the following features were observed.

One positive going band at 2168 cm^{-1} and two negative going bands at 2260 cm^{-1} and 2343 cm^{-1} were observed as major features. The intensity of the positive going band at 2168 cm^{-1} increases as the potential is increasingly made more anodic. In this particular technique this positive going band is due to the loss of cyanate ion content in the thin layer electrolyte solution. This occurs due to the adsorption of cyanate ions to the gold electrode and irreversible electrooxidation

to CO_2. In support of this explanation, the intensity of the negative going band at 2343 cm^{-1} increases (because more negative) with more positive potential. The band was assigned to the asymmetric stretching mode for solution CO_2. The negative going band at 2260 cm^{-1} was assigned to HNCO. This mechanism is consistent with the appearance of a negative going 2260 cm^{-1} band observed at both gold and platinum electrodes. The SPAIR spectra on gold was more likely due to the association with cyanate adsorption and this was evident in the appearance of a weak broad feature around 2220-2230 cm^{-1} was this may be due to a Au-OCN complex $[Au(NCO)_2]^-$.

2.4.3.2 Gold/thiocyanate electrochemical studies

Bron and Holze [45] carried out an investigation of the adsorption of thiocyanate ions at gold electrodes from an alkaline solution using the SNIFTIRS technique. The SNIFTIR spectra were obtained with the gold electrode in an electrolyte containing 0.01 mol L^{-1} KOH and 0.001 mol L^{-1} KSCN at various concentrations in aqueous solution.

In spectra using only p-polarized light, a band at about 2120 cm^{-1} was seen due to the CN-stretching vibration of adsorbed thiocyanate. The negative going band (in this study "negative" means a loss from the thin layer) at 2065 cm^{-1} can be assigned to the CN-stretching vibration of solution thiocyanate. It was consumed from the thin layer at more positive electrode potentials due to the formation of gold thiocyanate complex which gave a peak in IR spectra at 2145 cm^{-1} and 2168 cm^{-1} attributed to the formation of a gold-thiocyanate complex and solution cyanate, respectively. The cyanate was formed from the thiocyanate by oxidation. In higher thiocyanate concentrations (0.01 mol L^{-1}), the formation of a complex was mainly observed, whereas the oxidation of the thiocyanate ion itself occurred in more alkaline solutions. Therefore, the two bands 2145 and 2168 cm^{-1} are strongly detected and their relative intensities are dependent on the electrolyte composition.

2.4.4 Copper/pseudohalide electrochemical studies

2.4.4.1 Copper/cyanate electrochemical studies

Bron and Holze et. al [46] have also reported in situ IR studies on copper electrodes and cyanate in aqueous electrolytes. They conducted a series of

SNIFTIRS spectra of cyanate adsorbed on a copper electrode at more negative potentials. During the spectroelectrochemical experiment, the electrodes were pushed against a ZeSe window in order to form a thin-layer. The electrolyte solutions were prepared from 0.01 mol L^{-1} KOCN and 0.1 mol L^{-1} $KClO_4$ in aqueous media. A negative-going band at 2168 cm^{-1} was observed, which (in this technique employed) increases with more positive potential due to the consumption from the thin layer of solution cyanate. In addition, a potential-dependent positive going band at 2200 cm^{-1} appeared and shifted to higher values with the more positive potential and it also rose in intensity. The results indicated that adsorbed cyanate species had been detected on the copper electrode and the adsorption starts at more negative potentials.

2.4.4.2 Copper/thiocyanate electrochemical studies

Bron and Holze et. al [46] also studied copper electrodes in thiocyanate electrolyte using SNIFTIRS. The electrolyte was used as 0.01 mol L^{-1} KSCN and 0.1 mol L^{-1} $KClO_4$ in aqueous media in a thin-layer cell with ZnSe windows.

The SNIFTIRS spectra featured a bipolar band at 2100 cm^{-1} due to the v(CN) stretching frequency of SCN^- adsorbed to Cu. This peaks shifted to higher wavenumbers with more positive potentials as would be expected of a surface adsorbed species. They observed a band at 2068 cm^{-1} which exhibited negatively increased intensity at a potential more positive than -50 mV and also observed another band at 2122 cm^{-1}. They assigned these two bands to solution thiocyanate and copper thiocyanate complexes respectively. The negative increase in intensity indicated loss of free thiocyanate ion in the thin layer. Two possible reasons for the loss of solution thiocyanate in the thin layer were identified as being due to additional adsorption or the formation of a kind of copper thiocyanate complex ion species.

2.4.5 Platinum/pseudohalide electrochemical studies

In another study, PM-IRRAS was carried out and applied to platinum electrodes in thiocyanate electrolytes. This was also carried out by Bron and Holze [47].The electrolyte solution consisted of 0.1 mmol L^{-1} KSCN and 0.1 mol L^{-1} $KClO_4$ in aqueous solution. They observed a potential dependent band at 2100 cm^{-1} which was assigned to the CN-stretching vibration of adsorbed thiocyanate ions. The

shift of this band to higher wavenumber with increasingly anodic applied potentials could be explained in terms of the Stark effect as observed with all other systems where an adsorbed species was detected. Another peak at 2068 cm^{-1} was assigned to thiocyanate ions in bulk solution.

Kitamura et.al. [48] also studied anodic reaction at the Pt/OCN^- in methanol solution In addition, IRRAS spectra were obtained for 0.01 mol L^{-1} KOCN and 0.1 mol L^{-1} LiCl in methanol solutions. They observed bands at 2258 and 2342 cm^{-1} when potentials of +1 V(Ag/AgCl) were applied. These were due to HNCO and CO_2 species respectively. As for the KOCN/methanol solution, however, a further anodic reaction occurred. In contrast to the case in aqueous solution, the intensity of the HNCO band is much higher than that of CO_2. The appearance of the minor product CO_2 might be due to a water impurity in methanol.

2.4.6 Nickel/pseudohalide electrochemical studies

Mucalo and Li [37] studied the dissolution of nickel electrodes in aqueous pseudohalide-containing electrolytes in a thin-layer spectroelectrochemical cell by SNIFTIRS. In general, the electrolyte solutions prepared for use in SNIFTIRS experiments were 0.05 mol L^{-1} in the pseudohalide (NaOCN, KSCN, and KSeCN) salt and 0.01 mol L^{-1} in KNO_3. They reported the formation of electrochemically generated Ni(II) pseudohalide complex ions, i.e. Ni(II) complexes involving NCO^-, NCS^- and $NCSe^-$ ions which gave peaks at 2225 cm^{-1}, 2121 cm^{-1} and 2123 cm^{-1} respectively. In the same study, they also showed that a *negative-going* intensity peak (at the wavenumber value for the free pseudohalide ion) also appeared in spectra acquired at the more anodic potentials due to consumption of the free pseudohalide ions in the thin-layer (relative to the background spectrum acquired at more cathodic applied potentials) via complexation or via oxidation as Ni(II) ions were made available by anodic dissolution for complexation. They observed that CO_2 (2343 cm^{-1}) featured in the Ni/NCO^- system and was attributed to electro-oxidation of the cyanate ions at the working electrode surface. CO_2 was also observed in the Ni/$NCSe^-$ system and at a much less anodic potential (compared to the Ni/NCO^- system) which was reasoned to be due to some form of

surface activation by the decomposition of the $NCSe^-$ ion on the surface of the electrode.

2.5 Aim of the present study

Previous in situ IR studies of the electrochemistry of metal electrodes polarised in the presence of pseudohalide ions have been done for a number of systems but mostly they have involved species adsorbed on the electrode surface in aqueous electrolytes. Less emphasis had been placed on infrared studies of solution species being formed in the thin layer. Non-aqueous electrolytes with pseudohalides have also not been studied to any great extent by in situ IR spectroscopic techniques judging from previous literature [49-52]. This study will concentrate on the anodic polarisation of various metals Ni, Cu, and Au in DMSO and DMF using in situ IR spectroscopy and electrochemical techniques such as cyclic voltammetry, U.V./Vis. Spectroscopy, XAS and electrospray ionization mass spectroscopy to probe differences in 1) electrochemical behaviour 2) speciation of products resulting in solution based products from anodisation of the electrode in the non-aqueous solvent in the presence of various pseudohalide ions. The aims of each chapter are described as below.

Chapter 3 focuses on the use of SNIFTIRS for studying the anodic polarization of nickel electrodes in DMSO or DMF solutions of pseudohalide (NCO^-, NCS^-, $NCSe^-$) ions using tetrabutylammonium perchlorate as the supporting electrolyte. Conventional transmission IR and U.V./Vis. Spectrophotometry are also used for study of model solutions that serve to independently confirm the identity of species detected as a result of electrochemical processes. These techniques have also been used in the analysis of the cell solution at the conclusion of an in situ IR experiment.

Further this research will not only investigate in situ IR spectroelectrochemical behaviour but also study the electrochemistry of systems that have not previously been investigated because in earlier literature, there is little to no electrochemical data available on some metal/pseudohalide systems in pure DMF or DMSO. In chapter 4, novel techniques for probing electrogenerated products will be investigated such as the use of EXAFS/XANES which can be used to probe the coordination geometry of electrochemically generated products directly without

the need for their isolation which may be impossible. Hence the aim was to apply X-ray absorption near edge spectroscopy (XANES) and extended X-ray absorption fine structure (EXAFS) to these systems to obtain information on the complex ion species present in 1) solutions electrogenerated via the anodic dissolution of Ni in pseudohalide containing DMSO solutions and 2) the model solutions prepared to mimic these electrogenerated species.

The aim of chapter 5 is to better understand the anodic polarization behaviour and speciation of copper electrodes in non-aqueous, polar aprotic solvents, DMSO or DMF-containing solutions of pseudohalide ions (NCO^-, NCS^- and $NCSe^-$) through investigation of electrogenerated products in solution. This is achieved by using a similar suite of techniques as has been used in the in situ IR spectroelectrochemical studies of the Ni electrodes anodically polarized in pseudohalide-containing DMSO or DMF electrolytes covered in chapter 3. In addition, highly useful information has been provided by the use of synchrotron-based techniques such as X-ray absorption near edge spectroscopy (XANES) of the cell solutions containing electrogenerated products and the model solutions prepared that mimic these species independently of the electrolysis process undertaken when conducting the in situ IR investigations.

The aim of chapter 6 is to better understand the anodic polarization behaviour and speciation of gold electrodes in the non-aqueous, polar aprotic solvents, DMSO or DMF which contain pseudohalide ions such as NCO^-, NCS^- and $NCSe^-$. The approach is to use the one followed in previous work through investigation of electrogenerated products in solution as a function of potential using the in situ IR techniques and a thin-layer spectroelectrochemical cell used in the work in earlier chapter. To aid in and confirm assignments made for molecular species generated in the electrochemical studies, model solutions were made using Au(III) salts with added pseudohalide ions to synthesise the electrogenerated species independently of the electrochemical cell to prove their existence. These model solutions were characterized by FTIR transmission spectroscopy and Electrospray Ionisation Mass Spectrometry (ESI-MS) to confirm the presence of such species and to characterize other by-products formed in the model solutions. Some further work was done to generate and to confirm the identity of some Au(I) complexes

detected in electrochemical studies through some fortuitous redox chemistry between Au(III) and NCS^-, $NCSe^-$ ions.

In addition, the work will include in chapter 7, IR spectroelectrochemical studies of metal electrodes polarised in the presence of the unstable tellurocyanate ion for which no in situ IR data exists presently in the chemical literature. The aim of this study was thus, to investigate for the first time via IR spectroelectrochemistry the electrochemical behaviour of the $TeCN^-$ ion on several anodically polarised electrodes, namely Ni, Cu and Au and to understand better what kind of species are produced and to make comparisons with some earlier studied systems involving other pseudohalide systems as well as computational studies where the vibrational frequencies of hypothetical M-TeCN complexes (M=Ni,Cu and Au) are calculated. This study conveniently used the fact that free $TeCN^-$ ion can be prepared [41, 53, 54] and is stable in dry DMSO and DMF solutions.

Chapter 3

Anodically polarized nickel electrodes in DMF or DMSO solutions of pseudohalide ions

3.1 Introduction

Subtractively normalised interfacial Fourier transform infrared spectroscopy (SNIFTIRS) has afforded valuable information on the species formed at an electrode/electrolyte interface when anodic dissolution of an electrode occurs. Previous work has also led to detection of electrosorbed species using special configurations [55]. However much useful information can still be obtained by monitoring solution species generated in the thin layer between the working electrode and the IR window using a simple thin layer electrochemical cell. Using this approach, several systems have been studied in past work [36, 37] involving anodic dissolution of nickel in aqueous, cyanide and pseudohalide-containing electrolytes. Electrolytes containing -C≡N groups allow easy detection by IR spectroscopy because the ν(C≡N) stretch occurs in the 2500-1800 cm^{-1} area of the IR spectrum where few other fundamental IR vibrations are detected.

Mucalo et al. [36] studied corrosion of Ni electrodes in aqueous KCN and detected $[Ni(CN)_4]^{2-}$ (2124 cm^{-1}), NCO^- (2168 cm^{-1}) and other species. Cyanide ion was observed to oxidise to NCO^- ion and then to CO_2 at anodic potentials. Interfacial pH changes in the thin layer during the SNIFTIRS experiment were indicated by detection of species such as HCN and HNCO (2256 cm^{-1}). Mucalo and Li [37] studied the anodic dissolution of nickel electrodes in aqueous pseudohalide-containing electrolytes and reported the formation of Ni(II) pseudohalide complex ions, i.e. Ni(II) complexes involving NCO^-, NCS^- and $NCSe^-$ ions which gave peaks at 2225 cm^{-1}, 2121 cm^{-1} and 2123 cm^{-1} respectively. Dissolved CO_2 (2343 cm^{-1}) was also detected and attributed to electro-oxidation of the cyanate ions at the electrode surface.

Spectroelectrochemical studies of pseudohalide electrolytes and their interaction with nickel electrodes are rare, although several in situ spectroelectrochemical Raman and IR studies have been reported [45, 50].

IR spectroelectrochemical or electrochemical only studies of nickel electrodes anodically polarised in pseudohalide ion-containing *non-aqueous* solvent media such as dimethyl formamide (DMF) or dimethyl sulfoxide (DMSO), have not been previously reported in the literature. Instead, studies of Ni electrodes in mixed electrolytes of DMSO, DMF and aqueous acids exist. Delgado et al. [56] report that nickel electrodes in DMSO/HCl electrolytes exhibit distinct dissolution and passivation regions with passivation films consisting of an insoluble Ni(II) salt such as when ClO_4^- ion is present forming $Ni(DMSO)_6(ClO4)_2$. They comment that this is preceded by an irreversible active dissolution process where Ni(II)-DMSO complex ions form. Bellucci et. al. [57] studied the passivation of nickel electrodes in 0.1 mol L^{-1} aqueous H_2SO_4 and acetonitrile and DMF solutions and found that water content strongly affected the passivation process because the NiO/ $NiSO_4$ film was of poor protective character. Abrashkina et al. [58] studied the anodic behaviour of Ni electrodes in acidic perchlorate solutions of DMSO showing that anodic dissolution rate for Ni was much lower in DMSO than in water or DMF solvents. This was due to the strong adsorption of DMSO to the nickel surface. It was also shown that addition of surface activators like Cl^- and water molecules can substantially increase the rate of dissolution of nickel to the point of electrode pitting. Passivation by strong adsorption of DMSO to Ni was envisioned to occur via interaction of Ni with the oxygen atom on DMSO causing substantial loss of the double bond character of the S=O group. In contrast, for DMF or acetonitrile (AN), interaction with Ni occurs via the N-atom and no passivation occurs. Ercolano et al [59] state that properties of organic solvents like dielectric constant, dipole moment and values of acid dissociation constants (if ionisable species are present like SO_4^{2-}) strongly influence electrochemical and corrosion behaviour of metals in non-aqueous organic solvents. Banas et al [60] investigated the corrosion and passivity of nickel in pure (non-aqueous) methanol solutions of electrolytes due to the application of alcohols to chemical engineering-related areas such as oxide nanoparticle synthesis, use as fuels and others. In methanol, Ni passivates via direct interaction with the oxygen in the methanol solvent to form a nickel(I) methoxide species which then loses a further electron to form a Ni(II) methoxide species.

IR spectroelectrochemical studies on nickel/pseudohalide systems and their speciation in DMF or DMSO solvents are of interest for understanding the electrochemistry of non-aqueous electrolyte systems used in different technical areas such as in the chemical and fibre industries [59, 61]. Other systems where Ni electrochemistry has been studied in DMSO is in the formation of Ni-Au interfaces for catalyst or nanodevice development where the avoidance of hydrogen evolution during Ni deposition is desirable [62]. In studying the interaction of nickel with pseudohalide solutions in DMF and DMSO, there is also growing interest as reported by Vecchio-Sadus [63] in seeing whether unusual speciation occurs by study of the direct dissolution of the metal electrodes in various organic (non-aqueous) media. In this sense, the use of pseudohalide ions containing a –CN group makes the use of IR spectroelectrochemistry very convenient due to the fact that the CN stretching mode occurs in a region of the IR spectrum which is relatively unpopulated by other intense fundamental stretching vibrations. In addition there is also a rich literature of inorganic chemistry reports on discrete metal complexes containing pseudohalides where IR data has normally been obtained. Previous literature existing on the inorganic solution chemistry, spectroscopy and thermodynamics of the interaction of nickel ions and other transition metals with pseudohalide ions in DMF and DMSO solvents [64, 65] assists such studies.

The aim of this work is, therefore, to study using SNIFTIRS the anodic polarization of nickel electrodes in DMSO or DMF solutions of pseudohalide (NCO^-, NCS^-, $NCSe^-$) ions using tetrabutylammonium perchlorate as the supporting electrolyte. Conventional transmission IR and U.V./Vis. Spectrophotometry are also used for study of model solutions that serve to confirm the identity of species detected as a result of electrochemical processes.

3.2 Material and methods

3.2.1 Reagents and Solutions

DMF (Ajax Finechem Pty, analytical (UNIVAR) reagent grade) and DMSO (Scharlau, synthesis grade) solvents were used without further purification for all experimental work. The level of water impurity in the DMSO and DMF was quoted as being 0.1% and 0.15% respectively by Karl Fischer Titration. All

glassware used in experiments was cleaned thoroughly, prior to commencing experiments with double distilled water. Sodium hydroxide (NaOH,>99.5% (Merck), potassium selenocyanate (KSeCN,>97.0%), tetrabutylammonium perchlorate (TBAP, >97.0%) and potassium tetrabromoaurate(III) were supplied by Aldrich Chemical Co, USA. Other salts, i.e. ($Ni(NO_3)_2.2H_2O$,>99%), sodium thiocyanate (NaSCN, >98%) and potassium cyanate (KOCN, >98.0%) were all sourced from BDH chemicals. Apart from the hydrated nickel(II) salts, all were used as received from the manufacturer without further purification or treatment. Prior to their use in preparation of model solutions, the hydrated nickel(II) nitrate salt was partially dehydrated in an oven (50 °C) for 3-5 hours. This led to the originally blue salt turning a green colour after heating. Not all water was removed as confirmed by spectroscopic analysis, however this was not believed to affect results obtained to any great extent.

In general, the electrolyte solutions prepared for use in SNIFTIRS experiments (here and in other studies involving different metal electrodes) had a concentration of either 0.025 or 0.05 mol L^{-1} in the pseudohalide salt and 0.1 mol L^{-1} in TBAP, which acted as the supporting electrolyte in the DMF or DMSO solvent.

3.2.2 Spectroelectrochemical cell and electrode design used in this study

The thin layer IR spectroelectrochemical cell used in this study (see Figure 3.1 and Figure 3.2) was modelled on the specialised three electrode cell used by Mucalo et al. [37] in an earlier study. The glass cell was placed on a fixed angle (30°) Spectra Tech FT-30 specular reflectance accessory and made use of a vertically erected working electrode (WE) setup. In this cell, the angle of the IR beam relative to the electrode surface was always thus approximately 30 degrees. In addition the Luggin capillary designed for minimising *IR* drop was more favourably placed relative to the working electrode (see Figure 3.1) compared to the design used and reported in the Mucalo et al.'s study from 2004 [37]. The IR window employed was a circular 32 x 3 mm (Buck Scientific) CaF_2 disc glued to the bottom of the glass cell with silicone glue. When inserted into the spectroelectrochemical cell, the WE rested on the window's surface during IR spectral acquisition as a function of applied potential.

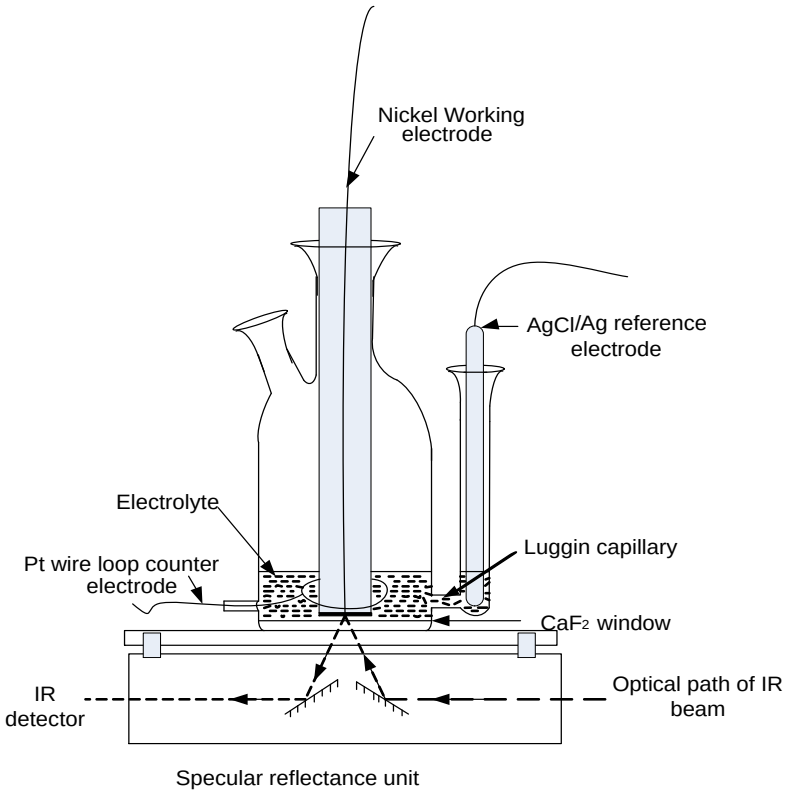

Figure 3.1: Schematic diagram of the three electrode thin-layer IR spectroelectrochemical cell and the 30^0 fixed angle specular reflectance unit with the optical path of the IR beam.

This created a thin layer of electrolyte solution between the electrode and the window, for which changes in species resident in this layer were studied by IR spectroscopy and cyclic voltammetry. The change to the cell configuration used in the 2004 study was made to the Luggin capillary part which was connected through a hole near the bottom side of the glass cell, so that better potential control of the electrode might be possible and also for allowing the solution levels in the arm holding the Radiometer AgCl/Ag "red rod" reference electrode to equilibrate naturally with the solution level in the cell without constant topping up of solution as was required in the case of the old style cell illustrated in reference [37]. The secondary electrode consisted of a circular Pt wire ring through which the WE was placed occupying a central position (see Figure 3.1).

The working electrode consisted of a flat, circular polycrystalline piece of nickel (7 mm diameter, (BDH and Aldrich Chemical, 99.98% purity)) which was embedded into a glass syringe barrel using Araldite epoxy glue and which was mechanically polished with Struers 0.01 μm grade aluminium paste on a chamois polishing cloth and subsequently with a Struers DP-lubricant red solution.

Remaining or excess aluminium polish was removed by rinsing in running water followed by in an ultrasonic bath.

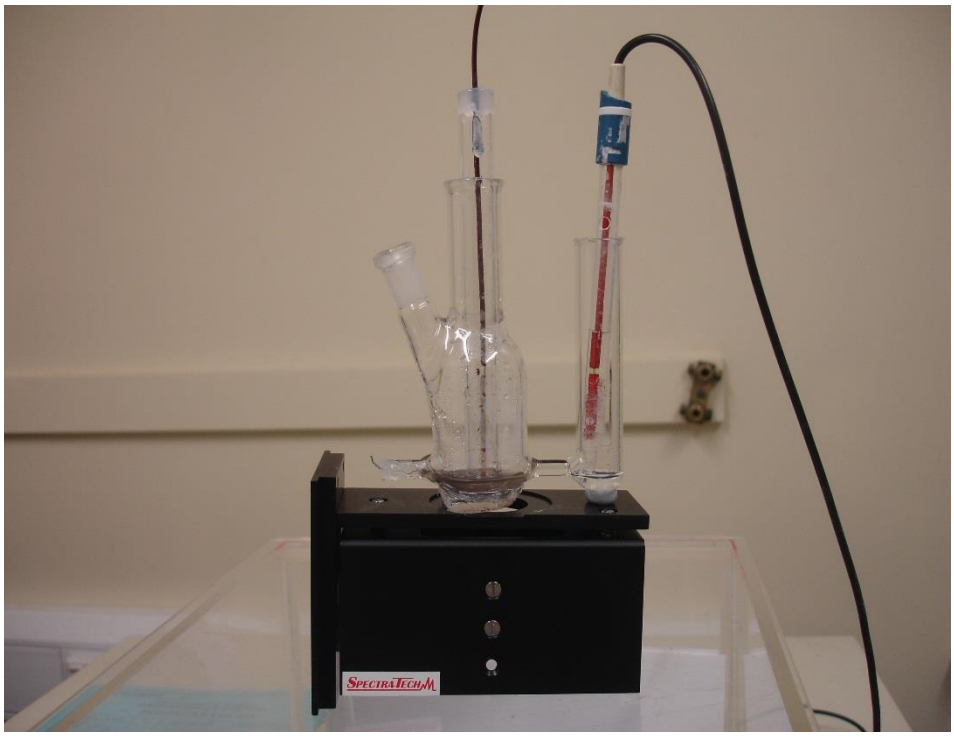

Figure 3.2: Photograph of spectroelectrochemical cell used in this study complete with electrodes and filled with electrolyte and placed atop the SpectraTech FT-30 specular reflectance unit.

3.2.3 The thin- layer cell

The thickness of the thin layer in front of the electrode in the cell was ultimately determined through obtaining the Beer's law plot of five accurately known concentrations (see Figure 3.3) of potassium ferricyanide (BDH Anala-R grade) between 0.025 mol L^{-1} and 0.4 mol L^{-1} in water via IR absorbance measurements of the $\nu(C\equiv N)$ stretching peak of the $[Fe(CN)_6]^{3-}$ ion peak at 2114 cm^{-1} from solutions held in a Buck Scientific fixed path length cell using two 32 x 3 mm CaF_2 windows and a Teflon 0.015 mm spacer. The extinction coefficient measured from this graph and accounting for solution thickness (0.0015 cm) was subsequently used to determine the thickness of the thin layer in the cell employed in experiments by measuring the intensity of the same five accurately known concentrations of potassium ferricyanide in the thin layer cell set up in the specular reflectance unit and calculating it from the slope of the Beer's Law plot obtained from the earlier exercise. Due to the fact that a double pass of the IR beam is involved in the thin layer cell (i.e. as the IR beam enters the thin layer cell and then emerges again by reflection off the working electrode surface), the

measured absorbances were divided by two before plotting them on the Beer's Law graph of absorbance vs. concentration. This led to a value of 1.31 μm which is in the region of values expected for thin layer cell thicknesses [11].

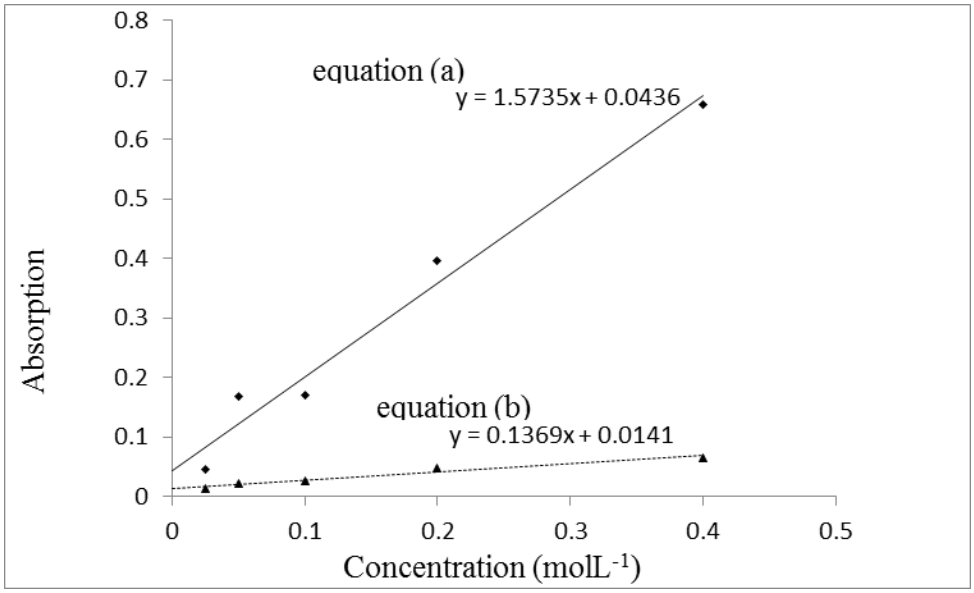

Figure 3.3: Graph illustrating absorption vs concentration of potassium ferricyanide between 0.025 mol L^{-1} and 0.4 mol L^{-1} in water. The equation (a), represents the fixed path length (0.0015 cm) between two CaF_2 window cell and equation (b) gives thin layer b2 between electrode and CaF_2 window.

According to Beer's law, absorbance (A) can be represented by

$$A = \varepsilon bc \tag{3-1}$$

where ε is molar absorptivity, b is the distance travelled through the solution by radiation (or solution thickness) and c is concentration of the solution.

If the thickness between two CaF_2 window cells is represented by b_1, and b_1 =0.0015 cm, ε can be determined using $\varepsilon = \frac{slope}{b_1}$

Therefore, according to equation (a) on the graph in Figure 3.3,

$\varepsilon = \frac{1.5735}{0.0015} = 1049$ L $mol^{-1}cm^{-1}$

Following on, equation (b) on the same graph is used to calculate the unknown solution thickness as $b_2 = \frac{0.1369}{1049} = 0.0001305\ cm$ =1.305 μm

(b_2 is thin layer between electrode and CaF_2 window)

In addition, some experiments were conducted to investigate the difference in the CV obtained when a thin layer of electrolyte was maintained between the electrode and the IR window and when a thicker layer was maintained. The thicker layer was created by lifting the Ni working electrode to a distance of 1 cm above the IR window and fixing in place before acquisition of the CV. (see Figure 3.4)

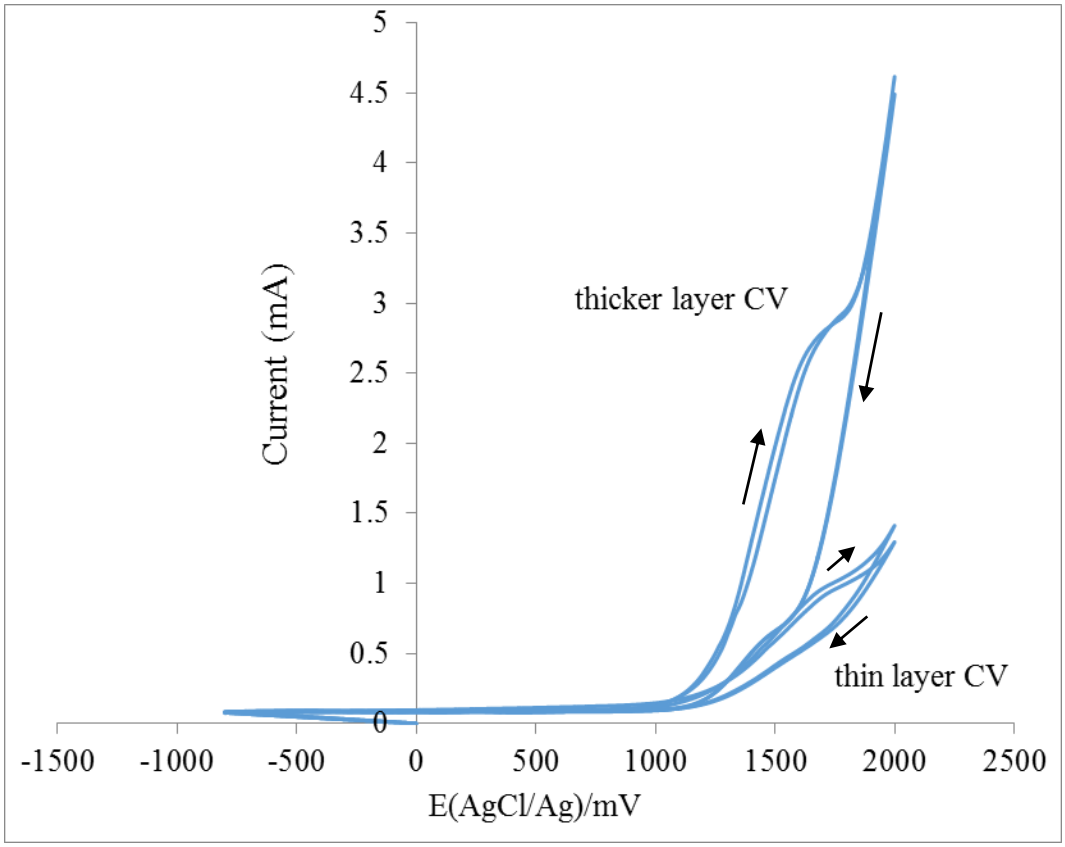

Figure 3.4: Cyclic voltammograms (2 sweeps) of the nickel electrode in DMF solvents containing 0.025 mol L^{-1} KOCN ions and 0.1 mol L^{-1} TBAP (sweep rate = 20 mV/s): The same concentration electrolyte solution and same electrode was used for the thicker layer and thinner layer CVs.

The CV of the thin-layer or thicker layer cell solutions are very similar. In the passivation region between -800 mV(AgCl/Ag) to 1200 mV(AgCl/Ag) the current monotonically increases after 1200 mV(AgCl/Ag) in both systems. Figure 3.4 shows the difference in current of the thicker layer and thin layer cell when a potential is applied between 1200 mV (AgCl/Ag) to 2000 mV (AgCl/Ag). This is because of the greater availability of solution in the thicker layer and lesser availability in the thin layer cell. However, the features were similar in both CVs of the thicker layer and thin layer cell which was evidence of the same electrochemistry happening in both systems.

3.2.4 Equipment for recording CV's, IR spectra and U.V./Vis. spectra

All cyclic voltammetry was carried out using a computer controlled potentiostat system supplied by EDAQ Pty Australia. This consisted of a potentiostat box and a 4-channel unit connected to the three electrode cell which was controlled by *Echem* computer software. The instrumentation was capable of variation voltages between -2000 mV and 2000 mV with respect to the AgCl/Ag reference electrode. In studying a typical electrochemical system, a preliminary voltammetric characterisation was carried out by recording a one sweep cycle from -800 mV to 2000 mV (AgCl/Ag) to generate a cyclic voltammogram.

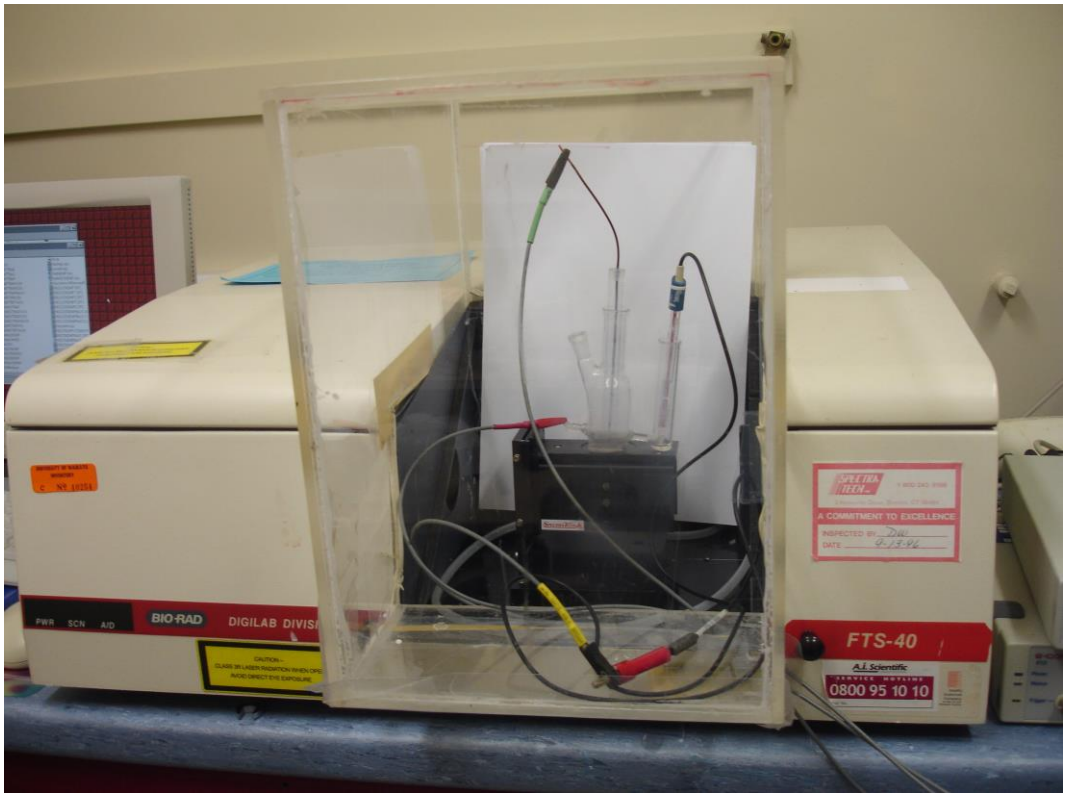

Figure 3.5: Photograph of Biorad FTS-40 FTIR spectrometer used in this study complete with electrodes and filled with electrolyte on the Spectra Tech FT-30 specular reflectance unit.

All SNIFTIRS spectra acquired off the polished metal nickel electrode was obtained using a Biorad FTS-40 FTIR spectrometer (see Figure 3.5) which was purged with dry nitrogen and which employed a Globar infrared source with detection of signals achieved by use of either a liquid nitrogen-cooled MCT (mercury cadmium telluride) detector or an InSb (indium antimonide) detector. The room temperature operated DTGS (deuterated triglycine sulphate) detector can also be used for acquiring the IR spectra. But, MCT and InSb detectors are

highly sensitive when compared to the DTGS. Further, it is evident from Figure 3.6, that the InSb detector has a high detectivity in the 2500-2000 cm^{-1} frequency range and also illustrates that the MCT detector has high detectivity in the 2500-1900 cm^{-1} frequency range. In the present study the all SNIFTIRS spectra were acquired by use of InSb detector.

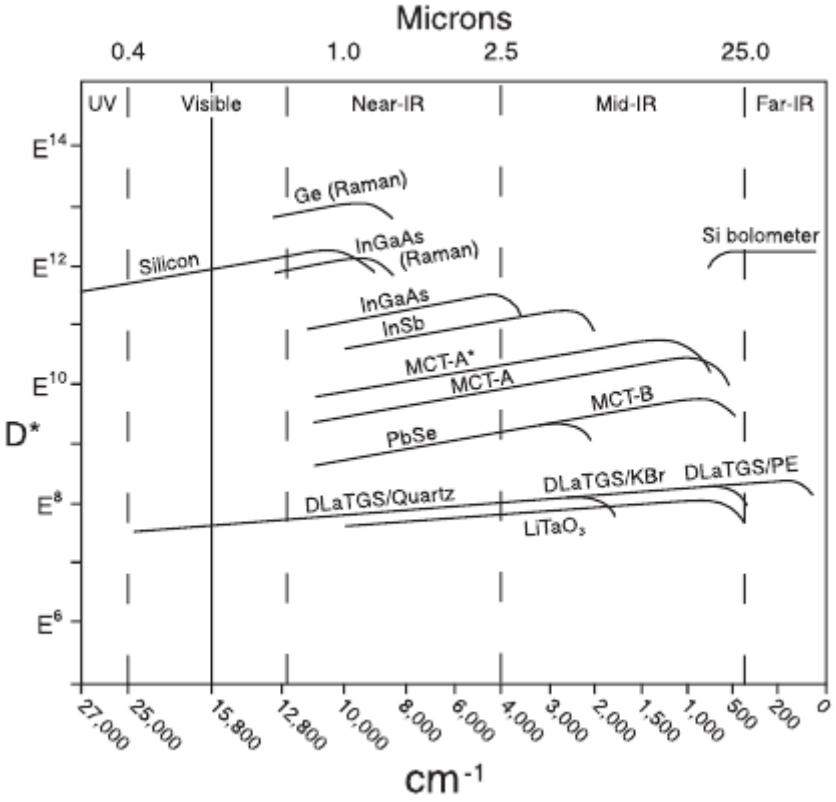

Figure 3.6: Detectivity (D*) versus the spectral range for the detectors represented. D* is proportional to the signal from the detector relative to the energy flux reaching the detector [66].

The usual procedure for acquiring a series of IR spectroelectrochemical spectra was to place the thin-layer spectroelectrochemical cell atop the specular reflectance unit and acquire a background spectrum of the electrochemical cell at a potential where no spectroscopically detectable cathodic or reduction processes were assumed to take place. In the present study the SNIFTIRS spectra were acquired by recording a background spectrum of the thin-layer cell at -900 mV(AgCl/Ag) (depended though the exact value of this potential on the system under study). The potential was then adjusted to more anodic values at the same electrode/electrolyte interface and the IR spectrum thus obtained ratioed against that background spectrum acquired at the more cathodic potential yielding an absorbance spectrum which was essentially that of the thin layer between the electrode and the CaF_2 window at the more anodic potential. Acquisition of

spectra at higher potentials led to a series of spectra that could be analysed in terms of the changes that occurred at the electrode/electrolyte interface as a function of applied potential at electrode. A resolution of 4 cm^{-1} and accumulation of 100 scans were the usual conditions followed. Current-potential data were also collected at the same time as the IR spectra. To do this during each SNIFTIRS run for a given electrode/electrolyte system, an average current calculated from summing the initial current observed at the beginning of an IR spectral acquisition (at a given potential value) and at the end of that same acquisition was collected and later plotted as current-potential plots. This effectively represented "single sweep" voltammograms of the (nickel/ pseudohalide) systems recorded at what would effectively be very slow sweep rates. (as it was recorded over the length of the SNIFTIRS experiment)

All U.V./Vis. spectra of model solutions (see below) and solutions from the electrochemical cell after SNIFTIRS experiments were acquired using a double beam Cary 1E UV-VIS spectrophotometer with a combined Tungsten and Hydrogen-Deuterium source. Scanning conditions used a data interval of 1 nm and a scanning rate of 600 nm/min. All samples were placed in 1 cm pathlength quartz cuvettes and spectra acquired over the 800 nm-200 nm range. The reference (blank) solvent used in all cases was DMF or DMSO depending on the samples being analysed. Baseline correction was not used as this technique was being used to provide qualitative assessments of the electrochemically generated species that were present in the cell solutions after electrochemical polarisation or spectrum present in model solution (see below) rather than quantification.

3.2.5 Sample preparation for model solution

Model solutions were made from mixing of partially dehydrated $Ni(NO_3)_2$ and pseudohalide salts in various $Ni(NO_3)_2$:pseudohalide salt mole ratios (from 1:1 to 1:8 depending on the combination of $Ni(NO_3)_2$, and pseudohalide salts and solvent used DMF or DMSO) to verify species detected in electrochemical experiments.

As for IR spectra of model solutions that were prepared to seek experimental confirmation of species generated in the electrochemical experiments, these were

recorded in conventional IR transmission mode (using a Spectra Tech Press-Lok^{TM} cell with 32x3 mm CaF_2 windows) on a Perkin Elmer Spotlight 200 FTIR instrument with a Spectrum 400 optical bench. Sample preparation consisted of placing a small drop of liquid between two CaF_2 windows in the Press-Lok^{TM} cell and creating a thin layer by the bringing together of the two windows. Detection of these IR transmission spectra (presented in absorbance mode) were carried out using a conventional DTGS room temperature detector with air being used as the background spectrum for ratioing.

3.3 Results and discussion

3.3.1 Anodically polarised nickel electrodes in DMF solutions of Pseudohalide ions

The first experiments investigating the dissolution of a nickel electrode in the polar aprotic solvent, DMF, involved initially the use of tetrabutylammonium bromide (TBAB) as an electrolyte. However this was later changed to terabutylammonium perchlorate (TBAP) because perchlorate ion was considered to be non-coordinating and it was desired to see what kinds of dissolution species involving pseudohalide ion would be produced without the complications of a potential strongly coordinating ligand present, i.e. the Br^- ion. In general, however, it was found that the CV and spectra obtained for when either TBAB or TBAP were used as supporting electrolytes were very similar but for consistently all the results to be discussed for the dissolution of nickel in pseudohalide-containing solutions (and other electrode system) will be for systems using TBAP as a supporting electrolyte.

In these studies a cyclic voltammogram (CV) was typically measured first of the various systems studied and following that, a series of IR spectroelectrochemical spectra at different values of the applied potential at the working electrode was measured using the thin-layer cell. During the IR experiment, potential-current data were collected also by measuring the current averaged over the values obtained before and after each spectral acquisition at a certain applied voltage. Using these approaches, the behaviour of the nickel electrode in the (separate) presence of the three pseudohalide ions, NCO^-, NCS^- and $NCSe^-$ was probed. Table 3.1 summarises all the data (6 system with DMF and DMSO solvent) for

the Ni systems studied. However, nickel/pseudohalide DMSO systems are discussed later in this chapter (section 3.3.5).

3.3.2 Ni/DMF /TBAP/NCO^- system

Figure 3.7 shows the CV for the nickel electrode in DMF solvent containing 0.025 mol L^{-1} KOCN and 0.1 mol L^{-1} TBAP.

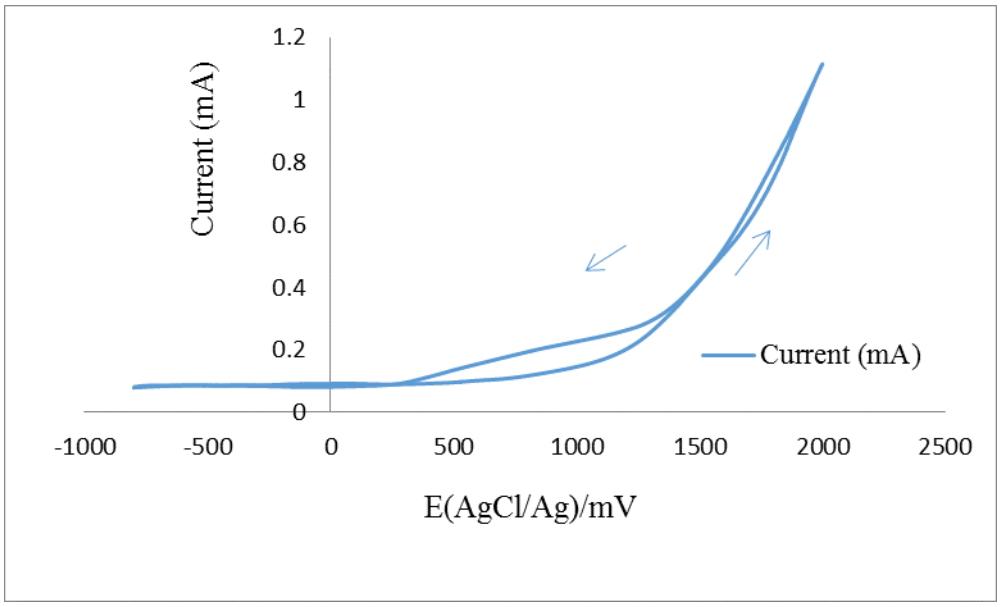

Figure 3.7: Cyclic voltammogram of the nickel electrode in DMF solvent containing 0.025 mol L^{-1} KOCN and 0.1 mol L^{-1} TBAP (sweep rate = 20 mV/s. Arrows show the path actually traced upon conducting the sweep of potentials.

The CV showed a featureless region from -800 mV (AgCl/Ag) to +500 mV (AgCl/Ag) (see arrows in Figure 3.7 which indicate how the curve was generated). After +500 mV, an increase in current was observed which is interpreted as being due to the oxidation of Ni to Ni(II) species. It is obvious that there is significant passivation of the nickel electrode below this voltage value because of the very low currents observed. After +500 mV, the current increases monotonically until the voltage reverses at 1000 mV at which point current decreases back to the baseline value at cathodic potentials.

Table 3.1: FTIR and U.V./Vis. data from in situ IR spectroelectrochemical studies of Ni/NCX^- systems electrochemically polarised in 0.1 mol L^{-1} TBAP in DMSO or DMF solvents

System studied	ν(CN) of free NCX^- ion (X = O, S, Se) cm^{-1}	ν(CN) of Ni^{2+}/NCX^- complex ion cm^{-1}	ν(CN) of CO_2 dissolved in solvent cm^{-1}	U.V./Vis. spectral features (nm)	Colour of cell solution after SNIFTIRS experiment
Ni/DMF/NCO^-	2134	2200, 2250	2337	280s, 430w, 648m, 670m	blue
Ni/DMF/NCS^-	2056	2092	2339	271s, 403w,	light green
Ni/DMF/$NCSe^-$	2064	2094	2337	278s, 397w	yellow green
Ni/DMSO/ NCO^-	2136	2199, 2244	2337	273s,430w , 602m, 650m	blue
Ni/DMSO/ NCS^-	2055	2094	2337	265s, 404w	light green
Ni/DMSO/ $NCSe^-$	2065	2095	2337	275s, 401w	yellow green

s=strong, m=medium, w=weak

No reduction feature is observed in the CV which appears to indicate that the oxidation processes occurring at the Ni WE are irreversible and that the species like Ni(II) complexes generated have been released from the electrode surface into the thin layer but are not amenable to reduction on the backward sweep. This irreversibility is also supported by the obvious hysteresis observed in the reverse CV curve (see Figure 3.7) and the forward and reverse directions. The CV while acting as an electrochemical "fingerprint" characterising, for instance, oxidation and reduction events occurring on the nickel surface, provides no molecular information and hence this is the reason IR spectroelectrochemistry is employed to provide a molecular picture of the detectable changes occurring as a function of applied potential at the electrode/electrolyte interface.

Figure 3.8 represents a series of IR spectroelectrochemical (SNIFTIRS) spectra that were recorded of the Ni/TBAP/NCO^-/DMF system using 0.025 mol L^{-1} KOCN in the presence of 0.1 mol L^{-1} TBAP. Figure 3.9 represents the single-sweep voltammogram that shows the average current at each applied potential in the thin layer cell during the SNIFTIRS experiment. Figure 3.10 represents the plot of the intensity changes of peaks observed in the Ni/TBAP/NCO^-/DMF system as a function of applied potential. They are shown in the same figure to facilitate matching of spectral intensity trends with those appearing in the single sweep voltammogram.

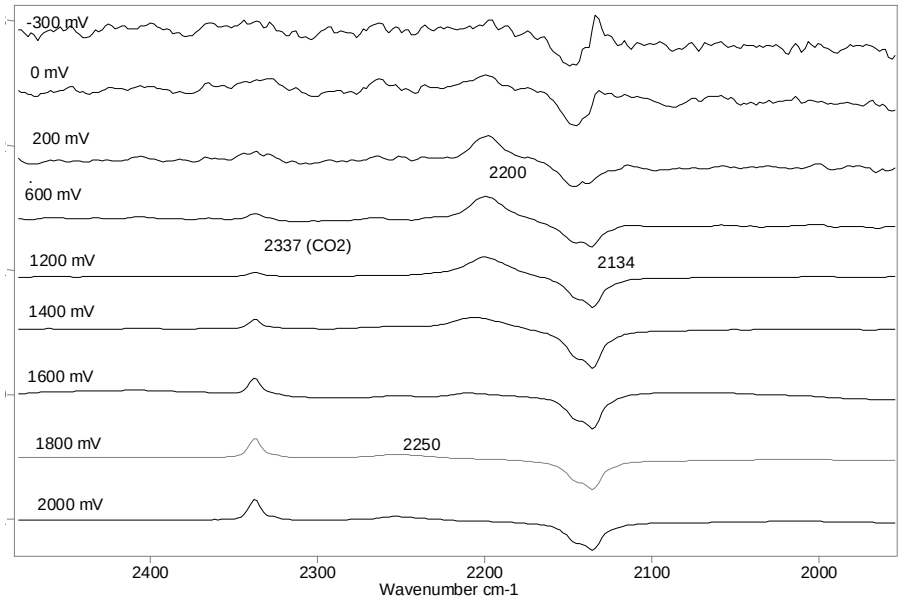

Figure 3.8: Series of SNIFTIRS spectra of the Ni/0.025 mol L^{-1} NCO^-/TBAP/DMF system as a function of applied potential at the nickel WE. The peak absorbance at 2337 cm^{-1} at 1600 mV is 0.14254 and negative peak at 2134 cm^{-1} is -0.23469.

In general the spectra mostly reflect the passive nature of the electrode over the -800 mV to +500 mV (AgCl/Ag) potential region as a largely featureless IR spectral pattern is obtained over this large range of applied potentials. At -300 mV (AgCl/Ag), a negative peak at 2134 cm^{-1} is observed which corresponds to free cyanate ion. At potentials more cathodic to -300 mV(AgCl/Ag) a featureless spectral trace was obtained. The negative-going peak indicates that there is less cyanate ion present at this applied potential relative to the background spectrum recorded at the more cathodic -900 mV (AgCl/Ag). This is indicating consumption of the cyanate ion because this peak would be expected to *increase* in intensity as the electrode is becoming more anodic due to diffusion of this negatively charged ion into the thin layer caused by the electrode becoming increasingly more anodic and hence more positively charged. In fact, when the free cyanate ion peak intensity vs. applied potential was plotted (in a system where tetrabutylammonium bromide was used as the electrolyte) over the -800 mV (AgCl/Ag) to +200 mV (AgCl/Ag) region a gradual increase in intensity *was* observed for the free cyanate ion before the peak became very negative in intensity due to consumption to form nickel-cyanate complexes at the more anodic potentials. Sometimes the spectral behaviour of free pseudohalide ion in these systems was spectroscopically variable because, at times, the peak appeared negative or positive in intensity in this passivation region (-800 mV to +500 mV (AgCl/Ag) prior to the onset of the electrochemically induced anodic dissolution of the nickel electrode. When viewing the spectra in which the free cyanate ion is observed to go negative, it is also apparent that two components develop in the *negative* peak, this additional component being at 2147 cm^{-1}. Because of the proximity of the free cyanate ion peak to the broad 2200 cm^{-1} peak due to the Ni(II) complexes species, it was thought that this may be a ratioing artefact that occurs. Later work in other systems including model solution data indicted this was a natural peaks shape of cyanate ion based in the complexity of its solid state IR signal [67].

In Figure 3.8 changes begin to occur in the IR spectra after ca. +200 mV (AgCl/Ag) which indicates definitively the region where the nickel electrode is undergoing anodic dissolution to Ni(II) species. When this happens, the Ni(II) ions released from the electrode form complex ions with the solvent and the available pseudohalide ion (i.e. NCO^-) in the thin layer. This is manifested in the

spectra by the appearance of a very broad and complex peak centred at *ca.* 2200 cm^{-1} (see Table 3.1). This peak is assigned to a nickel-cyanate-solvent complex ion. When the ion is generated electrochemically the solution turns a distinct blue colour. However the peak observed in the IR is broad meaning there could be several species (consisting of different numbers of solvent and/or NCO^-ligands) contributing to the peak shape. Another possibility could be (as with the peak due to free pseudohalide ion and its spectral variability) that there is some influence of the weak DMF solvent peaks in this region of the spectrum. The exact stoichiometry of the ion is difficult to prove using the methods employed in this work. Pilarczyk et al [64] have done a substantial body of work into the solution and complexation chemistry of Ni(II) (and other metals) with pseudohalide ions in non-aqueous solvents like DMF. In their studies it was shown that the complexation geometry of Ni(II) ions in polar aprotic solvents like DMF is predominantly octahedral, however for this particular system involving Ni(II) ions and cyanate ion, evidence from EXAFS on model solutions (see chapter 4) and on actual electrochemically generated (blue) dissolution solutions has suggested that the coordination for the blue-colour dissolution complex formed could indeed be 5-coordinate which may suggest another scenario in the solution. Given the blue colour of the cell solution at the conclusion of the SNIFTIRS experiment, a U.V./Vis. analysis was acquired of the undiluted cell solution which produced spectral features (see later, Figure 3.19) at 280, 430, 648 and 670 nm. The peaks at 280, 648 and 670 nm are unique to the complex when it forms. Although there are a number of previous U.V./Vis. studies providing data for the Ni-NCS^- complexes formed in DMF or DMSO [64, 65], there are almost no data reported for Ni-NCO^- complexes generated in DMF or DMSO. An older study from Fackler et al. [68] reported that Ni(II) forms *tetrahedral* complexes when bound to cyanate ligands and moreover that an "intense blue colouration" is observed. This is in contrast to the geometry formed when Ni(II) binds to NCS^- in DMF or DMSO where the geometry of the ion (which will be bonded to both solvent and the thiocyanate ion) is recognized as being octahedral [64, 65]. If the dissolution complex being formed in the SNIFTIRS experiment is a tetrahedral complex (if Fackler's early work is acknowledged as being correct) or if it is a 5 coordinate complex, then this behaviour of Ni(II) in DMF is different to what is observed in the SNIFTIRS studies of the Ni/NCS^- and Ni/$NCSe^-$ systems as will be discussed later.

The SNIFTIRS spectra of the Ni/NCO^- systems is provided by the appearance of a weak peak at 2244-2250 cm^{-1} at +1000-1300 mV(AgCl/Ag). Further voltammetric evidence is seen in the single sweep voltammograms of the Ni/NCO^- systems (see Figure 3.7 and Figure 3.9) in DMF where the current is observed to peak which is attributable to solid film formation on the electrode [55]. In addition, Ni electrodes inspected after a SNIFTIRS experiment in Ni/NCO^-/DMF system show visible evidence of a film. The IR peak at 2244-2250 cm^{-1} suggests the surface film may contain nickel oxide and cyanate ion though its nature is unknown. Previous workers [69] studying α-$Ni(OH)_2$ and Ni-Al layer double hydroxides (LDHs) precipitated by urea have assigned peaks of this value to intercalated cyanate ion in nickel hydroxide film in which cyanate ion is O-bonded to Ni rather than N-bonded.

In Figure 3.8, the change in the 2200 cm^{-1} Ni/NCO^- complex ion peak observed in the SNIFTIRS experiment as a function of applied potential indicates the possibility of the electrogenerated dissolution species changing in character over the potential range in question though it is difficult to indicate what these changes are. After *ca*. +1200 mV(AgCl/Ag), there is a shift to *ca.* 2250 cm^{-1}. They could be due to the complex ion undergoing solvent or ligand exchange inside the thin layer due to changes in complex equilibria. These may result from increases in concentration of the nickel ion or changes in concentration of the cyanate ion especially at higher applied potentials where the demand for cyanate ion could be greater so changing the concentration of free cyanate ion available for complexation in the thin layer. This could affect the number of cyanate ligands coordinated to the Ni(II) centre. At very high applied potentials, e.g. from +1200 mV (AgCl/Ag), a small peak at 2337 cm^{-1} begins to appear (see Table 3.1). This is due to dissolved CO_2 in the DMF medium which will be referred to as "$CO_{2(DMF)}$". The origin of this CO_2 could be from three sources. It may come from electro-oxidation of cyanate ion which is either free or bound with nickel or from oxidation of the solvent, DMF, itself or even from the alkyl chains in the TBAP. The presence of CO_2 in spectra may indicate some water presence in the DMF solvent used as well. However it was noted in some spectroelectrochemical experiments where nickel electrodes were polarised in DMF in the presence of

TBAP but in the *absence* of cyanate ion that peaks due to CO_2 at 2337 cm^{-1} were still observed. This would indicate the solvent is becoming electro-oxidised and hence is a source of the CO_2 as well. In the Ni/TBAP/NCO^-/DMF system, it was nevertheless felt that some cyanate or cyanate containing Ni(II) complexes must be involved to some extent in this electro-oxidation process as the nickel(II) complex ion peak at *ca.* 2200 cm^{-1} disappears from IR spectra at very high potentials suggesting the scavenging of cyanate ion by the electrode at the high applied potentials for oxidation to CO_2.

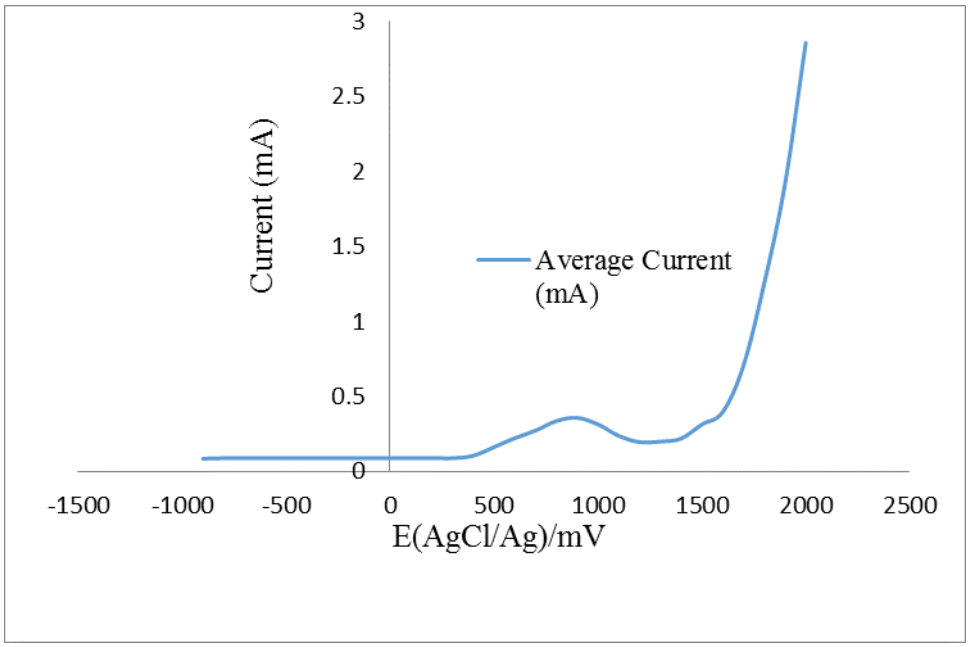

Figure 3.9: Single sweep voltammogram of the Ni/0.025 mol L^{-1} NCO^-/TBAP/DMF electrochemical system constructed from average current data acquired at each applied potential at which SNIFTIRS spectra were acquired

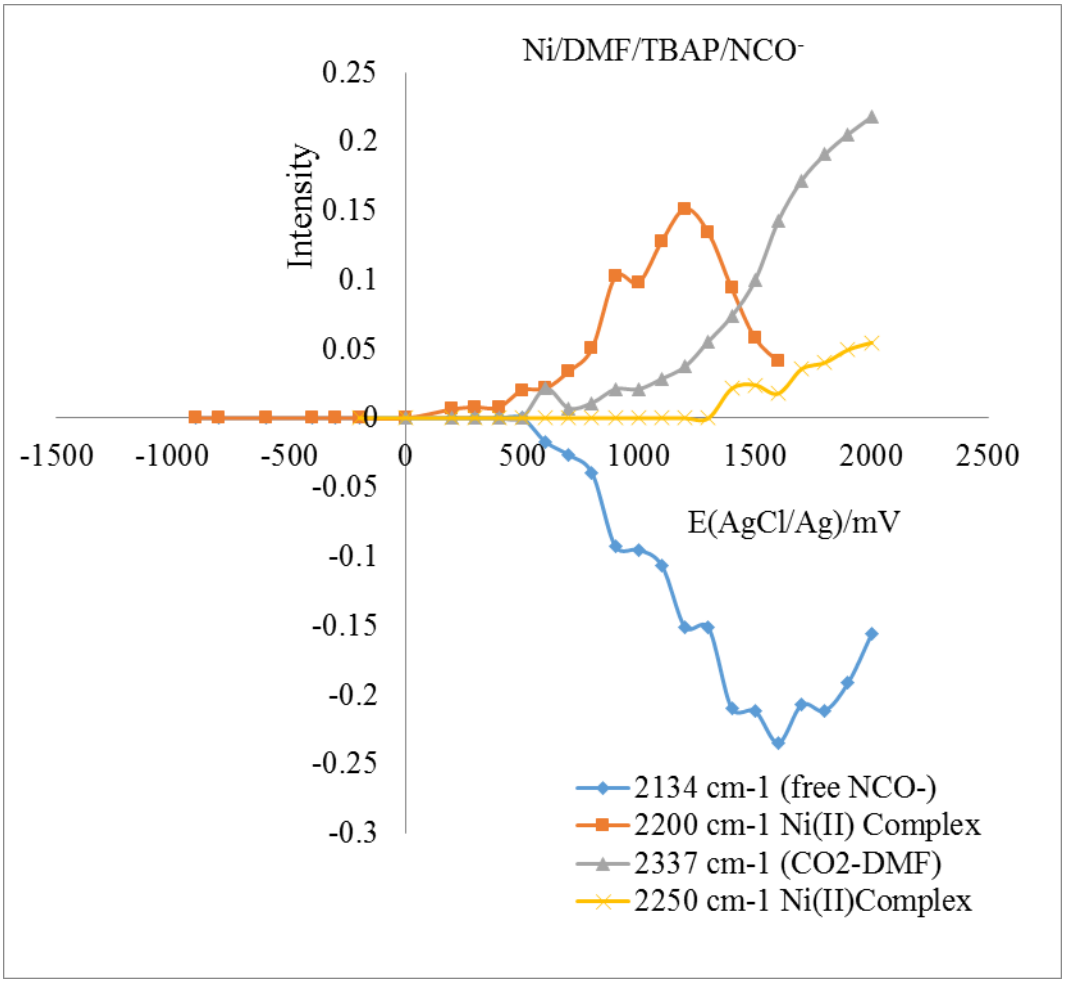

Figure 3.10: Plots of the intensity changes of the various molecular species generated in the thin layer during electrochemical polarisation and observed in the SNIFTIRS spectra as a function of applied potential in the Ni/0.025 mol L^{-1} NCO^-/TBAP/DMF system

Figure 3.9 and Figure 3.10 show how the appearance and disappearance of features observed in the SNIFTIRS spectra correlate with applied potential at the Ni electrode surface. In particular it shows the rise and fall of the Ni(II) dissolution species. The fall in intensity of this species correlates with an increase in the $CO_{2(DMF)}$ intensity. This proves the involvement of the Ni cyanate dissolution species with contributing to the $CO_{2(DMF)}$ signal and is supported by the observation of the large increase in cell current as very anodic potentials are approached as the $CO_{2(DMF)}$ peak beings to appear after +1200 mV (AgCl/Ag). In addition, as the $CO_{2(DMF)}$ forms, bubbles form at the working electrode surface which caused issues in detection due to 'thin layer' turbulence leading to fluctuating in SNIFTIRS spectra (see Figure 3.10).

3.3.3 Ni/DMF /TBAP/NCS^- system

Identical electrochemical and spectroscopic investigations were done by polarizing a nickel electrode in the presence of NCS^- instead of NCO^- and also with $NCSe^-$. The spectroscopic data are summarized in Table 3.1. The solutions tested were mostly identical in composition except higher concentrations of NCS^- and $NCSe^-$ could be used (i.e. 0.05 mol L^{-1}) due to the higher solubility of these pseudohalide ions in the DMF solvent. CVs obtained with the nickel electrode in 0.05 mol L^{-1} KSCN and 0.1 mol L^{-1} TBAP in DMF electrolyte solution are shown in Figure 3.11 shows similar behaviour to the NCO^- system except that the passivation region is a little more extended and there is an increase in current despite the potential being reversed because the electrode has partially exposed fresh metal on its surface due to anodica dissolution. On the forward sweep, the cell current does not increase until *ca.* +600 mV (AgCl/Ag) after which it increases sharply. As the potential reverses back to more cathodic potentials, there is some obvious hysteresis (see arrows which indicate the pathway of the current curve as potential was swept from cathodic to anodic potentials) in the CV which reflects the irreversibility of the electrochemical processes taking place and the phenomena described above with regard to exposed metal surface. This was also observed in the cyanate system discussed above. It is obvious that the increase in current after +600 mV (AgCl/Ag) is due to anodic dissolution processes where the Ni is forming to Ni(II) complex ion species in the solvent.

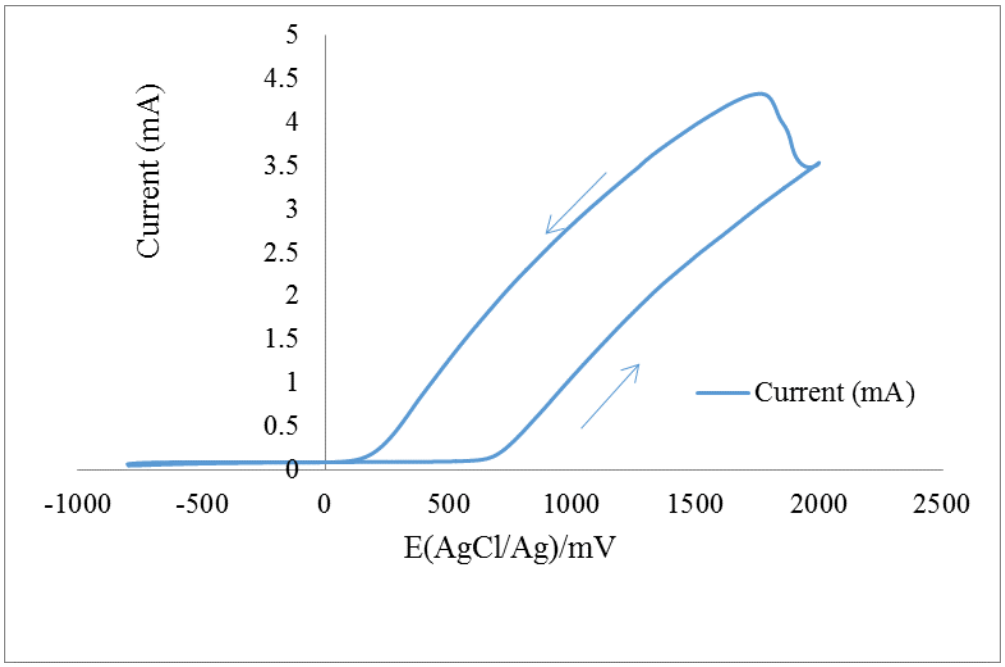

Figure 3.11: Cyclic voltammogram of the nickel electrode in DMF solvent containing 0.05 mol L^{-1} KSCN and 0.1 mol L^{-1} TBAP (sweep rate = 20 mV/s. Arrows show the path actually traced upon conducting the sweep of potentials.

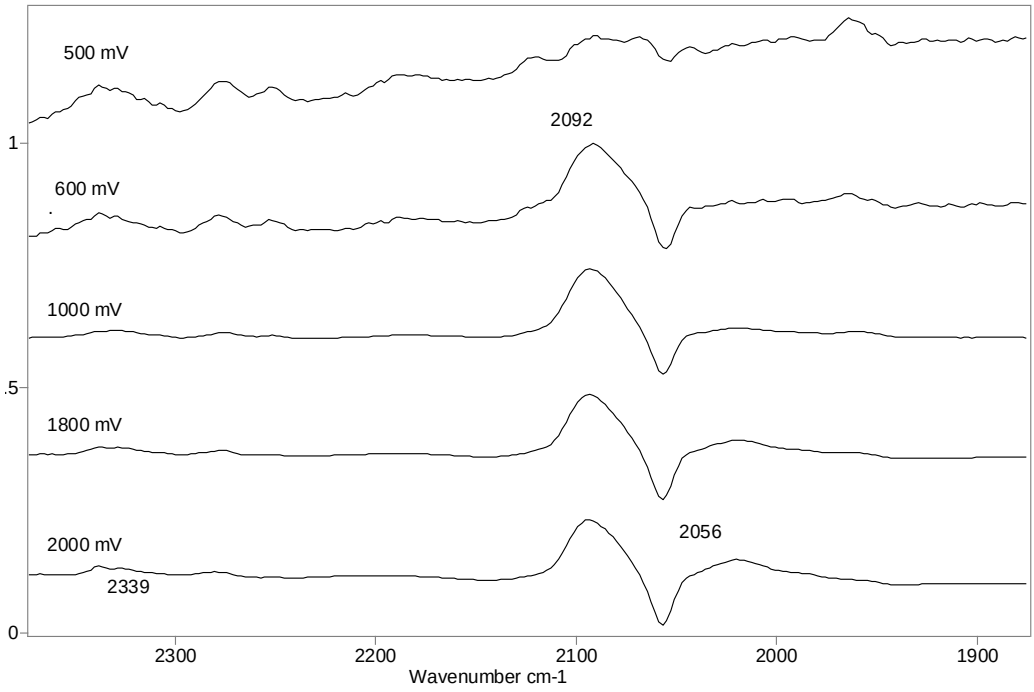

Figure 3.12: Series of SNIFTIRS spectra of the Ni/0.05 mol L^{-1} NCS^-/TBAP/DMF system as a function of applied potential at the nickel WE. The peak absorbance at 2096 cm^{-1} at 1600 mV is 0.13 and negative peak absorbance at 2056 cm^{-1} is -0.092.

Figure 3.12 show the series of SNIFTIRS spectra acquired as a function of applied potential at the nickel electrode surface of the Ni/0.05 mol L^{-1} NCS^-/TBAP/DMF system. At very cathodic applied potentials, the spectra only reveal a peak at 2055 cm^{-1} due to free thiocyanate ion. Other peaks are detected and these are uncompensated minor solvent related (DMF) peaks. The free thiocyanate ion peak remains unchanged in spectra until about +600 mV (AgCl/Ag) after which it starts to appear as a negative-going peak. This would indicate consumption of the thiocyanate ion due to its involvement in Ni(II) complex ions formed by dissolution. As reflected in the CV, +600 mV (AgCl/Ag) corresponds to the onset of anodic dissolution of the Ni to Ni(II) species. The trend is similarly reflected in the single sweep voltammogram (Figure 3.13) and in the trends observed in graphs of the intensity of observed species as a function of applied potential (Figure 3.14). As the electrode anodically dissolves, a broad peak at 2092 cm^{-1} appears in IR spectra which can be definitively assigned to a

Ni/NCS^-/DMF complex. When this complex is formed in sufficient amounts in the thin layer solution by anodic dissolution, the cell solution is noticed to go a distinct yellow-green colour. The peak remains relatively unchanged in position and in shape throughout other spectra acquired at more anodic potentials.

At +1800 mV (AgCl/Ag), a very weak peak due to $CO_{2(DMF)}$ is observed. However, the lack of appearance of $CO_{2(DMF)}$ in this system compared to the Ni/NCO^- system discussed above suggests some support for the idea that the cyanate ion in the electrolyte medium was the source of the more intense $CO_{2(DMF)}$ peaks observed in that system. Overall the spectral and electrochemical behaviour in this system is largely similar to that of the Ni/NCO^- system in that anodic dissolution does not set in until moderately anodic potentials are applied to the electrode.

U.V./Vis spectral data recorded of the cell solutions after the SNIFTIRS experiment are also summarised in Table 3.1 for the Ni/NCS^- system.

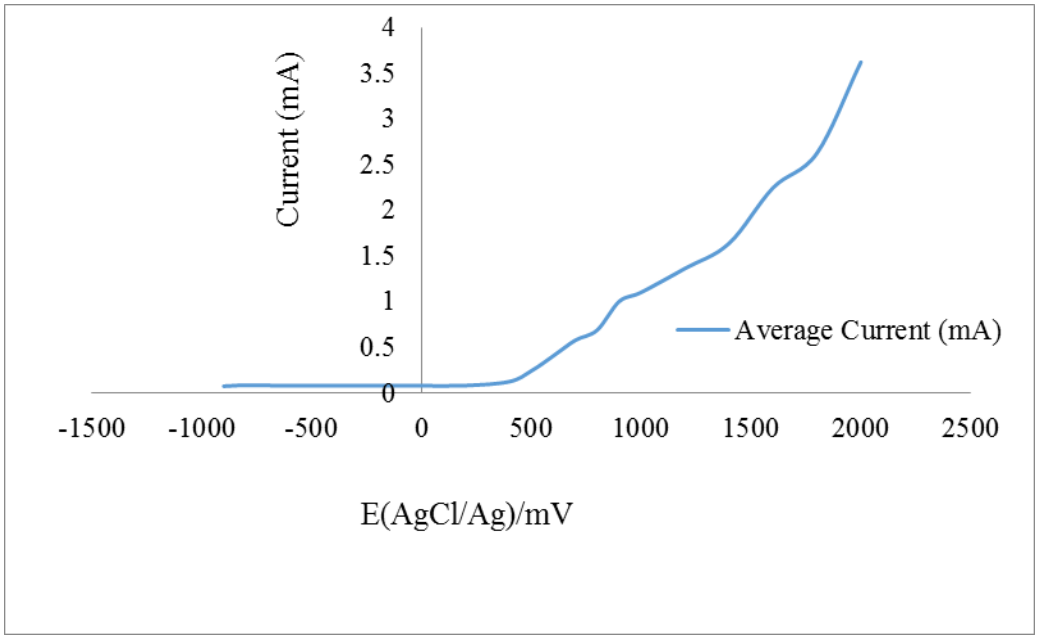

Figure 3.13: Single sweep voltammogram of the Ni/0.05 mol L^{-1} NCS^-/TBAP/DMF electrochemical system constructed from average current data acquired at each applied potential at which SNIFTIRS spectra were acquired.

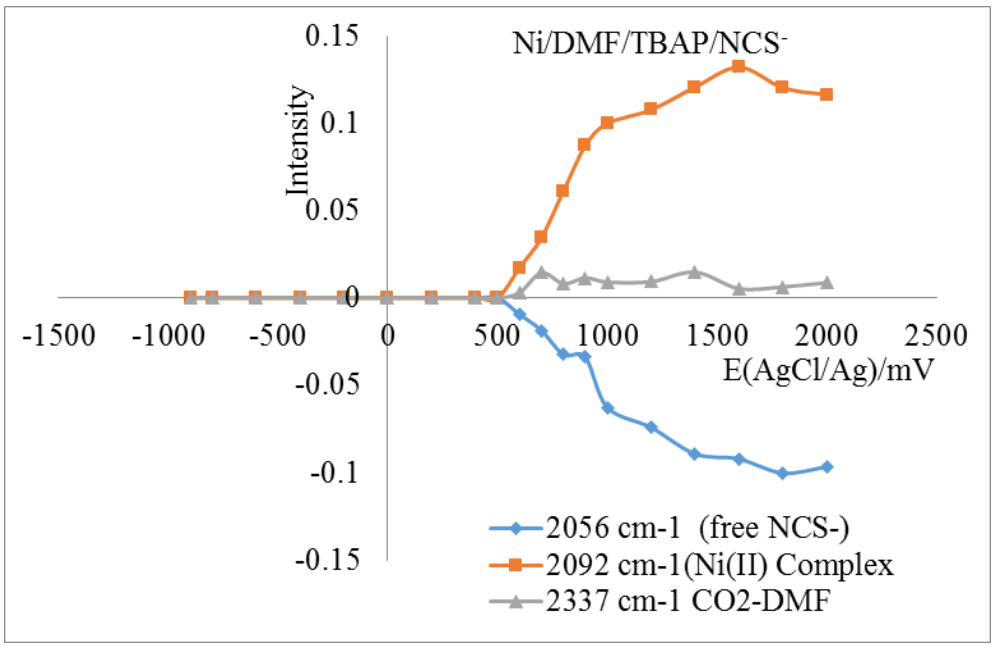

Figure 3.14: Plots of the intensity changes of the various molecular species generated in the thin layer during electrochemical polarisation and observed in the SNIFTIRS spectra as a function of applied potential in the Ni/0.05 mol L^{-1} NCS^-/TBAP/DMF system.

3.3.4 Ni/DMF /TBAP/$NCSe^-$ system

Figure 3.15, Figure 3.16, Figure 3.17 and Figure 3.18 represent all the electrochemical and spectral data for the nickel electrode in DMF solvent containing 0.05 mol L^{-1} KSeCN and 0.1 mol L^{-1} TBAP. Table 3.1 summarises spectroscopic and U.V./Vis data obtained from the SNIFTIRS study with U.V./Vis data being obtained of the cell solution after the SNIFITRS experiment. As with the previously discussed electrochemically polarised systems in KOCN and NaSCN, the behaviour when the nickel electrode is polarised in the KSeCN-containing DMF solutions is very similar to the system where NCS^- ion is present. As applied potential is shifted to more anodic values from a base potential of -900 mV(AgCl/Ag), low to zero current is observed until the electrode enters its anodic dissolution region which is in the +500-600 mV (AgCl/Ag) region as was typically observed in the last two systems discussed. The CV (Figure 3.15) is slightly different in appearance from the single sweep voltammogram of the same system acquired during the SNIFTIRS experiment (Figure 3.16) in that there is a small amount of current flow occurring after *ca.* +200 mV (AgCl/Ag). However the single sweep voltammogram is very similar to those observed in the Ni/NCO^- and Ni/NCS^- systems. In the SNIFTIRS spectra series, (see Figure 3.16) the Ni(II) dissolution species is manifested by a peak appearing at 2094 cm^{-1} which appears

at more anodic potentials (compared to where the equivalent Ni(II) species appears in the Ni/NCO^- and Ni/NCS^- systems) and remains unchanged in shape in the rest of the IR spectra acquired at more anodic potentials. In common with the Ni/NCS^- system, when the anodic dissolution of Ni occurs in solutions containing $NCSe^-$ ion, the cell solution turns a yellow-green colour. In agreement with the spectral behaviour of the free pseudohalide ion in the other two systems discussed, the peak due to free selenocyanate ion (2064 cm^{-1}) becomes negative-going in intensity as the electrode is moved more into the anodic dissolution region by the application of more positive potentials. Prior to the potential of +800 mV (AgCl/Ag) at which the Ni(II) complex ion species at 2094 cm^{-1} appears, there is little evidence for "positive-going" free selenocyanate ion peaks in the spectra. As with the Ni/NCS^- system, $CO_{2(DMF)}$ features as a relatively minor species in the Ni/DMF/$NCSe^-$ system.

U.V. /Vis spectral data for the Ni/DMF/$NCSe^-$ system are similar to that of the Ni/DMF/NCS^- system discussed previously (see Table 3.1). Hence it is assumed based on the interpretations offered by Pilarcyzk [64] that the geometry of the Ni/$NCSe^-$/DMF complex ion formed is octahedral as found with the complex ion generated in the Ni/DMF/NCS^- system.

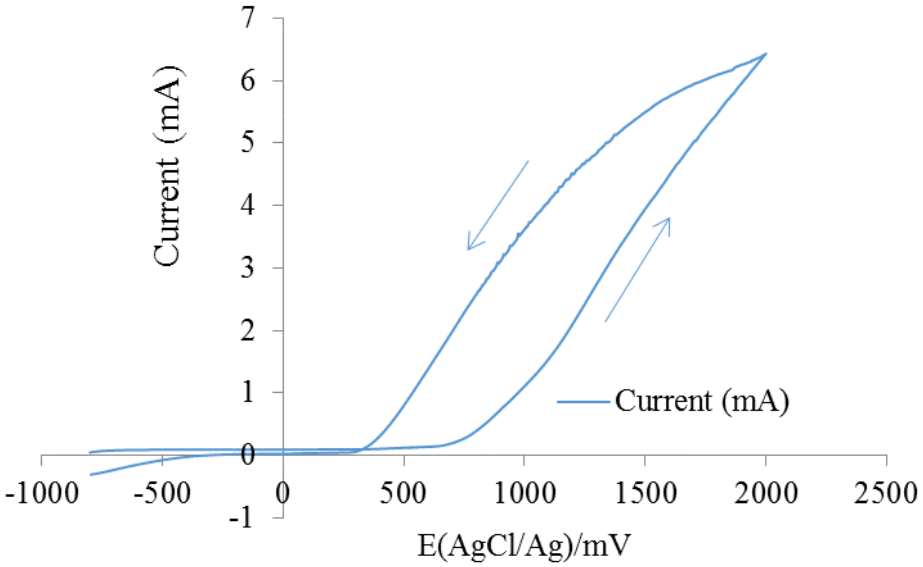

Figure 3.15: Cyclic voltammogram of the nickel electrode in DMF solvent containing 0.05 mol L^{-1} KSeCN and 0.1 mol L^{-1} TBAP (sweep rate = 20 mV/s). Arrows show the path actually traced upon conducting the sweep of potentials.

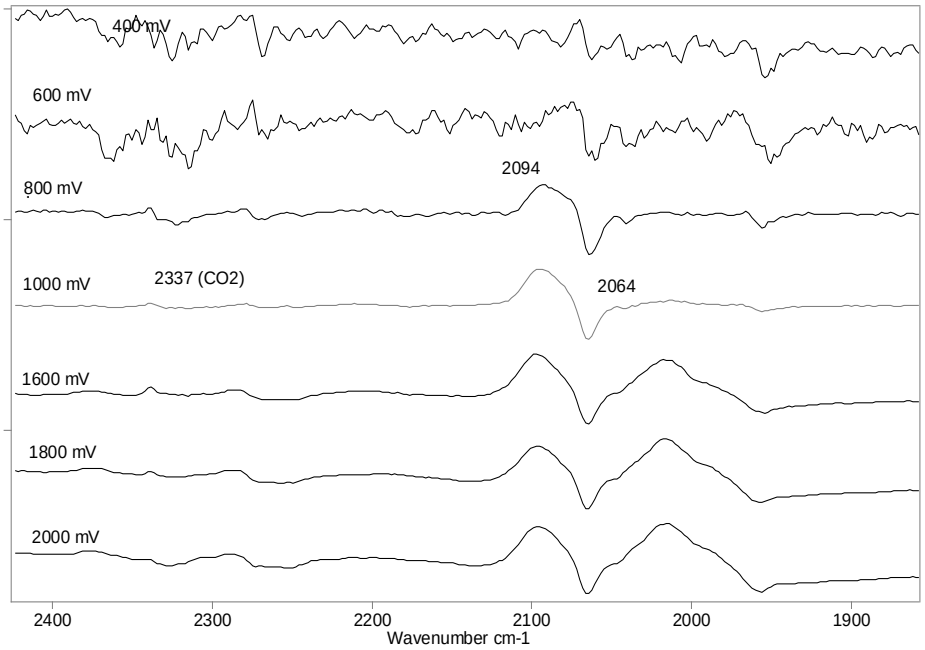

Figure 3.16: Series of SNIFTIRS spectra of the Ni/0.05 mol L^{-1} $NCSe^-$/TBAP/DMF system as a function of applied potential at the nickel WE. The peak height at 2094 cm^{-1} at 1600 mV is 0.43345 and negative peak at 2064 cm^{-1} is -0.23200.

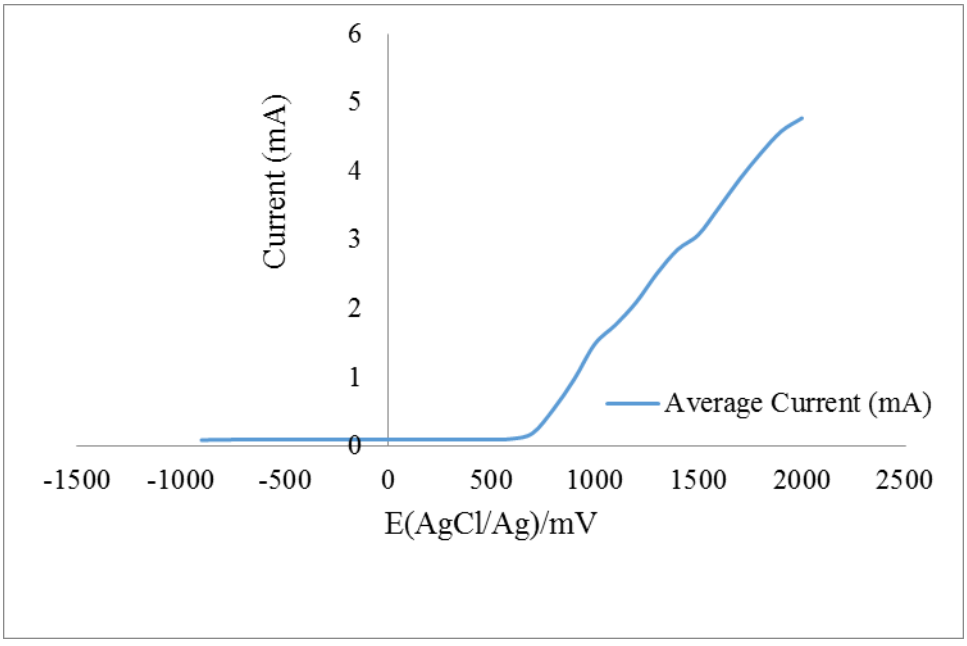

Figure 3.17: Single sweep voltammogram of the Ni/0.05 mol L^{-1} $NCSe^-$/TBAP/DMF electrochemical system constructed from average current data acquired at each applied potential at which SNIFTIRS spectra were acquired.

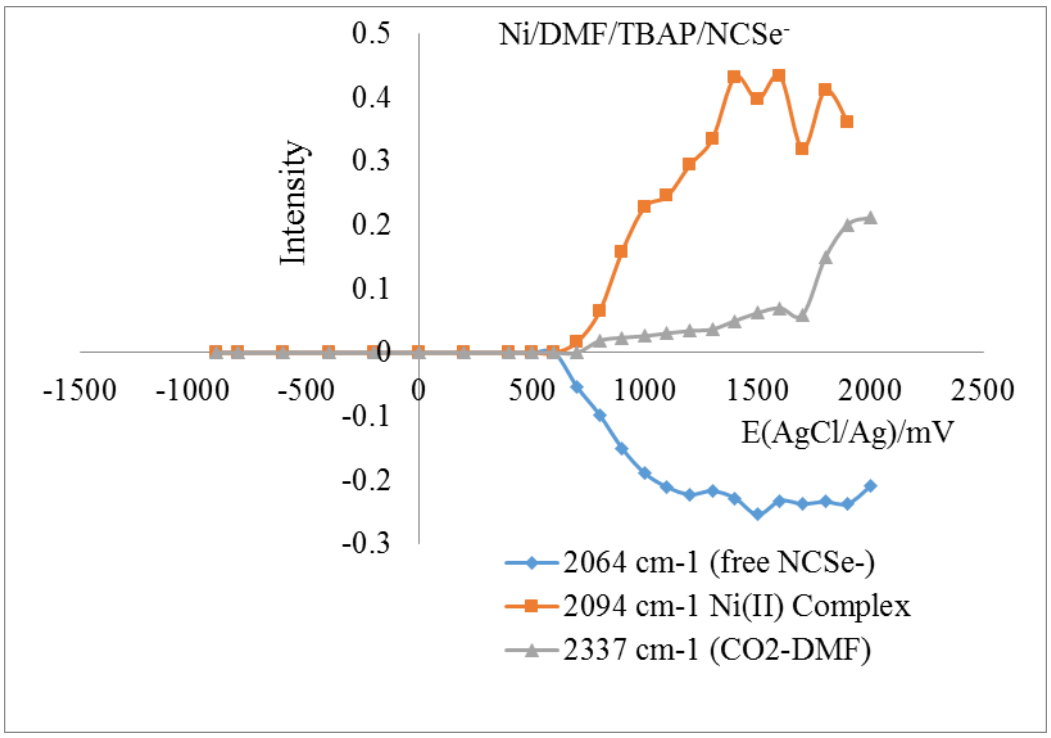

Figure 3.18: Plots of the intensity changes of the various molecular species generated in the thin layer during electrochemical polarisation and observed in the SNIFTIRS spectra as a function of applied potential in the Ni/0.05 mol L^{-1} $NCSe^-$/TBAP/DMF system.

3.3.5 Electrochemical and SNIFTIRS studies of Ni/DMSO systems containing NCO^-, NCS^- and $NCSe^-$ in 0.1 mol L^{-1} TBAP as supporting electrolyte.

Using another non-aqueous solvent, namely the common solvent, dimethyl sulfoxide (DMSO), more IR spectroelectrochemical studies were carried out of the anodic dissolution of Ni in this solvent in the presence of the pseudohalide ion series (and TBAP). DMSO was chosen because of the fact it was a polar aprotic solvent like DMF and hence it was reasoned that its behaviour with respect to the electrochemically driven anodic dissolution of nickel should be similar.

This was found to hold true. For example in the case of the electrochemical and spectroscopic studies of the nickel electrode in DMSO solvent containing 0.025 mol L^{-1} KOCN and 0.1 mol L^{-1} TBAP, apart from the single sweep voltammograms which showed some differences between the Ni/DMSO and Ni/DMF systems studied, the electrochemical and spectroscopic behaviour of the nickel electrode exposed to DMSO-containing solutions of cyanate, thiocyanate and selenocyanate were very similar to their DMF counterpart systems. The CVs of all the Ni/pseudohalide/DMSO systems demonstrated a passive region followed by an anodic dissolution region at applied potentials > *ca.* +500 mV (AgCl/Ag). The single sweep voltammograms though showing some variability in appearance between the different systems studied in Ni/DMF and Ni/DMSO systems also gave the same trend of an initial passivation period followed by an anodic dissolution region where current was observed to sharply increase. Sometimes peak currents were observed but mostly there was a monotonic increase in current as potentials were adjusted to more positive values.

Table 3.1 summarises the spectroscopic data for the 3 Ni/DMSO/NCX^-/TBAP (X=NCO^-, NCS^-, $NCSe^-$) systems studied by SNIFTIRS. Each system behaved in consistent fashion compared to the DMF-based systems in that a peak that was assigned to free pseudohalide ion was detected which invariably was seen as a negative-going peak in IR spectra acquired at potentials where anodic dissolution was actively occurring. This indicated consumption in the thin layer of the free

ion as Ni(II) complexes or as oxidation products like CO_2 which could be detected dissolved in the solvent used (as a peak at 2338-2339 cm^{-1}). Further, the intensity behaviour observed for the Ni(II)/pseudohalide ions in all the systems studied, i.e increasing to a maximum and then declining (see Figure 3.10, Figure 3.14, and Figure 3.18), has been tentatively attributed to the formation of an insoluble film on the electrode which forms at very high applied potentials.

In DMSO, however, the tendency to form detectable solvent-dissolved CO_2 was greater and the possible reason is that DMSO is more hygroscopic than DMF and hence there could be a greater tendency for water to be absorbed in this solvent during an experiment compared to DMF. Providing water to this system would increase the source of oxygen which could form as CO_2 in the medium at potentials where anodic processes were occurring. In Table 3.1, the characteristic Ni(II) complexes (effectively the product of anodic dissolution of nickel in the solvent concerned) are summarised. Each system studied had slightly different ν(CN) stretching frequencies for the dissolution product detected. Small differences in the ν(CN) stretching frequencies for Ni(II) complexes of the same type of pseudohalide ion in different solvents (e.g. Ni-NCO complexes in DMF *vs.* Ni-NCO complexes in DMSO, can be attributed to the influence of the solvent on the complex ions dissolved in it. Solvatochromic shifts are well known in IR spectra and would be expected in IR peaks of species solvated in DMF vs. DMSO. In addition, when the vibrational frequencies of species detected by IR in these systems are compared to similar systems reported earlier [37] involving the anodic dissolution of Ni in aqueous media containing pseudohalide ions and KNO_3 as supporting electrolyte, lower values are almost invariably detected relative to the aqueous solvent-supported electrochemical systems due to the large polarity difference between water and DMF and DMSO [70].

3.3.6 Model Solution work for elucidating Ni(II) complex species formed in anodically dissolved Ni solutions containing different pseudohalide ions.

In line with an earlier aqueous based study performed by Mucalo et al. [37], model solutions were prepared to identify what the Ni(II) complex species formed in the anodic dissolution experiments performed in aqueous media could be. In

general this was done by mixing a 1:1 mole ratio of Ni salt solutions prepared from partially dehydrated $Ni(NO_3)_2$ to the respective potassium (or in case of NCS^-, the sodium) pseudohalide salt (also prepared as a solution). In each study, this produced peaks due to the free pseudohalide ion and another higher wavenumber peak which was the ν(CN) stretching frequency of the Ni(II)-pseudohalide species in the aqueous media. In the present study, it was decided to prepare not only 1:1 mole ratio model solutions (using DMF or DMSO) of Ni^{2+}:NCX^- but also 1:2, 1:4 and 1: 8 mole ratio solutions to see if there was any difference in IR spectroscopic features observed and colour between the different mole ratio solutions. It was also to ascertain if Ni(II)-NCX or Ni(II)-$(NCX)_2$ (or higher) type complexes could form in the polar aprotic media supporting the systems under study. In general, only model solutions up to 1:4 mole ratio model could be prepared in DMSO due to the greater solubility of the NCO^- ion in this solvent compared to DMF where it is relatively less soluble at Ni^{2+}:NCO^- mole ratios of 1:2 and above. It was, however, impossible to prepare 1:8 mole ratio solutions in DMSO for cyanate ion due to solubility issues. IR transmission spectra and U.V./Vis. spectra were both acquired of these solutions and compared to the coloured cell solutions generated in the Ni/NCX^- systems after SNIFTIRS experiments in either DMF or DMSO. U.V./Vis. spectra were acquired to obtained spectroscopic information in addition to IR data. Table 3.2 summarises the transmission FTIR and U.V./Vis. spectra obtained of all 17 Ni^{2+}/NCX^- model solution systems (with differing Ni^{2+}:NCX^- mole ratios) studied. Previous authors have extensively studied Ni complexation of pseudohalides in DMF and have reported UV/Vis. data hence a comparison with that data from systems studied in the present investigation will be useful.

Table 3.2: : FTIR and U.V./Vis. data from IR studies of DMF or DMSO model solutions of $Ni(NO_3)_2$ and potassium (or sodium) pseudohalide ion salts prepared with different mole ratios.

Model solution studied and mole ratio of ($Ni(NO_3)_2$): NCX^- prepared in DMF or DMSO (X = O, S, Se)	ν(CN) of free NCX^- ion (X = O, S, Se) cm^{-1}	ν(CN) of Ni^{2+}/NCX^- complex ion cm^{-1}	U.V./Vis spectral features nm	Observed colour of solution
DMF				
$Ni(NO_3)_2$/ KOCN 1:1	nd	2210	276s, 412m,602w,656w	blue-green
$Ni(NO_3)_2$/ KOCN 1:2	nd	2200	280s, 416w, 600s, 647s	dark blue
$Ni(NO_3)_2$/ NaSCN 1:1	2056	2094	280s, 404m, 677w	light green
$Ni(NO_3)_2$/ NaSCN 1:2	2056	2094	280s, 404m, 681w	green
$Ni(NO_3)_2$/ KSeCN 1:1	2065	2098	288s, 401m, 680w	yellow green
$Ni(NO_3)_2$/ KSeCN 1:2	2065	2098	292s, 401m, 675w	light green
DMSO				
$Ni(NO_3)_2$/ KOCN 1:1	nd	2210	262s, 418m,	yellow-green
$Ni(NO_3)_2$/ KOCN 1:2	nd	2199	280s, 426w, 602s, 649s	blue-green
$Ni(NO_3)_2$/ KOCN 1:4	2137	2199	281s, nd, 601s, 648s	dark blue
$Ni(NO_3)_2$/ KOCN 1:8	2137	2199	281s, nd, 601s, 649s	dark blue
$Ni(NO_3)_2$/ NaSCN 1:1	2055	2094	263s, 416m, 700w	light green
$Ni(NO_3)_2$/ NaSCN 1:2	2055	2094	266s, 415m, 701w	green
$Ni(NO_3)_2$/ NaSCN 1:4	2055	2094	271s, 415m, 701w	green
$Ni(NO_3)_2$/ NaSCN 1:8	2055	2094	273s, 415m, 700w	green
$Ni(NO_3)_2$/ KSeCN 1:1	2065	2096	272s, 412m, 695w	yellow green
$Ni(NO_3)_2$/ KSeCN 1:2	2065	2096	273s, 416m, 697w	light green
$Ni(NO_3)_2$/ KSeCN 1:4	2065	2096	277s, 416m, 705w	light green
$Ni(NO_3)_2$/ KSeCN 1:8	2065	2096	297s, 416m, 700w	light green

s=strong, m=medium, w=weak

In general, when looking at the IR data in Table 3.1, it is obvious that a Ni^{2+}/NCX^- complex forms in every Ni^{2+}-NCX^- ion model solution mixture prepared. This is shown by the detection of peaks ranging from 2093-2210 cm^{-1} in the IR spectra of the model solutions. Furthermore the ν(CN) stretching frequencies of these peaks assigned to the Ni^{2+}-NCX^- complex ions are very similar in value to those observed in the SNIFTIRS spectra acquired for each system (see Table 3.1). The U.V. /Vis. data for the model solutions are also reasonably similar to the data presented for the cell solutions in Table 3.1. The only difference is that some weak peaks at wavelengths > 600 nm in the Ni/NCS^- and $Ni/NCSe^-$ cell solutions are not detected because the concentration of the $Ni\text{-}NCS^-$ and $Ni\text{-}NCSe^-$ complexes in these media must be lower than those in the model solutions. Moreover the observed colours of the model solutions parallel (when concentration differences are taken into account between the model and cell solutions) those observed in the cell solutions obtained after the SNIFTIRS experiment has concluded. This permanent colouration left in the cell solution supports the general observations from hysteresis in CV curves (See Figure 3.7, Figure 3.11 and Figure 3.15) that the dissolution of the nickel electrode during its anodic polarization is irreversible. Hence the model solutions are plausible representations of the Ni(II) complex ion species formed during the SNIFTIRS experiment.

The interesting aspect of these systems is the significant difference in colour between the cell solutions (after SNIFITRS) model solutions for the Ni/NCO^- system and the rest of the systems studied. Ni/NCO^- systems have always given a blue colour when the $Ni\text{-}NCO^-$ complex is present while complexes from Ni anodically polarized in NCS^- and $NCSe^-$ solutions are always observed to be green or yellow-green. The underlying reason for the colour of the Ni/NCO^- system has not been studied to a great extent in the literature. This is because the bulk of the literature (in regard to speciation of Ni^{2+} and NCX^- in DMF or DMSO media) reported, has concentrated on the NCS^- ligand [64, 65]. It is believed that a difference in coordination geometry of ligands around the central Ni^{2+} ion is responsible for the different colour observed in the case of the $Ni\text{-}NCO^-$ complex. Fackler et al. [68] had commented that qualitative studies of DMSO solutions containing $Ni(ClO_4)_2.6H_2O$ and KOCN were intense blue and that this was possibly due to a trisisocyanato Ni(II) or a tetraisocyanato Ni(II) complex. The

blue solid could only be formed by precipitation from aqueous solutions with large cations such as tetraphenylarsonium ions from Fackler's observations and it is likely the arrangement of the NCO^- ligands about the central Ni(II) ion is most likely tetrahedral. This is in distinct contrast to the complexes of Ni(II) (in DMF and presumably DMSO) [64] where the geometry of the attached pseudohalide and solvent ligands around the central ion are octahedral. Given the pseudohalide ions would all be bonded via the N atom to the central Ni, the crystal field splitting effect that may influence colour may not be so much the factor causing the difference in colour as the difference in geometry. Inorganic complexes of the transition metals with octahedral geometry are generally weakly coloured (i.e. green-yellow) compared to tetrahedral type complexes. [19]. Given these facts, it is apparent that the blue colour in the Ni/NCO^- systems is due to a tetrahedral complex or complex with a different geometry from either systems containing NCS^- or $NCSe^-$. Indeed when model solutions for the Ni/NCO^- system are prepared in DMSO in mole ratios of 1:1,1:2 and 1:4 and U.V./Vis. and IR spectra recorded changes can be seen that indicate the formation of different complexes depending on the mole ratio.

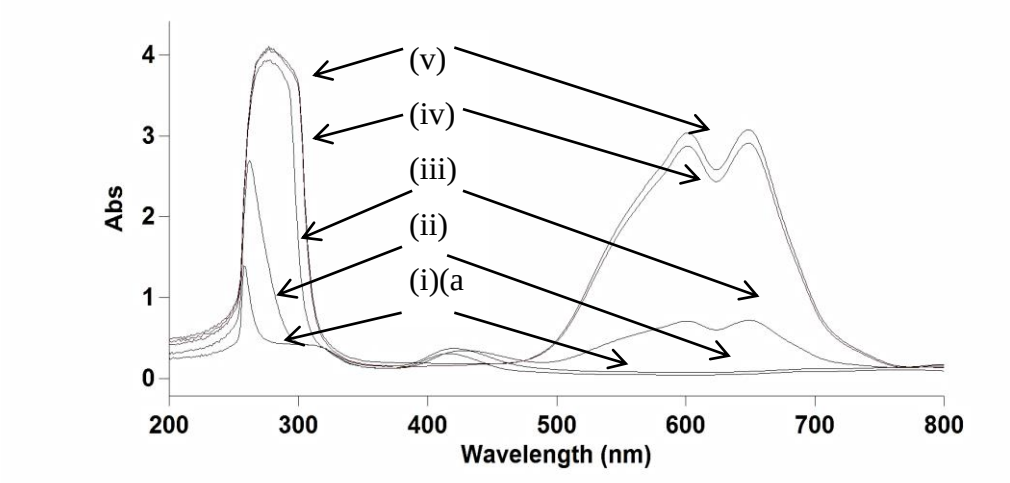

Figure 3.19: U.V./Vis spectra of various $Ni(NO_3)_2$/KOCN/DMSO model solutions where $[Ni(NO_3)_2]$ = 0.025 mol L^{-1} in each solution. Numbers (i) to(v) and arrows provide a guide to the U.V./Vis traces for each system: (i) $Ni(NO_3)_2$ dissolved in DMSO alone, (ii) $Ni(NO_3)_2$: KOCN 1:1 mole ratio solution, (iii) $Ni(NO_3)_2$: KOCN 1:2 mole ratio, (iv) $Ni(NO_3)_2$: KOCN 1:4 mole ratio solution, and (v) $Ni(NO_3)_2$: KOCN 1:8 mole ratio solution.

The U.V./Vis spectrum of the model solutions, are shown in Figure 3.19. There are only two features observed at 271 nm and 403 nm. One of these features based on previous U.V./Vis. spectral studies reported by Pilarcyzk et al [64] on

Ni(II) thiocyanate complexes in DMF could be assigned to "$Ni(NCS)_2$" when it is dissolved in DMF. The paper by Pilarczyk assigns these to *octahedral* Ni(II) thiocyanate complexes where the balance of the ligands attached to the Ni(II) centre are DMF solvent molecules. The peak at 403 nm is assigned to a "charge transfer" band while the peak at 271 nm though not detected in Pilarcyzk et al.'s paper is thought to be a charge transfer band which may be more closely associated with the coordinated thiocyanate ligand. When the U.V./Vis spectrum of NaSCN (alone) dissolved in DMF is taken, a peak in a similar position is observed but is much less intense. Moreover, U.V./Vis spectra of $Ni(NO_3)_2$ only dissolved in DMF also give a very weak peak in that same wavelength region. These observations prove that the strong enhancement in intensity leading to the peak at 271 nm is only observed upon complexation of the Ni(II) to the pseudohalide ion in DMF. For 1:1 mole ratio solutions, the colour of the solution is green but for 1:2 mole ratio solutions and above, the colour changes to blue and intensifies as is evident from the U.V./Vis spectra (see Figure 3.19) of 1:4 mole ratio solution and higher. Transmission IR spectra of the 1:1 to 1:4 mole ratio Ni/NCO^- solutions also show a shift in the ν(CN) stretching frequency to lower wavenumbers of the Ni-NCO complex that has formed which indicates an increase in the number of cyanate ligands coordinated to the Ni(II) centre that would decrease the large upward shift of ν(CN) brought about by sigma bonding of NCO^- to Ni(II).

Model solutions for the Ni/NCS^- and $Ni/NCSe^-$ systems were also prepared in 1:1, 1:2, 1:4 and 1: 8 mole ratio solutions for Ni^{2+}:NCX^- and these were different in terms of their appearance and spectroscopic behaviour from the systems involving the NCO^- ion. The colours were generally green yellow (as was observed after SNIFTIRS experiments involving Ni electrodes and these ions) and the ν(CN) stretching frequencies of the various model solutions were identical over all compositions. This suggested a stable possibly mono or disubstituted pseudohalide ion octahedral complex had formed as Ni(II) pseudohalide complex ion species in the Ni/NCS^- and $Ni/NCSe^-$ electrochemical systems.

3.3.7 Comparison of the present SNIFTIRS research on the corrosion of Ni in the non-aqueous polar aprotic solvents DMSO and DMF (containing pseudohalide ions) with earlier SNIFTIRS research carried out of the same systems in aqueous media

The systems in the present study have been studied before in aqueous media by Mucalo and Li [37]. In general when comparisons are made of the corrosion behaviour/electrochemistry between the earlier aqueous solvent-based and the present non-aqueous solvent-based systems, there are some strong similarities that are apparent in that the Ni(II) complex ion with the respective pseudohalide ion strongly features in all systems when Ni is anodically polarised. In the earlier study the colours of the model solutions made to explain the origin of the Ni(II) complex species were not mentioned in the paper. It is likely that they all appeared green in colour because they were only 1:1 mole ratio Ni^{2+}: NCX^- model solutions. To investigate this further in the present project, more model solutions were prepared in aqueous solvents to see whether there would be any colour changes in the solutions where the Ni(II) salt: pseudohalide ion mole ratio was > 1:1 and it was found that all solutions prepared were green in colour and in addition there was some precipitation observed. Hence it can be concluded that the characteristic blue colour in the Ni/NCO^- systems in DMF and DMSO is only observed in these polar aprotic solvents and not in aqueous solvent based systems. Hence the coordination chemistry occurring for these Ni/pseudohalide complexes do exhibit some differences between the aqueous and non-aqueous media.

Other points of difference in behaviour between the aqueous electrochemical systems studied and the non-aqueous systems were that most vibrational frequencies of the species detected in SNIFTIRS experiments were generally higher in value for the aqueous systems as opposed to those in the non-aqueous systems. This is merely due to a solvatochromatic shift as mentioned previously. The other major point of difference was the level of CO_2 generated in the aqueous vs. the non-aqueous systems. In the aqueous system, especially the Ni/NCO^- system, CO_2 formation features strongly while in the non-aqueous systems the formation of CO_2 appears to be repressed. This is probably due to the

general absence of water in the system which would be a source of OH^- ion which is what is consumed assuming an overall equation of oxidation as:

$$2NCO^- + 4OH^- \rightarrow 2CO_2 + 2H_2O + N_2$$

This may be due to the fact that aqueous solvents will have different anodic and cathodic limiting voltages to non-aqueous solvents such as DMF or DMSO. These limiting voltages [71] would indicate where solvent or electrolyte may themselves become oxidised or reduced at the electrode surface as a result of the applied potential existing there. Electrodes in aqueous media have a lower limiting voltage due to the greater reactivity of water. In a non-aqueous medium like DMF or DMSO, the limiting voltage is higher. Hence an electro oxidation reaction involving solvent or pseudohalide ion which leads to CO_2 formation at the electrode would be inhibited. However if small traces of water were present it could lead to some heightened CO_2 formation via the solvent as a feedstock. Indeed when the Ni/NCX^-/TBAB/DMF systems (i.e. systems using the tetrabutylammonium **bromide** salt) were carried out with *25% aqueous NaOH* added to the electrolyte, the SNIFTIRS spectra clearly showed significant peaks due to CO_2 electrogenerated at anodic potentials. The presence of the NaOH and water was also sufficient to enable the solvent alone (i.e DMF with no pseudohalide ion present) to become electro-oxidised to CO_2. It was believed that this was due to the influence of the OH^- ion on the keto enol equilibrium that an organic ketone like DMF would undergo [72]. It is possible that a shift to the enol form in NaOH/DMF mixtures may facilitate its oxidation to CO_2 at the electrode due to greater adsorption of the enol form at the Ni electrode surface. For instance it was found in an earlier study by Cho et al. [73] involving electrooxidation of β-dicarbonyl compounds using ceric methanesulfonate as a mediator that the enol-form created through coordination with ceric ion was more reactive to further transformations at the electrode/electrolyte interface. In the present study, UV/Vis evidence showed that the ketone functional group in DMF was affected (presumably by conversion to the enol form) by addition of OH^- to the DMF mixture.

The conclusion of this study, when the anodic dissolution of Ni electrodes in DMSO or DMF media containing pseudohalide ions, it was found that the nickel electrode anodically dissolved in these solvents to form Ni^{2+} complex ions formed by coordination to pseudohalide ions and solvent molecules.

Chapter 4

An X-ray absorption spectroscopy investigation of the coordination environment of electrogenerated Ni(II)-pseudohalide complexes arising from the anodic polarization of Ni electrodes in DMSO solution of NCO^-, NCS^- and $NCSe^-$ ions

4.1 Introduction

Additional data to probe the geometry observed for the Ni-pseudohalide complex ions formed during anodic dissolution experiments has been done using other techniques which involved X-ray absorption spectroscopy (XAS), (i.e Extended X-ray absorption fine structure / X-ray absorption near edge spectroscopy, (EXAFS/XANES). These data were obtained at the Australian Synchrotron on frozen DMSO-solution samples of model solutions and cell solutions (after SNIFTIRS) for the Ni/NCX^- systems (X=O, S, Se).

The XAS has been particularly useful in studies where the solvation structure around the metal ions needs to be known for understanding better the reactivities of the metal in solution [74]. It has also been useful in studying electrochemical processes such as corrosion, catalysis and the probing of unstable reactive species which are electrochemically generated in solution [75-78]. Most XAS studies on electrochemical systems have involved probing of the solid electrodes or solid product involved or formed in the electrochemical process which is inherently easy to do and can provide better quality results depending on the sample. In the case of the studies, however, involving the direct probing of species produced *in solution* by electrochemical action, there have not been many recent studies where XAS has been directly utilized to elucidate the molecular structure of species produced. For instance Yeo et al. [78] used XAS to study reactive electrogenerated tri-iron carbonyl sulfide clusters in mixed non-aqueous solvents by the method of freeze quenching. In this particular study, IR spectroscopy was used by Yeo et al. to fingerprint the different Fe-S species produced at various potentials. Charnock et. al. [75], on the other hand, have used a novel in situ electrochemical cell to study the XAS of Ni and Cu quinoxaline-2-3-dithiolene

complexes in solution. The point of this was to obtain structural information or changes to redox species that are often transitory in nature and cannot be isolated once solvent is removed or crystallization attempted.

The IR spectra provided a good replication of the species which had been electrogenerated during the anodic polarisation of nickel but did not provide specific information on the exact coordination environment of the Ni(II) ion in the electrogenerated solutions. This is of interest because of the different colours observed in the electrogenerated products when comparing the solutions produced as a result of anodic polarisation of Ni in NCS^- and $NCSe^-$ containing electrolytes (which were green-yellow in colour) to the colour produced when Ni was anodically polarised in NCO^- containing electrolytes, which was a clear blue. UV/Vis spectra showed definite differences in features between the green-yellow and blue solutions and previously reported UV/Vis spectra on solutions containing Ni(II) and NCS^- in papers by Pilarczyk et al. [79] were very similar in appearance (see Chapter 3). Pilarczyk et al. attributed their observed UV/Vis spectra to "an ability of the Ni^{2+} ion towards an octahedral environment". However similar UV/Vis work relating to Ni(II)-cyanate complexes has not been performed. It is of interest to determine what stoichiometry in the complex ion (in terms of the geometry and the numbers of coordinated pseudohalide ions versus numbers of coordinated solvent molecules in the complex ion species) could be giving rise to the blue colour when Ni was anodically dissolved in NCO^- containing solutions of DMSO. This requires an analysis of the solutions containing this species as well as the species giving rise to the green yellow colours in DMSO solutions where Ni has been anodically dissolved in the presence of NCS^- and $NCSe^-$ in order to determine the local coordination environment around the Ni(II) ion. Although symmetry arguments can provide an idea of the number of IR active CN^- stretching frequencies in an octahedral complex consisting for instance of $Ni(DMSO)_4(NCX)_2$ it may not describe the origin of the colour of complexes which may be related to differences in the geometry of coordination of solvent and pseudohalide ions with the central metal ion. Other techniques such as ^{13}C solution NMR are hindered by issues such as sensitivity and the fact that the Ni(II) ion is paramagnetic [80] which will tend to broaden any detected peaks. X-ray absorption spectroscopy (XAS) has the ability to probe short and medium range order in liquid and solid molecular samples providing information on bond

lengths, coordination numbers, geometry and oxidation states of atoms in a diverse range of samples, in particular coordination environments around inorganic metal ion centres [81-84]. Hence it was decided to apply X-ray absorption near edge spectroscopy (XANES) and extended X-ray absorption fine structure (EXAFS) to these challenging systems to obtain a more accurate picture of the complex ion species present in 1) solutions electrogenerated via the anodic dissolution of Ni in pseudohalide containing DMSO solutions and 2) the model solutions prepared to mimic these electrogenerated species.

4.2 Experimental

4.2.1 Solvents

Anhydrous DMSO (99.9%) solvents were used for all experiments. The pseudohalide salts used in experiments, i.e. potassium cyanate (KOCN, >96%), potassium thiocyanate (KSCN, >99%), and potassium selenocyanate (KSeCN, >97%) as well as other incidental chemicals that were needed in electrochemical, XAS work and in model solution preparations, i.e. nickel oxide (NiO, >99%), tetrabutylammonium perchlorate (> 98 %) were all supplied by Aldrich Chemical Co, Ltd. and used as received. The nickel nitrate ($Ni(NO_3)_2.6H_2O$, >99%) contained waters of crystallisation which were partially removed by drying in an oven at 50°C for 2-3 hours. This led to the originally blue salt turning a green colour after heating. Not all water was removed as confirmed by IR spectroscopic analysis. This was not believed to affect results obtained to any great extent.

Electrogenerated solutions were produced for XAS analysis using the appropriate hardware in a thin layer electrochemical cell containing a nickel working electrode, Pt secondary electrode and AgCl/Ag reference electrode as described previously. In general, the electrolyte solutions prepared for electrochemical experiments had a concentration of 0.05 mol L^{-1} in the pseudohalide salt with 0.1 mol L^{-1} TBAP used in the capacity of a supporting electrolyte in DMSO. Model solutions were prepared by mixing partially dehydrated (heated in an oven at 50°C for 2-3 hours) $Ni(NO_3)_2.6H_2O$ and potassium pseudohalide salts with Ni^{2+}:NCX^- mole ratios of 1:1 and 1:2 in DMSO.

4.2.2 Equipment and cell used in this study for XAS analysis

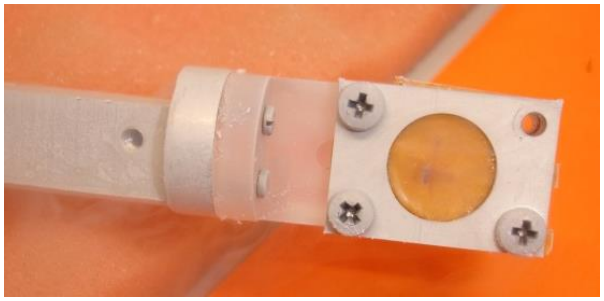

Figure 4.1: Custom made cell used in all XAS studies constructed from Perspex pellet holders and Kapton™

Liquid samples and standards were loaded into a custom made cell (see Figure 4.1) which was constructed by affixing Kapton™ tape to both sides of a Perspex holder which had a circular cavity of 1 cm diameter by 2 mm thickness. Liquid was injected into this Kapton™-sealed cavity (~2.5 mL) via a syringe. The liquid-filled cell was then flash frozen in liquid nitrogen and measured in a closed-cycle He cryostat (T<10K) at the XAS beamline at the Australian Synchrotron (Melbourne, Australia). Samples were frozen to avoid the formation of bubbles due to ionization of the solution by the X-ray beam. To verify that freezing did not alter the co-ordination environment of the complexes, the IR spectra of frozen samples were recorded and showed no difference compared to liquid samples. The nominal beam size at the sample was 2 × 0.5 mm (horizontal × vertical height). Frozen samples were measured in fluorescence mode using a Canberra 100-element Ge detector. Data were collected at the Ni K-edge (8333 eV) up to k = 12 $Å^{-1}$. The photon energy was controlled using a Si(111) double-crystal monochromator operating at the peak of the rocking curve ("fully tuned"), higher harmonics were rejected via X-ray mirrors. Solid standards (NiO) were measured in transmission mode by thoroughly mixing powders in cellulose powder. The liquid standard solutions were prepared as nominally 0.05 mol L^{-1} solutions of the dried nickel nitrate in distilled water and in neat DMSO solvent.

The following samples were measured:

Sample 1: NiO, powder standard

Sample 2: $Ni(NO_3)_2$ dissolved in water, liquid standard

Sample 3: $Ni(NO_3)_2$ dissolved in DMSO solvent, liquid standard

Sample 4: KOCN + $Ni(NO_3)_2$ 2:1 in DMSO model solution

Sample 5: KSCN + $Ni(NO_3)_2$ 2:1 in DMSO model solution

Sample 6: KSeCN + $Ni(NO_3)_2$ 2:1 in DMSO model solution

Sample 7: Ni/KOCN solution generated by anodic polarization of a Ni electrode at +800 mV(AgCl/Ag) in DMSO producing a blue solution. N.B. +800 mV(AgCl/Ag) is where the Ni(II)/cyanate complex ion produced by anodic polarization of the Ni electrode occurs at maximum intensity (when detected via SNIFTIRS). The concentration of the Ni(II) complex ions being analyzed in the electrogenerated solutions was expected to be lower than those in the model solutions (i.e. < 0.05 mol L^{-1}).

Data were processed using either beamline software (Average 2.0) or software developed in-house to remove diffraction peaks. These software packages allow scans from entire detector elements (or parts of scans, in the case of the in-house software) to be removed. The data from remaining elements were dead-time corrected and averaged. The EXAFS data were processed and analyzed using Athena and Artemis [85] with FEFF6 [86]. The background subtraction and normalization procedures were carried out using standard routines with default parameters determined by the Athena software. The data were fitted in R-space with k^1, k^2, and k^3 weightings simultaneously. The Fourier transformed data were not phase shift corrected.

4.3 Results and discussion

4.3.1 XANES

The XANES part of the spectrum can be used for 'fingerprinting' the valence state of the Ni complex ions being probed (from the position of the absorption edge, E_0), and their co-ordination environment (from the intensity and position of peak features near the edge).

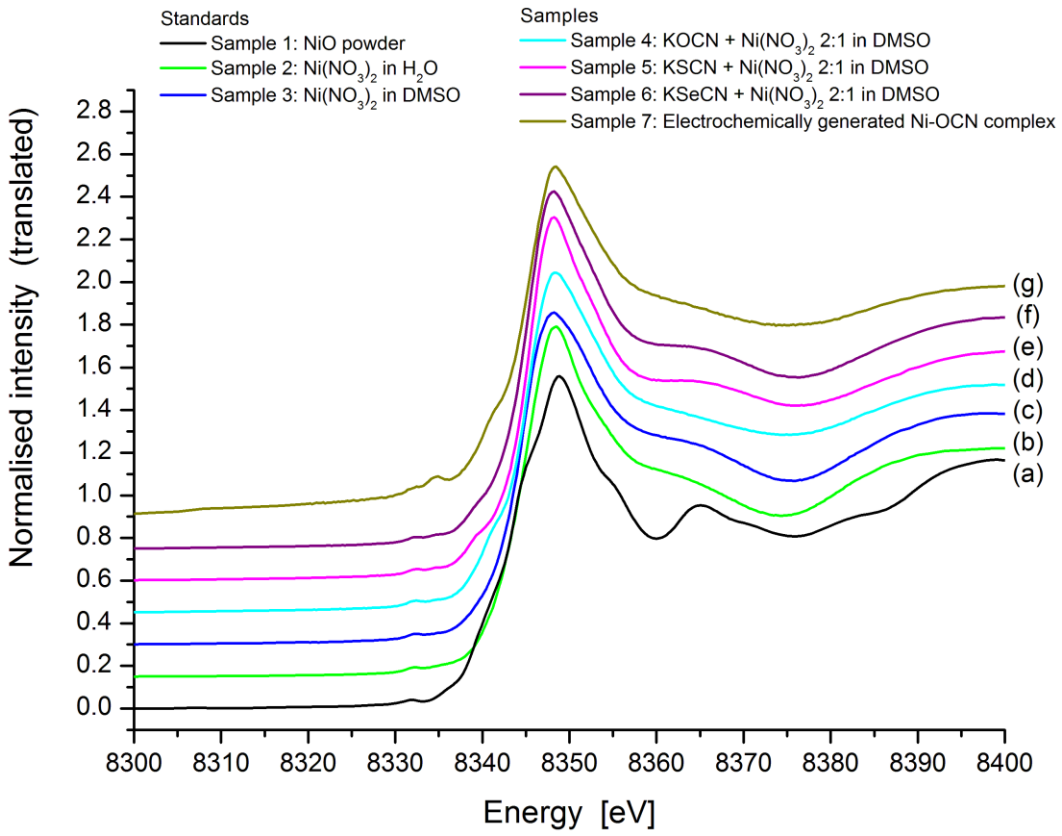

Figure 4.2: XANES data collected for standards: (a) NiO powder, (b) $Ni(NO_3)_2$ in H_2O, (c) $Ni(NO_3)_2$ in DMSO, (d) to (f) represent samples of model solutions with pseudohalide ion to nickel ratios of 2:1, hence (d) is Ni/NCO^- (sample 4), (e) is Ni/NCS^- (sample 5), (f) is $Ni/NCSe^-$ (sample 6) and (g) represents the sample of electrochemically generated Ni complex ions with NCO^- from the thin layer electrochemical cell (sample 7).

Figure 4.2(a-g) shows the XANES spectra for all standards and samples collected. Ni(II) ions tend to adopt octahedral or tetrahedral geometries [80], although square planar, 5-co-ordinate trigonal bipyramid and square pyramid geometries have also been observed. In many transition metals the XANES spectra for these different coordination geometries are reasonably distinct, but for Ni the differences can be subtle. [87-89] According to the literature, the following conclusions can be drawn: A weak pre-edge peak feature at ~8333 eV corresponds to a 1s - 3d electronic transition, which is forbidden in true centrosymmetric molecules. Thus it is more prominent in tetrahedrally co-ordinated Ni than octahedrally co-ordinated Ni. However, distortion of octahedral Ni(II) complexes will also result in this pre-edge peak feature being observed. Square planar and square pyramidal Ni often show a prominent feature or peak on the edge at ~ 8338 eV corresponding to the 1s - $4p_z$ transition. For Ni(II) in solution, the first minimum above the edge is lower in energy for 6

co ordinate Ni (8375 eV) than 4 co-ordinate Ni (8380 eV). [87] Other features present in XANES spectra, including the intensity of the "white line" (first maximum) and position of subsequent maxima, depend on the ligand species attached and cannot be used as a general fingerprint of co-ordination geometry. Similarly the average slope of the edge depends on the ligand hardness. [87] The position of the edge can also shift by up to 2 eV as a result of ligands conjugated through O or N, to S. [87].

From an examination of the XANES spectra from this study as illustrated in Figure 4.2, the following was noted. There is a small peak at 8332 eV in all of the spectra shown in Figure 4.2, which corresponds to the 1s - 3d electronic transition. All of the Ni samples and standards in solution have similar shapes, i.e., the white line at 8348 eV, a shoulder at 8365 eV, a minimum at 8374 -8376 eV, and subsequent oscillations. The two liquid standards (Ni(II) in H_2O and Ni(II) in DMSO; Figure 4.2(b) and Figure 4.2(c)) are expected to adopt symmetric octahedral geometries [79, 80] and display similar spectra to octahedral Ni(II) ions in solution [90]. The samples containing coordinated NCX^- ligands (X = O, S, Se) show a shoulder below the edge at 8340 eV, not present in the two liquid standards. This indicates a degree of asymmetry, possibly arising from having two different species of co-ordinating ligands (NCX^- and DMSO solvent molecules). For both the model and electrochemically generated samples with coordinated NCO^- (Figure 4.2(d) and Figure 4.2(g)), the intensity of this feature is noticeably higher than the samples with NCS^- and $NCSe^-$. This is most likely a $1s\text{-}4p_z$ transition as observed in the XANES of species possessing square planar and square-pyramidal geometries, and, by implication, in distorted octahedral geometries also [87-89]. This may indicate that the Ni(II) complex with NCO^- has a different co-ordination geometry, or adopts a mixture of different co-ordination geometries.

The shoulder above the edge at 8365 eV is significantly lower in intensity for the two samples with coordinated NCO^- ligands compared to the other samples and solution standards.

The peak at 8335 eV for the electrochemically generated Ni/NCO^- sample (Figure 4.2(g)) is due to a monochromator 'glitch'. The reason it is only seen in

this sample is due to the lower concentration of Ni that is expected in the electrochemically generated solution (relative to model solutions), which results in a lower overall absolute intensity.

In conclusion it appears that the Ni complexes with NCS^- and $NCSe^-$ in the model solutions are mostly octahedral in geometry, with varying degrees of distortion depending on the ligand, arising from the mixture of co-ordination species (NCX^- and DMSO). However the Ni complexes with NCO^- appear to have a different geometry, or possibly a mixture of geometries. The XANES spectra of the Ni/cyanate system produced by anodic dissolution of Ni in 0.05 mol^{-1} KOCN to the 2:1 KOCN:Ni(II) model solution (Figure 4.2(g) and Figure 4.2(d), respectively) are similar, indicating that the model solutions are accurate representations of the co-ordination environment existing in the electrochemically generated solutions, as also proven by IR spectroscopy in chapter 3. For this reason, and because the Ni(II) complex ion species can be prepared in higher concentrations than what would be produced in the electrochemical experiments, the bulk of the study presented here concentrates on the model solutions.

4.3.2 EXAFS

The EXAFS region of the XAS spectra was analysed to gain more information about the *average* coordination environment around the Ni(II) centres under study. The NiO powder standard was fitted simultaneously for k^1, k^2 and k^3 weightings in R-space, using a FEFF model based on the NiO crystal structure to a radial distance of R = 6 Å. All single- and multiple- scattering paths were used to fit the data to R = 5 Å. The data and fit for k^2 weighting is shown in Figure 4.3, and for all k-weightings in Figure S.1 in Appendix 1. The parameters used are given in the Table S.1 in Appendix 1. In the EXAFS equation, the co-ordination number, N, and the amplitude parameter, S_0^2, are combined as a product. For NiO, N is known to be 6. The value of S_0^2 obtained from the fit is 0.78 ± 0.07, which is in agreement with the usual expected value of 0.8. When fitting the samples, the unknown co-ordination number can be obtained if one assumes that S_0^2 has this same value.

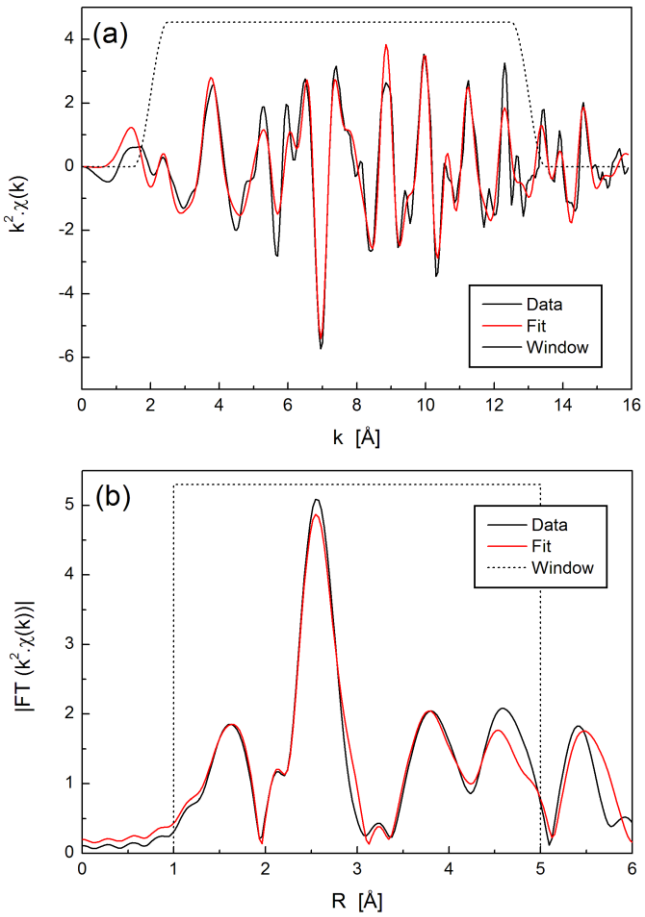

Figure 4.3: EXAFS data and fit for NiO powder standard ('Sample 1') in (a) k-space and (b) R-space, with k^2 weighting.

The same analysis method (constructing a model based on a known crystal structure) cannot be applied to complex ions in solution due to the lack of long-range order. Instead, a collection of single-scattering paths was used to fit the data, with limitations imposed on various parameters as appropriate.

Firstly, it was considered the two $Ni(NO_3)_2$ standards dissolved in H_2O and DMSO, shown in Figure 4.4 and Figure 4.5 respectively. A prominent peak in both spectra is observed at R ≈ 1.5 Å, corresponding to the first nearest neighbour shell. For Ni^{2+} in H_2O, a model was constructed using only oxygen atoms. Usually hydrogen is not observed in EXAFS. Two paths representing the first and second solvation shells were estimated to be located at 2.0 and 4.0 Å. Seven parameters were used: amplitude (amp), σ^2 (Debye-Waller Factor) and Δr (to account for the difference in the shell radius between the model and actual data) for each path, and ΔE_0 (same for both paths). A full list of parameter values is given in the

Appendix 2 (Table S.2). The data and fit for k^2 weighting are shown in Figure 4.4, and for all k-weightings in Figure S.2 in Appendix 2.

For Ni^{2+} in DMSO, it is assumed that the oxygen atom, with its lone electron pairs, is closest to the Ni^{2+} ion. A collection of single-scattering paths to represent the oxygen, sulfur, and two carbon atoms of DMSO at appropriate path distances based on the molecular geometry was used. This gave a good fit to the data and used 9 parameters, which are given in the Appendix 3 (Table S.3). The data and fit for k^2 weighting are shown in Figure 4.5, and for all k-weightings in Figure S.3 in Appendix 3.

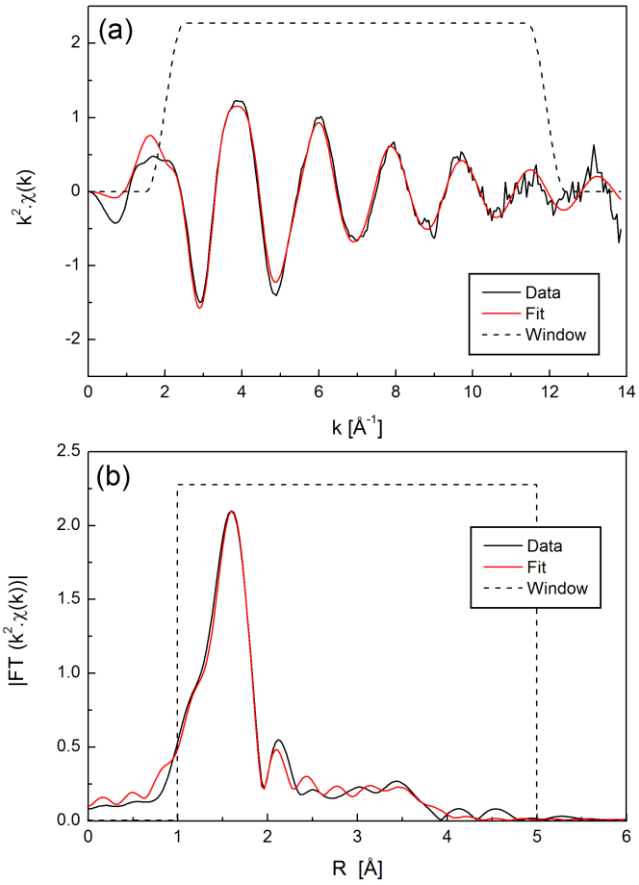

Figure 4.4: EXAFS data and fit for Ni^{2+} in H_2O standard ($Ni(NO_3)_2$ dissolved in water, 'Sample 2') in (a) k-space and (b) R-space, with k^2 weighting.

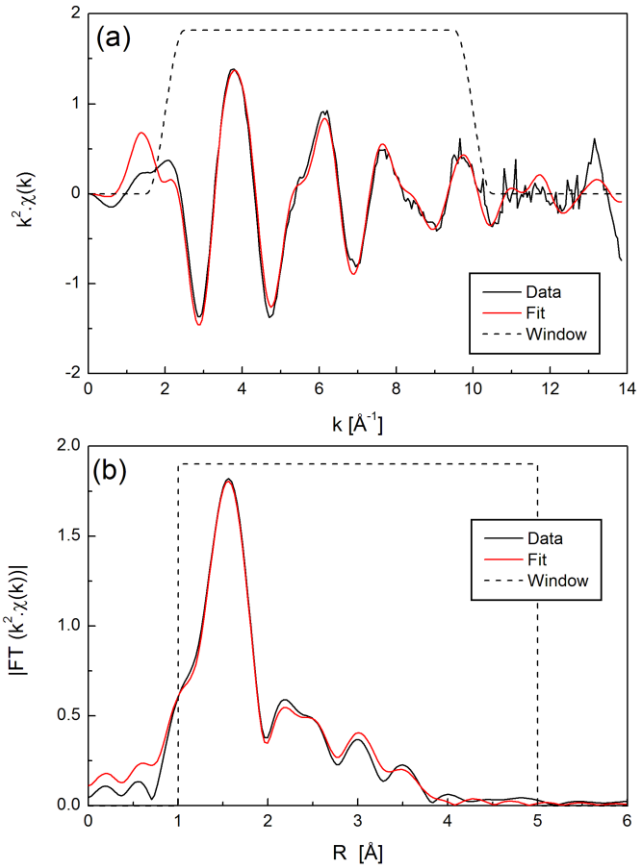

Figure 4.5: EXAFS data and fit for Ni^{2+} in DMSO standard ($Ni(NO_3)_2$ dissolved in DMSO solvent, 'Sample 3') in (a) k-space and (b) R-space, with k^2 weighting.

When comparing the product $N \times S_0^2$ for the three standards and dividing by the value of S_0^2 obtained from the NiO fit of 0.78 ± 0.07, it is possible to obtain values for the co-ordination number of Ni^{2+} in the two liquid standards (Table 4.1). These are the same as each other within uncertainty. The average co-ordination numbers may be 5 or 6 within uncertainty, but are most likely to be 6. According to literature, the predominant species in such solutions are likely to be $[Ni(H_2O)_6]^{2+}$ [80] and $Ni(DMSO)_6^{2+}$ [79]. This is consistent with the XANES spectra of Ni^{2+} in H_2O and in DMSO which are very similar to one another, and to literature data for octahedrally co-ordinated Ni^{2+} ions [90].

Table 4.1: Extraction of co-ordination numbers for standards. The co-ordination number is calculated assuming the global value of S_0^2 of 0.78 ± 0.07, as obtained from the NiO standard, applies to all samples.

Sample	N in model	Fitted value of S_0^2	$N \times S_0^2$	Calculated coordination number, N
NiO	6	0.78 ± 0.07	4.68 ± 0.42	6.00 ± 0.60
$Ni(NO_3)_2$ in H_2O	1	4.00 ± 0.15	4.00 ± 0.15	5.13 ± 0.65
$Ni(NO_3)_2$ in DMSO	1	4.16 ± 0.20	4.16 ± 0.20	5.33 ± 0.74

Then the nickel DMSO-pseudohalide complexes were considered, which are expected (based on assumptions of octahedral coordination geometry as suggested by XANES) to have the *average* stoichiometry $Ni(NCX^-)_n(DMSO)_m$ (X = O, S, or Se), most likely with n = 2 and m = 4, resulting in a 6-co-ordinate, possibly distorted, octahedral geometry.

The first question that arises when proposing a model structure for this complex is which terminus of the pseudohalide ion complexes to Ni^{2+}? This was done by considering the case of a Ni(II) complex containing $NCSe^-$ as the coordinated pseudohalide ion. Selenium has the highest atomic number of the species studied and will therefore lead to different spectral responses at different k-weightings compared to lower atomic number species such as C, N, and O (specifically, at higher k-weightings Ni-Se components will show an increase in intensity relative to Ni-C, Ni-N and Ni-O components).

A model was constructed from a collection of single-scattering paths as follows. The DMSO molecule was included with paths based on the Ni^{2+} in DMSO standard. The number of parameters for the DMSO molecule was reduced by fixing the amplitude ratios of the four paths, and using a single amplitude scale factor, and common σ^2 parameter. The NCX^- (X = O, S, or Se) molecule was modelled in two different ways. In the first, three separate paths were included corresponding to N, C, and either O, S, or Se at appropriate distances from the central Ni atom. These paths shared a common σ^2 parameter, and each had separate independent parameters for 'amp' and Δr. This resulted in a total number of parameters of 13. For consideration of the case involving Ni(II) coordinated to $SeCN^-$, models were constructed for both Ni-NCSe and Ni-SeCN. The Ni-NCSe model gave a much more stable fit than Ni-SeCN, indicating that the pseudohalide ion is complexed to the Ni(II) central atom via the nitrogen atom – an observation that is consistent with IR data reported by previous workers [32, 39, 79]. Therefore in considering Ni(II) complexes coordinated to the other pseudohalide ions, similar models were also constructed for Ni-NCS and Ni-NCO. (However, note that due to the similarity in atomic number between N and O, it is impossible to distinguish between Ni-NCO and Ni-OCN by EXAFS alone.) A list of the fitted values for the parameters for each sample is given in Table S.4 in Appendix 4, and the data and fits are shown in Figures S.4-S.7 in Appendix 4.

Although the first method gave reasonable fits and values for the amplitude parameters, the shell radii for some of the atoms - particularly Ni-N and Ni-C in the Ni-NCX ligand - resulted in unphysical bond lengths for N-C (< 1.0 Å) in the NCX^- molecule. For collinear paths, multiple scattering can often be significant. Since all ions in the NCX^- series are linear, a second model was constructed that included multiple scattering paths for NCX^-. Once again, single-scattering paths were used for DMSO. This resulted in more realistic values for N-C bond lengths within the NCX^- molecules. Note that the Ni-X (X = O, S, Se) distances are indicative only as these are close to the limit of the fitting range used. Once again both Ni-NCX and Ni-XCN models were considered, and for X = Se and S the Ni-XCN model failed (these results are not shown). The fitted values of the parameters are given in Table 4.2, and the data and fits are shown for k^2-weighting in Figures 4.6-4.9 and all k-weightings in Figures S.8-S.11 in Appendix 5.

Table 4.2: Parameters used in EXAFS fits with a multiple-scattering model for NCX^- and a single-scattering model for DMSO.

Parameter	X = O	X = S	X = Se	echem X = O
Reduced χ^2	106	484	301	32.5
ΔE^0 (all paths)	-4.1 ± 1.0	-5.7 ± 2.5	-4.8 ± 1.4	-6.4 ± 1.3
σ^2 (DMSO paths)	0.005 ± 0.004	0.005 ± 0.007	0.003 ± 0.003	0.004 ± 0.005
σ^2 (NCX^- single scattering paths)	0.002 ± 0.004	0.002 ± 0.005	0.001 ± 0.005	0.001 ± 0.003
σ^2 (NCX^- multiple scattering paths)	0.005 ± 0.011 [c]	0.007 ± 0.015 [c]	0.018 ± 0.010	0.004 ± 0.008 [c]
scale (DMSO)[a]	0.71 ± 0.13	0.94 ± 0.45	0.70 ± 0.19	0.62 ± 0.09
amp_O (DMSO)[b]		3.34 ± 0.87		
amp_S (DMSO)[b]		2.87 ± 1.36		
amp (NCX^-)	0.52 ± 0.49	0.64 ± 1.10	1.34 ± 1.10	0.59 ± 0.32
r_O (DMSO)	2.06 ± 0.01	2.06 ± 0.03	2.08 ± 0.026	2.04 ± 0.01
r_S (DMSO)	3.19 ± 0.03	3.14 ± 0.02	3.14 ± 0.04	3.15 ± 0.03
r_C1 (DMSO)	3.87 ± 0.09	3.94 ± 0.09	3.98 ± 0.063	3.95 ± 0.07
r_C2 (DMSO)	4.18 ± 0.05	4.13 ± 0.09	4.16 ± 0.063	4.05 ± 0.10
r_N (NCX^-)	1.99 ± 0.15	1.97 ± 0.19	2.01 ± 0.05	1.98 ± 0.06
r_C (NCX^-)	3.10 ± 0.09	3.00 ± 0.26	3.34 ± 0.14	3.09 ± 0.14
r_X (NCX^-)	4.14 ± 0.07	4.84 ± 0.06	5.11 ± 0.08	4.31 ± 0.06

[a] For the DMSO paths, amp(O) = scale*4.14, amp(C) = scale*4.61.

[b] X = S only.

[c] Set to $3*\sigma^2$(NCX^- single scattering).

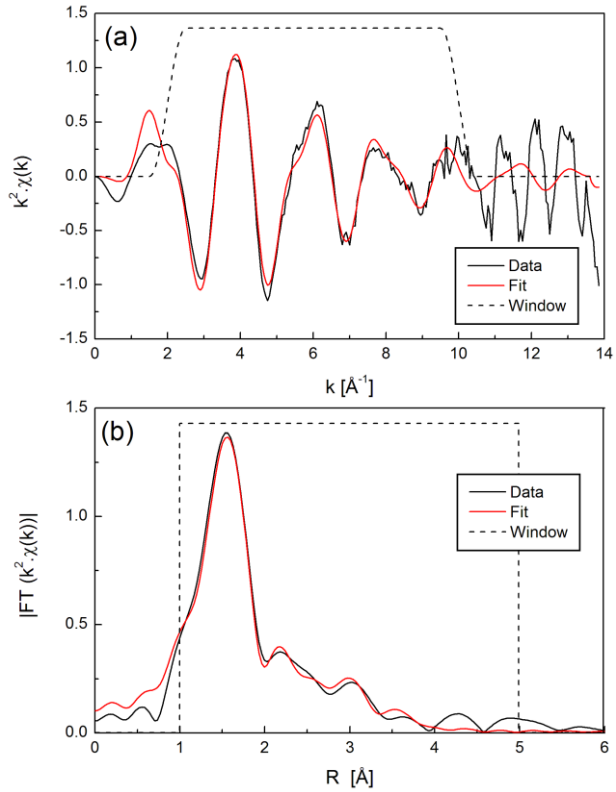

Figure 4.6: EXAFS data and fit for 2:1 KOCN + Ni^{2+} in DMSO model solution ('Sample 4') in (a) k-space and (b) R-space, with k^2 weighting. Single-scattering paths were used for DMSO, and multiple-scattering paths for NCO^-.

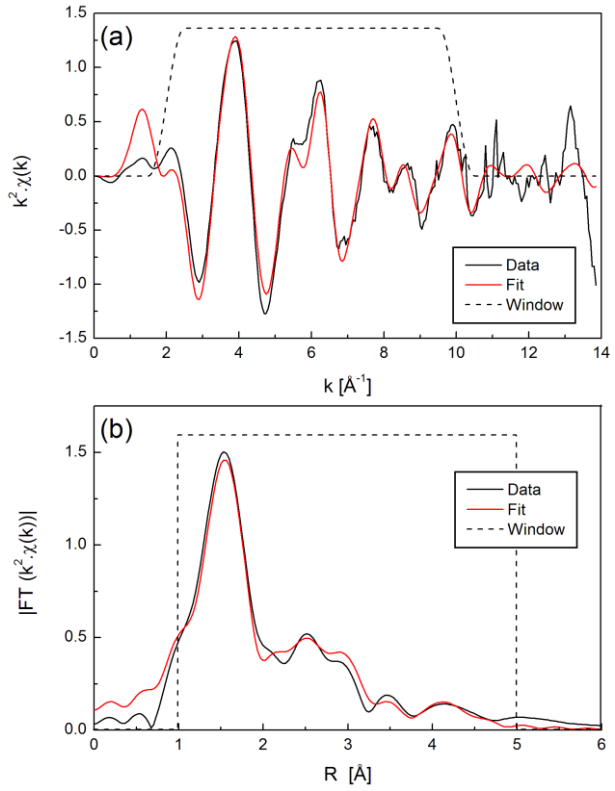

Figure 4.7: EXAFS data and fit for 2:1 KSCN + Ni^{2+} in DMSO model solution ('Sample 5') in (a) k-space and (b) R-space, with k^2 weighting. Single-scattering paths were used for DMSO, and multiple-scattering paths for NCS^-.

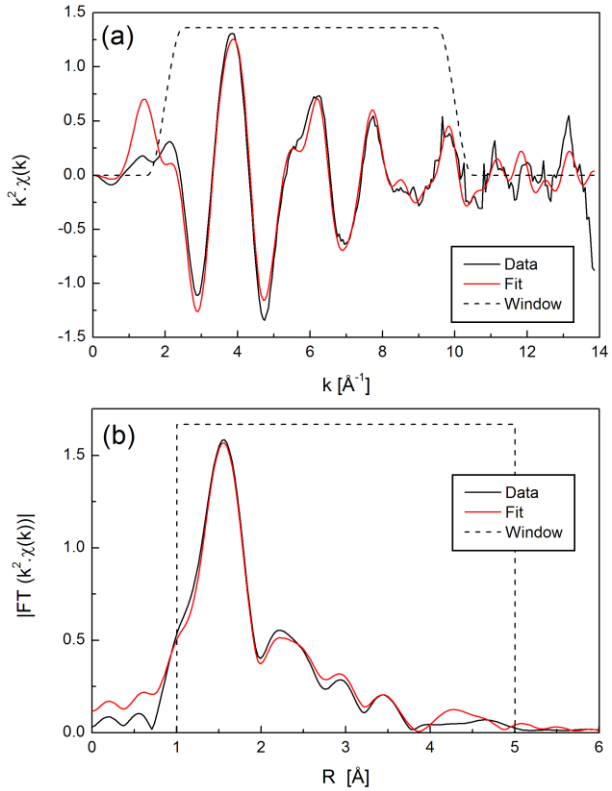

Figure 4.8: EXAFS data and fit for 2:1 KSeCN + Ni^{2+} in DMSO model solution ('Sample 6') in (a) k-space and (b) R-space, with k^2 weighting. Single-scattering paths were used for DMSO, and multiple-scattering paths for $NCSe^-$.

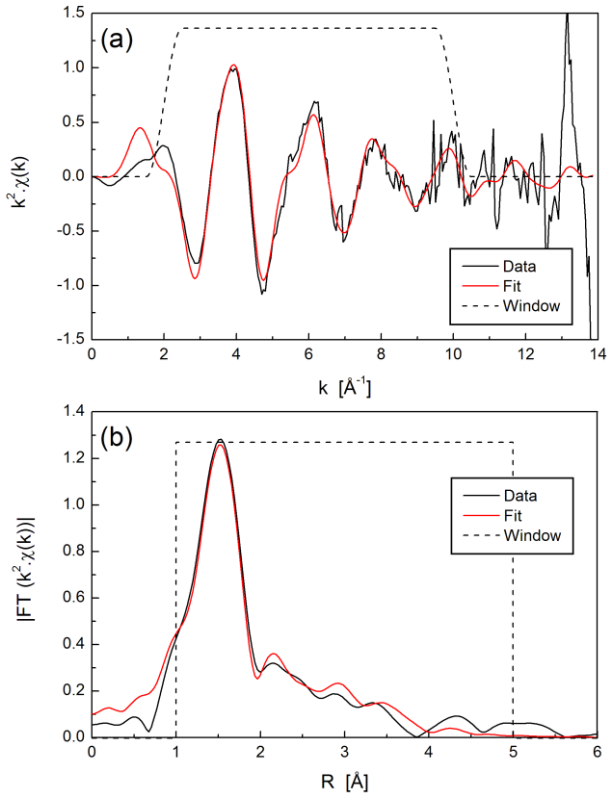

Figure 4.9: EXAFS data and fit for electrochemically generated Ni^{2+}:NCO^- complex ions in DMSO solution ('Sample 7') in (a) k-space and (b) R-space, with k^2 weighting. Single-scattering paths were used for DMSO, and multiple-scattering paths for NCO^-.

Figure 4.10 shows the path distances graphically for the two approaches used (i.e. single scattering only for all and multiple scattering (NCX^-) and single scattering (DMSO)). Given that the NCX^- ligand is linear, the bond distances can be directly read off the graph. For all of the fits that were performed using a single-scattering model (as labelled in Figure 4.10) for NCX^-, the N-C bond is less than 1 Å, which is unreasonable, even though the reduced χ^2 is lower for these fits. The N-C bond acquires values > 1 Å when multiple scattering paths are included. This demonstrates the necessity of including multiple scattering paths for the linear NCX^- ligand. As mentioned above, the Ni-X (X = O, S, Se) distances are indicative only as these are close to the limit of the fitting range used. However these show consistent trends with size, as expected, and the model and electrochemically generated Ni-NCO data yield quite consistent distances for the furthest Ni-O shell of this ligand.

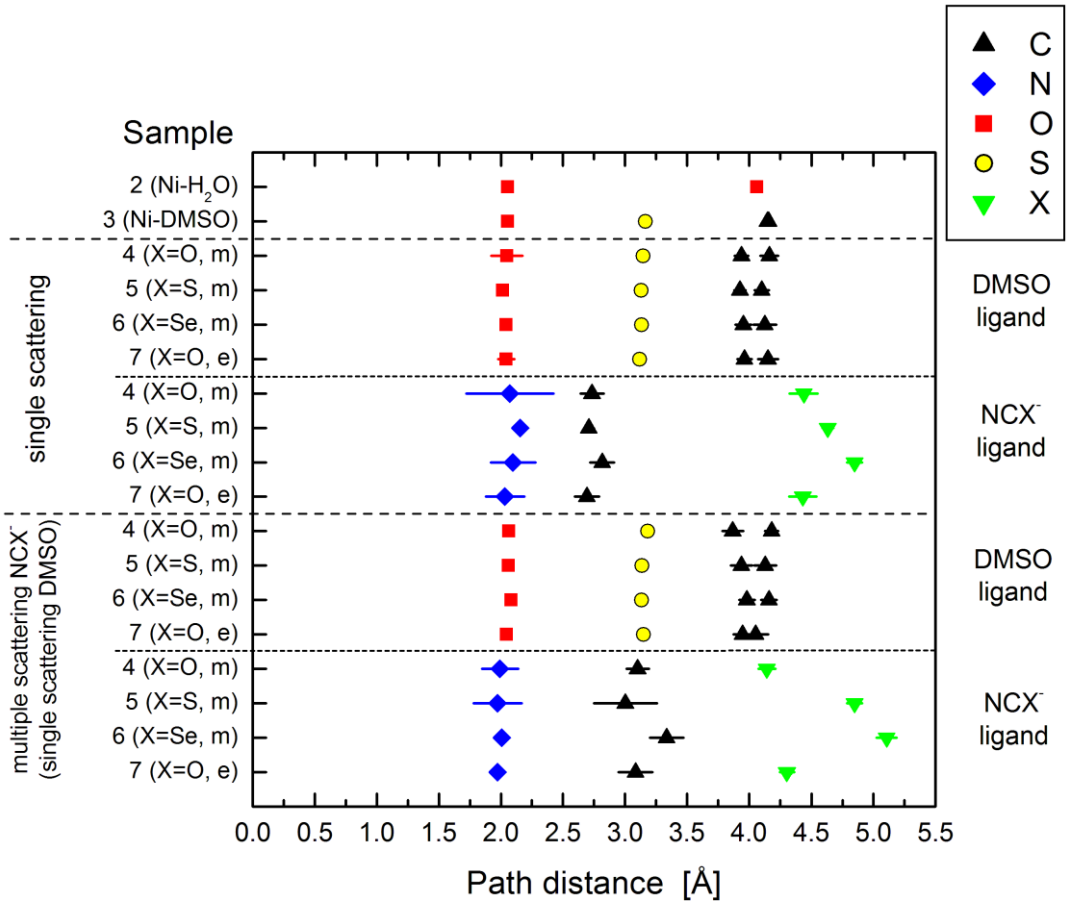

Figure 4.10: Graphical representation of path distances obtained from EXAFS fitting. Sample ID numbers have been described in the experimental section. 'm' = 2:1 NCX^-:Ni^{2+} model solutions, 'e' = electrochemically generated solution.

The overall co-ordination environment can be ascertained by considering the various amp (S_0^2) parameters. If the assumption is that the co-ordination numbers of the Ni^{2+} in H_2O and Ni^{2+} in DMSO liquid standards are both 6, then it is possible to obtain the co-ordination numbers for both types of ligands in the $[Ni(NCX)_x(DMSO)_{6-x}]^{(2-x)+}]$ complex ions, i.e. to determine N(DMSO) and $N(NCX^-)$. These values are given in Table 4.3.

Table 4.3: Extraction of co-ordination numbers for samples from fits with single scattering paths for DMSO and multiple scattering paths for NCX^-.

Sample	N (DMSO)	N (NCX^-)	Total N
4 (Model Ni-NCO)	4.3 ± 0.4	0.8 ± 0.4	5.0 ± 0.8
5 (Model Ni-NCS) [a]	4.8 ± 1.5	0.9 ± 0.8	5.7 ± 2.3
6 (Model Ni-NCSe)	4.2 ± 0.5	1.9 ± 0.8	6.1 ± 1.3
7 (Echem Ni-NCO)	3.7 ±0.3	0.9 ± 0.2	4.6 ± 0.5

[a] Based on Ni-O path from DMSO only, since the uncertainties on amplitude for the Ni-S and Ni-C paths were large (~50%).

The average co-ordination numbers obtained from the model including multiple-scattering NCX^- paths showed 6-co-ordinate Ni for $NCSe^-$ and NCS^-, and 5-co-ordinate Ni for NCO^-.

Hence there is a mixture of 4 and 6 coordinate species present in both the electrochemically generated solution and the model solution so that the EXAFS/XANES method effectively is sensing on average a 5-coordinate species based on the calculated N numbers. This also accounts for the different features observed for Ni-NCO XANES compared to the other, octahedrally co-ordinated, Ni-NCS and Ni-NCSe samples and standards. It is strongly believed that the "6 coordinate" species is $[Ni(DMSO)_6]^{2+}$ because the N values for DMSO in the "average" 5 coordinate complex are weighted toward the DMSO ligand.

An X-ray absorption spectroscopy investigation of the coordination environment of electrogenerated Ni(II)-pseudohalide complexes arising from the anodic polarization of Ni electrodes in DMSO solution of NCO^-, NCS^-, and $NCSe^-$ ions. In the EXAFS studies two structural models were used to fit the data and hence gain information on the coordinative environment around Ni(II) in the model and electrogenerated solutions. One was using the single scattering path and second was the multiple scattering path. It is important to include multiple scattering path in the EXAFS fitting for the linear NCX^- ligand.

Chapter 5

Anodically polarised copper electrodes in DMSO and DMF solutions of pseudohalide ions: A combined IR spectroelectrochemical and XANES study.

5.1 Introduction

The electrochemistry of metal electrode/pseudohalide systems has often been of interest in past work. Though there have been numerous studies on the adsorption and oxidation of pseudohalide ions on copper electrode in alkaline solution, only a few studies on the electrochemical processes occurring in copper-pseudohalide in the polar aprotic solvents have been published until now. This is surprising given the large number of organic systems used in technology [91]. For instance, even though copper in DMF is of wide use in industry, electrochemical studies of copper in DMF are not extensive. It has also been of interest to find new ways to electrodeposit copper from non-aqueous solutions [92]. Previous work by Bowmaker et al [93, 94] and Kilmartin et al [49, 50] have looked at thiocyanate interaction with copper anodes and platinum electrodes. Thiocyanate has often been used in electrochemistry with copper as it can mimic the behaviour of halide ions like chloride [49] which can seriously disrupt the passivation layer of oxide coatings formed on copper, thus increasing the corrosion rate. The benefit of using thiocyanate (and other pseudohalide ions) for the characterisation is that the presence of the –CN moiety allows detection by IR spectroscopy in a region of the spectrum where few other fundamental vibrations can be detected (2500-1800 cm^{-1}), thus allowing any speciation that occurs as a result of electrochemical processes to be followed. Given the scarcity of data on corrosion of copper in non-aqueous media, it is of interest to use a probe electrolyte like a pseudohalide ion which, because of the presence of the -CN group in the ion, will allow facile detection of species such as metal-pseudohalide complex ions that might form from anodic polarisation of the metal in the non-aqueous electrolyte containing pseudohalide ion. In addition, some highly useful information has also been provided by the use of synchrotron-based techniques such as X-ray (as a function of applied potential via the use of thin layer spectroelectrochemical cell) by IR spectroscopy and X-ray absorption near edge spectroscopy (XANES).

Further, this study may assist in understanding better the electrochemical behaviour in the solvents used (DMF or DMSO) which are of interest in various chemical industries [59-61] but also in the area of electrowinning and refining of metals using the electrolyte solutions in these solvents [95]. They may also allow comparisons of chemical behaviour between aqueous based and non-aqueous based electrolytes. In particular, the electrochemical characterisation of metal electrode action (e.g. corrosion etc) in non-aqueous (organic) media has been lacking.

The aim of this work is, therefore, to study using SNIFTIRS the anodic polarization of copper electrodes in DMSO or DMF solutions of pseudohalide (NCO^-, NCS^-, $NCSe^-$) ions using tetrabutylammonium perchlorate as the supporting electrolyte. In addition, some useful information has been provided by the use of synchrotron-based techniques such as X-ray absorption near edge spectroscopy (XANES) of the cell solutions containing electrogenerated products and the model solutions prepared that mimic these species independently of the electrolysis process undertaken when conducting in situ IR investigations.

5.2 Experimental

5.2.1 Reagents and Solutions

Solvents: DMSO, DMF, pseudohalide salts and TBAP used in experiments same as described in chapter 3. XAS standards (Cu_2O and CuO powders, Cu foil) were obtained either from Aldrich Chemical Co, Ltd. or BDH Chemicals and were used as received. Cu(I) and Cu(II) salts were used to prepare model solutions in DMSO and DMF. Cupric chloride ($CuCl_2.2H_2O$, Anal-R grade BDH chemicals) which contained waters of crystallisation was partially dehydrated in an oven at 50°C for 2-3 hours. This led to the originally blue salt turning a brown colour after heating. Not all water was removed as confirmed by spectroscopic analysis, however this was not believed to affect results obtained to any great extent. The model solutions involving $CuCl_2$ were made by mixing partially dehydrated $CuCl_2$ and pseudohalide salts in various $CuCl_2$:pseudohalide salt mole ratios (from 1:1 to 1:8 depending on the combination of $CuCl_2$ and pseudohalide salts and solvent used) to verify species detected in electrochemical experiments. Another set of model solutions was made by mixing CuI (Ajax Chemicals Ltd. Australia) and

pseudohalide salts in mole ratios (CuI : pseudohalide salt) of 1:1, 1:2 and 1:4 in DMSO and 1:1 and 1:2 only in DMF (due to solubility issues of the pseudohalide salt in DMF).

5.2.2 Spectroelectrochemical cell and electrode cell design

The working electrode was a flat, circular polycrystalline piece of copper (Aldrich, 99.98% purity) of 7 mm in diameter. The construction of this electrode has been described in chapter 3. The thin layer IR spectroelectrochemical cell employed in this study is as described and illustrated in chapter 3.2.3 with an expected thickness of the thin layer being determined to be *ca.* 1.31 μm. The thin layer cell was placed on top of a fixed angle (30°) Spectra Tech FT-30 specular reflectance accessory as has been used in chapter 3.

5.2.3 Instrumentation (IR spectroelectrochemistry)

Cyclic voltammetry was carried out on all systems studied using an EDAQ computer-interfaced potentiostat system which was controlled by Echem software as described in chapter 3. Reference electrodes and counter electrodes were identical as described in earlier studies involving anodic dissolution of Ni in DMSO and DMF (chapter 3). When systems were initially voltametrically characterized, a single sweep from -800 mV to +2000 mV(AgCl/Ag) was performed. Subtractively normalized interfacial Fourier transform infrared spectra (SNIFTIRS) were obtained on a dry N_2-purged Biorad FTS-40 FTIR spectrometer using liquid N_2-cooled InSb detectors as described in chapter 3. Using a procedure as described in chapter 3, the SNIFTIRS spectra were acquired by recording a background spectrum of the thin-layer cell at -900 to -1500 mV(AgCl/Ag) (depending on the system under study). IR spectra were then recorded at potentials more anodic than the chosen background potential and were ratioed against the background spectrum to yield a SNIFTIRS spectrum. As in chapter 3, current potential data collected at the same time as the actual SNIFTIRS experiment was acquired by calculating the average current drawn during the experiment. These data were hence regarded as “slow”, “single sweep” voltammograms of the Cu/pseudohalide systems.

IR transmission spectra of model solutions and other confirmatory solution preparation experiments were acquired as thin layers in conventional Press-Lok™ cells on a Perkin-Elmer Spotlight 200 FTIR instrument.

5.2.4 XANES

X-ray absorption near edge spectroscopy (XANES) measurements were performed on the XAS beamline at the Australian Synchrotron (Melbourne, Australia). Extended X-ray absorption fine structure (EXAFS) was also attempted but due to severe beam damage did not yield usable data. XANES results were also subject to beam damage during acquisition. To assess the extent of beam damage, multiple XANES scans were collected and the first was used for analysis. To measure XANES, liquid samples were mounted in a custom made Perspex cell which has been described previously (chapter 4) which was fabricated by affixing Kapton^{TM} tape to both sides of a conventional solid pellet holder. The liquid-filled holder was then quickly frozen by immersion in liquid nitrogen and the XANES measured in a cryostat at 77 K to avoid the formation of bubbles due to ionisation of the solution by the X-ray beam. The nominal beam size at the sample was 2 x 0.5 mm (horizontal x vertical height). XANES spectra were recorded in fluorescence mode at the Cu K-edge (8979 eV) using a Canberra 100-element Ge detector. Solid standards (Cu foil, Cu_2O, CuO) were measured in transmission mode by mixing the powdered oxide samples in cellulose powder. Liquid standard solutions were prepared as nominally 0.05 mol L^{-1} solutions of the partially dried cupric chloride in distilled water and in neat DMSO solvent respectively.

The following samples were measured:

Sample 1: CuO, powder standard

Sample 2: Cu_2O powder

Sample 3: $CuCl_2$ dissolved in DMSO, liquid standard

Sample 4-7: $CuCl_2$/ KOCN dissolved in DMSO solvent (with mole ratios of Cu^{2+}:NCO^- of 1:1, 1:2, and 1:4 (model solutions) and cell solution from Cu electrode/KOCN electrochemical system after polarising at +500 mV (AgCl/Ag) in the thin layer cell.

Sample 8-11: $CuCl_2$/ KSCN dissolved in DMSO solvent (with mole ratios of Cu^{2+}:NCS^- of 1:1, 1:4 (model solutions) and 2 cell solutions from the Cu electrode/KSCN electrochemical system after polarising at (i) +200 mV (AgCl/Ag) for 2-3 hours and at (ii) +1000 mV (AgCl/Ag) for 2-3 hours in the thin-layer cell.

Sample 12-14: $CuCl_2$/KSeCN dissolved in DMSO solvent (with mole ratios of Cu^{2+}:$NCSe^-$ of 1:1, 1:4 (model solutions) and 1 cell solution from the Cu electrode/KSeCN electrochemical system after polarising at +400 mV(AgCl/Ag) for 2-3 hours in the thin-layer.

5.3 Results and discussion

5.3.1 Cu/NCO^- systems

5.3.1.1 Cyclic voltammetric investigations

The cyclic voltammogram (CV) of the copper electrode in DMF and DMSO solvents containing 0.025 mol L^{-1} KOCN and 0.1 mol L^{-1} TBAP recorded under the thin-layer condition as an inert supporting electrolyte are shown in Figure 5.1(a) and Figure 5.1(b). The voltage was adjusted between -800 mV(AgCl/Ag) and +2000 mV(AgCl/Ag), this range being used for all electrochemical systems studied. The CVs for the Cu/NCO^- electrochemical systems in both DMF and DMSO showed a largely unremarkable region (feature-wise) from -800 mV(AgCl/Ag) to +0 mV(AgCl/Ag) (see arrows in Figure 5.1(a) and Figure 5.1(b)) but there was not a true flatline of current observed in any one potential. The current was either a nett positive or negative current being observed, with the common trend that it became increasingly positive as the applied potential was made more anodic at the electrode. The CVs showed the general trend that after +0 mV(AgCl/Ag), an increase in (positive) current was observed which was interpreted as being due to the oxidation of Cu and other concurrent processes such as solvent oxidation, pseudohalide ion oxidation and film formation. In the CVs, it can be seen that the current increases monotonically with applied potential > 0 mV(AgCl/Ag) until the voltage reversed at +2000 mV at which point it decreased back to the baseline current. No apparent reduction feature was observed in the CVs of all systems which would indicate that the oxidation of copper was irreversible and that the species have been released from the electrode surface into the thin solution layer. The lack of specific detail in the CV traces of this system makes it a highly suitable candidate for analysis by in situ IR spectroscopy especially in terms of obtaining more molecular information on the system.

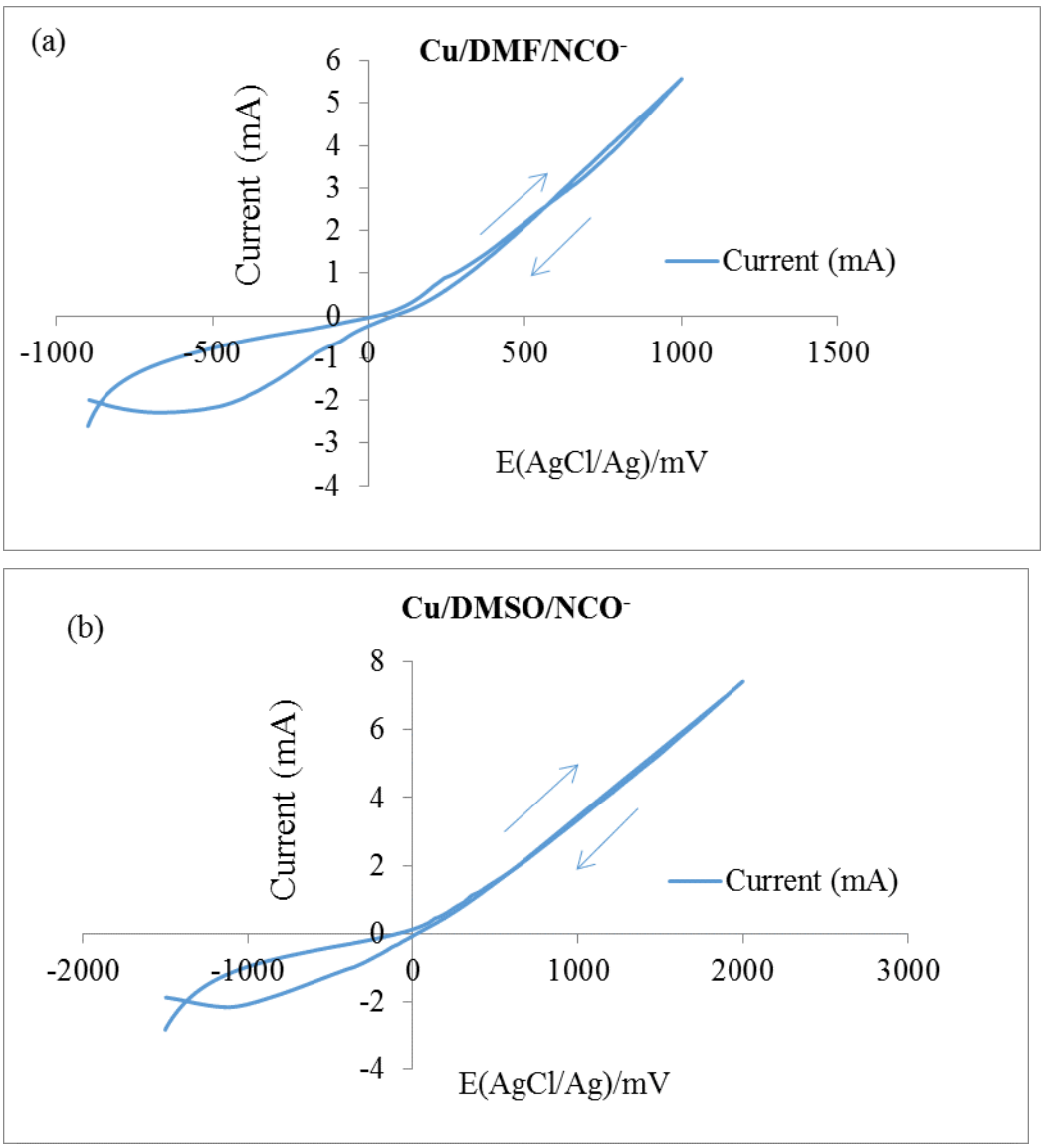

Figure 5.1: Cyclic voltammograms of the copper electrode in DMF and DMSO solvents containing pseudohalide ions and 0.1 mol L^{-1} TBAP in the thin layer cell (sweep rate = 20 mV/s): (a) 0.025 mol L^{-1} KOCN in DMF, (b) 0.025 mol L^{-1} KOCN in DMSO

5.3.1.2 IR spectra of Cu/TBAP/NCO^-/DMF and DMSO

Figure 5.2(a) and Figure 5.2(b) present a series of IR spectroelectrochemical (SNIFTIRS) spectra that were recorded of the copper electrode using 0.025 mol L^{-1} KOCN and 0.1 mol L^{-1} tetrabutylammonium perchlorate (TBAP) in the polar aprotic solvents (DMF or DMSO). Figure 5.3(a) and Figure 5.3(b) present the single-sweep voltammogram that shows the average current at each applied potential in the thin layer cell during the SNIFTIRS experiment. Figure 5.4(a) and Figure 5.4(b) show the plots of the intensity changes of SNIFTIRS peaks observed in the Cu/TBAP/NCO^-/DMF or DMSO system as a function of applied potential.

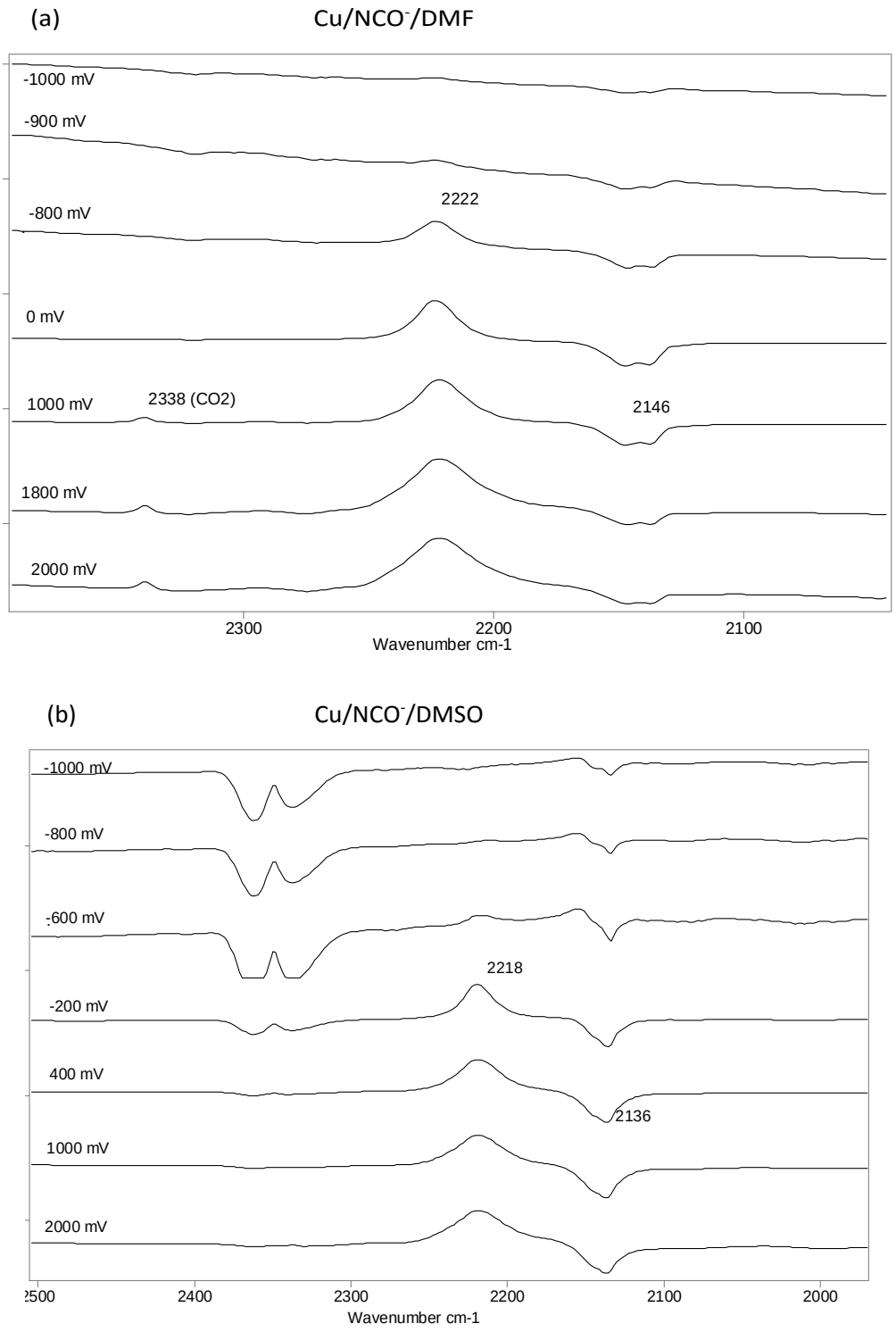

Figure 5.2: Series of SNIFTIRS spectra of the copper electrode as a function of applied potential in DMF and DMSO solvents containing pseudohalide ions and 0.1 mol L^{-1} TBAP in the thin layer cell. (a) 0.025 mol L^{-1} KOCN in DMF, (b) 0.025 mol L^{-1} KOCN in DMSO

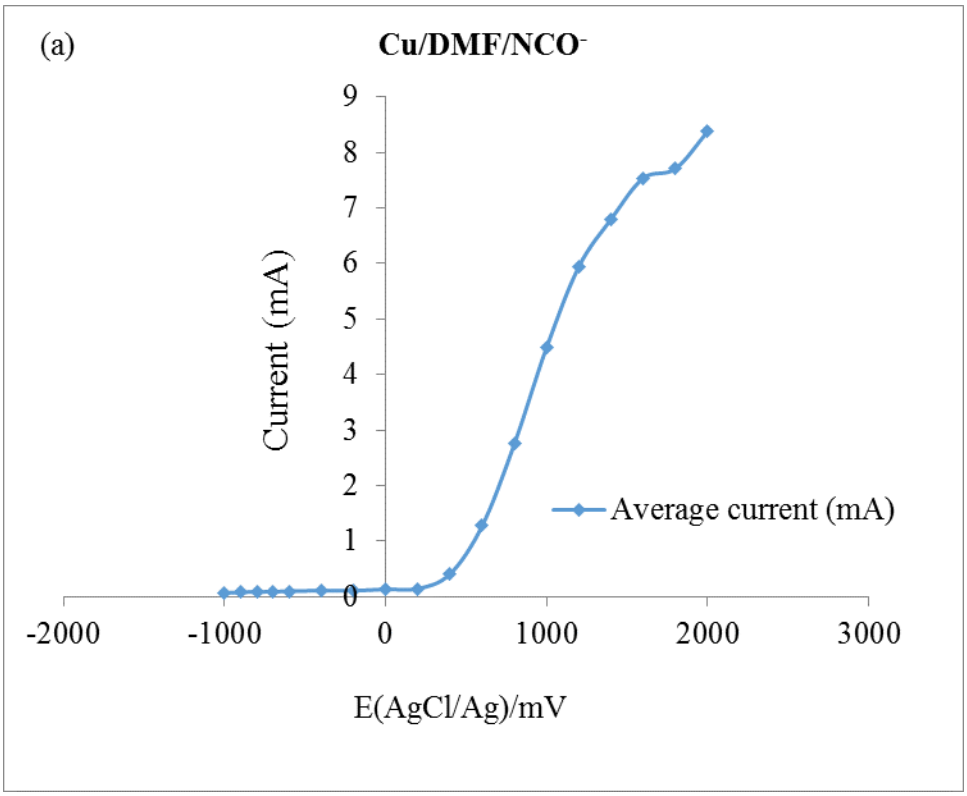

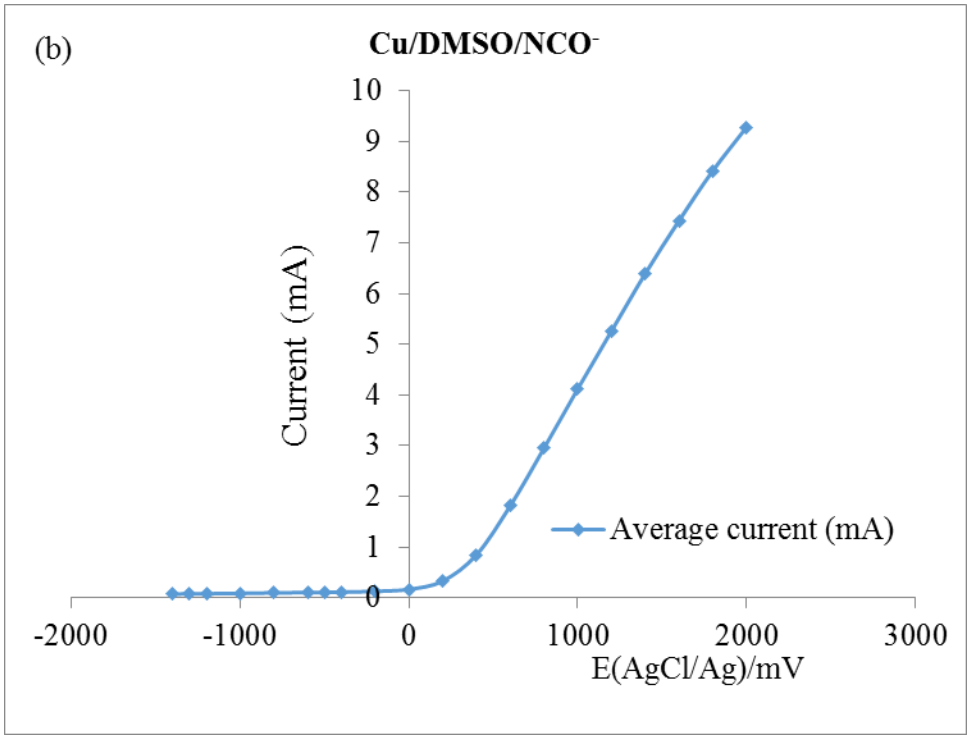

Figure 5.3: Single sweep voltammograms acquired of the copper electrodes during a SNIFTIRS experiment in DMF and DMSO solvents containing pseudohalide ions and 0.1 mol L^{-1} TBAP in the thin layer cell: Data were obtained from calculating the average current at the beginning and end of the spectral acquisition period for each applied potential at which SNIFTIRS spectra were acquired. (a) Cu electrode and 0.025 mol L^{-1} $KOCN^-$ in DMF, (b) Cu electrode and 0.05 mol L^{-1} KOCN in DMSO.

Table 5.1: FTIR data from in situ IR spectroelectrochemical studies of Cu/NCX^- systems electrochemically polarised in 0.1 mol L^{-1} TBAP in DMSO or DMF solvents

Electrolytes	ν(CN) of free NCX^- ion (X = O, S, Se,) cm^{-1}	ν(CN) of Cu^+/ NCX^- complex ion cm^{-1}	ν(CO) of CO_2 dissolved in solvent cm^{-1}	Colour of cell solution after SNIFTIRS experiment
Cu/DMF/NCO^-	2136	2220	2338	light green
Cu/DMF/NCS^-	2055	2087, 2173	2338	red
Cu/DMF/$NCSe^-$	2066	2087, 2140	nd	gold yellow
Cu/DMSO/NCO^-	2136	2218	nd	light green
Cu/DMSO/NCS^-	2055	2087, 2171	nd	red-yellow
Cu/DMSO/$NCSe^-$	2065	2089, 2138	nd	gold yellow

nd=not detected

Table 5.1 (which summarises the in situ IR spectroelectrochemical data obtained from all the systems studied in this investigation) describes the data of relevance to the Cu/NCO^- systems.

The single-sweep voltammograms for the Cu/NCO^- systems in DMSO and DMF have similar features, i.e. a flatline (almost zero current) at cathodic potentials and an increasing current the applied potential is adjusted above +500 mV(AgCl/Ag). Although "zero current" profiles were observed in the single sweep voltammograms, it was still apparent from spectral features observed in the in situ IR spectra recorded (see Figure 5.2(a) and Figure 5.2(b)), that anodic-type processes involving the oxidation of Cu were occurring in both solvent systems. Firstly the detection of negative going peaks (as observed at 2136 cm^{-1} in Figure 5.2(a) and (b) and attributed to free NCO^- ion) indicated that there was less cyanate ion present at the applied potential of interest relative to the potential at which the background spectrum was recorded i.e. -1100 mV (AgCl/Ag). Secondly in Figure 5.2(a) and (b), a weak broad peak at 2220 cm^{-1} began to emerge. This peak has been assigned to a copper cyanate complex ion in solution and is believed to be $[Cu(NCO)_2]^-$, a Cu(I) complex ion species. No specific IR data exists on this assigned species in the literature. The following authors discuss spectroscopic data from Cu(II) cyanate species. Forster and Goodgame [96] have reported that nujol mull IR spectra of $(Et_4N)_2Cu(NCO)_4$ salts have ν(CN) stretching frequencies at 2183 cm^{-1} (strong) with a shoulder peak at 2247 cm^{-1}. Melendres et al. [97] had assigned a peak observed at 2234 cm^{-1} in the in situ IR spectra of a Cu electrode in 0.0001 M KOCN and 0.1 M $NaClO_4$ solution at -0.25 V (SCE) to "a few monolayers of $Cu(OCN)_2$". An interesting recent study

by Ray et al. [98] reported crystallographic, electrochemical, and IR data on an end-on-end bridged Cu I-II/cyanate compound, $[Cu_2L_2Na(NCO)_2Cu]^n$ where L = N,N' bis (2hydroxyacetophenone propylenediimmine) which gave a ν(CN) stretch of 2228 cm^{-1} in IR spectra. This is the closest frequency to what is observed in the in situ IR spectra of the Cu/NCO^- system in the present study so is the strongest literature evidence that the 2220 cm^{-1} peak is a Cu(I) complex.

Other experimental evidence collected from the present study also suggested that this peak was due to a Cu(I) solution species. IR transmission spectra were collected of the cell solution from the Cu/NCO^-/DMSO electrochemical system after performing an anodic polarisation (without the involvement of in situ IR spectroscopy) by keeping the Cu electrode at an initial potential of -800 mV(AgCl/Ag) for one hour, extracting the electrolyte and recording IR transmission spectra. The IR transmission spectrum showed two features at 2220 cm^{-1} and 2136 cm^{-1} due to the Cu-cyanate complex ion species and free cyanate in DMSO. (see Appendix 6, Figure S.12).This constituted experimental proof of the Cu(I) species existing in solution.

This uncertainty of assignment was the reason for performing further analysis on the cell solutions (and model solutions to be discussed) to clarify the identity of this species. The XANES study of the electrogenerated cell solution and comparison with XANES of model solutions prepared from mixing Cu(II) and cyanate solutions (together with more infrared data) provided convincing evidence that the species being observed in the in situ IR spectra were more likely to be Cu(I) cyanate complexes as opposed to Cu(II).

Another minor feature observed in the Cu/NCO^- systems in DMSO and DMF (and also observed in previously studied Ni/NCO^-/DMF or DMSO electrochemical systems) was a weak peak at 2338 cm^{-1}. This was observed to appear at very positive potentials i.e. at potentials > +1000 mV (AgCl/Ag), and was attributed to electrogenerated, dissolved CO_2 in the DMF solvent. This would have formed from oxidation of dissolved cyanate in the electrolyte medium.

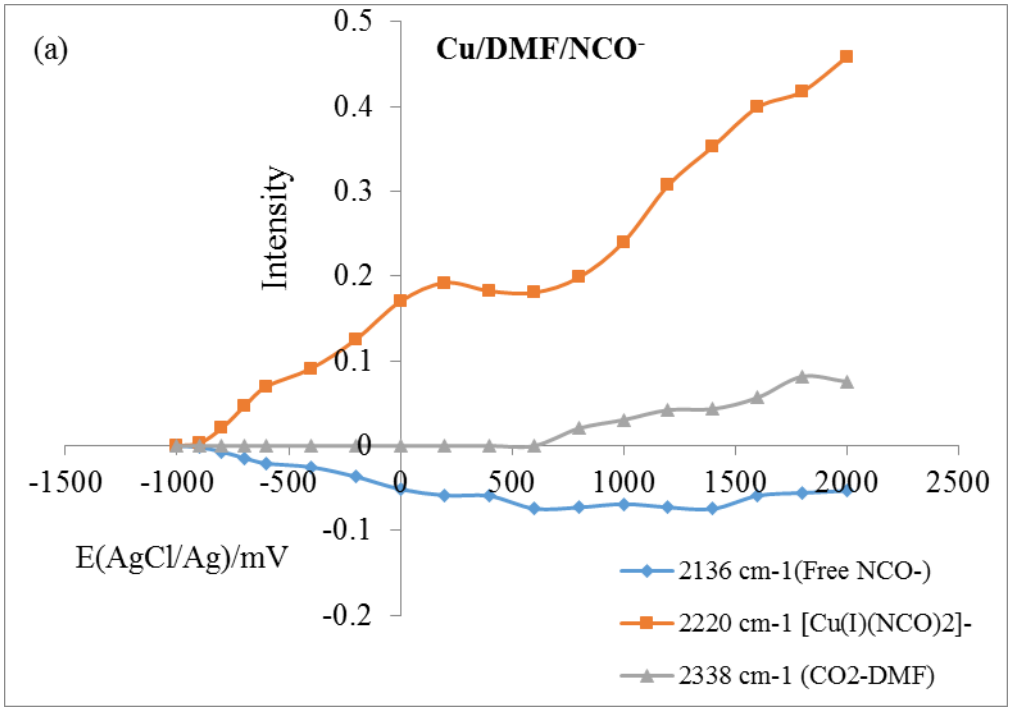

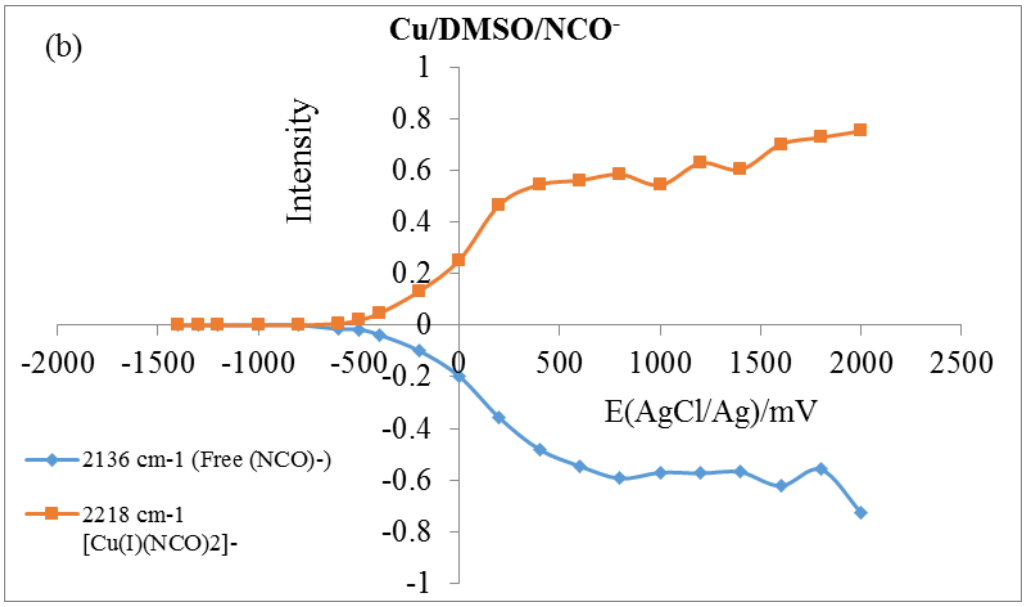

Figure 5.4: Plots of the intensity changes of the various molecular species generated in the thin layer during electrochemical polarisation and observed in the SNIFTIRS spectra as a function of applied potential in the copper electrode as a function of applied potential in DMF and DMSO solvents containing pseudohalide ions and 0.1 mol L^{-1} TBAP in the thin layer cell. (a) 0.025 mol L^{-1} KOCN in DMF, (b) 0.025 mol L^{-1} KOCN in DMSO.

Further information on the species detected above was provided by examination of Figure 5.4(a) and (b) which summarise intensity trends of species observed in the in situ IR spectra as a function of applied potential. In these, negative intensity trends reflect the consumption of the free cyanate ion species giving rise to the (negative-going) peak at 2136 cm^{-1} due to the free cyanate ion in the solvents used. This indicates there is more of the free ion present in the thin layer recorded at the background potential of -1100 mV(AgCl/Ag) (DMF) or -1500 mV(AgCl/Ag) (DMSO) as already stated. The increasingly negative intensity observed for the free ion at more anodic potentials, shows the demand of the Cu interface for free cyanate ion in forming the Cu(I) cyanate complex ions (this agrees with the increasing intensity observed at 2218-2220 cm^{-1}) and for the production of CO_2 from electro-oxidation of the cyanate ion. The single sweep voltammograms (see Figure 5.3(a) and (b)) support this by indicating a monotonically increasing current for the Cu/DMSO/NCO^- system on applying potentials >0.00 mV(AgCl/Ag) with the same being observed for the Cu/DMF/NCO^- system which would correspond to release of Cu as "Cu^+" and its combination with cyanate ion to form Cu(I) cyanate complexes and electro oxidation of cyanate to form CO_2. These represent the extent of detectable species and their behaviour as a function of applied potential in these systems.

5.3.1.3 Cu/NCO^-/DMF or DMSO model solutions

The model solutions were made by combining either solutions of cupric chloride (containing Cu^{2+}) or cuprous iodide (containing Cu^+) with pseudohalide salts in various Cu: pseudohalide salt mole ratios (1:1 to 1:4 depending on the solvent used). They were carried out to lend support to assignments made in in situ IR spectra as summarised above. Table 5.2 (for solutions of cupric chloride and pseudohalide salts) and Table 5.3 (for solutions of cuprous iodide and pseudohalide salts) summarise all the IR spectroscopic data and physical observations of solution colour made from the model solution systems. The reason for preparing model solutions for both Cu(I) and Cu(II) systems was to determine what the possible frequencies were for cyanate complexes with both oxidation states of Cu.

Table 5.2 shows that when copper (II) chloride/ potassium cyanate solutions in DMSO or DMF are prepared in Cu^{2+}: NCO^- mole ratios from 1:1 to 1:4 (DMF) or

to 1:8 (DMSO), peaks in the ν(CN) stretching region are detected. In DMF and in DMSO a peak at 2136 cm^{-1} is detected which is the typical vibrational peak exhibited by free cyanate ion in the DMSO and DMF solvents. The 2136 cm^{-1} feature did not appear in the 1:1 and 1:2 mole ratio spectra of the model solution series but did appear in the 1:4 and 1:8 mole ratio model solution spectra.

Table 5.2: FTIR data from IR studies of DMF or DMSO model solutions of $CuCl_2$ and potassium (or sodium) pseudohalide ion salts prepared with different mole ratios.

Model solution studied and mole ratio of ($CuCl_2$): NCX^- prepared in DMF or DMSO (X = O, S, Se)	ν(CN) of free NCX^- ion (X = O, S, Se) cm^{-1}	ν(CN) of Cu^{2+}/NCX^- complex ion cm^{-1}	Observed colour of solution
DMF			
$CuCl_2$/ KOCN 1:1	nd	2194	green
$CuCl_2$/ KOCN 1:2	nd	2194	green
$CuCl_2$/ KOCN 1:4	2136	2196	blue green
$CuCl_2$/ NaSCN 1:1	2056	2090	blood red
$CuCl_2$/ NaSCN 1:2	2056	2088	blood red
$CuCl_2$/ NaSCN 1:4	2056	2084	blood red
$CuCl_2$/ KSeCN 1:1	nd	nd	gold yellow
$CuCl_2$/ KSeCN 1:2	2065	2092	orange brown
$CuCl_2$/ KSeCN 1:4	2065	2089	orange brown
DMSO			
$CuCl_2$/ KOCN 1:1	nd	2115	green
$CuCl_2$/ KOCN 1:2	nd	2198	green
$CuCl_2$/ KOCN 1:4	2136	2196	blue
$CuCl_2$/ KOCN 1:8	2136	2196	blue
$CuCl_2$/ NaSCN 1:1	2055	2093	light red
$CuCl_2$/ NaSCN 1:2	2055	2093	red
$CuCl_2$/ NaSCN 1:4	2055	2090	blood red
$CuCl_2$/ NaSCN 1:8	2055	2089	blood red
$CuCl_2$/ KSeCN 1:1	2065	2096	gold yellow
$CuCl_2$/ KSeCN 1:2	2065	2096	gold yellow
$CuCl_2$/ KSeCN 1:4	2065	2096	orange brown
$CuCl_2$/ KSeCN 1:8	2065	2088	orange brown

nd=not detected

This most likely indicates its total complexation by copper ions in the model solutions as another feature observed in the 1:1 and 1:2 model solution spectra for this system was a peak at 2194 cm^{-1} which has been assigned to the a CN stretch for cyanate ligand complexed to a Cu(II) metal centre, i.e. $[Cu(II)(NCO)_4]^{2-}$ complex ion [99]. However, in comparison to the observations made in the in situ

IR spectra, the dominant solution species noted was instead a peak at 2220 cm^{-1}. Hence this cannot be due to a Cu(II) species coordinating to cyanate ligand and so must be due to a Cu(I) cyanate species. Indeed, this has been proven via XANES spectra of the cell solutions obtained after conclusion of the in situ IR spectroelectrochemical experiments for the Cu/NCO^- system as discussed further below. To prove this unequivocally, a Cu(I) salt, namely CuI, was directly dissolved in DMSO and DMF and made up to 1:1 to 1:4 CuI:pseudohalide salt mole ratio solutions and the IR spectra acquired. As shown in Table 5.3, a peak at 2220 cm^{-1} is clearly obtained which agrees well in position and in shape with that observed in the in situ IR spectra. This hence confirms the assignment of the peak to $[Cu(NCO)_2]^-$.

Table 5.3: FTIR data from IR studies of DMF or DMSO model solutions of CuI and potassium (or sodium) pseudohalide ion salts prepared with different mole ratios.

Model solution studied and mole ratio of (CuI): NCX^- prepared in DMF or DMSO (X = O, S, Se)	**ν(CN) of free NCX^- ion (X = O, S, Se) cm^{-1}**	**ν(CN) of Cu^+/NCX^- complex ion cm^{-1}**	**Observed colour of solution**
DMF			
CuI/ KOCN 1:1	nd	2220	green
CuI/ KOCN 1:2	nd	2220	light green
CuI/ NaSCN 1:1	nd	2089	green
CuI/ NaSCN 1:2	2056 sh	2088	colourless
CuI/ KSeCN 1:1	2065 sh	2088	orange brown
CuI/ KSeCN 1:2	2065 sh	2088	colourless
DMSO			
CuI/ KOCN 1:1	nd	2220	green
CuI/ KOCN 1:2	nd	2220	light green
CuI/ KOCN 1:4	2136, 2147	2220	colourless
CuI/ NaSCN 1:1	nd	2088	green
CuI/ NaSCN 1:2	2055 sh	2088	yellow/green
CuI/ NaSCN 1:4	2055 sh	2088	colourless
CuI/ KSeCN 1:1	2065 sh	2088	red brown
CuI/ KSeCN 1:2	2065 sh	2088	yellow
CuI/ KSeCN 1:4	2065 sh	2088	colourless

nd=not detected sh= shoulder

5.3.2 Cu/TBAP/NCS^-/DMF and DMSO

5.3.2.1 Cyclic voltammetric investigations

The cyclic voltammogram (CV) of the copper electrode in DMF and DMSO solvents containing 0.05 mol L^{-1} NCS^- and 0.1 mol L^{-1} TBAP is shown in Figure 5.5(a) and Figure 5.5(b). As observed with the Cu/NCO^- electrochemical systems, the CVs for this system were unremarkable but generally showed an increase in current as the applied voltage was adjusted to more anodic potentials. In the Cu/DMSO/NCS^- system, the CV showed some hysteresis which indicated a level of irreversibility in the systems. In the anodic region of the CV, concurrent processes such as metal and solvent oxidation could be jointly linked to the increase in current in this region.

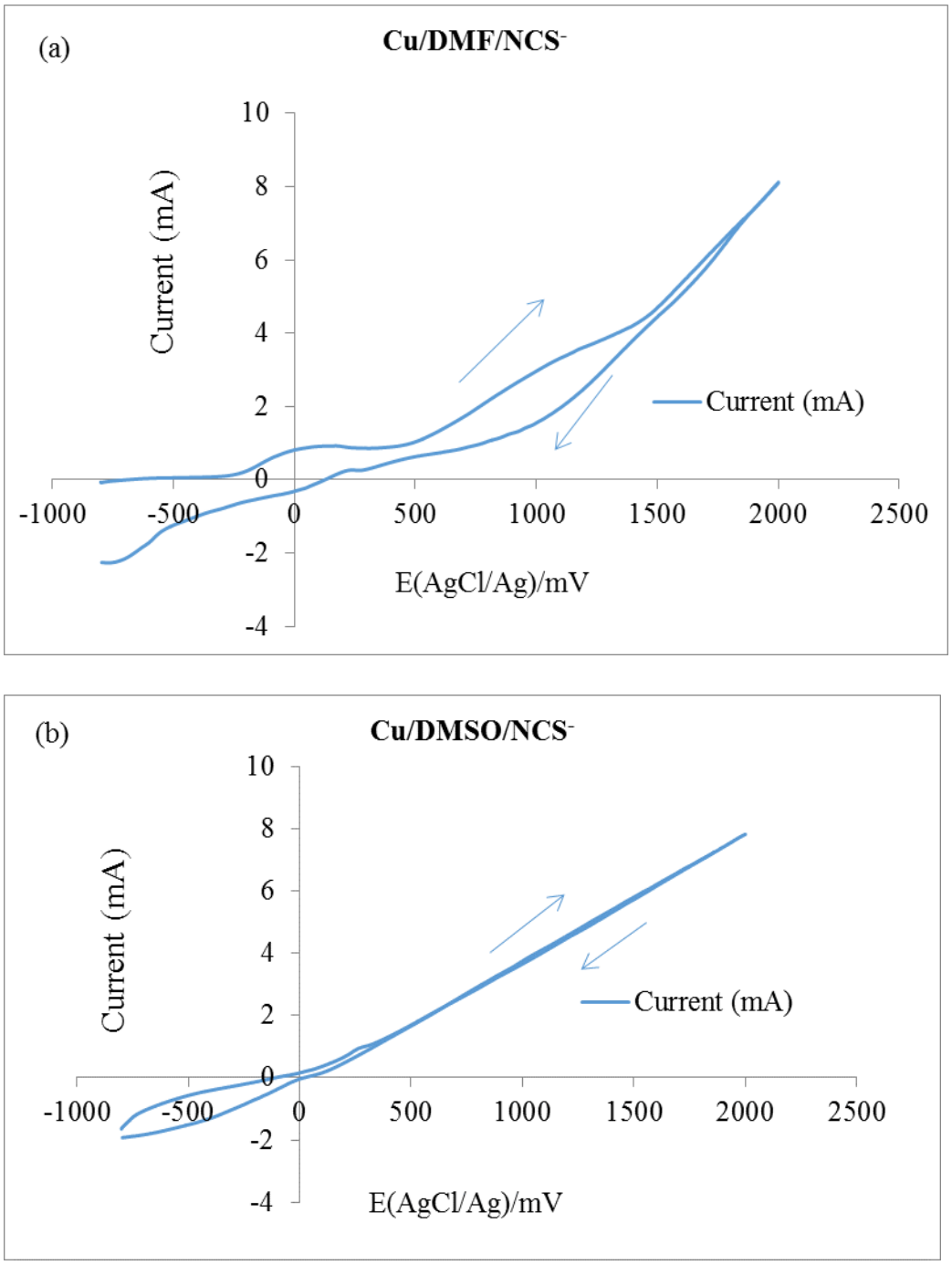

Figure 5.5: Cyclic voltammograms of the copper electrode in DMF and DMSO solvents containing pseudohalide ions and 0.1 mol L^{-1} TBAP in the thin layer cell (sweep rate = 20 mV/s): (a) 0.05 mol L^{-1} NaSCN in DMF, (b) 0.05 mol L^{-1} NaSCN in DMSO.

5.3.2.2 IR spectra of Cu/TBAP/NCS^-/DMF and DMSO

Figure 5.6(a) and Figure 5.6(b) show the series of SNIFTIRS spectra acquired as a function of applied potential at the copper electrode surface of the

Cu/NCS^-/TBAP/DMF and DMSO systems. Figure 5.7(a) and Figure 5.7(b) represent the single sweep voltammograms that shows the average current at each applied potential in the thin layer cell during the SNIFTIRS experiment. Figure 5.8(a) and Figure 5.8(b) represent the plot of the intensity changes of peaks observed in the Cu/TBAP/NCS^-/DMF or DMSO system as a function of applied potential. Table 5.1 summarises the in situ IR data from this system.

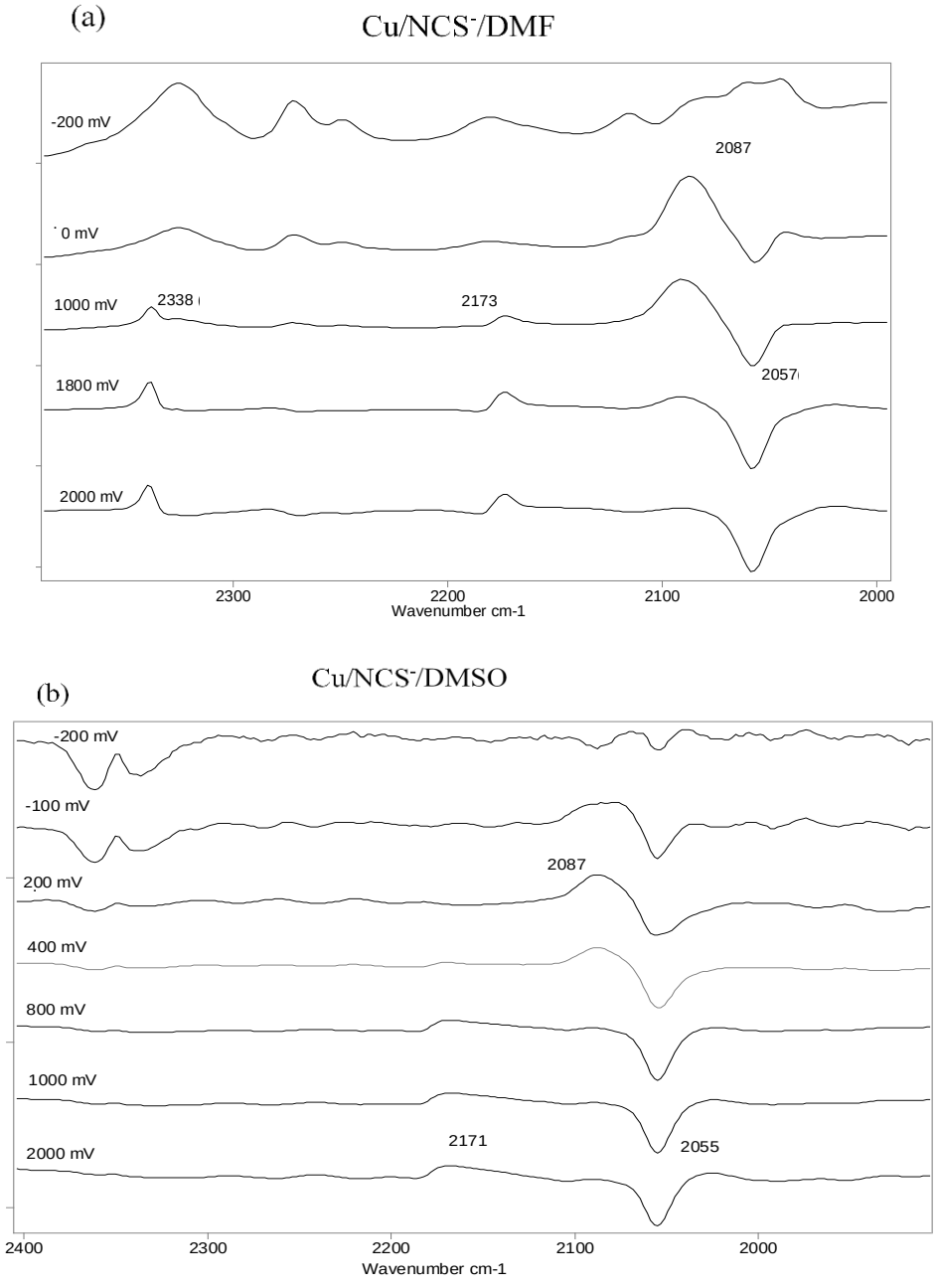

Figure 5.6: Series of SNIFTIRS spectra of the copper electrode as a function of applied potential in DMF and DMSO solvents containing pseudohalide ions and 0.1 mol L^{-1} TBAP in the thin layer cell. (a) 0.05 mol L^{-1} NaSCN in DMF, (b) 0.05 mol L^{-1} NaSCN in DMSO.

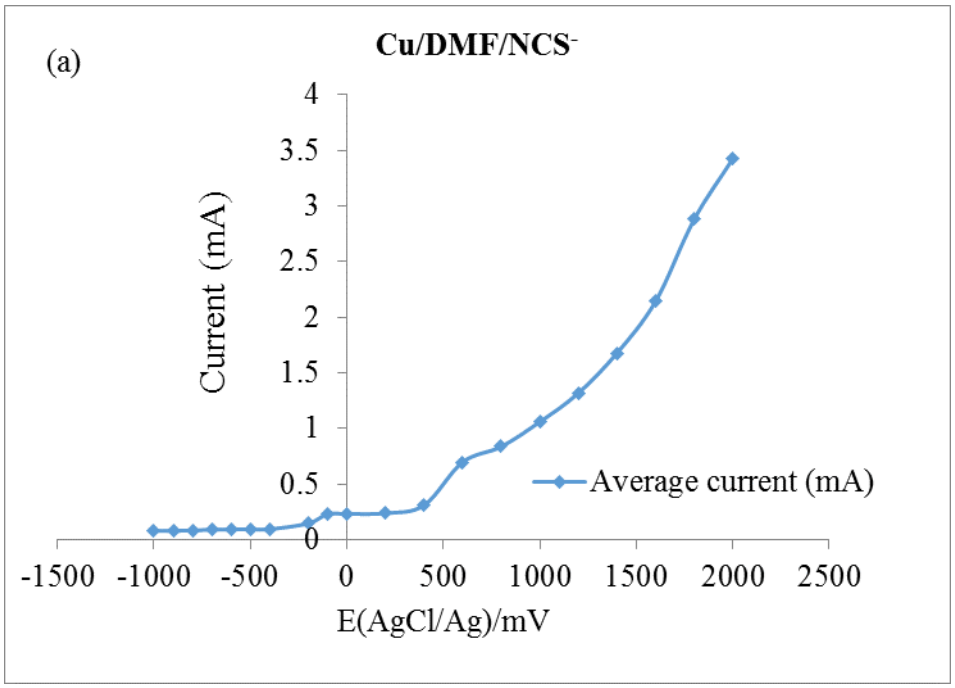

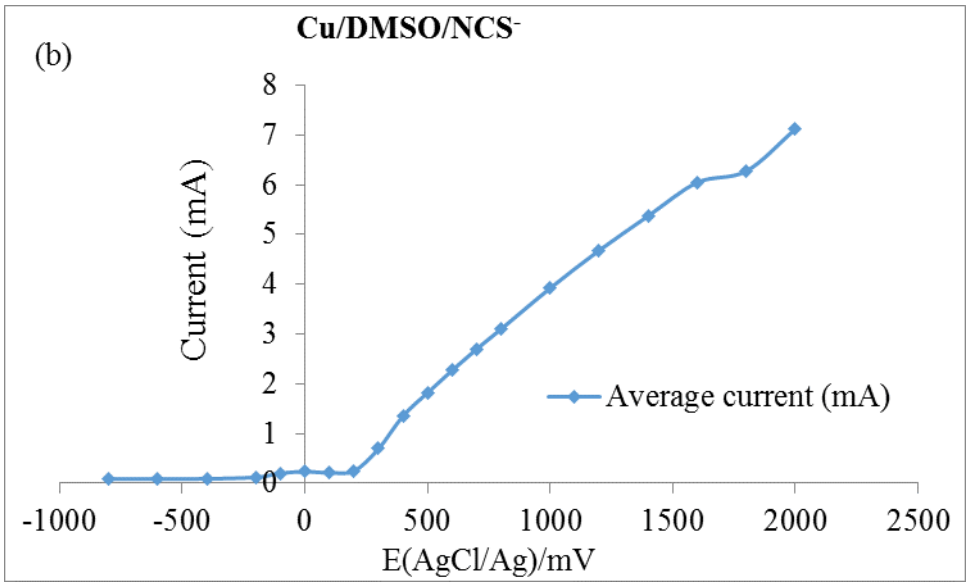

Figure 5.7: Single sweep voltammograms acquired of the copper electrodes during a SNIFTIRS experiment in DMF and DMSO solvents containing pseudohalide ions and 0.1 mol L^{-1} TBAP in the thin layer cell: Data were obtained from calculating the average current at the beginning and end of the spectral acquisition period for each applied potential at which SNIFTIRS spectra were acquired. (a) Cu electrode and 0.05 mol L^{-1} NaSCN in DMF, (b) Cu electrode and 0.05 mol L^{-1} NaSCN in DMSO.

At applied potentials between -100 mV and 0 mV(AgCl/Ag), peaks specific to the system (apart from weak solvent related peaks that appear in spectra more cathodic than -100 mV(AgCl/Ag)) appear. These consisted of a negative-going peak at 2055 cm^{-1} and a broad positive-going peak at 2087 cm^{-1}. The negative peak at 2055 cm^{-1} is due to free thiocyanate ion, as has been detected before in chapter 3 involving the corresponding Ni/NCS^-/DMSO or DMF systems studied by in situ IR spectroscopy. The peak at 2087 cm^{-1} has been subject to various interpretations in the chemical literature [94, 100, 101]. Forster and Goodgame reported IR data (run as nujol mulls) of some isothiocyanato complexes of Ni(II) and Cu(II) in 1965. IR spectra of a $(C_2H_5)_4NCu(NCS)_4$ salt prepared by these authors showed a strong ν(CN) stretching frequency at 2074 cm^{-1}. The solid was described as being either green or purple depending on the counter cation used to precipitate the solid [100] but which dissolves in nitromethane or acetone solutions to produce characteristic blood red solutions. In the present study, a red solution was observed to develop over the time in the thin layer cell while the in situ IR experiment was being conducted. Given literature reports, the colouration must be due to a complex of Cu^{2+} and NCS^- ion especially given the characteristic colour seen when Fe^{3+} complexes with NCS^- (which is used as a test of Fe^{3+} presence in solution and as an indicator of excess NCS^- in the Volhard Method [102]). The exact identity of the copper/thiocyanate species giving rise to the red colour in solution has been subject to various interpretations. Forster and Goodgame [100] only reported the IR spectrum of the solid as a nujol mull which gave a ν(CN) stretch which was slightly less (i.e. 2074 cm^{-1}) than the one detected in the in situ IR spectra in the present study (which is at 2087 cm^{-1}). While reporting that the solid dissolves in organic solvents to produce a red solution, they did not report an IR spectrum of this red solution. However, Rannou et al. [101] who studied the dissolution of "CuSCN" solutions in various polar aprotic solvents (including DMSO) and who used IR spectroscopy to probe the vibrational spectra of dissolved copper/thiocyanate species in these systems reported a peak at 2089 cm^{-1} for saturated (~10^{-2} mol L^{-1}) solutions of CuSCN in DMSO which they assigned to a copper-isothiocyanate ion-pair "Cu^+NCS^-" because it was thought that the Cu^+ ion would be poorly solvated by oxygen donors provided by these solvents. However, work done in the present study involving model solutions disputes that earlier judgement by Rannou and it is believed that the situation is a little more complex than that. It was found that

when model solutions (see later) prepared from mixing cupric chloride and NCS^- in DMSO or DMF were prepared in a 1:1 to 1:8 mole ratio for Cu^{2+}:DMSO (and 1:1 to 1:4 for Cu^{2+}:DMF), red to intense red solutions were invariably observed to form and the transmission IR spectra featured a peak over the 2084-2093 cm^{-1} range which includes the 2089 cm^{-1} value reported by Rannou et al. [101] as discussed earlier. It was observed however that these peaks were very broad in nature suggesting that there may be a mixture of different oxidation state copper-thiocyanate complex ions present which have similar ν(CN) stretching frequencies. Indeed, later work reported by Bowmaker et al. [94] supports this suggestion. In Bowmaker et al's study, complexes of $[AsPh_4]M(SCN)_2$ and $N(PPh_3)_2[M(SCN)_2]$ (M=Cu(I) or Au(I)) were prepared and characterised by IR spectroscopy as nujol mulls and when dissolved in tributylphosphate solvent. In the nujol mull (solid state) spectra, two strong peaks were observed for the compounds at 2105-2109 and 2084 cm^{-1} due to ν(CN) stretching in the compounds however, in solutions of the compounds in tributyl phosphate, only one peak centred at 2085 cm^{-1} was observed which is very similar to the peak observed at 2087 cm^{-1} in the Cu/NCS^-/DMF or DMSO systems in the present study (see Figure 5.6(a) and (b)). Bowmaker et al attributed this peak to the discrete complex ion species $[Cu(SCN)_2]^-$ and it is believed that part of the in situ IR spectral peak observed at this frequency is due to that discrete Cu(I) thiocyanate complex ion. However, the red colour being observed in the cell solution after the in situ IR experiment cannot be attributed to a Cu(I) thiocyanate complex which is known to be colourless (see later for evidence) but must be due to the additional presence of Cu(II) thiocyanate complexes to which this red colour has been normally attributed in earlier studies [103].

Examination of Figure 5.6(a) and (b) reveal another weak, broad peak which is centred at ca. 2173 cm^{-1} (in systems with DMF) and 2170 cm^{-1} (in systems with DMSO) respectively. This peak at 2169-2173 cm^{-1} is believed to be due to the same species, namely a solid film on the Cu electrode. The nature of this film in the present study is uncertain but is believed, on the basis of previous reports, to be due to a solid "CuSCN" species. Kilmartin et al. [49] studied the mechanism of formation of electrochemically deposited copper thiocyanate films on a copper anode. In general, they had observed three ν(CN) stretching peaks in their Raman spectra of the electrode at different times. A peak at 2175 cm^{-1} was the first to

appear and persisted in the applied potential regions of the electrode where primary-film and secondary film regions existed on the electrode. This peak was observed to dominate in Kilmartin's spectra though was found to quickly disappear on reduction and was replaced by smaller peaks at 2165 and 2157 cm^{-1} which were similar to those observed in an IR spectrum of a discrete solid CuSCN sample (peaks at 435, 743, 2165 and 2154 cm^{-1} observed) [49] Kilmartin commented that the peak at 2175 cm^{-1} which was dominant in Raman spectra obtained from the Cu electrode surface was due to the underlying CuSCN barrier film while other peaks observed at 2165 and 2157 cm^{-1} were due to loosely held solid on top of the barrier film which would have been more akin to free crystalline solid CuSCN. On the basis of this study (which has the strongest correlation to the present study of in situ IR studies of anodically polarised copper electrodes in DMF and DMSO), the 2173 cm^{-1} peak observed can therefore be assigned with reasonable confidence to a CuSCN film on the Cu electrode. No evidence of peaks at 2165 and 2157 cm^{-1} (which might appear as a broadening on the low wavenumber end of the peak at 2173 cm^{-1}) are observed in Figure 5.6(a). However in Figure 5.6(b), corresponding to systems possessing DMSO electrolytes, a distinct tail was observed to lower wavenumbers in the 2170 cm^{-1} CuSCN-associated peak. These could conceivably be due to loosely bound CuSCN on the electrode as discussed above though without further evidence this may be subject to speculation.

Other workers reporting spectroscopic data for this material in other, non-electrochemical studies [94, 101, 104] have also reported peaks at 2173 cm^{-1} and these studies have suggested what the nature of the solid CuSCN film on the Cu electrode in the present study could be. Clark et al. [104] reported the IR spectrum of solid CuSCN to have a strong ν(CN) stretching peak at 2165 cm^{-1} which was assigned to S-bonded CuSCN. However he also attributed a weak shoulder at 2173 cm^{-1} in the same spectrum to a bridge-bound Cu(I) species with thiocyanate. Kabesova et al [105] have discussed the effect of bridged thiocyanates on copper/thiocyanate compounds in IR spectra. They report that the infrared spectrum of "CuNCS" features a peak at 2173 cm^{-1} due to ν(CN) stretching and that the mode of bridging present in this compound occurs involve Cu-N and Cu-S bonds. Hence it is possible that the solid film on the electrode could contain some bridged structures.

Further evidence supporting the assignment of the 2087 cm^{-1} and 2173 cm^{-1} peaks in the in situ IR spectra to solution and solid species respectively was provided by acquiring IR transmission spectra of the red-coloured cell solution that resulted in the thin layer cell after carrying out the in situ IR spectroelectrochemical experiment. These spectra featured a peak at 2087 cm^{-1} and no peak at 2173 cm^{-1} which proves that the former peak is definitely due to solution species (i.e. a mix of Cu(I) and Cu(II) complex ions with thiocyanate as discussed earlier) which has resulted from the anodic polarisation while the latter peak must have arisen as a thin film existing on the electrode surface.

The only other species to be detected in the spectra exhibited in Figure 5.6(a) and (b) was a peak at 2338 cm^{-1} which can be attributed to dissolved CO_2 species in the electrolyte. This peak may arise from oxidation of either the pseudohalide ion or the solvent. It was found to be more prevalent in the DMF systems than in the DMSO systems. The difference in CO_2 levels detected could be due to a surface blocking effect by the deposition of a solid film, i.e. CuSCN, which would inhibit access to the surface for the presumed electro-oxidation reaction leading to CO_2 species to take place.

The trends relating to intensities of FTIR-detected species in the thin layer as a function of applied potential in the Cu/NCS^-/DMF or DMSO electrochemical systems studied appear consistent in behaviour (see Figure 5.8(a) and Figure 5.8(b)). They reveal that the intensity of the peak at 2055 cm^{-1} attributed to the free NCS^- ion in the solvent is negative for all applied potentials at the electrode studied and becomes increasingly negative in the applied anodic potential region where there is a stronger demand for free thiocyanate ion to form soluble complexes, solid deposited films and electrogenerated CO_2. The intensity trends also indicate that in the anodic region there is an increase in the intensity due to the soluble Cu(I) and Cu(II) thiocyanate complex ion species (broad peak at 2087 cm^{-1} in both systems) which starts to ramp up between - 400 and -200 mV(AgCl/Ag) and peaks at +400-600 mV(AgCl/Ag) in the anodic applied potential region. The drop off in intensity is then followed by the increase in intensity of peaks at 2171-2173 cm^{-1} and 2337-2338 cm^{-1} due to solid CuSCN films and solvent-dissolved CO_2 respectively. This shows that film deposition is occurring as a result of limited solubility of the copper/thiocyanate

complex ions formed in the solvents used (DMSO and DMF). Intensities due to these species (film and the electrogenerated CO_2) level off and increase only gradually as increasingly anodic potentials are applied.

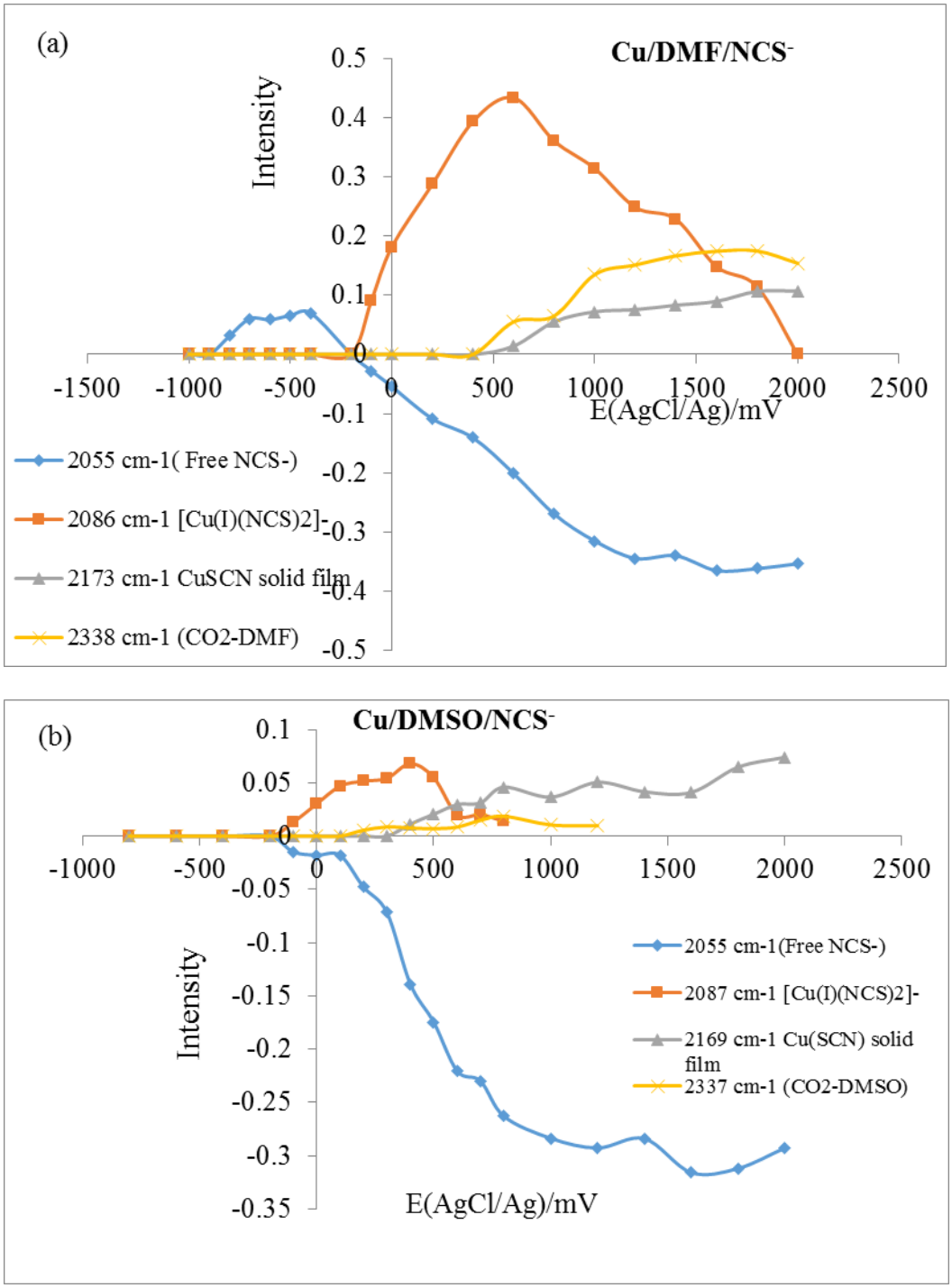

Figure 5.8: Plots of the intensity changes of the various molecular species generated in the thin layer during electrochemical polarisation and observed in the SNIFTIRS spectra as a function of applied potential in the copper electrode as a function of applied potential in DMF and DMSO solvents containing pseudohalide ions and 0.1 mol L^{-1} TBAP in the thin layer cell. (a) 0.05 mol L^{-1} NaSCN in DMF, (b) 0.05 mol L^{-1}NaSCN in DMSO.

5.3.2.3 Cu/NCS^-/DMF or DMSO model solutions

Table 5.2 and Table 5.3 summarise the model solution IR experiments which involved the mixing of cupric chloride or cuprous iodide salts with sodium thiocyanate to prove the identity of species detected in the in situ IR experiments. A complicating factor is that the electrochemically generated cell solution probably contains two oxidation states of copper present. This is indicated by 1) the colour (red) that develops in the cell solution during the experiment which probably indicates a Cu(II) thiocyanate species [106] and 2) the single, broad peak at 2087 cm^{-1} (see Figure 5.6(a) and (b)) which has been assigned in previous literature as a Cu(I) species [94]). It is however hypothesised that the broadness of the IR peak at 2087 cm^{-1} in Figure 5.6(a) and (b) may be caused by spectral contributions from two complex ion species of copper ions with thiocyanate which have closely occurring ν(CN) stretching vibrational frequencies.

One set of model solutions involving the $CuCl_2$/NaSCN combinations may fortuitously prove the above hypothesis because of some known redox chemistry that occurs [106] when Cu^{2+} and NCS^- ion are mixed in solution. Such redox chemistry is not expected to occur when the CuI salt is dissolved and mixed with NCS^-.

When mixed, CuCl2 and NCS^- solutions in DMF or DMSO form a characteristic blood red solution which is the typical colour of Cu(II)-thiocyanate complex ion species [106]. Furthermore as the mole ratio ($CuCl_2$:NaSCN) is increased from 1:1 to 1:4 the peak maximum decreases from 2093 to 2091 cm^{-1} (in DMSO) or 2090 to 2084 cm^{-1} (in DMF). It is believed that this shift is due to the production of Cu(I) thiocyanate species by a redox process in the $CuCl_2$/NaSCN model solutions especially when more NCS^- ion is added relative to $CuCl_2$ salt. The downward shift in ν(CN) stretching is towards values observed for ν(CN) stretching in the CuI/NaSCN mixtures where it is known that the peak is due to a Cu(I) species i.e. $[Cu(NCS)_2]^-$. CuI/pseudohalide salt mixtures also do not exhibit a red colour (they are in fact green to colourless) which supports this observation. In the $CuCl_2$/NaSCN model solution mixtures, there will be a mixture of the two oxidation states with the colour of the solution dominated by the Cu(II) thiocyanate complex ions. Further evidence to support the mixture of the Cu(I) and Cu(II) thiocyanate complexes in the $CuCl_2$/NaSCN model solutions

may be given by comparison of $CuCl_2$/NaSCN and CuI/NaSCN model solution IR spectra at the different mole ratios, see Figure 5.9(a-c). In these it is clear that the ν(CN) stretching frequencies of the Cu(I) appeared relatively more sharp and narrow compared to the broader peaks due to ν(CN) stretching in the Cu(II) salt/pseudohalide solutions. From these spectra it appears that the Cu(II)-thiocyanate complex ion may be contributing at higher wavenumbers relative to a Cu(I) thiocyanate complex which (as shown by spectra recorded for the CuI/NaSCN) model solutions) produces a ν(CN) stretching peak at lower wavenumber.

The observations were regarded as sufficient experimental proof that 1) the two oxidation states of Cu are produced in the in situ IR experiment and 2) they are also produced in the model solution spectra produced from $CuCl_2$/NaSCN mixtures in DMSO (and also DMF) due to redox chemistry. This was supported later by XAS work on the model solutions and the electrochemically generated cell solution samples.

In addition to features caused by Cu(I) and Cu(II) thiocyanate complexes in the model solutions, it is also possible to observe peaks at 2055-2056 cm^{-1} which are due to the free NCS^- ion in the DMSO medium (see Figure 5.9(a) to (c)).

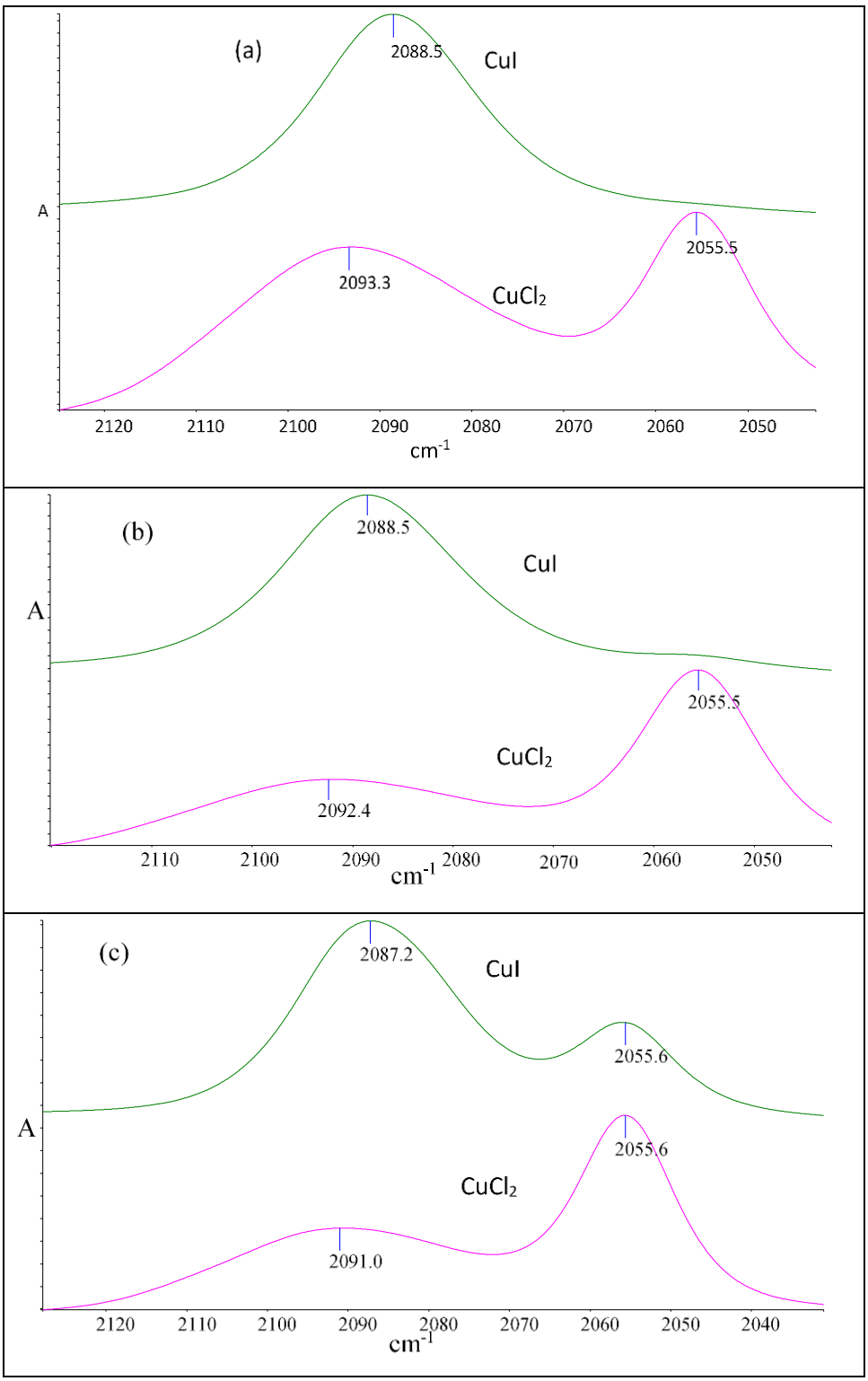

Figure 5.9: Transmission IR spectra of the Cu(I) and Cu(II) pseudohalide complexes in the model solutions prepared with CuI or $CuCl_2$ salts at different mole ratios of Cu salt:pseudohalide salt in NaSCN salt/ DMSO model solution where [CuI] or [$CuCl_2$] = 0.025 mol L^{-1} in each solution. (a) 1:1 CuI: NCS^- and 1:1 $CuCl_2$: NCS^- mole ratio solutions., (b) 1:2 CuI: NCS^- and 1:2 $CuCl_2$: NCS^- mole ratio solutions., (c) 1:4 CuI: NCS^- and 1:4 $CuCl_2$: NCS^- mole ratio solutions.

5.3.3 Cu/$NCSe^-$/DMF and DMSO

5.3.3.1 Cyclic voltammetric investigations

The cyclic voltammogram (CV) of the copper electrode in DMF and DMSO solvents containing 0.05 mol L^{-1} $KSeCN^-$ and 0.1 mol L^{-1} TBAP is shown in Figure 5.10(a) and Figure 5.10(b). As observed with the other electrochemical systems discussed above, the CVs for this system were also unremarkable in their appearance apart from showing an increase in current as the applied voltage was adjusted to more anodic potentials that features in CV are due to metal oxidation and solvent oxidation. However in contrast to the other systems, the observed hysteresis of the CV was strongly evident in the Cu/$NCSe^-$ system which was evidence for large level of irreversibility in the system caused possibly by loss of solid from or modification of the electrode by deposition of a film on the surface.

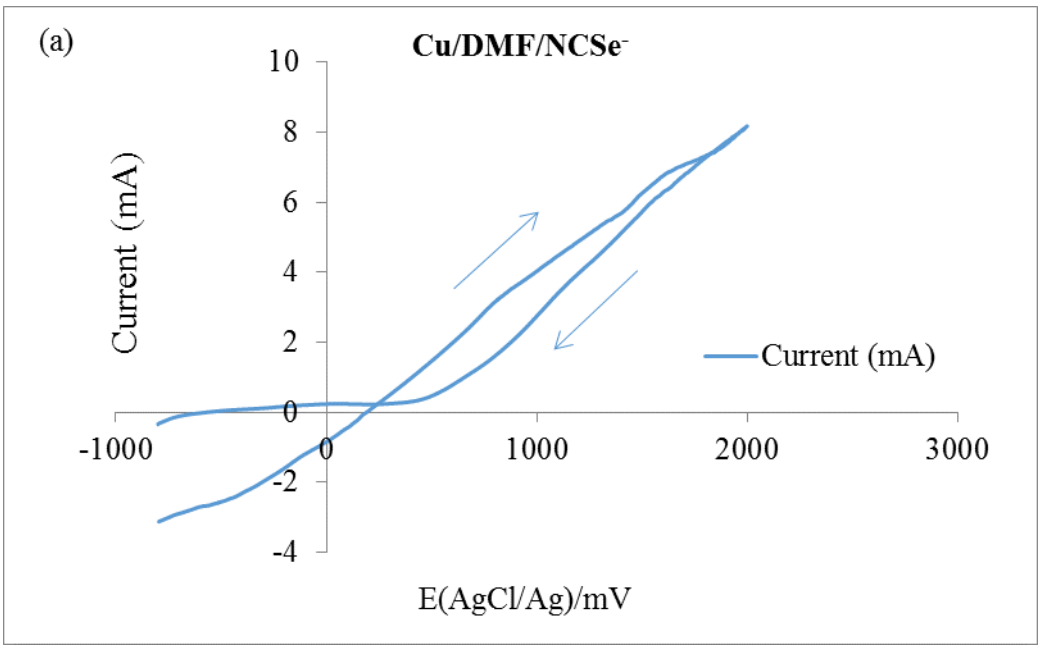

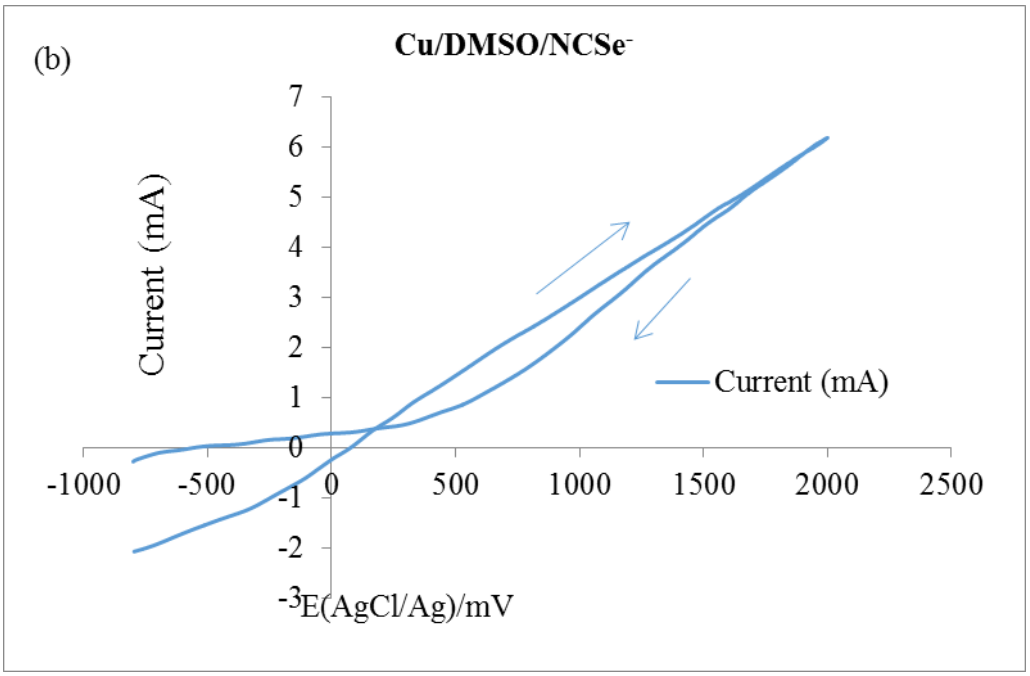

Figure 5.10: Cyclic voltammograms of the copper electrode in DMF and DMSO solvents containing pseudohalide ions and 0.1 mol L^{-1} TBAP in the thin layer cell (sweep rate = 20 mV/s): (a) 0.05 mol L^{-1} KSeCN in DMF, and (b) 0.05 mol L^{-1} KSeCN in DMSO. Arrows show the path actually traced upon conducting the sweep of potentials.

5.3.3.2 IR spectra of Cu/TBAP/$NCSe^-$/DMF and DMSO

Figure 5.11(a) and Figure 5.11(b) show the series of SNIFTIRS spectra acquired as a function of applied potential at the copper electrode surface of the Cu/$NCSe^-$/DMF and DMSO systems. Figure 5.12(a) and Figure 5.12(b) represent the single sweep voltammograms that shows the average current at each applied potential in the thin layer cell during the SNIFTIRS experiment in DMF and

DMSO. Figure 5.13(a) and Figure 5.13(b) represent the plot of the intensity changes of peaks observed in the Cu/TBAP/$NCSe^-$/DMF and DMSO systems respectively as a function of applied potential. Table 5.1 may be referred to for a summary of the in situ IR data.

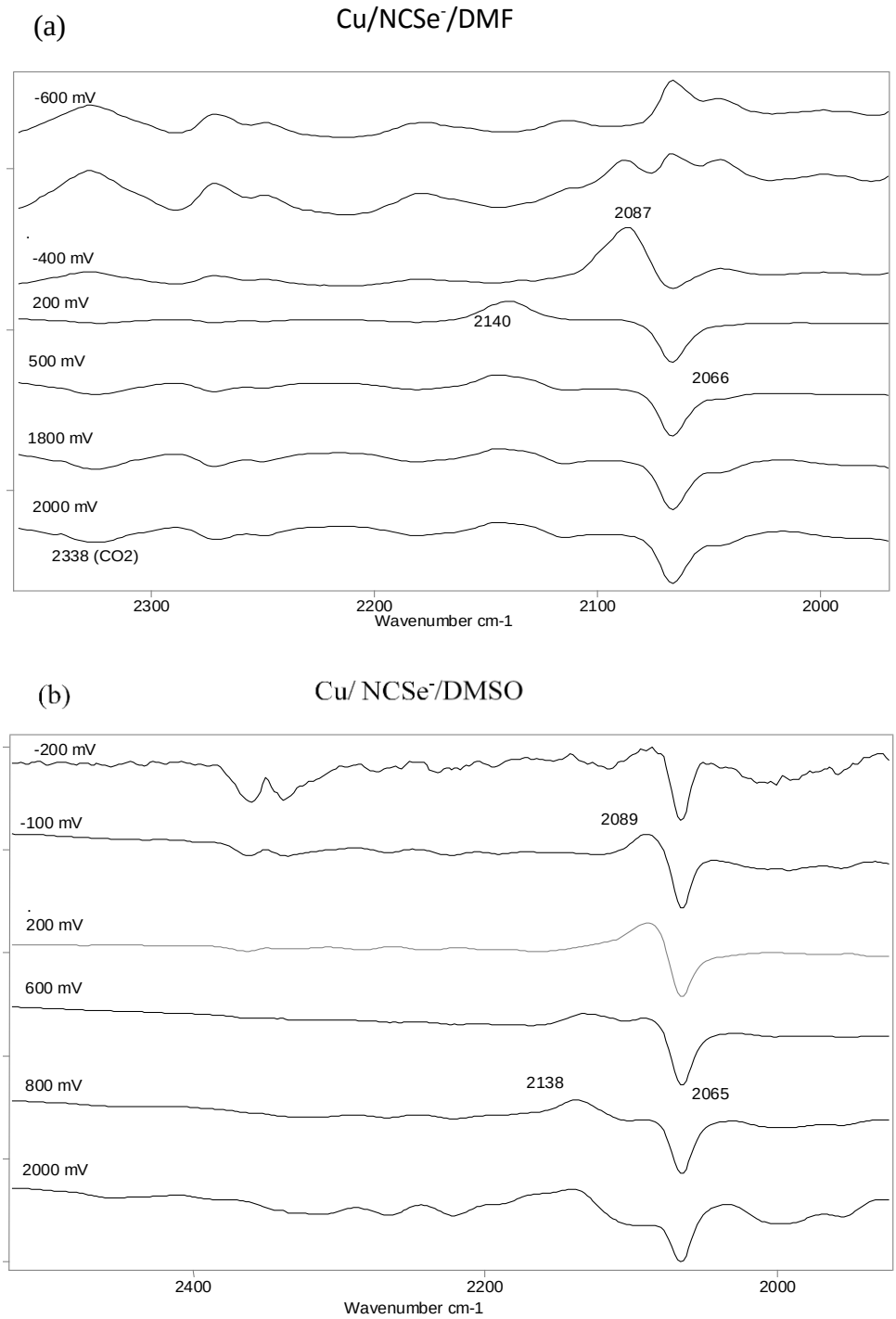

Figure 5.11: Series of SNIFTIRS spectra of the copper electrode as a function of applied potential in DMF and DMSO solvents containing pseudohalide ions and 0.1 mol L^{-1} TBAP in the thin layer cell. (a) 0.05 mol L^{-1} KSeCN in DMF, (b) 0.05 mol L^{-1} KSeCN in DMSO.

In Figure 5.11(a) and (b), at applied potentials between -400 mV (AgCl/Ag) and +500 mV (AgCl/Ag), a broad positive-going peak at 2087 cm^{-1} is observed as well as a negative-going peak at 2066 cm^{-1}. This pattern of peaks is analogous to that observed in the Cu/NCS^-/DMF and Cu/NCS^-/DMSO systems, and can be interpreted similarly in that the negative-going peak at 2066 cm^{-1} and the broad positive-going peak at 2087 cm^{-1} are due to free selenocyanate ion and possibly a mixture of Cu(I) and Cu(II) selenocyanate complex ions assuming similar chemistry as observed in the Cu/thiocyanate systems discussed above. As data on Cu-selenocyanate complex ion systems are lacking in the literature, it was difficult to confirm the assignment of the 2087 cm^{-1} peak observed in Figure 5.11(a) and (b) to a mixture of the Cu(I) and Cu(II) selenocyanate species. There is however literature where entities containing -SeCN moieties have been studied experimentally and subject to calculations of the expected IR frequencies for ν(CN) stretching. For instance Burchell et al. [107] have studied the series of molecules $Se_x(CN)_2$ (x=1-3) and have reported spectroscopic and structural data. Both the calculated and observed ν(CN) stretching frequencies in these molecules are higher (i.e. > 2100 cm^{-1}) than 2087 cm^{-1}. Another paper by Solangi et al. [108] is a more directly relevant paper in that they conducted an electrochemical study in $NCSe^-$ containing electrolytes at a glassy carbon electrode (i.e. no metals involved). The system studied was described as a "$SeCN^-$, $(SeCN)_2^-$, $(SeCN)_3^-$" electrochemical system and the solvent medium supporting the system under study was a room temperature ionic liquid. Unfortunately only NMR spectroscopic data was acquired relating to the $NCSe^-$ ion. The most useful study which confirms the assignment of the 2087 cm^{-1} peak to a mixture of Cu(I) and Cu(II) selenocyanate complex ions is a comprehensive review by Bailey et al. [38] which states that the ν(CN) stretching frequency of a nujol mull of "$CuL_2(SeCN)_2$" (L= N,N,diethyl 1,2-diaminoethane) is 2072 cm^{-1}. This is regarded by the authors as the typical IR stretching frequency for "apparently N-bonded" Cu-SeCN complexes but the paper states that Se-bonded analogues give higher ν(CN) stretching frequencies. According to Norbury [39], Cu can bond via the N or the Se atom in the $SeCN^-$ ligand. It is also stated by Norbury that complexes of $Cu(en)_2(SeCN)_2$ are probably isostructural with the equivalent NCS^- based complexes.

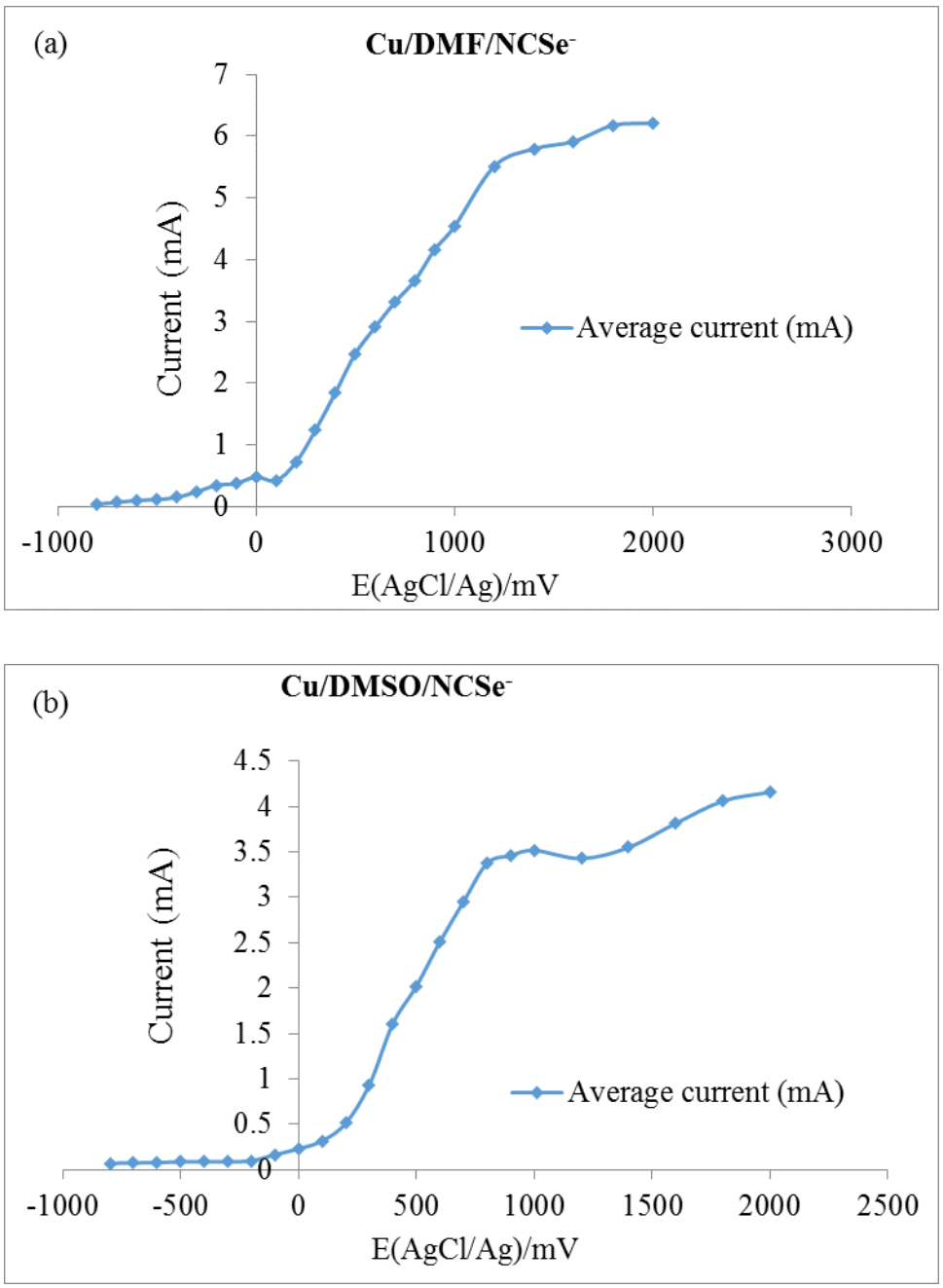

Figure 5.12: Single sweep voltammograms acquired of the copper electrodes during a SNIFTIRS experiment in DMF and DMSO solvents containing pseudohalide ions and 0.1 mol L^{-1} TBAP in the thin layer cell: Data were obtained from calculating the average current at the beginning and end of the spectral acquisition period for each applied potential at which SNIFTIRS spectra were acquired. (a) Cu electrode and 0.05 mol L^{-1} KSeCN in DMF, (b) Cu electrode and 0.05 mol L^{-1} KSeCN in DMSO.

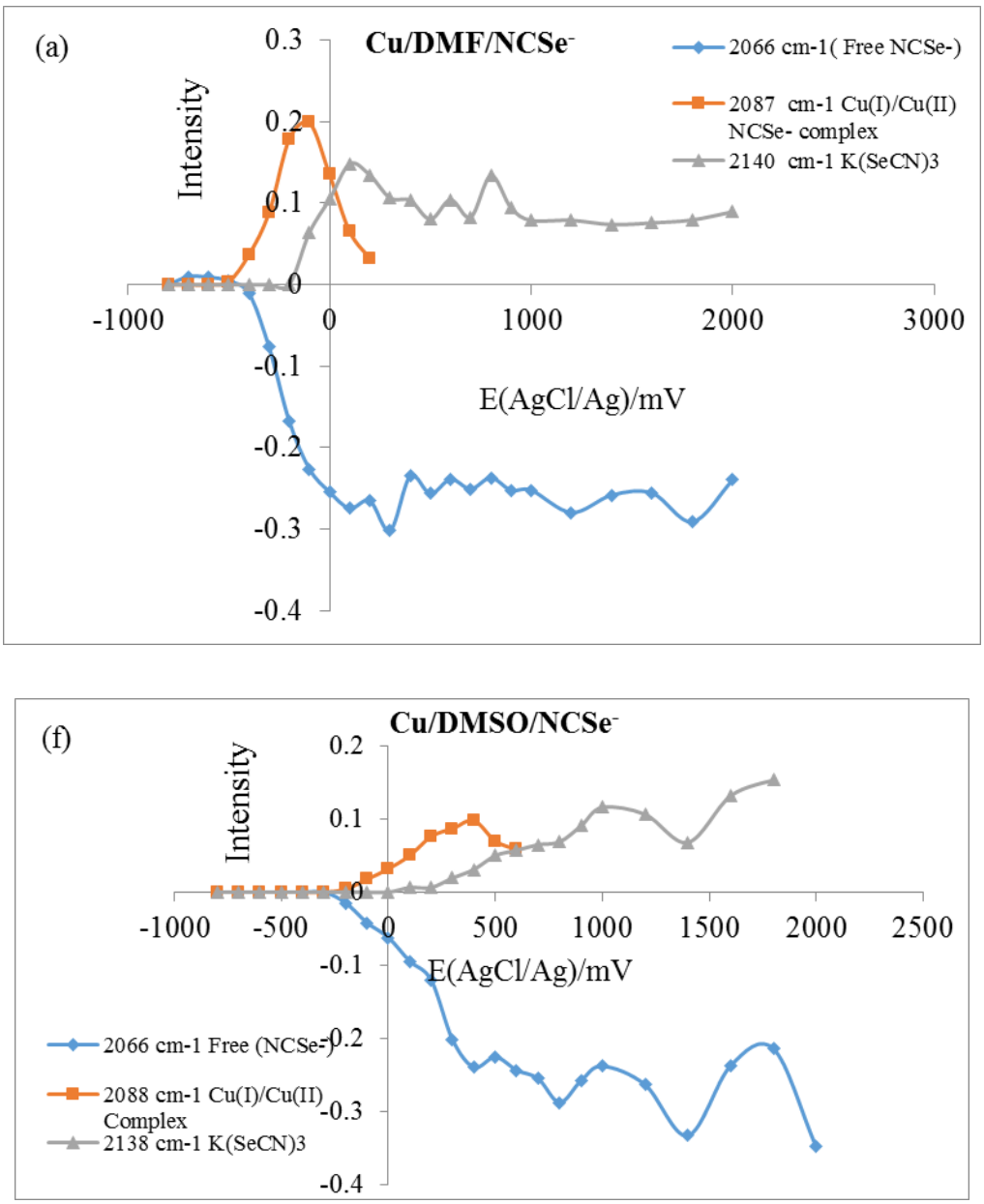

Figure 5.13: Plots of the intensity changes of the various molecular species generated in the thin layer during electrochemical polarisation and observed in the SNIFTIRS spectra as a function of applied potential in the copper electrode as a function of applied potential in DMF and DMSO solvents containing pseudohalide ions and 0.1 mol L^{-1} TBAP in the thin layer cell (a) 0.05 mol L^{-1} KSeCN in DMF, (b) 0.05 mol L^{-1} KSeCN in DMSO.

Hence in Figure 5.11(a) and (b), the assignment of the observed 2087 cm^{-1} band in in situ IR spectra to a mixture of Cu(I) and Cu(II) selenocyanate complex ions is plausible but not as easy to prove using colours of solution as in the Cu/NCS^- electrochemical systems and the model solutions.

In general, the colour of the solutions were both (i.e. in DMF and DMSO) gold-yellow, a colour. Such colours were also shown later in model solution work

where $CuCl_2$ and CuI salts with mixed with the pseudohalide salts in various copper salt: pseudhalide salt mole rises (see Table 5.2).

Another peak that appears in in situ IR spectra from the spectroelectrochemical cell (see Figure 5.11(a) and (b)) is a weak, broad feature at 2138-2140 cm^{-1} which is observed at applied potentials of +200 (± 100) mV onwards for Cu electrodes in DMF solutions, and from +600 mV (± 100) mV onwards for Cu electrodes in DMSO solutions. It was initially thought that this feature was due to a solid film of "CuSeCN" however this was not supported by literature. Kilmartin et al. [50] attributed a weak band (detected by Raman spectroscopy) at 2164 cm^{-1} to a copper selenocyanate passive film that had formed on a copper anode. Assuming the detected 2164 cm^{-1} peak (in Kilmartin's work) would be at the same position had IR been used (assuming low point group symmetry of CuSeCN)) then the observed peak of 2138-2140 cm^{-1} in the present IR spectroelectrochemical study is reasonably distant in value from Kilmartin's observed peak. Furthermore Manceau et al. [109] has reported data relating to ν(CN) stretching frequencies of various thiocyanate and selenocyanate compounds. The ν(CN) stretching frequencies of α-CuSCN, β-CuSCN, α-CuSeCN, and β-CuSeCN are reported at 2157, 2173, 2157 and 2174 cm^{-1} respectively, which are all very similar to Kilmartin et al.'s [50] observed peak. In Manceau's paper [109] it was stated that these IR frequencies were typical of Cu-Se bonded compounds. One of Manceau et al.'s source papers for the CuSCN IR data [110] reports that two different polytypes of CuSCN and CuSeCN, namely the α and β forms exhibit different ν(CN) stretching frequencies.

Hence the 2138-2140 cm^{-1} peak is probably unlikely to be due to a Cu-$SeCN^-$ containing solid compound and it is necessary to consider other possibilities for this peak where Cu is not involved. It is known that selenocyanogen can be isolated as a yellow solid from dichloromethane where it is formed by reaction of silver selenocyanate with iodine. Aynsley et al. [111] have reported that the yellow chloroform (or benzene) solutions of selenocyanogen exhibit ν(CN) stretching frequencies of 2152 cm^{-1} while Cataldo [112], who reported the first IR spectrum of *solid* selenocyanogen (as a KBr disk) has stated that a very intense ν(CN) stretching frequency can be observed in the FTIR spectra at 2143 cm^{-1}. Hence the peak observed in the in situ IR spectrum for the Cu/$NCSe^-$/DMSO or

DMF systems might be deposited selenocyanogen solid but this is unclear. A more likely assignment for the peak is a $(NCSe)_3^-$ species which according to Solangi et al [108] is the thermodynamically favoured species in an equilibrium involving the formation of $(NCSe)_3^-$ from $(SeCN)_2$ and $NCSe^-$. In the presence of K^+ ion (from use of KSeCN), the $(NCSe)_3^-$ may precipitate in the thin layer cell on the electrode as $K(SeCN)_3$. This compound is known from earlier studies [93] involving the oxidation of selenocyanate on platinum electrodes in aqueous electrolytes containing 0.5 mol L^{-1} KSeCN and 0.1 mol L^{-1} NH_4O_2CMe at pH 7. According to these authors, an intense band at 2143 cm^{-1} was observed in their systems when applied potentials > 0.8 V (NHE) were used. It is proposed that the peak at 2138-2140 cm^{-1} is hence due to the solid compound $K(SeCN)_3$. That this peak is due to a solid phase species (in the form of a film) is supported by the observation that IR transmission spectra of the cell solutions obtained after doing in situ IR experiments on the Cu/KSeCN in DMSO only show peaks at 2088 cm^{-1} and 2065 cm^{-1} which are known and assigned solution species. The peak at 2138-2140 cm^{-1} is not observed under these conditions indicating it must exist only on the electrode and hence only amenable to detection during the in situ IR experiment (see Table 5.1).

In the Cu/NCO^-/DMF or DMSO and Cu/NCS^-/DMF or DMSO systems, a peak at 2338 cm^{-1} was also observed in situ IR spectra due to dissolved (electrogenerated) CO_2 in the electrolyte and arising from electro oxidation processes. This peak was characteristically not observed in any of the Cu/$NCSe^-$ electrochemical systems investigated by in situ IR. It is possible that the copper surface becomes poisoned or blocked during the in situ IR experiment by a layer of solid $K(SeCN)_3$ or even elemental Se which would inhibit some electrochemical reactions. Selenocyanate compounds or derivatives are known to decompose to elemental Se [50, 93]. Observations of the Cu electrode at the conclusion of the in situ IR experiment with electrochemical polarisation revealed that the surface was a black colour which supports the conclusion that a film of material has deposited during the experiment.

Examination of the intensity-potential plots (see Figure 5.13(a) and (b)) for the Cu/$NCSe^-$/DMF or DMSO electrochemical systems studied by in situ IR revealed some unavoidable problems with data acquisition during runs. Generally

fluctuations in intensities were observed which suggested that the thin layer was subjected to "thin layer turbulence" during the electrochemical experiment which is interpreted as being caused by gas production during the experiment. In the case of the Cu/$NCSe^-$/DMF or DMSO systems it was not obvious what gas was causing this problem as CO_2 was not observed in the in situ IR spectra at any of the potentials applied to the electrode. Despite this fluctuating intensity behaviour being superimposed on the intensity plots for these systems, very similar intensity trends in species to what was observed in the Cu/NCS^-/DMF or DMSO systems, were seen. Hence the intensity of the Cu-selenocyanate complex ion species observed at 2087-2088 cm^{-1} increased and peaked at -100 mV and -400 mV(AgCl/Ag) in the DMF and DMSO systems respectively while the intensity of the 2138-2140 cm^{-1} peak attributed to solid $K(SeCN)_3$ started increasing as the intensity of the 2087-2088 cm^{-1} peak began to drop (see Figure 5.13(a) and (b)) and plateaued in intensity at more anodic potentials. Hence this is a species which appears to have limited solubility in the polar aprotic solvent systems being used. Also in common with all the copper/pseudohalide/DMF and DMSO systems being investigated, the intensity of the peak at 2066 cm^{-1} attributed to free selenocyanate ion was always observed as a negative peak over the entire potential range and decreased sharply to increasingly negative intensities as the electrochemical demand for selenocyanate ion increased in the anodic region of the electrode. It is interesting to note that no CO_2 was observed in this system at all.

5.3.3.3 Cu/$NCSe^-$/DMF or DMSO model solutions

As shown in Table 5.2, mixing DMF and DMSO solutions of Cu^{2+} and $NCSe^-$ in different Cu^{2+}: $NCSe^-$ mole ratios produced gold yellow coloured solutions starting with a Cu^{2+}: $NCSe^-$ mole ratio of 1:1 and increasing in intensity of colour when progressing to solutions with a mole ratio of 1:8 where an orange brown colour was observed. This colour was similar to (though more intense) than the cell solution colour observed in Cu/ $NCSe^-$ electrochemical systems after the in situ IR experiments. The transmission IR spectra of the DMF model solutions containing Cu^{2+} and $NCSe^-$ feature a peak at 2084-2090 cm^{-1} (the peak position decreases as the Cu^{2+}:$NCSe^-$ mole ratio is changed form 1:1 to 1:4), and a peak at 2065-2066 cm^{-1}. The peak at 2065-2066 cm^{-1} is detectable in all model solutions examined except for the 1:1 model solution. This peak is due to free

selenocyanate ion in DMF. For the model solutions prepared in DMSO, the peak corresponding to free selenocyanate ion is easily observed at the same wavenumber position (as in DMF) at 2065-2066 cm^{-1} in all solutions scanned.

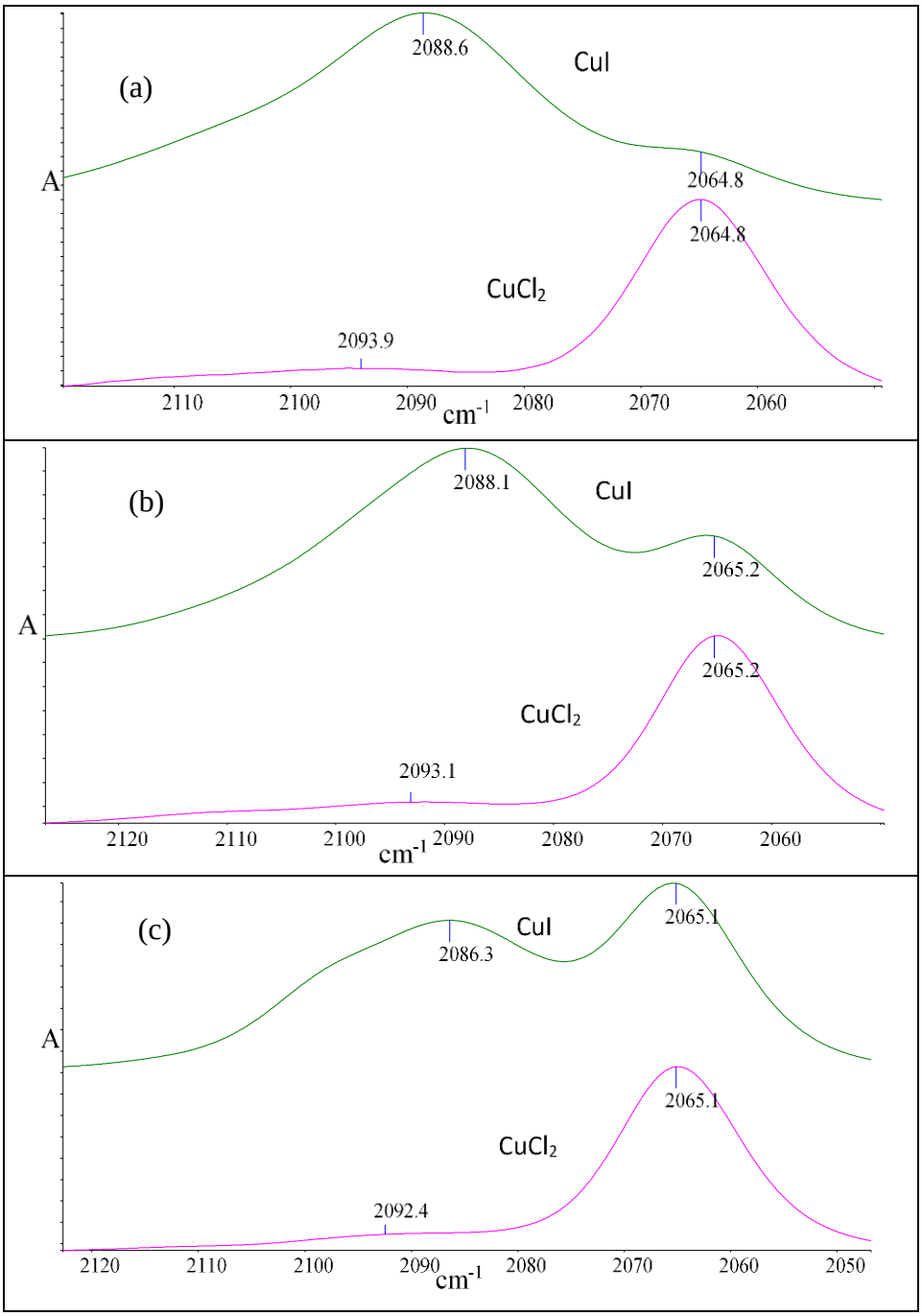

Figure 5.14: Transmission IR spectra of the Cu(I) and Cu(II) pseudohalide complexes in the model solutions prepared with CuI or $CuCl_2$ salts at different mole ratios of Cu salt:pseudohalide salt in KSeCN salt/ DMSO model solution where [CuI] or [$CuCl_2$] = 0.025 mol L^{-1} in each solution. (a) 1:1 CuI: $NCSe^-$ and 1:1 $CuCl_2$: $NCSe^-$ mole ratio solutions., (b) 1:2 CuI: $NCSe^-$ and 1:2 $CuCl_2$: $NCSe^-$ mole ratio solutions, (c) 1:4 CuI: $NCSe^-$ and 1:4 $CuCl_2$: $NCSe^-$ mole ratio solutions.

However, in the 2080-2120 cm^{-1} region of the DMSO Cu^{2+}/ $NCSe^-$ model solution IR spectra, there is a broad absorption peak which is made up of contributions from both the solvent and a putative Cu/selenocyanate complex ion species giving

rise to the 2084-2090 cm^{-1} peak in the DMF spectra. It was hence impossible to resolve the two peaks due to DMSO solvent and the other species hence these have not been summarised in Table 5.2 (see "nd" entry).

Compared to the model solutions and cell solution observations made for the Cu/thiocyanate ion systems as discussed above, the evidence for generation of a mixture of Cu(I) and Cu(II) selenocyanate complex ions in the electrochemical cell during anodic dissolution (and also in the model solutions involving $CuCl_2$/KSeCN vs. CuI/KSeCN model solutions) is not as clearly demonstrated as it is when examining the Cu/thiocyanate solution data (see Figure 5.14(a) to (c)) . It is also difficult to make comparisons of the colours of model solutions with what develops in the cell solution during anodic dissolution of copper in DMF or DMSO solutions of $NCSe^-$ ion. However it is known that redox chemistry also occurs when mixing Cu^{2+} with $NCSe^-$ ions in solution [113]

5.3.4 XAS studies of Cu/NCX^-/DMSO systems and Cu(II)/NCX^-/DMSO model solutions.

To provide further evidence in support of the interpretations provided by FTIR spectroscopy and to more importantly provide new evidence to suggest the presence of specific oxidation states for the soluble Cu complex ion species produced in these in situ IR studies, the electrochemical cell solution and model solution systems were subjected to analysis using synchrotron radiation at the Australian Synchrotron in Melbourne. One important and very serious aspect of these studies discovered was that the synchrotron radiation was found to chemically modify the Cu-containing frozen solution samples being studied so that only limited information could be derived. This effectively stymied the use of EXAFS for analysing the exact coordination environment of the Cu ions in the frozen solution samples. In contrast, the solid Cu-containing standard samples (e.g. Cu_2O and CuO) were unaffected by the beam. Hence for this reason, *only* XANES spectra could be analysed in depth in this study. It was however discovered that even XANES spectra of solutions analysed also changed with scanning them repeatedly (due to ionisation problems) hence only XANES spectra from the *first* scan of the systems being investigated were discussed, as it was

important to keep the illumination time as short as possible to minimise beam damage.

XANES can yield information about the valence state and average co-ordination geometry. This information is customarily obtained by comparing the spectra of the samples of interest to spectra of appropriate standards chosen for the study.

5.3.4.1 XANES data collected for the Cu/pseudohalide systems.

XANES carried out on spectra of copper-based systems are known to vary dramatically with co-ordination geometry due to the different possible orbital configurations ($4s^2\ 3d^9$ / $4s^1\ 3d^{10}$) that can be manifest with this element. These configurations allow various electronic transitions to occur, which are evident in the XANES spectra as peaks near the absorption edge. Copper can also adopt +1 and +2 valence states, which are evidenced by a shift in the absorption edge [80]. Cu(II), in particular, with its d^9 electronic configuration is strongly susceptible to Jahn Taller distortion [80] which leads to alterations in the geometry of ligands around the metal centre. In isocyanato-copper(II) complexes, coordination numbers can be 4,5, or 6 and the geometry can be pseudo-octahedral, coplanar, pseudotetrahedral, tetragonal pyramidal or trigonal bipyramidal depending on the ligands involved and the way the crystal structure is packed in the solid [114] .

5.3.4.2 Standards used in the Cu XANES study

Figure 5.15 shows the XANES spectra of the various standards measured. Solid samples of Cu (foil), Cu_2O (powder) and CuO (powder) show characteristic features, namely for Cu_2O, a prominent peak at 8983 eV (the 1s-4p transition, indicative of Cu^+); and for CuO a small peak at 8979 eV (the 1s-3d transition, indicative of Cu^{2+}) and a peak at the absorption edge that is less prominent than that of Cu_2O. The XANES spectra of these solid samples were not affected by beam damage.

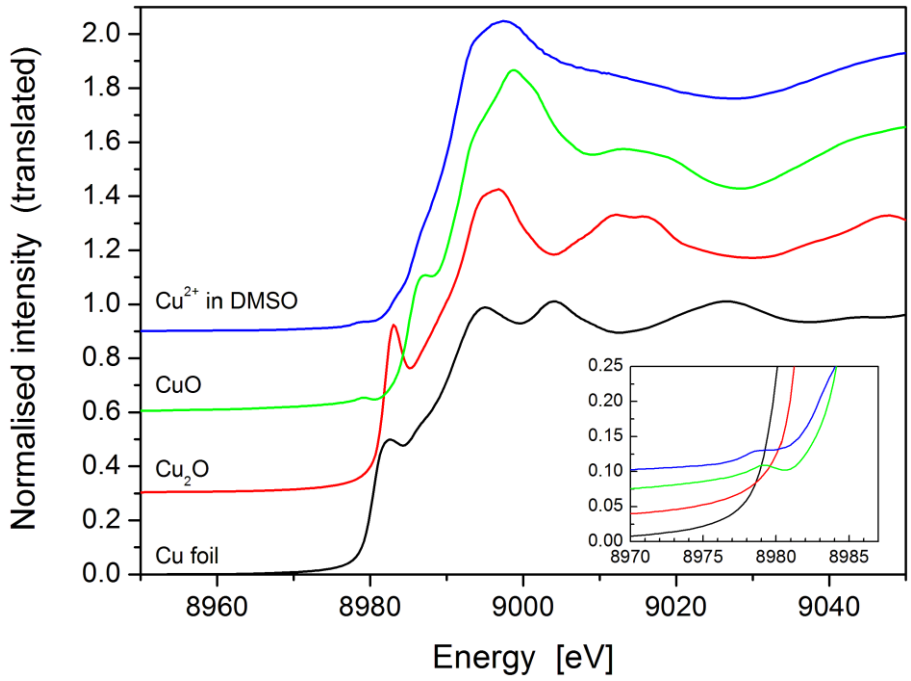

Figure 5.15: XANES spectra of Cu standards as labelled.

Cu^{2+} in DMSO was also measured as a standard as a liquid N_2-frozen solution of partially oven dried $CuCl_2$ dissolved in DMSO. The same experiment using CuI was not thought of at this point, however later in the study the model solution IR experiments which involved the mixing of CuI and pseudohalide were carried out. The XANES spectrum of the Cu^{2+} in DMSO standard was found to have a similar shape to XANES spectra run for other known octahedral Cu^{2+} species as reported by Huggins et al. [115] in that it exhibited a small pre-edge peak, and had a single peak at the white line in contrast to the two peaks observed in square planar and square pyramid complexes [116].

5.3.4.3 XANES spectra of the Cu/pseudohalide systems studied (model solutions and electrochemically generated samples)

5.3.4.3.1 Cu/ NCO^-

Figure 5.16 shows XANES spectra of the model solutions intended to mimic the solution chemistry occurring in the in situ electrochemical cell for the Cu/NCO^-/DMSO system, and the electrochemically generated solution. The XANES spectra for the model solutions all show a very small peak below the edge at 8979 eV indicating Cu^{2+}. The shapes of the curves closely resemble those for Cu^{2+} in an octahedral geometry as reported for $[Cu(H_2O)_6]^{2+}$ by McEwen et al [117] as well as the XANES spectrum for $CuSO_4.xH_2O$ as reported by Huggins et al. [115] and observed in the $CuCl_2$ in DMSO standard, Figure 5.16. The edge

positions for all scans lie between 8982.1 and 8982.7 eV (c.f. 8981.8 eV for Cu_2O, 8985.1 eV for CuO, 8985.8 eV for Cu^{2+} in DMSO). According to Gardea-Torresdey et al [118], the edge position can shift to lower energies due to donation of electrons by the ligand. Hence as expected Cu(II) species are dominant in these model solutions.

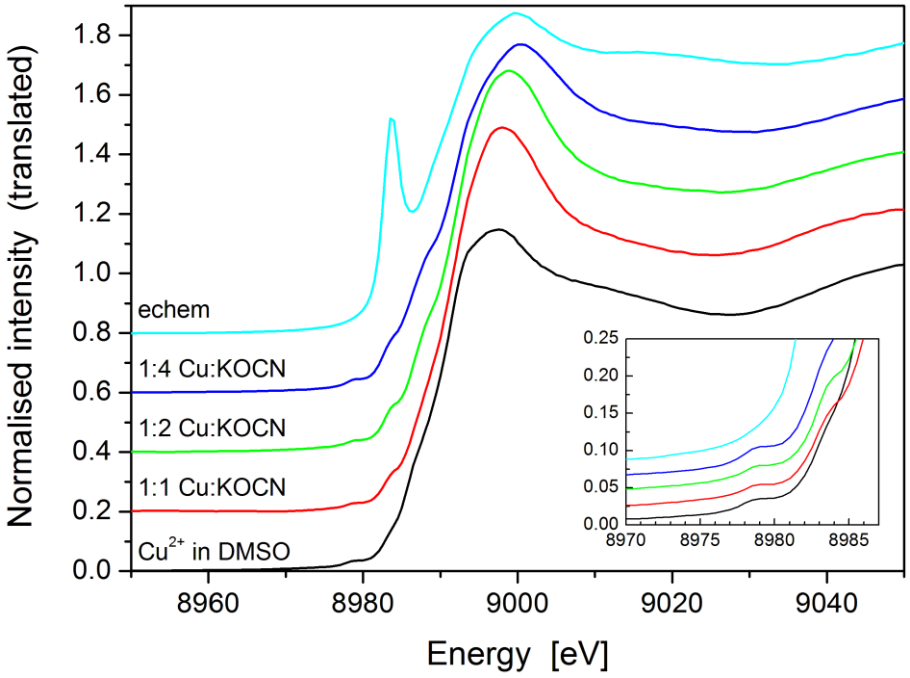

Figure 5.16: XANES scans of the model solutions prepared from adding Cu^{2+} and NCO^- in mole ratios of 1:1, 1:2 and 1:4 compared to the a green-coloured electrochemically generated sample from the Cu/NCO^-/DMSO electrochemical system previously anodically polarized at +500 mV(AgCl/Ag) for 2 hours. The Cu^{2+} in DMSO standard is also shown for comparison. The inset shows the pre-edge region.

In contrast, the electrochemically generated solution spectrum does not show a peak at this position, but does have a prominent peak at 8983.5 eV, which is in a similar position to the peak in the Cu_2O standard (8983.0 eV), and indicates the presence of Cu(I). This peak, which corresponds to the 1s-4p transition, is stronger than in the Cu_2O standard and indicates Cu^+ is present in a 2-fold co-ordination environment [19, 119]. The intensity of the peak depends on the co-ordination environment and the specific ligand bound to the metal ion centre.

To test the extent of beam damage, a series of XANES scans was recorded in rapid succession of the light green coloured cell solution that was generated by polarizing the Cu electrode at +500 mV(AgCl/Ag) in 0.025 mol L^{-1} KOCN and 0.1 mol L^{-1} TBAP in DMSO for 1-2 hours. These are shown in

Appendix 6 (Figure S.13). Each XANES scan took *ca.* 7 minutes, and the series of 12 scans acquired took approximately the same length of time as would be required to obtain two EXAFS scans (the minimum required to check repeatability). These spectra effectively showed that any attempt to analyze EXAFS data from this system was futile given the variability of the data. This was because the XANES spectra changed rapidly with exposure time. In general this was a problem with all XANES analyses of frozen solutions involving copper pseudohalide solution species.

Over time the peak at 8983.5 eV (indicative of Cu^{+} in a 2-fold co-ordination environment) decreased dramatically in intensity until it was just a shoulder (see Appendix 6 Figure S.13); however the edge position (i.e. point of inflection) of the spectra remained unchanged. The white line changes in intensity: increasing during the first few scans and then decreasing and broadening out. It is for this reason that only the first XANES scan of any given Cu/pseudohalide system was used.

In summary for the electrochemically generated sample, analysis of the XANES spectra indicate that copper is present as Cu(I). In the in situ IR spectra, Cu/cyanate complex ions were observed that had been produced as a result of anodic action at the Cu electrode and this copper species was in the +1 oxidation state when electrochemically generated in DMSO (as proven by XANES, see Figure 5.17) and (by inference) in DMF solutions.

5.3.4.3.2 Cu/ NCS^{-}

In contrast to XANES spectra of the electrochemically generated sample from the Cu/NCO^{-}/DMSO system, that of the Cu/NCS^{-}/DMSO electrochemical system produced XANES spectra (Figure 5.17) which featured a small peak at 8979 eV and a peak on the edge at 8983 eV, but the white line and subsequent features mirror those of the model solutions of Cu^{2+} and NCS^{-} shown in the same figure (see Figure 5.17). In later scans of the electrochemically generated solutions for the Cu/NCS^{-}/DMSO system, the edge peak was noted to increase in intensity and become a shoulder on the edge. The edge position for all the repeated scans of this sample was 8982.1 eV. Generally the XANES shows some evidence of Cu(I) species in the electrochemically generated samples (though Cu(II) species were also detected).

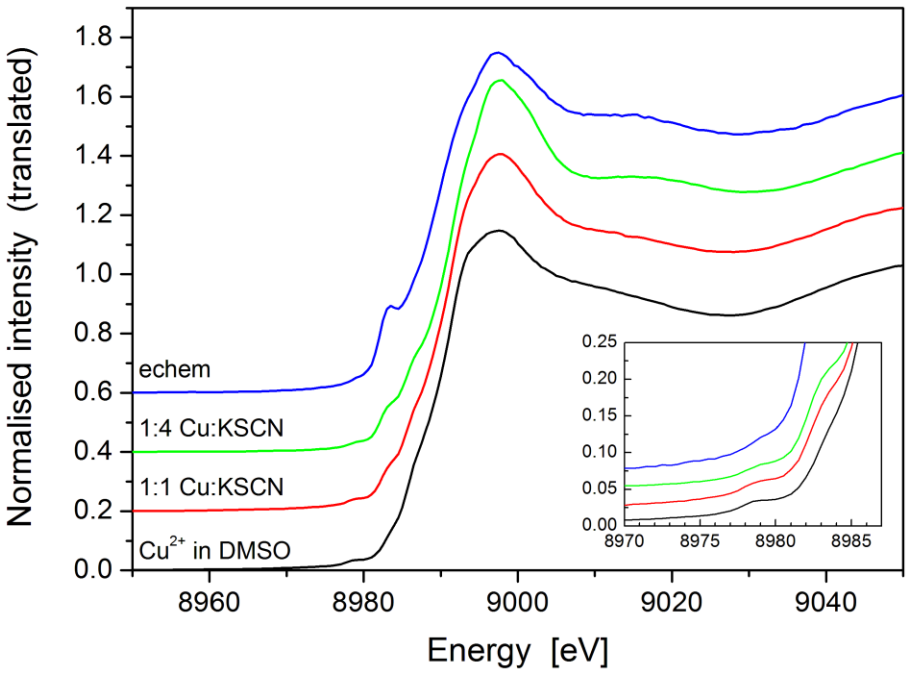

Figure 5.17: XANES scans of the electrochemically generated cell solution from the Cu/NCS^-/DMSO electrochemical systems (produced after polarising electrode at 200 mV for 2-3 hours) and of the model solutions prepared from adding Cu^{2+} and NCS^- in mole ratios of 1:1, and 1:4. The Cu^{2+} in DMSO standard is also shown for comparison. The inset shows the pre-edge region.

The model solutions prepared which were intended to mimic the solution species produced in the in situ IR cell of the Cu/NCS^-/DMSO system when anodically polarized gave XANES spectra (see Figure 5.17) which appeared to indicate that both Cu(I) and Cu(II) species existed in the solution. Hence, there was a small peak at 8979 eV, a small shoulder on the edge, and a single white line, all indicative of Cu^{2+} in an octahedral geometry, though intensity observed at 8982 eV (see Figure 5.17) illustrates that there is a mixture of Cu(I) and Cu(II) oxidation states present in the model solutions. This corroborates the earlier discussed IR evidence from studies performed on the Cu(II) salt/pseudohalide salt mixtures discussed above. It also agrees with the observed colour (red) that develops in the cell solution during the in situ IR experiment. Hence XANES and IR studies of the electrochemical systems and the model solutions prepared in the presence of CuI and $CuCl_2$ with NCS^- ion show that a mix of Cu(I) and Cu(II) pseudohalide complex ions are generated in the electrochemical cell.

5.3.4.3.3 Cu/ $NCSe^-$

The XANES spectra for the electrochemically generated solutions and model solutions associated with the Cu/$NCSe^-$/DMSO electrochemical systems are shown in Figure 5.18. The 1:1 mole ratio ($CuCl_2$:KSeCN) model solution

resembles the Cu/NCS^-/DMSO XANES (Figure 5.17), except that the white line is not as symmetric. The 1:4 mole ratio ($CuCl_2$:KSeCN) model solutions and the electrochemically generated solution both exhibit a prominent peak on the edge at 8983 eV, and little to no pre-edge peak at 8979 eV. Now like the $CuCl_2$/KSCN model solution systems when combined, there is a known redox reaction [24] between Cu^{2+} ion and $NCSe^-$ ion which results in a Cu(I) species being produced in the model solutions which becomes more predominant in the model solutions as the mole ratio of $CuCl_2$:KSeCN increases. In the 1:1 mole ratio model solution, the feature at 8983 eV is minor indicating a relatively small amount of Cu(I) produced by the reaction so that the XANES spectrum resembles more a solution which is dominated by Cu(II) species. This is because there are equimolar amounts of $NCSe^-$ and Cu^{2+} in solution. As the mole ratio of $NCSe^-$ relative to Cu^{2+} increases, there is observed a more prominent peak at 8983 eV which indicates relatively more Cu(I) species being produced in the model solutions as a result of the redox reaction.

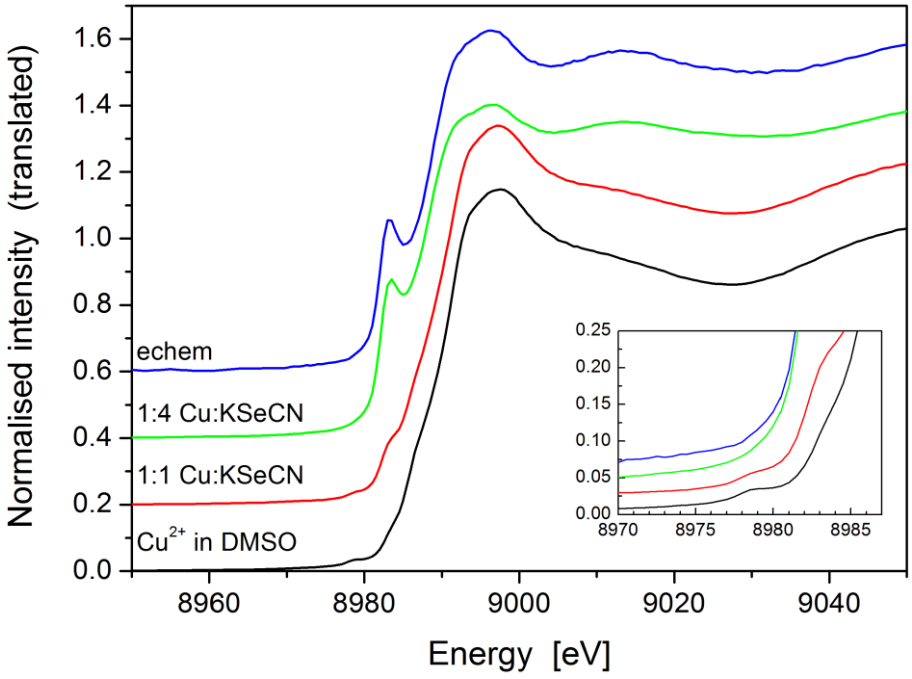

Figure 5.18: XANES scans of the electrochemically generated cell solution from the Cu/ $NCSe^-$/DMSO electrochemical system (produced after polarising electrode at + 400 mV for 2-3 hours) and of the model solutions prepared from adding Cu^{2+} and $NCSe^-$ in mole ratios of 1:1, and 1:4. The Cu^{2+} in DMSO standard is also shown for comparison. The inset shows the pre-edge region.

Hence in general, the XANES spectra support the IR studies of the electrochemical systems involving Cu and $NCSe^-$ which show that a Cu(I) species is predominantly generated as a result of the anodic dissolution process in KSeCN.

This is supported by the IR spectra of the model solutions as a function of mole ratio as these all indicate the appearance of a peak at 2096 cm^{-1} due to a $Cu(I)(NCSe)_2^-$ complex ion though in the lower mole ratio solutions Cu(II) species will also exist as shown by the XANES work. Although the colours of solutions observed for the cell solutions and the model solutions in the $CuCl_2$/NaSCN, CuI/NaSCN and the cell solution colours generated in the electrochemical Cu/NaSCN system during the in situ IR studies were helpful in confirming the presence of the Cu(II) and Cu(I) species, the colours observed in the $CuCl_2$/KSeCN, CuI/KSeCN and the cell solution colours from the electrochemical Cu/KSeCN systems in DMF and DMSO were less helpful in elucidating mixed oxidation state presence.

5.3.5 Comparison with electrochemical studies from other systems

It is important to compare the results obtained in the present study with the few reported electrochemical studies conducted on Cu electrode systems that are related to this area.

For instance, Pyun and Park [120] have carried out in situ spectroelectrochemical studies on anodic oxidation on copper electrodes in an alkaline medium and showed that oxides of Cu(I) and Cu(II) are formed by anodic oxidation. Their CV recorded from -1.2 V (Ag/Ag_2SO_4) shows a rich array of peaks which correspond to oxidation and reduction features associated with copper oxides. Two peaks identified by the authors in their publication as "IIA" and IIIA" at *ca.* -0.45 V and -0.2 V (Ag/Ag_2SO_4) correspond to Cu(I) oxide species. The other peak at *ca.* - 0.1 V is due to Cu(II) oxide species formed either directly from Cu or Cu(I). On the reverse sweep they attribute sharp peaks at -0.6 V and -0.9 V (Ag_2SO_4/Ag) to reduction of these oxides on the electrode surface. The CV reported by Pyun and Park [120] bears no resemblance to the CVs reported for the present systems under investigation as illustrated in all system in CV which showed monotonically increasing profiles with unremarkable voltammetric features. A more relevant study to the present systems being investigated is the paper by Gonçalves et al, [91] which reports electrochemical studies of copper electrodes in DMF in the presence of water, ethanol and acetic acid as additives. They also studied the system in the presence and absence of oxygen. The CVs from this system also showed features due to the oxidation of Cu to Cu(I) and Cu to Cu(II). The

experiments that Gonçalves performed in the presence and absence of oxygen definitively showed that oxygen gas is involved with the formation of Cu(II) oxide species in the system. Water concentration increased the extent of electro-oxidation, altering ethanol concentration had the same effect as water but acetate formation was found to significantly inhibit oxide formation suggesting the formation of a passive film, possibly cuprous acetate though this was not mentioned by Gonçalves et al. [91]. Melendres et al. [121] carried out an electrochemical study of Cu electro oxidation in aqueous solution in the presence of similar concentrations of KSCN as used in the current study (i.e. 0.025 mol L^{-1}). In aqueous solution their CV contained distinct peaks due to Cu(I) and Cu(II) relative to the present study's CV. It appears that the presence of water can have a large influence on the appearance of the CVs. However, of interest in their study was the finding that they detected by far-IR spectra the presence of a CuSCN film on the electrode.

In the present study the CVs of the systems being studied did not yield much detail on the species being produced given the absence of features that could be attributed to either Cu to Cu(I) or Cu to Cu(II) oxidation. However it was obvious that the speciation of copper compounds produced in the thin layer electrochemical cell solutions were exclusively based on compounds/complex ion species where Cu was in +1 oxidation state. It is difficult to provide a mechanism in light of the previous reported electrochemical evidence on these systems which states that Cu(I) and Cu(II) species should be produced. Possibly a mechanism involving oxidation of Cu to a Cu(I) species involving a pseudohalide ion could be invoked. Alternatively given the known redox chemistry of Cu(II) and the pseudohalide ions, it is plausible that a Cu(I)-pseudohalide complex ion species was being formed initially, but also at higher anodic applied potentials due to a redox reaction between Cu(II) oxide and the pseudohalide ion. Another explanation could be that as in the study by Melendres et al. [121], a partially insoluble passivating film of a Cu(I) salt forms which may release Cu(I)-pseudohalide complex ions into solution.

The anodic dissolution of copper electrodes in DMSO and DMF solutions containing pseudohalide ions, it was found that the copper electrode anodically dissolved in these solvents to form Cu(I) complex species. This has been

supported by XANES data which show the presence of Cu(I) species in the electrochemically generated solutions in all systems but also a mixture of Cu(I) and Cu(II) in the Cu/NCS and Cu/NCSe system.

Chapter 6:

In situ IR study of the anodic polarisation of gold electrodes in polar aprotic solvents: DMSO and DMF solutions of cyanate, thiocyanate and selenocyanate ions.

6.1 Introduction

The importance of the chemistry of gold and its interaction with pseudohalide ions such as cyanide, thiocyanate, cyanate and selenocyanate cannot be overestimated given its relevance in areas such as the recovery and recycling of gold [122]. In addition, the reason for studying pseudohalide interactions with Au electrodes is because the pseudohalide ions mimics chemically halide ions [123] which may be useful for understanding electrochemical phenomena as the pseudohalide ion has an easily detectable IR signature (i.e. ν(CN) stretching vibrations) that occurs in the 2500-1800 cm^{-1} region of the IR spectrum without interferences from strong fundamental vibrations coming from the solvent. Hence it can be used to verify or understand earlier electrochemical studies which report that electrochemical oxidation of Au to Au(I) is facilitated in media containing halide ions because of the tendency of halide ions to adsorb strongly to the electrode surface and the fact that Au complexes with the halide ions to form stable species in solution. This is said to then facilitate the dissolution of the electrode in polar aprotic solvents such as acetonitrile even in the presence of small traces of water which run the risk of passivating the electrode at anodic potentials. This then forms the rationale of using a pseudohalide ion in such studies as it will allow this complex ion behaviour to be visualised spectroscopically.

To date most of the in situ IR work probing such complexes with gold has been done in aqueous electrolytes [42, 44-46, 124]. This previous work has shown the importance of species such as Au(I)-pseudohalide complexes as anodic dissolution species and the earlier work has also led to adsorbed pseudohalide ions being detected on the electrode surfaces as well as oxidation by-products of the pseudohalides themselves. In addition, previous work has demonstrated the bonding modes of the gold to the pseudohalide ion in the complex ion species. For instance cyanate (NCO^-) ions have been shown to predominantly bond via the N atom to gold centres whereas thiocyanate can coordinate via S atoms to the gold

centres [46]. No papers have been reported where the in situ IR spectra of Au anodically dissolving in polar aprotic solvents containing pseudohalide ions have been discussed. However, authors such as Martins et al. [51, 52] and Benari et al. [95] have investigated the anodic dissolution of gold in either acetonitrile or DMSO solvent media containing NaSCN, there have been no reports of in situ IR studies from such electrochemical interfaces. Martins [51] has commented, however that the electrochemical behaviour is similar to that in aqueous solution and that gold complex ion speciation is expected at such interfaces. It is stated that the $Au/Au(SCN)_2^-$ redox couple is the potential determining reaction at the electrode. Benari et al [95] showed that the electrode metals of Ag, Cu, Pd and Au oxidized more readily than Pt and glassy carbon electrodes in DMSO media. In the case of Au dissolving in the presence of chloride ion, the $AuCl_n^{(1-n)+}$ complex ions are formed. Hence it is of interest to extend the understanding of the electrochemical behaviour of gold in non-aqueous media by using in situ IR spectroscopy to detect the molecular species being formed at such interfaces to support existing electrochemical data. It is also of interest to extend studies to ions not previously studied to any extent such as selenocyanate ion for which little electrochemical and in situ IR data exist to see if the electrochemical behaviour is comparable to that of other pseudohalide ions.

6.2 Experimental

6.2.1 Reagents and Solutions

DMF and DMSO used in this study were sourced from Ajax Finechem Pty and Scharlau and used without further purification as described in previously. All glassware was cleaned prior to beginning experiments with doubly distilled water and dried. Other reagents used being KOCN, NaSCN, KSeCN, $KAuBr_4$, gold foil (99.99%, 0.1 mm thick) and tetrabutylammonium perchlorate (TBAP) were supplied by Aldrich Chemical Co USA as previously described. When used either as (DMSO/DMF) electrolyte solutions or in model solutions the concentration of the TBAP (used as an inert supporting electrolyte) was 0.1 mol L^{-1}. For the pseudohalide salts, the concentrations used were 0.025 mol L^{-1} in the case of potassium cyanate (owing to its limited solubility in the polar aprotic solvents used) and 0.05 mol L^{-1} in the case of the thiocyanate and selenocyanate salts. This

is in common with what has been done in early chapters studying anodic dissolution of metal electrodes in pseudohalide.

6.2.2 Spectroelectrochemical cell and electrode design.

The thin layer cell used for this work has had details illustrated in chapter 3. The gold electrode was a flat, circular polycrystalline piece of gold of 0.1 mm thickness embedded in a glass syringe barrel using Araldite epoxy glue. The preparation of this electrode has been also covered in chapter 3. The gold electrode was polished using alumina paste.

6.2.3 Instrumentation:

As described previously in chapter 3, cyclic voltammetry (CV) was acquired over the region of -800 to 2000 mV (AgCl/Ag) using an EDAQ computer controlled potentiostat system which was run using Echem software. A Radiometer "red rod" (AgCl/Ag) reference electrode was employed with a platinum metal ring utilised as the counter electrode. Typically a CV scan was run first of the electrochemical system under study these being: Au/DMSO/NCO^-, Au/DMSO/NCS^-, Au/DMSO/$NCSe^-$, Au/DMF/NCO^-, Au/DMF/NCS^-, and Au/DMF/$NCSe^-$. In situ IR (SNIFTIRS) spectra were acquired using a Biorad FTS-40 FTIR spectrometer equipped with a liquid N_2-cooled indium antimonide (InSb) detector as previously described in chapter 3. In situ IR spectra were normally acquired at 4 cm^{-1} resolution as the accumulation of 100 scans at different potentials above the background potential where the background spectrum used was that of the thin layer created when the polished gold electrode in the electrolyte-filled cell was pressed against (resting on) the calcium fluoride IR window with the electrode adjusted to a static potential of -900 mV(AgCl/Ag). Further spectra acquired at potentials more positive than this value and ratioed versus this background were acquired to provide a series of spectra as a function of voltage. Additionally the practice of acquiring electrochemical current measurements during the IR spectral acquisition at each potential was carried out to provide effectively a "single sweep voltammogram" over the timescale of the experiment. The procedure for doing this was described in chapter 3.

IR spectra of model solutions prepared in DMSO and DMF consisting of mixtures of $KAuBr_4$ and the respective pseudohalide salts at various $KAuBr_4$:pseudohalide

salt mole ratios (1:1, 1:2 and 1:4) were also acquired using a Press-Lok© cell containing calcium fluoride windows. Scanning conditions on the Perkin Elmer Spotlight 200 FTIR spectrometer used for the transmission IR spectra were identical to what has been described previously.

In contrast to earlier studies, additional information was acquired in these studies by measure of electrospray ionisation mass spectrometry. ESI-MS spectra were acquired on a Bruker Electrospray Ionisation Time-of-Flight (ESI-TOF) mass spectrometer in negative ion mode of model solutions and other solutions prepared for the purpose of confirming the identity of species detected in the electrochemical cells. Samples for analysis were prepared by adding a drop of model solution (1 μL) to 1 mL of methanol to a small capped plastic vial and vortexed for 10 seconds to allow thorough mixing. This mixture was then injected via hypodermic syringe into the instrument. The parameters set on the instrument were -80.0 V for the capillary exist and 60.0 V for the hexapole RF (radio-frequency) ion guides. The skimmer voltage was -40 to -50 V and the hexapole 1 voltage in the instrument was -23.5V. The m/z range scanned was 800.

6.3 Results and discussion

6.3.1 Cyclic voltammetric studies of the Au/pseudohalide systems in DMSO and DMF

Figure 6.1(a) to Figure 6.1(f) illustrate the CVs of Au electrode systems recorded in the presence of NCO^- (0.025 mol L^{-1}), NCS^-(0.05 mol L^{-1}) and $NCSe^-$ (0.05 mol L^{-1}) ions co-dissolved in DMSO and DMF solvents with 0.1 mol L^{-1} TBAP as a supporting electrolyte. The CVs for all three pseudohalide ions give different looking traces with most (apart from $NCSe^-$) exhibiting some commonality of appearance between CVs done in DMSO and DMF for the same ion.

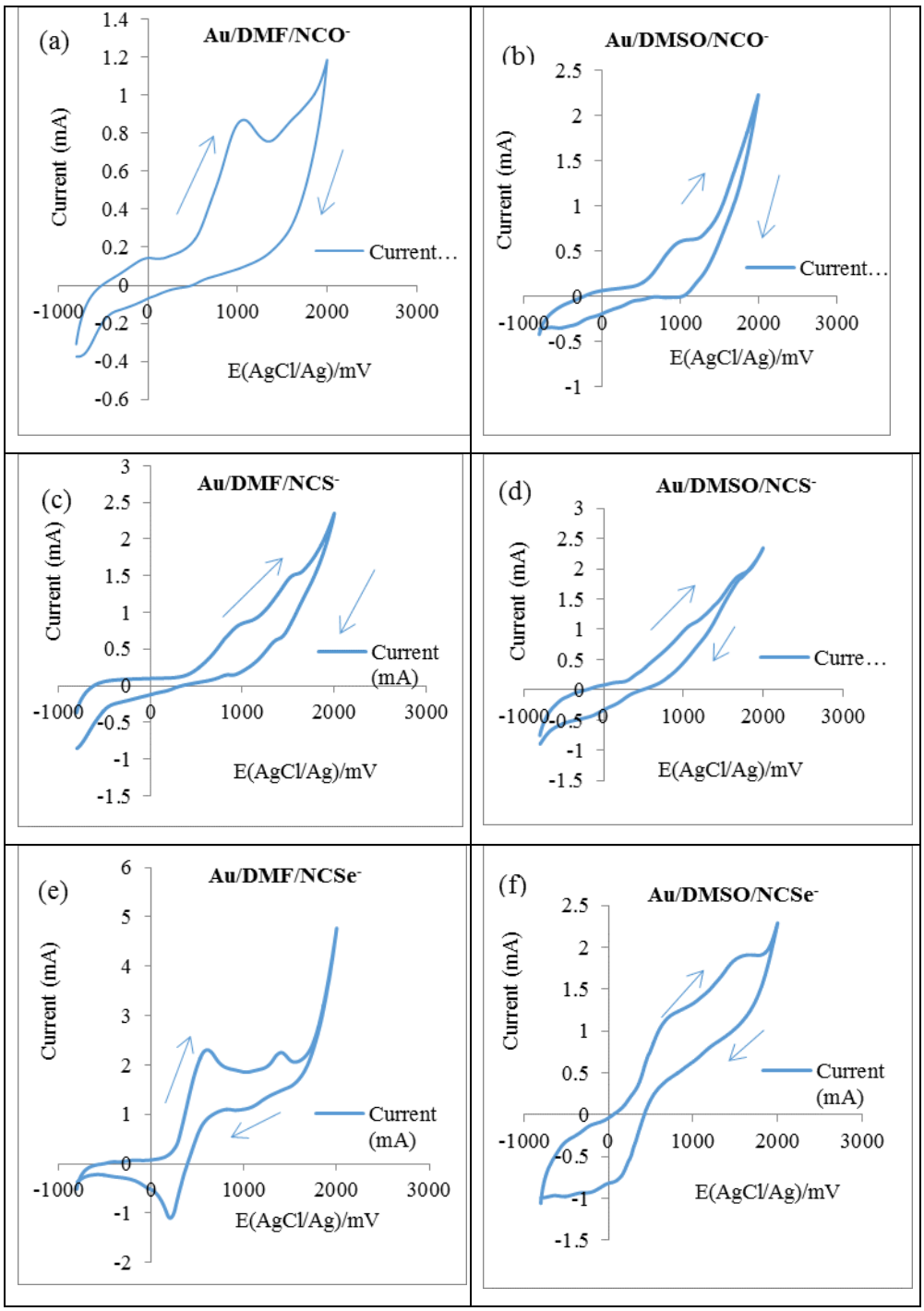

Figure 6.1: Cyclic voltammograms of the gold electrode in DMF and DMSO solvents containing pseudohalide ions and 0.1 mol L^{-1} TBAP (sweep rate = 20 mV/s) 0.025 mol L^{-1} KOCN in (a) DMF and (b) DMSO , 0.05 mol L^{-1} NaSCN in (c) DMF and (d) DMSO 0.05 mol L^{-1} KSeCN in (e) DMF and (f) DMSO. Arrows show the path actually traced upon conducting the sweep of potentials.

In the case of Au/NCO^-/ DMSO or DMF systems (Figure 6.11(a) and (b)), the CV shows a distinct broad peak at *ca.* 1000 mV(AgCl/Ag) which is most likely associated with Au to Au(I) electrodissolution [95]. In the Au/NCS^-/DMF system (Figure 6.1(d)) there are two peaks observed in the CV recorded in the DMF

solvent at *ca.* 1000 mV(AgCl/Ag) and 1500 mV(AgCl/Ag) and both could be due to the formation of Au(I) species [95], though the literature often provides conflicting views of this. For instance, in the paper by Dickinson and Povey (1975) [125], the potential at which Au^{3+} oxide is produced on Au electrode in sulphuric acid is *ca.* 1.5 V(SCE) however this is for the (Au) electrode immersed in an aqueous electrolyte. In general, the later in situ IR work (to be discussed) did not demonstrate the detection of any Au^{3+}-based species (see later).

The CV produced for the Au/NCS^-/DMSO system (Figure 6.1(c)) does not demonstrate distinct peaks. The CVs for the Au/$NCSe^-$/DMSO and Au/$NCSe^-$/DMF systems (Figure 6.1(e) and (f)) exhibit two peaks also with the CV for the Au/$NCSe^-$/DMF system showing the most well defined peaks. The difference between the CV for this system and those exhibited in Figure 6.1(a) to (d) is that the first peak occurs at a lower potential of 550-600 mV(AgCl/Ag). Also in the Au electrode systems involving $NCSe^-$ in both DMSO and DMF, there are distinct negative-going features evident in the CVs which indicate the reduction of a deposited film on the electrode. When observing the "single sweep voltammograms" of the electrode systems (Figure S.14(a) to (f) in Appendix 7) [acquired during the course of the SNIFTIRS experiment, see later], the appearance of the voltammograms is visibly different from the CVs illustrated in Figure 6.1. This is due to the fact that the time scale of the potential at the electrode surface is different for the single sweep voltammogram from that observed for the CVs which were recorded at a sweep rate of 20 mV/s operating over a potential span of 2800 mV each way (corresponding to 4.7 minutes for the entire sweep). In contrast the single sweep voltammograms are recorded over the time scale of the SNIFTIRS experiment which averages approximately 45 minutes per run and are only for data that occur when potential is adjusted in one direction, i.e. anodically. Nevertheless in the case of the Au/NCS^- and Au/$NCSe^-$ systems, two peaks in the single sweep voltammogram can still be mostly discerned (Figure S.14(d), (e) and (f) in Appendix 7).

Martins et al. [52] have done an electrochemical study of Au dissolution kinetics in DMSO solutions of KSCN containing $LiClO_4$ as the supporting electrolyte. They state that whilst the faradaic processes of NCS^- ion on Pt electrodes in

acetonitrile (ACN) involve transformations of the NCS^- ion itself into various oxidation products such as $(SCN)_2$ (at lower NCS^- concentrations and T < 30°C) and NCS^- based polymers (at higher concentrations of NCS^- and T > 30°C), the situation on Au electrodes is different. This is because the faradaic processes involve not just the pseudohalide ion undergoing transformations but in fact electrodissolution of the Au electrode itself to produce complex-ion species. This is supported by a later study by Benari et al. [95] although these authors make no reference to $(SCN)_2$ type by-products as Martins did.

6.3.2 In situ IR spectra of the Au/pseudohalide systems in DMSO and DMF

Table 6.1 summarises all the vibrational frequencies observed in the in situ IR spectra reported for the Au/pseudohalide systems in DMSO and DMF. Further details on these assignments are provided below under each system discussed.

6.3.2.1 Au/NCO^-/DMSO and Au/NCO^-/DMF

Figure 6.2(a) and Figure 6.2(b) are the SNIFTIRS spectra of the Au electrode anodically polarised in the presence of 0.025 mol L^{-1} KOCN/0.1 mol L^{-1} TBAP dissolved in DMSO and DMF respectively. Figure 6.3(a) and Figure 6.3(b) are the corresponding intensity/applied potential plots showing intensity changes in detected molecular species as a function of applied potential for the Au/NCO^-/DMSO and Au/NCO^-/DMF respectively. The single sweep voltammograms pertaining to these systems are illustrated in Figure S.14(a) and S.14(b) in Appendix 7.

Inspection of the spectra in Figure 6.2(a) and (b) reveal three main species in this system which give peaks at 2137/2147 cm^{-1}, 2230 cm^{-1} and 2337 cm^{-1}. The characteristically double-headed peak at 2137/2147 cm^{-1} is due to free cyanate ion in DMSO and DMF electrolyte. This characteristic shape seen in DMSO and DMF is due to its being dissolved in a solvent with which it interacts less strongly and hence shows up more fine structure [67] present in the IR absorption band compared to aqueous solvents where the expectedly stronger intermolecular forces of water have caused the vibrational peaks of the cyanate ion to blend together to form a mostly symmetrical/smoother looking peak. This smoother peak has been observed in earlier SNIFTIRS studies involving aqueous electrolytes [36, 37].

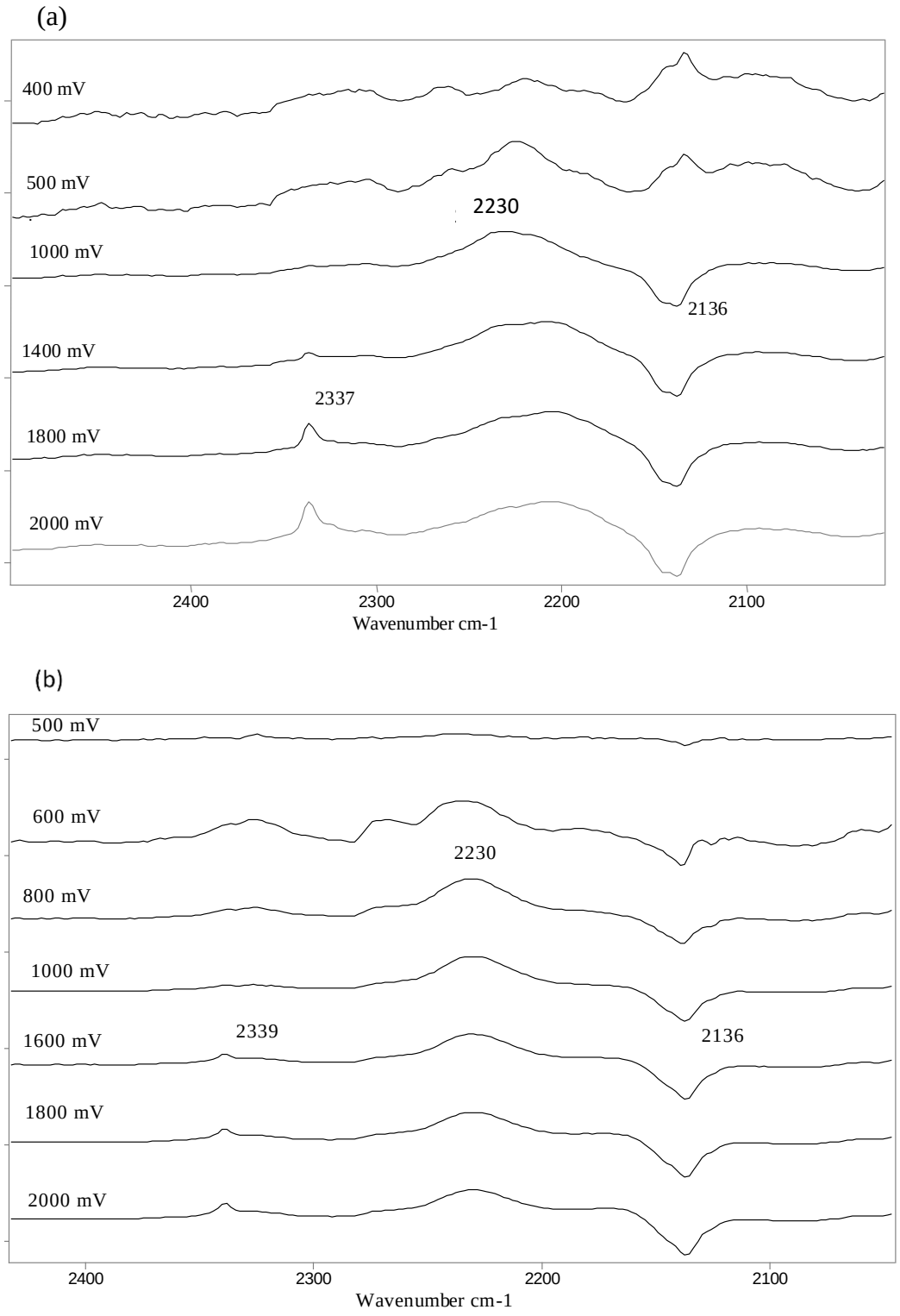

Figure 6.2: Series of SNIFTIRS spectra of the gold electrode as a function of applied potential in DMSO and DMF solvents containing pseudohalide ions and 0.1 mol L^{-1} TBAP. (a) 0.025 mol L^{-1} KOCN in DMSO, (b) 0.025 mol L^{-1} KOCN in DMF.

Table 6.1: FTIR data from in situ IR spectroelectrochemical studies of Au/NCX$^-$ systems electrochemically polarised in 0.1 mol L^{-1} TBAP in DMSO or DMF solvents

System studied	ν(CN) of free NCX$^-$ ion (X = O, S, Se) cm^{-1}	ν(CN) of Au$^+$/ NCX$^-$ complex ion cm^{-1}	ν(CO) of CO_2 dissolved in solvent cm^{-1}	Colour of cell solution after SNIFTIRS experiment
Au/DMF/NCO$^-$	2137/2147	2230	2339	no colour change
Au /DMF/NCS$^-$	2056	2123	2337	no colour change
Au /DMF/NCSe$^-$	2064	2125	nd	light yellow
Au /DMSO/ NCO$^-$	2136/2147	2234	2337	no colour change
Au /DMSO/NCS$^-$	2055	2124	nd	no colour change
Au /DMSO/NCSe$^-$	2065	2124	nd	light yellow

nd= not detected

The spectral behaviour of the 2137/2147 cm^{-1}(due to from cyanate ion) peak does not change until the anodic region is entered where it shows negative intensity relative to the background recorded at -900 mV(AgCl/Ag). This indicates the ion is being consumed at the Au electrode surface as it is anodically polarised to form complex ion species via Au(I) formation and undergo electro oxidation. The drop in intensity as seen in Figure 6.3(a) and (b) is sharp over the region 700 - 1000 mV(AgCl/Ag) for the Au electrode in DMF and over the 500 - 700 mV(AgCl/Ag) region for DMSO before it levels off. Paralleling this decrease in intensity of the 2137/2147 cm^{-1} peak in Figure 6.3(a) and (b) is an increase in the intensity of the broad 2230 cm^{-1} peak. The origin of peaks observed in this region of the spectrum has been subject to various interpretations. One study by Zhen et al. [124] states that a weak, broad peak was observed at 2230 cm^{-1} in their in situ IR spectra of a Au(III) (not Au^{3+}) single crystal electrode (adjusted to 0.5 V (SCE)) in the presence of 0.1 mol L^{-1} NaOH and 50 mmol L^{-1} glycine.

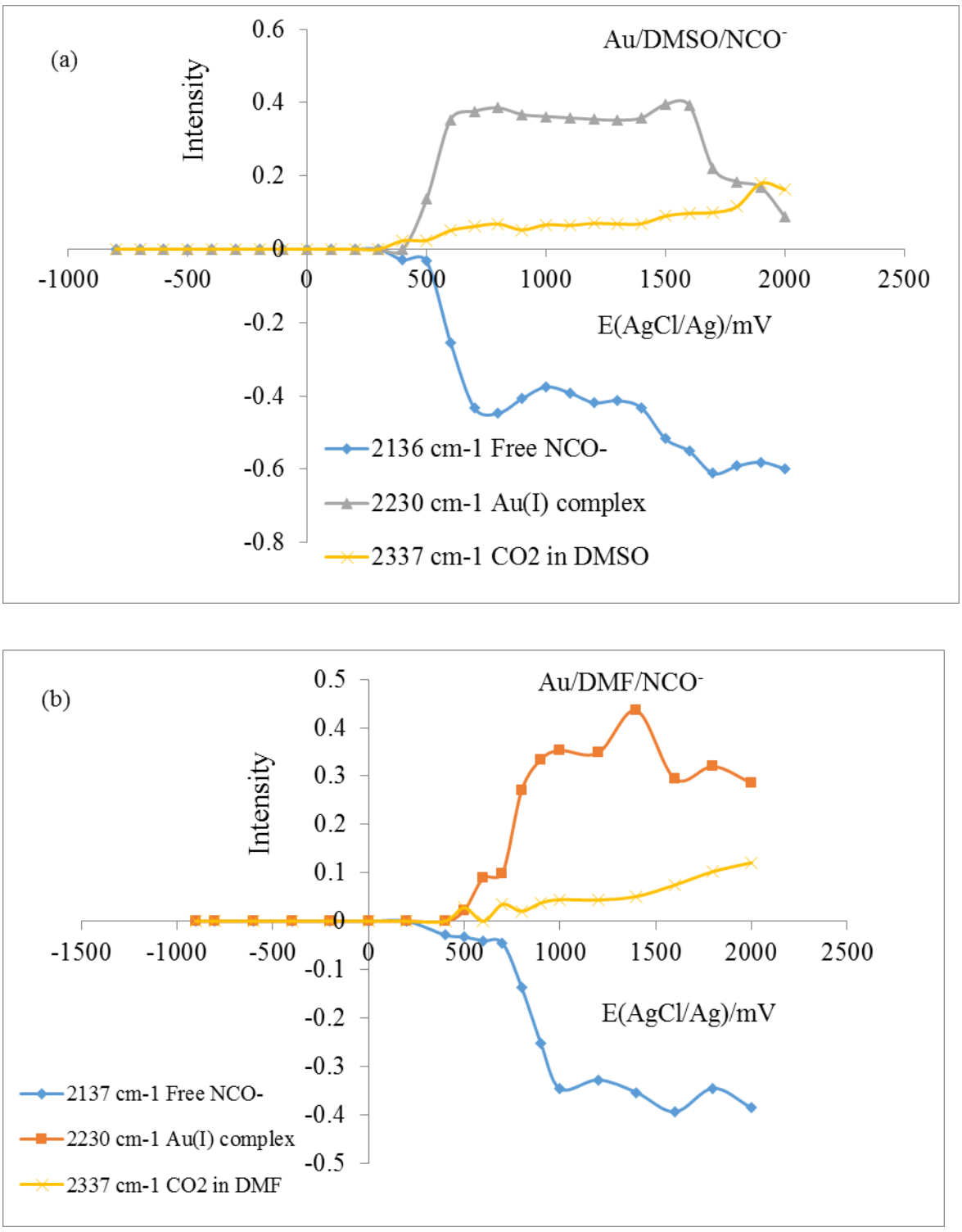

Figure 6.3: Plots of the intensity changes of the various molecular species generated in the thin layer during electrochemical polarisation and observed in the SNIFTIRS spectra as a function of applied potential in the gold electrode as a function of applied potential in DMSO and DMF solvents containing pseudohalide ions and 0.1 mol L^{-1} TBAP. (a) 0.025 mol L^{-1} KOCN in DMSO, (b) 0.025 mol L^{-1} KOCN in DMF.

This was interestingly assigned to an insoluble AuCN film. However, in the present study involving polar aprotic solvents, it is believed that this peak is due to a Au(I) complex ion species forming through electrodissolution of the Au to

Au(I) and subsequent complexation with cyanate ion to form a species thought to be $Au(NCO)_2^-$. Although no study has reported the IR stretching frequency of this simple ion in DMSO, DMF or even aqueous solution, the CN stretching frequency is close in magnitude to the 2251 cm^{-1} CN stretching frequency detected in the KBr disk IR spectrum of solid $[Ph_4As]Au(NCO)_2$ as reported by Beck et al. [126] (1969). Model solution work reported later in this paper also supports the assignment of this species to the $[Au(NCO)_2]^-$ ion. The observation of this species hence supports the views of Benari et al. and Martins et al [52, 95] that the Au is undergoing active dissolution in this region to form Au(I) complex ion species. The intensity of this peak as a function of applied potential at the Au electrode increases sharply as stated earlier but then levels off which could indicate the deposition of an insoluble film on the electrode surface containing the Au(I) species. This may have occurred due to large onset of formation of Au(I) at the electrode followed by complexation, increase in concentration and then precipitation due to saturation of the thin layer with this compound. The other peak observed in SNIFTIRS spectra Figure 6.2(a) and (b)) is a peak at 2337 cm^{-1} which based on earlier works (chapter 3 and 5) can be assigned to electrogenerated CO_2 dissolved in the DMSO or DMF solvent. The source of this CO_2 is likely to be from the oxidation of cyanate ion and or solvent oxidation.

Its intensity as a function of applied potential (Figure 6.3(a) and (b)) is low with a slight increase being observed as more anodic potentials are applied at the Au electrode. The difference in electrochemical behaviour between the DMSO and DMF solvents was small. Apart from the region corresponding to the sharp drop in free cyanate ion intensity in SNIFTIRS spectra, DMSO and DMF generally exhibit almost identical behaviour in terms of speciation observed at the electrode surface.

6.3.2.2 Au/NCS^-/DMSO and Au/NCS^-/DMF

Figure 6.4(a) and Figure 6.4(b) are the SNIFTIRS spectra of the Au electrode anodically polarised in the presence of 0.05 mol L^{-1} NaSCN/0.1 mol L^{-1} TBAP dissolved in DMSO and DMF respectively. The higher concentration of NCS^- used in this experiment was due to the greater solubility of this salt in the electrolyte relative to KOCN which remained partially undissolved at the same concentration. Figure 6.5(a) and Figure 6.5(b) are the corresponding intensity/applied potential plots showing intensity changes in detected molecular

species as a function of applied potential for the Au/NCS^-/DMSO and Au/NCS^-/DMF respectively. The single sweep voltammograms pertaining to these systems are illustrated in Figure S.14(c) and S.14(d) in Appendix 7.

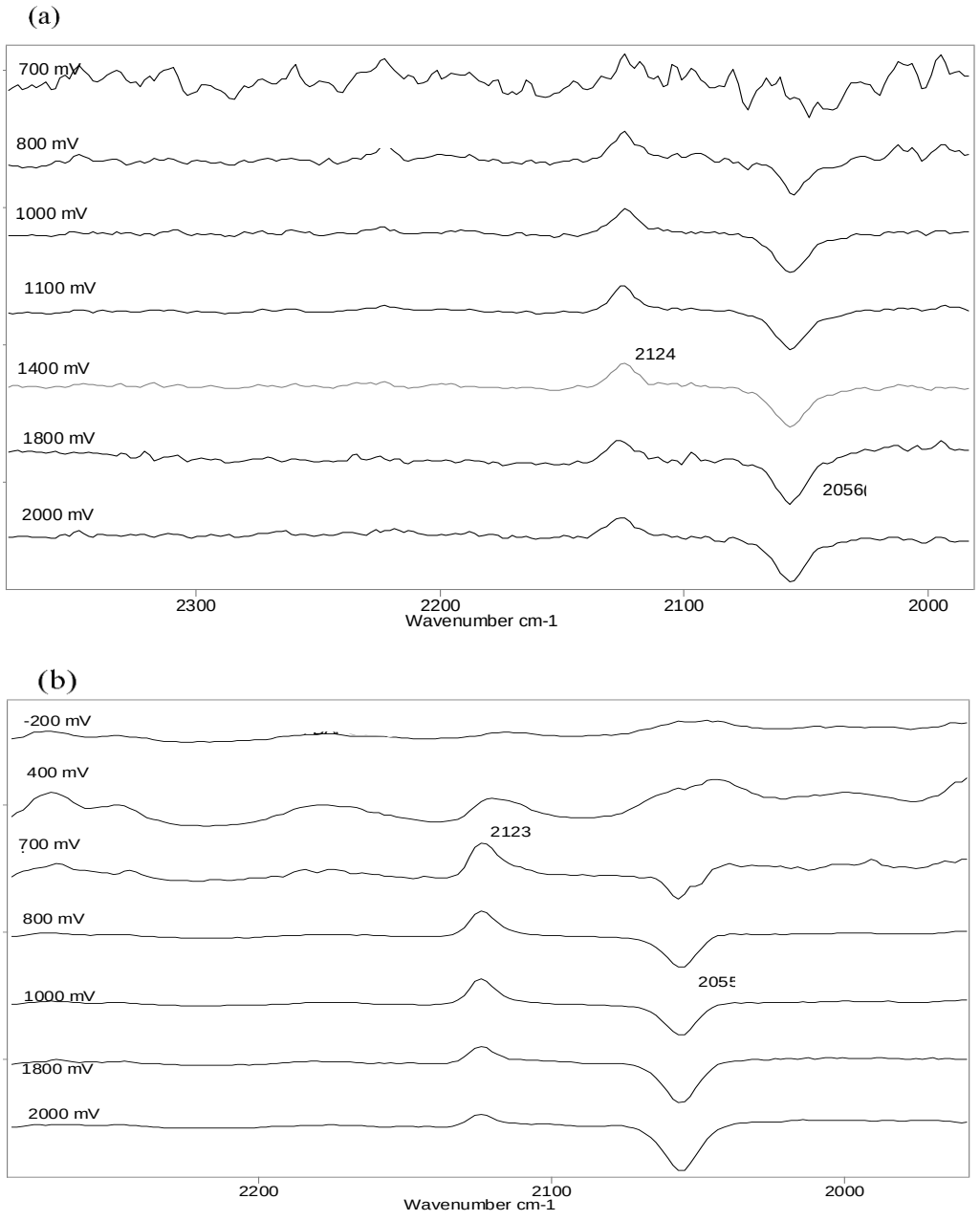

Figure 6.4: Series of SNIFTIRS spectra of the gold electrode as a function of applied potential in DMSO and DMF solvents containing pseudohalide ions and 0.1 mol L^{-1} TBAP. (a) 0.05 mol L^{-1} NaSCN in DMSO, (b) 0.05 mol L^{-1} NaSCN in DMF.

Inspection of the spectra in Figure 6.4(a) and (b) reveal two main species in this system (as well as a third minor one) all of which give peaks at 2055 cm^{-1}, 2123 cm^{-1} and 2337 cm^{-1}.

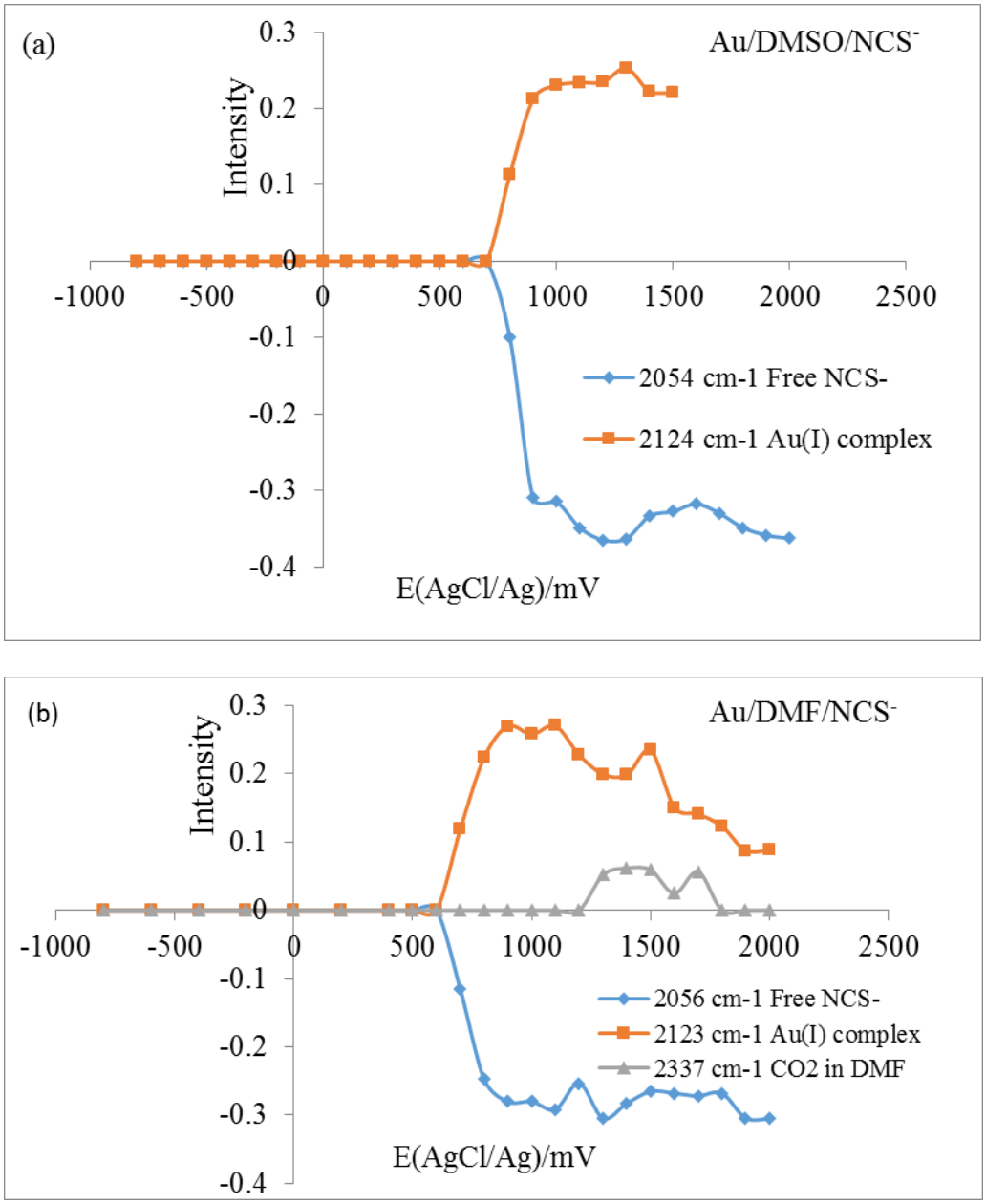

Figure 6.5:Plots of the intensity changes of the various molecular species generated in the thin layer during electrochemical polarisation and observed in the SNIFTIRS spectra as a function of applied potential in the gold electrode as a function of applied potential in DMSO and DMF solvents containing pseudohalide ions and 0.1 mol L^{-1} TBAP. (a) 0.05 mol L^{-1} NaSCN in DMSO, (b) 0.05 mol L^{-1} NaSCN in DMF.

The spectral behaviour of the 2055 cm^{-1} peak (similar to the NCO^- system) attributed to free thiocyanate ion does not change or even register a peak until the

anodic region is entered where it shows negative intensity relative to the background recorded at -900 mV(AgCl/Ag). This indicates, as in the Au/NCO^- system case that the free thiocyanate ion is being consumed at the Au electrode surface as it undergoes anodic dissolution to form complex ion species and also when the NCS^- ion undergoes electro oxidation itself at the electrode (the products of which are not immediately observed in the CN stretching region). The drop in intensity as seen in Figure 6.5(a) and (b) is very sharp over the region 700 - 900 mV(AgCl/Ag) for the Au electrode in DMSO and over the 600 - 800 mV(AgCl/Ag) region for DMF before it fluctuates/levels off. Paralleling this decrease in intensity of the 2055 cm^{-1} peak in Figure 6.5(a) and (b) is an increase in the intensity of the broad 2123 cm^{-1} peak. This peak can be unequivocally attributed to an Au(I) complex ion species with NCS^- ion, i.e. $[Au(SCN)_2]^-$.

This is well supported by literature studies [94, 127] in which the CN stretching frequency of this has been determined for this complex ion in non-aqueous media. For instance, Bowmaker and Rogers [94] reported that a peak observed at 2120 cm^{-1} in a dichloromethane solution of $[NBu_4]Au(SCN)_2$ was due to the $[Au(SCN)_2]^-$ ion in solution. In the same study, it is also shown that Au bonds to S in this complex and not N as would be the case with $[Au(NCO)_2]^-$ discussed earlier. Hence it is obvious that at 500-600 mV (AgCl/Ag), Au dissolves to form Au(I) which then is complexed by NCS^- ion to form $[Au(SCN)_2]^-$. Figure 6.5(a) and (b), show a levelling off of the intensity of 2123 cm^{-1} peak at about 1000 mV(AgCl/Ag) which may be indicative of an insoluble film of the complex ion forming on the electrode surface due to the burst of formation of the Au(I) complex and its release into the thin layer so saturating the solution. There is a distinct peak observed in the single sweep voltammogram of the Au/NCS^-/DMF system at ca. 700 mV(AgCl/Ag) (Figure S.14(d) in Appendix 7) which can be clearly associated with the Au to Au(I) electrodissolution event. An additional peak just before +1500 mV(AgCl/Ag) could be a Au to Au(III) oxidation peak but it does not appear to be associated with the emergence in the IR of any $[Au(SCN)_4]^-$ species which has been reported to be isolated as an unstable insoluble red solid from cold aqueous reaction mixtures of Au^{3+} and thiocyanate ion [128]. In the present study, the cell solution was observed to remain colourless during this in situ IR experiment so suggesting that this

complex ion species had not formed. Furthermore, the IR spectrum did not reveal any new peaks other than those discussed above which might be associated with this species.

The other peak observed in SNIFTIRS spectra is a peak at 2337 cm^{-1} which can be assigned to electrogenerated CO_2. This was only observed in the DMF solvent. The source of this CO_2 is likely to be from the oxidation of DMF. This is supported by the fact that it is only observed as a minor species at 1200-1500 mV(AgCl/Ag) where DMF would be expected to become oxidised at the electrode surface.

6.3.2.3 Au/$NCSe^-$/DMSO and Au/$NCSe^-$/DMF

Figure 6.6(a) and Figure 6.6(b) are the SNIFTIRS spectra of the Au electrode anodically polarised in the presence of 0.05 mol L^{-1} KSeCN/0.1 mol L^{-1} TBAP dissolved in DMSO and DMF respectively. The higher concentration of $SeCN^-$ used in this experiment was due to the greater solubility (in common with NaSCN) of this salt in the electrolyte. Figure 6.7(a) and Figure 6.7(b) are the corresponding intensity/applied potential plots showing intensity changes in detected molecular species as a function of applied potential for the Au/$NCSe^-$/DMSO and Au/$NCSe^-$/DMF respectively. The single sweep voltammograms pertaining to these systems are illustrated in Figure S.14(e) and S.14(f) in Appendix 7.

Inspection of the in situ IR spectra in Figure 6.6(a) and (b) reveals two main species in this system which give peaks at 2065 cm^{-1} and 2124-2126 cm^{-1}. The 2065 cm^{-1} peak can be attributed to free selenocyanate ion dissolved in the polar aprotic solvent. This agrees with the vibrational frequency reported for KSeCN dissolved in butanone solution [129] and has a lower vibrational frequency compared to that observed for the ion dissolved in water [37] as expected for this lower polarity solvent. In common with the Au/NCS^- and Au/$NCSe^-$ systems, the free ion peak does not appear in the IR spectrum until the anodic region is entered where it shows negative intensity relative to the background recorded at -900 mV(AgCl/Ag).

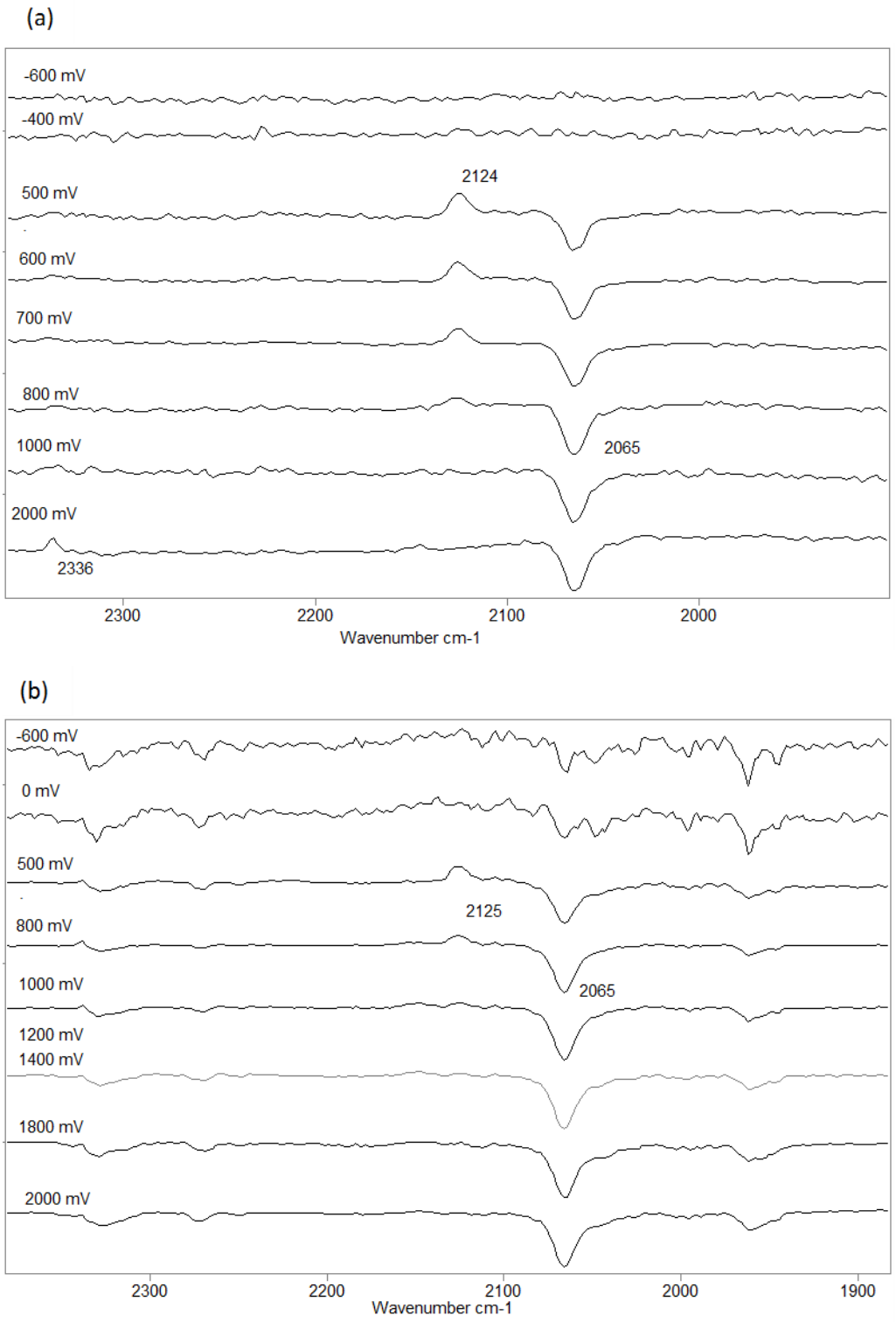

Figure 6.6: Series of SNIFTIRS spectra of the gold electrode as a function of applied potential in DMSO and DMF solvents containing pseudohalide ions and 0.1 mol L^{-1} TBAP. (a) 0.05 mol L^{-1} KSeCN in DMSO, (b) 0.05 mol L^{-1} KSeCN in DMF.

This indicates, as in the other systems that the free selenocyanate ion is being consumed at the Au surface as the electrode undergoes anodic dissolution to form complex ion species and also when the $NCSe^-$ ion, itself, undergoes electro-oxidation at the electrode (the products of which are not immediately observed in

the CN stretching region). When observing the intensity vs applied potential plots in Figure 6.7(a) and (b), sharp/sudden increases/decreases in the intensities of the peaks due to the free ion and the peak at 2124-2126 cm^{-1} followed by a drop and levelling off of the intensities indicates an anodic dissolution event where Au is oxidised to Au(I) after 500 mV(AgCl/Ag) and then probably forms an adherent film on the surface of the electrode.

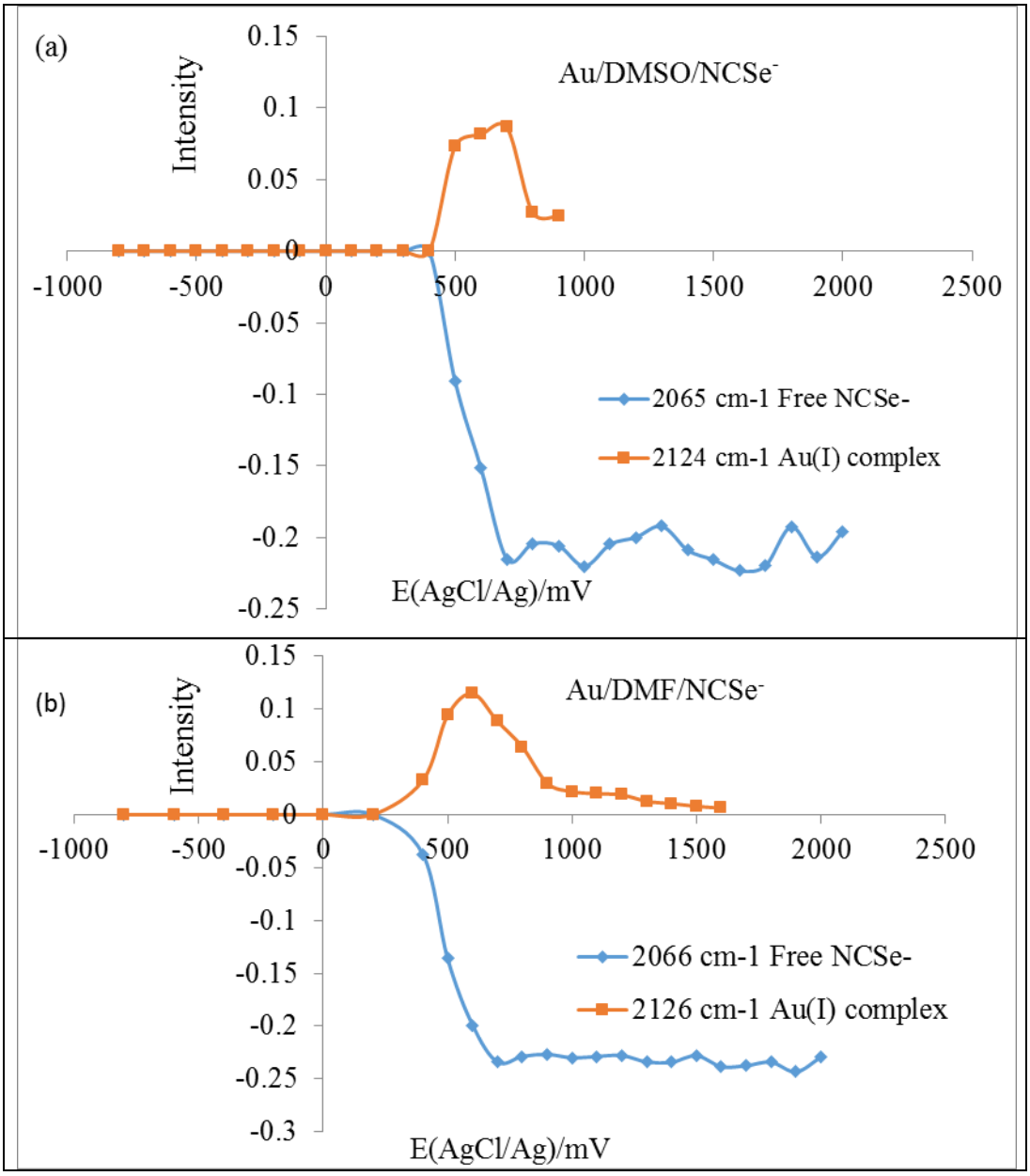

Figure 6.7: Plots of the intensity changes of the various molecular species generated in the thin layer during electrochemical polarisation and observed in the SNIFTIRS spectra as a function of applied potential in the gold electrode as a function of applied potential in DMSO and DMF solvents containing pseudohalide ions and 0.1 mol L^{-1} TBAP. (a) 0.05 mol L^{-1} KSeCN in DMSO, (b) 0.05 mol L^{-1} KSeCN in DMF.

This is supported also by the single sweep voltammograms (Figure. S.14(e) and (f) in Appendix 7) which show a plateau of current after 500 mV(AgCl/Ag). This lasts until 1600 mV(AgCl/Ag) after which the current increases sharply due most likely to events like oxidation of the solvent (DMSO or DMF). Furthermore, after the in situ IR experiment, a black film was observed on the Au electrode surface.

The drop in the intensity to more negative values of the 2065 cm^{-1} free selenocyanate ion peak is paralleled by an increase in intensity of the peak at 2124-2126 cm^{-1}. As in the Au/NCS^- system, this peak can be unequivocally attributed to an Au(I) complex ion species with $NCSe^-$ ion, It is strongly believed this is due to the $[Au(SeCN)_2]^-$ ion dissolved in DMSO or DMF. While direct spectroscopic evidence does not appear to exist in the literature for this ion, it can be inferred to be the case from the similarity of its vibrational frequency to that of the $Au(SCN)_2^-$ ion as detected in the Au/NCS^- electrochemical system discussed previously.

6.3.3 Model Solution work for verifying species observed in in situ IR spectra

In order to provide a verification of the species observed in the in situ IR spectra provided of the Au/NCO^-, Au/NCS^- and Au/$NCSe^-$ systems as discussed above, model solution work was carried out in order to make species detected in in situ IR spectra independently of their electrochemical method of generation in order to prove the identity of them. This involved the mixing of DMSO/DMF solutions of $KAuBr_4$ and the pseudohalide salts (NCO^-, NCS^- and $NCSe^-$ in 1:1 and 1:2 mole ratios for solutions made in DMF (due to solubility issues of the salts in this solvent) and 1:1, 1:2 and 1:4 mole ratio solutions for solutions made in DMSO (in which the solubility of the pseudohalide salts were better than in DMF). These model solutions were then examined using transmission IR spectra of a thin layer of the solutions created between calcium fluoride windows as previously described.

Table 6.2 is a summary of the IR data collected from the model solution spectra.

Table 6.2: FTIR data from IR studies of DMF or DMSO model solutions of $KAuBr_4$ and potassium (or sodium) pseudohalide ion salts prepared with different mole ratios.

Model solution studied and mole ratio of $KAuBr_4$: pseudohalide salt prepared in DMF or DMSO (X = O, S, Se)	ν(CN) of free NCX^- ion (X = O, S, Se) cm^{-1}	ν(CN) of Au(I)/Au(III)/NCX^- complex ion cm^{-1}	Observed colour of solution
DMF			
$KAuBr_4$/ KOCN 1:1	nd	2168 s	Blood red
$KAuBr_4$/ KOCN 1:2	nd	2168 s	
$KAuBr_4$/ NaSCN 1:1	nd	nd	Blood red
$KAuBr_4$/ NaSCN 1:2	2055	2120 w	
$KAuBr_4$/ KSeCN 1:1	nd	nd	Orange/yellow
$KAuBr_4$/ KSeCN 1:2	2065	2126 w	Yellow
DMSO			
$KAuBr_4$/ KOCN 1:1	nd	2166	Blood red
$KAuBr_4$/ KOCN 1:2	nd	2165	
$AuBr_4$/ KOCN 1:4	2136	2165	
$KAuBr_4$/ NaSCN 1:1	2055 w	nd	Blood red
$KAuBr_4$/ NaSCN 1:2	2055	2120	
$AuBr_4$/ NaSCN 1:4	2055	2120, 2143w	
$KAuBr_4$/ KSeCN 1:1	nd	nd	
$KAuBr_4$/ KSeCN 1:2	2065	2124	Orange/yellow
$KAuBr_4$/ KSeCN 1:4	2065	2124, 2143w	Yellow

nd=not detected, s=strong, w=weak

6.3.3.1 $KAuBr_4$/KOCN model solutions

As is evident in Table 6.2, the IR spectra show a peak ranging from 2163-2168 cm^{-1} in the two solvents. No peak due to the free cyanate ion was observed apart from the $KAuBr_4$:KOCN 1:4 mole ratio solution where a small shoulder at 2136 cm^{-1} was observed on the more intense peak at *ca.* 2163 cm^{-1}. The wavenumber value at 2163-2168 cm^{-1} is obviously not the same as the wavenumber value observed in the in situ IR spectra of the Au/NCO^- electrochemical system which was at 2230 cm^{-1}. This is because in the model solutions consisting of $KAuBr_4$ and KOCN, another species different to that observed in the electrochemical experiments has formed, and this species is a Au(III)-cyanate complex or complexes. To test this, it was decided to carry out an

ESI-MS spectrum of the 1:4 mole ratio (Au(III):NCO^-) model solution to gain an idea of what species are likely to be present in the actual solution. Figure 6.8(a) illustrates the ESI-MS spectrum of this sample diluted in methanol before introducing it into the ESI-MS instrument. The spectrum is dominated by an intense peak at m/z= 364.97 which can be assigned to the species $[Au(NCO)_4]^-$, a gold(III) complex ion. This agrees with the expected isotopic splitting of the peak which will only show weak splitting due to ^{13}C which gives a weak peak at m/z = ~366. In addition there are other peaks which are much weaker than the m/z=364.97 peak. These species are easy to identify due to the more significant isotopic patterns produced by the Br^- ion which is present in these complexes. Table 6.3 is a summary of the assignments made for this system and others to be discussed. Hence characteristic peaks at m/z 401.90 and 440.82 are observed which are assigned to $[Au(NCO)_3Br]^-$ and $[Au(NCO)_2Br_2]^-$ respectively. Another weak peak is also observed at m/z= 280.98. This is believed to be due to the species $[Au(NCO)_2]^-$ which is not likely to be present in the solution but has occurred as an artefact as a result of reduction arising out of the use of a negative cone voltage in the ESI-MS experiment [23]. The ESI-MS work hence confirms that the peaks observed at 2162-2168 cm^{-1} in the IR spectra (in both DMF and DMSO) of the $KAuBr_4$/KOCN model solutions are due to Au(III)-cyanate complexes. Literature with IR data for discrete simple Au(III)-NCO complexes to support this assignment appears, however, to be lacking hence this work reports this for the first time. In DMSO solutions, there is a small shift of the ν(CN) stretching frequency in going from 1:1 to 1:4 $KAuBr_4$:KOCN mole ratio solutions which indicates the formation of higher order complexes such as $[Au(NCO)_4]^-$. It remains however to prove that $[Au(NCO)_2]^-$ can be synthesised in solution independently of the electrochemical cell. This was provided in later experiments where the Au(III) starting salt was reduced initially to Au(I) by premixing with NaSCN (see later).

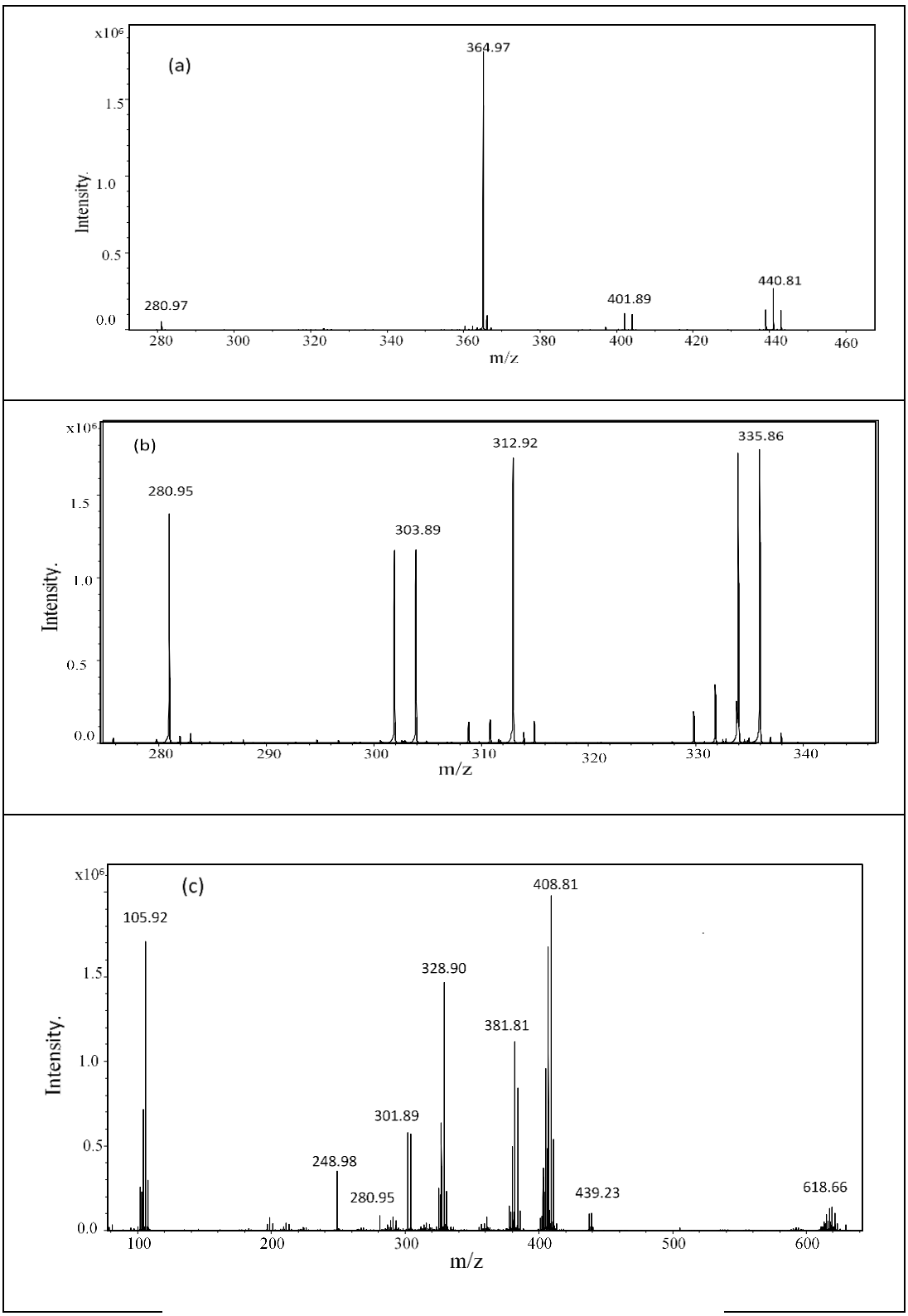

Figure 6.8: Electrospray ionisation mass spectra (ESI-MS) of the Au(III) pseudohalide complexes in the model solutions prepared with $KAuBr_4$ salts and pseudohalide salts in DMSO solution where [$KAuBr_4$] = 0.025 mol L^{-1} and [pseudohalide salt] = 0.1 mol L^{-1}. The sample was diluted in methanol before introducing into the ESI-MS by adding a drop of model solution (1 µL) to 1 mL of methanol. (a) 1:4 $KAuBr_4$:KOCN mole ratio solutions, (b) 1:4 $KAuBr_4$:NaSCN mole ratio solutions, (c) 1:4 $KAuBr_4$:KSeCN mole ratio solutions.

6.3.3.2 $KAuBr_4$/NaSCN model solutions

Table 6.2 shows that when mixing $KAuBr_4$ and NaSCN in different mole ratios (varying from 1:1 to 1:4 $KAuBr_4$:NaSCN) three peaks were generally observed in the IR spectra. These peaks occurred at 2055, 2120.5 and 2143 cm^{-1}. The peak at 2055 cm^{-1} is due to the free NCS^- ion as expected. The other weak peak at 2120.5 cm^{-1} can be assigned to $[Au(SCN)_2]^-$ ion although it is 3-4 cm^{-1} different from the peak observed in the in situ IR experiment (see Table 6.1). This result from the model solution IR experiments proves that NCS^- ion is reducing the Au(III) present in $KAuBr_4$ to Au(I) which subsequently forms a complex with NCS^- ion in solution to generate the complex ion, $[Au(SCN)_2]^-$. This was confirmed by recording the ESI-MS spectrum of the 1:4 $KAuBr_4$: NaSCN model solution in DMSO which is shown in Figure 6.8(b). This featured a group of 4 major peaks at m/z 280.95, 303.90, 312.93 and 335.87 which can be assigned to $[Au(SCN)(CN)]^-$, $[Au(CN)Br]^-$, $[Au(SCN)_2]^-$ and $[Au(SCN)Br]^-$. All of these species are Au(I) species which reflects that redox reactions have occurred in this solution reducing Au(III) to Au(I). This agrees with previous literature on the subject [130]. Of note is the m/z peak at 312.9 due to the stable $[Au(SCN)_2]^-$ ion which is proof the ion exists in the model solution. It is interesting to note that the other species are mixed ligand species with one involving Br^- and CN^- ion. The detection of a Au-cyano species suggests that the NCS^- ion itself has been induced to convert to CN^- due to the strong thermodynamic driving force of forming a Au(I) cyano complex ion. This would explain the peak observed at 2143 cm^{-1} in the IR transmission spectrum which on the basis of its similarity to the vibrational frequency of $[Au(CN)_2]^-$ in solution is probably due to a C-N stretch of a coordinated cyanide group bound to a Au(I) centre [7]. Conversion of NCS^- to CN^- is known [130, 131] to occur in acidic aqueous solution via thiocyanous acid formation. In DMSO, however, NCS^- is more stable as an ion [132], however mixing Au(III) with thiocyanate ion leads to a redox reaction as discussed above producing Au(I) species which may induce side reactions in which the NCS^- is converted to CN^-. The driving force for such a reaction is the stability of the resultant Au-CN-type complex ion formed in solution. This is because the $[Au(CN)_2]^-$ ion is reported to have one of the highest formation constants known for a transition metal complex ion with K values in the vicinity of 10^{37} L^2 mol^{-2} [133].

6.3.3.3 $KAuBr_4$/KSeCN model solutions

In common with the $KAuBr_4$/NaSCN model solution systems, the IR spectra of the KSeCN based model solutions also feature three peaks which occur at 2065, 2124 and 2143 cm^{-1}. On the basis of assignments provided for the $KAuBr_4$/NaSCN model solution discussed above, these peaks may be assigned to free selenocyanate ion (2065 cm^{-1}), the $[Au(SeCN)_2]^-$ complex ion (2124 cm^{-1}) and a gold-cyano complex (2143 cm^{-1}) respectively. The wavenumber value of the peak assigned to $[Au(SeCN)_2]^-$ is identical to that observed in the in situ IR spectra of the Au/$NCSe^-$ electrochemical system (compare Table 6.1 and Table 6.2, and Figure 6.6). The ESI-MS spectrum for the 1:4 mol ratio $KAuBr_4$/KSeCN model solution in DMSO is shown in Figure 6.8(c).

In systems involving Se-containing species, the distinct isotopic splitting patterns produced by the natural isotopes of selenium facilitate identification of species as the Se atom has 6 stable isotopes [134]. The ESI-MS spectra hence predictably gave very rich isotopic splitting patterns which could be easily matched by simulation and ascribed to Se-containing species (see Table 6.3). For example, free $NCSe^-$ ion gave a characteristic pattern of peaks centred at m/z 105.9. In addition, there was a peak assignable to $[Au(SeCN)_2]^-$ (m/z= 408.8) which confirmed the existence of this ion in solution as intimated by the IR spectra. This confirmed that a redox process had occurred also in this model solution where Au(III) had become reduced to Au(I). There was also evidence of a weak peak due to the Au(III)-selenocyanate complex, i.e. $[Au(SeCN)_4]^-$ at m/z 618.66. In addition there was evidence of other complex ion species (also noticed in the $KAuBr_4$/NaSCN DMSO model solution ESI-MS spectra), which involved the Br^- $NCSe^-$ and CN^- ions. These species occurred at m/z 381.8 ($[Au(SeCN)Br]^-$), m/z 328.9 ($[Au(CN)(SeCN)]^-$), m/z 301.9 ($[Au(CN)Br]^-$) and m/z 248.9 ($[Au(CN)_2]^-$). All of these ions involved Au in the +1 oxidation state with the Au(I)-cyano species being of particular note as the presence of these confirmed that $NCSe^-$ had also undergone chemical conversion to CN^- as had happened in the $KAuBr_4$/NaSCN model solution in DMSO. The detection of a peak at 2143 cm^{-1} in the IR spectrum of the 1:4 mole ratio $KAuBr_4$/KSeCN model solution in DMSO is IR proof of the existence of these Au(I) cyano complexes in solution.

6.3.3.4 Further experiments to prove the existence of $[Au(NCO)_2]^-$ ion through the use of model solutions.

Earlier it was shown that the mixing of $KAuBr_4$ with KOCN in DMSO in 1:1, 1:2 and 1:4 mole ratio solutions (with respect to $KAuBr_4$:KOCN) did not lead to the formation of a Au(I) complex ion as evidenced by the different ν(CN) stretching frequencies observed in the FTIR transmission spectrum of the model solution. Instead Au(III) –cyanate complexes were formed. In order to use model solutions to prove that the complex ion $[Au(NCO)_2]^-$ hypothesised to form during the anodic dissolution of Au in cyanate-containing DMSO (and DMF) solutions (see Figure 6.2) could be formed independently, a strategy exploiting the redox chemistry described above for the Au/NCS^- and $Au/NCSe^-$ model solution systems had to be used. It is known that in $KAuBr_4$/NaSCN model solutions, a redox reaction occurs to produce Au(I) complexes in solution. To exploit this reaction to generate the $[Au(NCO)_2]^-$ ion, "flooding" of an initially mixed $KAuBr_4/NCS^-$ model solution preparation was done in order to form a complex of $[Au(NCO)_2]^-$ by displacement of the existing NCS^- ion from $[Au(SCN)_2]^-$ ions present. Upon doing this experiment and running the IR spectra, the strategy appeared to work as is shown in Figure 6.9(a-d) which illustrate a series of IR spectra of $KAuBr_4$/NaSCN and $KAuBr_4$/NaSCN/KOCN solutions where the latter ("cyanate-flooded") system is studied as a function of $KAuBr_4$:KOCN mole ratio (varying from 1:1 to 1:4) with the $KAuBr_4$:NaSCN mole ratio kept constant at 1:4. In Figure 6.9(a), 3 peaks are observed at 2055.4, 2120.5 and 2143 cm^{-1}. As indicated in Table 6.2, the peaks detected in the IR spectrum are due to the free thiocyanate ion at 2055.4 cm^{-1} with the two weaker peaks being to complex ion species $[Au(SCN)_2]^-$ (2120.5 cm^{-1}) and the putative Au-cyano complex (2143 cm^{-1}) as discussed above.

In Figure 6.9(b) to (d), the spectra presented represent model solutions where relatively more cyanate ion has been added to the $KAuBr_4$/NaSCN model solutions. In Figure 6.9(c) and (d) the consequences of the cyanate addition to the solution was to cause the appearance of an additional broad peak at 2246 cm^{-1} (Figure 6.9(c)) which shifted to 2234 cm^{-1} in Figure 6.9(d). An additional asymmetrical peak was also observed at 2147.5 cm^{-1} in Figure 6.9(d) corresponding to the solution with the greatest amount of cyanate ion added. These extra peaks can be readily assigned to cyanate-containing species.

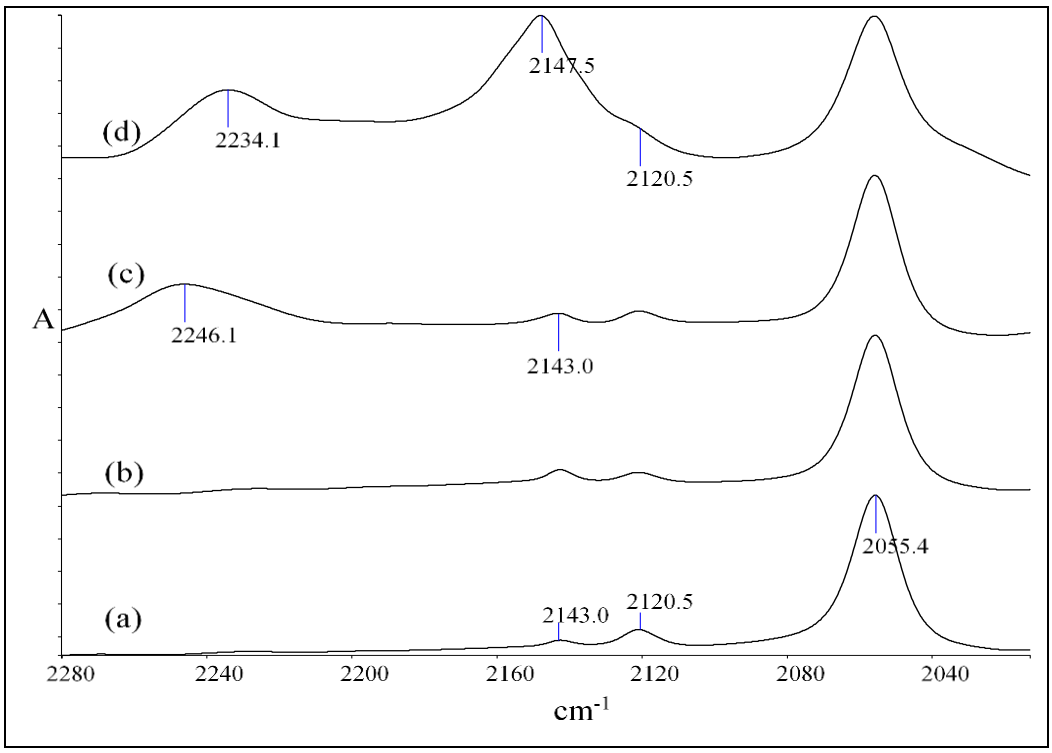

Figure 6.9: Transmission IR spectra of the model solutions prepared with $KAuBr_4$ salts and pseudohalide salts in DMSO solution where [$KAuBr_4$] = 0.025 mol L^{-1}, [NaSCN] = 0.1 mol L^{-1} and different amounts of KOCN salt. (a) 1:4 $KAuBr_4$: NCS^- mole ratio solutions., (b) 1:4:1 $KAuBr_4$: NCS^- : NCO^- mole ratio solutions., (c) 1:4:2 $KAuBr_4$: NCS^- : NCO^- mole ratio solutions. (d) 1:4:4 $KAuBr_4$: NCS^- : NCO^- mole ratio solutions.

The peak at 2147.5 cm^{-1} observed in Figure 6.9(d) is due to the free cyanate ion and has the typical peak shape expected for this ion when it is dissolved in DMSO solution. More importantly, the broader peaks occurring over the 2234-2246 cm^{-1} range are similar in frequency and shape to the weak, broad peak observed in the in situ IR spectra of Au electrodes anodically polarised in KOCN/DMSO/TBAP electrolytes. This peak is hence assigned to an Au(I)-cyanate complex ion. The shift in peak maximum in the IR spectra in going from Figure 6.9(c) to (d) is symptomatic of a mixed complex ion (e.g. $[Au(CN)(NCO)]^-$) being initially formed which is likely to convert to $[Au(NCO)_2]^-$ as more cyanate is added to the solution. The peak at 2234 cm^{-1} is very close in frequency to that peak observed in the in situ IR spectra as shown in Figure 6.2(a) earlier and hence is likely to be the same solution species, i.e $[Au(NCO)_2]^-$. Given the model solution is more complex in composition than the electrolyte cell solutions discussed earlier, it is important to recognise that other species such as the mixed $[Au(CN)(NCO)]^-$ ion could also be present in the model solutions investigated .

Table 6.3: Electrospray mass data of the species observed in the model solutions prepared with KAuBr4 salts and pseudohalide salts which are present in a $KAuBr_4$:pseudohalide salt 1:4 mole ratio in DMSO solution. (Mass (m/z) values are rounded to whole numbers)

$KAuBr_4$/KOCN model solutions		**$KAuBr_4$/NaSCN model solutions**		**$KAuBr_4$/KSeCN model solutions**	
Au(III) complexes	**Mass (m/z)**	**Au(I) complexes**	**Mass (m/z)**	**Au(I)/Au(III) complexes**	**Mass (m/z)**
$[Au(NCO)_2Br_2]^-$	441	$[Au(SCN)_2]^-$	313	$SeCN^-$	106
$[Au(NCO)_3Br]^-$	402	$[Au(SCN)Br]^-$	336	$[Au(SeCN)_2]^-$	409
$[Au(NCO)_4]^-$	365	$[Au(CN)Br]^-$	304	$[Au(SeCN)Br]^-$	382
		$[Au(SCN)(CN)]^-$ and	281	$[Au(SeCN)_4]^-$	619
		$[Au(NCO)_2]^-$		$[Au(SeCN)CN]^-$	329
		*$[Au(NCO)(CN)]^-$	265		

*This is a mixed solution containing $KAuBr_4$, NaSCN and KOCN in a 1:4:4 $KAuBr_4$: NCS^- : NCO^- mole ratio.

6.3.3.5 ESI-MS investigations of the mixed $KAuBr_4$/NaSCN/KOCN model solutions in DMSO

Evidence to support some of the interpretations made from the IR spectra discussed in 6.3.3.4 was provided by the recording of ESI-MS spectra of the $KAuBr_4$/NaSCN (1:4 mole ratio solutions) and the mixed $KAuBr_4$/NaSCN/KOCN (1:4:4 mole ratio) solutions. The typical peaks detected in the 1:4 mole ratio $KAuBr_4$:NaSCN solution were illustrated in Figure 6.8(b). Figure 6.10 is the ESI-MS spectrum of the $KAuBr_4$/NaSCN/KOCN mixed solution. This spectrum (Figure 6.10) shows 5 prominent to medium intensity mass spectral peaks. Of these, the most prominent is the $[Au(SCN)_2]^-$ ion at m/z= 312.93 which indicates this ion is still present in the mixed solution. However other ions at m/z 264.98, 280.95, 303.9 and 335.9 are due to $[Au(NCO)(CN)]^-$, ($[Au(CN)(SCN)]^-$ and $[Au(NCO)_2]^-$) , $[AuBr(CN)]^-$ and $[Au(SCN)Br]^-$ respectively. The appearance of the m/z= 264.98 and 280.95 peaks due to $[Au(NCO)(CN)]^-$ and ($[Au(CN)(SCN)]^-$ and $[Au(NCO)_2]^-$) are the most significant observations as they prove the existence of Au(I) cyanate complexes in solution as intimated by the IR spectra. The m/z = 280.95 peak actually occurs in ESI-MS spectra of 1) the 1:4 mole ratio ($KAuBr_4$:NaSCN)model solution and 2) the mixed $KAuBr_4$/KOCN/NaSCN

model solutions and is probably mostly due to the species $[Au(CN)(SCN)]^-$ especially so in Figure 6.8(b) where no cyanate ion is present.

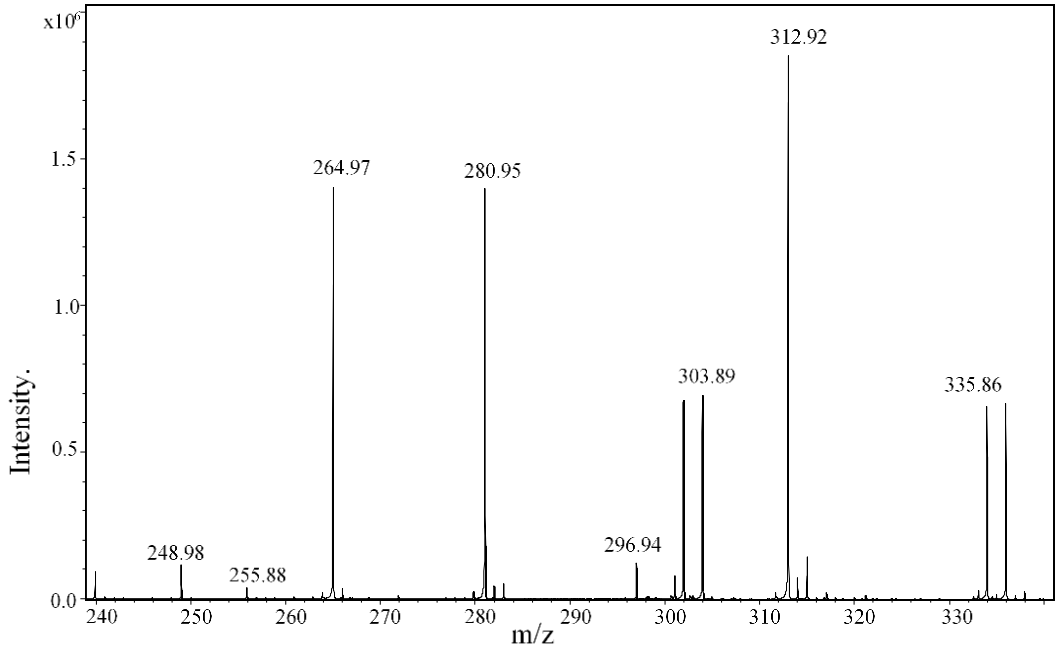

Figure 6.10: Electrospray mass spectra of the model solutions prepared with $KAuBr_4$ salts and pseudohalide salts in DMSO solution where $[KAuBr_4] = 0.025$ mol L^{-1}, [NaSCN] = 0.1 mol L^{-1} and different amounts of KOCN salt.

However this peak could also potentially contain some contribution from an $[Au(NCO)_2]^-$ species as it has a very similar mass to $[Au(CN)(SCN)]^-$. The peak at m/z= 264.98 in Figure 6.10 is, hence believed to be stronger evidence (for the presence of Au(I)-cyanate species existing in the mixed $KAuBr_4$/KOCN/NaSCN solution) than the appearance of the m/z 280.95 peak.

When a $KAuBr_4$/KSeCN/KOCN mixed solution in a 1:4:4 mole ratio was prepared and examined in similar manner by FTIR and ESI-MS (Figure 6.11 and Figure 6.12), identical peaks in the IR were detected which confirmed the presence of Au(I) cyanate species. In addition (in ESI-MS spectra), the same peak at m/z = 264.98 (albeit at weaker intensity) due to the mixed gold-cyanate-cyanide complex ion species was observed. Additional peaks observed in the ESI-MS spectrum (Figure 6.12) of the $KAuBr_4$/KSeCN/KOCN model solution (mole ratio = 1:4:4) at m/z= 301.9/303.9, 328.90, 381.80, and 408.82, were assigned (as discussed above) to $[Au(CN)Br]^-$, $[Au(SeCN)(CN)]^-$, $[Au(SeCN)Br]^-$ and $[Au(SeCN)_2]^-$ respectively. The peak at m/z=408.82 was the dominant peak in this ESI-MS spectrum which reflects its importance in the mixed

$KAuBr_4$/cyanate/selenocyanate model solution. In conclusion, ESI-MS spectra of these mixed model solution systems reflect a common species, namely the m/z - 264.98 peak corresponding to $[Au(NCO)(CN)]^-$ which was deemed to be a more reliable indicator of the presence of the Au(I)cyanate complex ion in these systems. This hence proves that such a species can be prepared independently of an electrochemical cell and therefore confirms that a Au(I) cyanate species has been prepared and detected in the IR spectroelectrochemical experiments.

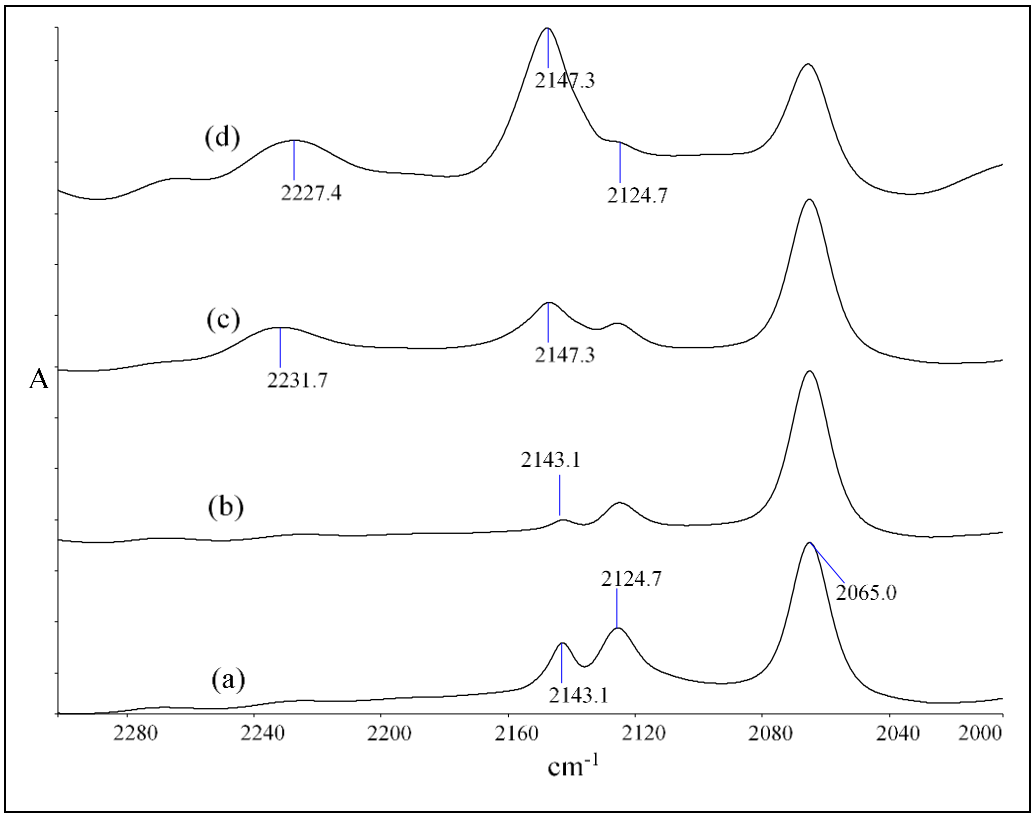

Figure 6.11: Transmission IR spectra of the model solutions prepared with $KAuBr_4$ salts and pseudohalide salts in DMSO solution where $[KAuBr_4]$ = 0.025 mol L^{-1}, [KSeCN] = 0.1 mol L^{-1} and different amounts of KOCN salt. (a) 1:4 $KAuBr_4$: $NCSe^-$ mole ratio solutions., (b) 1:4:1 $KAuBr_4$: $NCSe^-$:NCO^- mole ratio solutions., (c) 1:4:2 $KAuBr_4$: $NCSe^-$: NCO^- mole ratio solutions. (d) 1:4:4 $KAuBr_4$: $NCSe^-$: NCO^- mole ratio solutions.

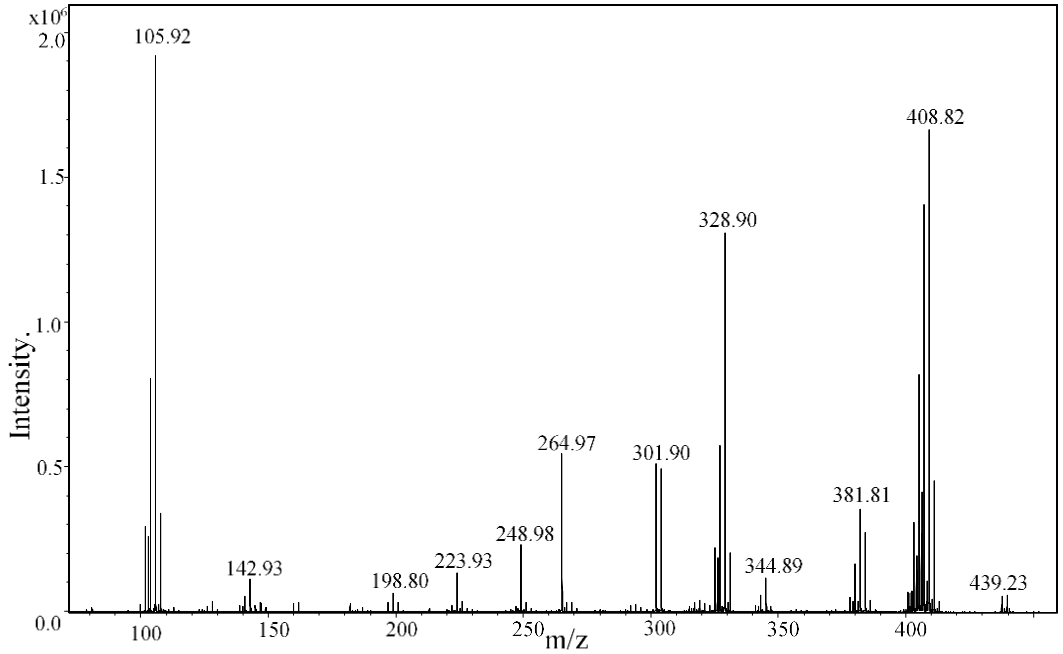

Figure 6.12: Electrospray mass spectra of the model solutions prepared with $KAuBr_4$ salts and pseudohalide salts in DMSO solution where [$KAuBr_4$] = 0.025 mol L^{-1}, [KSeCN] = 0.1 mol L^{-1} and different amounts of KOCN salt.

This chapter discussed a gold electrodes anodically polarised in DMSO and DMF solutions containing pseudohalide ions with tetrabutylammonium perchlorate as supporting electrolyte. In general, Au electrodes dissolve to form Au(I) pseudohalide complex ions (i.e. $[Au(NCO)_2]^-$, $[Au(SCN)_2]^-$ and $[Au(SeCN)_2]^-$. Further, model solution studies involving mixture of KAuBr4 and pseudohalide salt in DMSO have proven the above assignments by ESI- MS.

Chapter 7

A fundamental IR spectroelectrochemical study of the anodic polarisation of nickel, copper and gold electrodes in the presence of the unstable tellurocyanate ion in DMF and DMSO solutions

7.1 Introduction

The focus of the research in the previous 4 chapters has been done the study of the anodic dissolution of metal electrodes (Ni, Cu, and Au) in polar aprotic solvents containing the stable and well known pseudohalide ions (NCO^-, NCS^- and $NCSe^-$). In this chapter, the study was extended to include the unstable tellurocyanate ion and its interaction electrochemically with Ni, Cu and Au electrodes. The in situ IR study of tellurocyanate interaction with any metal electrode has not been attempted before in the electrochemical literature.

The successful preparation of the tellurocyanate ion was reported in 1968 by Downs [53] who prepared it from the reaction (in dimethyl formamide (DMF)) of tetraethylammonium cyanide and elemental tellurium and isolated pale yellow crystals which were highly moisture and oxygen sensitive. A Raman spectrum of a solution of the ion showed a peak at 2080 cm^{-1}. The use of "feebly polarizing" cations was necessary in the isolation of the salt because tellurocyanate ion cannot exist in a solid in the presence of strongly polarizing cations like potassium or even the larger cesium cation. Although the tellurocyanate ion ($TeCN^-$) is relatively stable in DMF or acetone, the addition of water will instantly lead to decomposition to elemental tellurium and cyanide ion. Austad et.al. [41] isolated pure tetraphenylarsonium tellurocyanate, after the reaction of tetraphenylarsonium cyanide and tellurium powder in acetonitrile solution. It was demonstrated that the tetraphenylarsonium salt of tellurocyanate was reasonably stable on storage as long as no solvent traces were left on the pale yellow cystals formed. Austad et al. also published UV. and IR data for the tellurocyanate ion in acetonitrile reporting the ν(CN) stretching frequency of the ion at 2081 cm^{-1}. The IR stretching frequencies for the -TeCN group in solid $(CH_3)_4NTeCN$ and $(C_6H_5)_4AsTeCN$ were reported in 1972 by Ellestad et al. [135]. Spencer et.al. [54] reported the first

preparation of tellurocyanate ion in dimethyl sulfoxide (DMSO) and described its use in organic reactions to produce stable benzyl tellurocyanates. This and other aspects of its use in inorganic chemistry have been discussed further by Al-Rubaie et al. [136]. Klaeboe et al. [137] stated that the Te-C bond is very weak which is the reason it can only be isolated as a salt of large non-polarising cations like tetraethylammonium ion or tetraphenylarsonium ion.

Owing to the stability of the tellurocyanate ion in only a limited range of non-aqueous solvents, the number of electrochemical studies carried out with this ion as an electroactive species has been few in number. There have also been challenges in performing these studies. For instance, Cauquis et al [138] reported a voltammetric study in 1975 in which the electrochemical oxidation of the tellurocyanate ion in acetonitrile at a platinum microelectrode was discussed and compared with the electrochemistry of other pseudohalide ions, namely NCO^-,NCS^- and $NCSe^-$. Using fast sweep rates, they were able to detect the electrochemical oxidation of $TeCN^-$ ion via a series of reactions where formation of "tellurocyanogen", $(TeCN)_2$ was proposed from the combination of two tellurocyanate free radical species. This was then reasoned to react further with a $TeCN^-$ ion to form $[(TeCN)_3]^-$ ion. This species is then regarded to oxidise further to reform $(TeCN)_2$ which subsequently decomposes to form elemental Te and $(CN)_2$. It was found that fast sweep rates minimized the importance of the decomposition of the ion to elemental Te and $(CN)_2$ species. Cauquis et al. [138] had commented on how the instability of the $TeCN^-$ ion can make the detection of such transitory species generated during electrolysis a difficult exercise.

Given the fact that $TeCN^-$ has reasonable stability when prepared in DMSO and DMF solvents and no previous attempts in the literature have been made to study the IR spectroelectrochemistry of this ion when anodically polarized at various metal electrodes, it was regarded as being of interest to investigate this system to extend previous investigations to this unstable ion. Therefore, the aim of this study was anodically polarised electrodes (i.e. Ni, Cu, and Au) in DMF and DMSO solvents containing $TeCN^-$ ion to investigate via IR spectroelectrochemical method and computational studies where the vibrational frequencies of hypothetical metal-TeCN complexes. IR spectroelectrochemistry of CN^-containing systems are easy to follow due to the occurrence of the

ν(CN) stretching vibration in the 2500-1800 cm^{-1} region of the IR spectrum hence useful information can be easily obtained.

7.2 Material and methods

The solvents used in the study (DMF, Ajax Finechem Pty, UNIVAR grade and DMSO, Scharlau, synthesis grade) were used without further distillation. However due to the moisture sensitivity of the $TeCN^-$ ion, both solvents were dried over activated type 3A molecular sieve pellets to remove any traces of water. Before drying over molecular sieves, the solvents, DMF and DMSO are quoted in their specifications as having 0.1% and 0.15% water impurity as measured by Karl Fischer titration. All glassware was cleaned thoroughly with doubly distilled water prior to its use in experiments.

$TeCN^-$ ion was prepared following the procedure of Spencer et al.[54]. An excess amount (0.40 g) of preground elemental tellurium (Aldrich Chemical Co, USA, 99.9%) was mixed with 0.163 g of KCN (BDH, Anala-R grade) which had been pre-dried in a desiccator containing activated silica gel. 50 mL of dried DMSO or DMF were added to the mixture and heat applied (with the mixture having a N_2 gas flow from an oxygen free N_2 (OFN) cylinder (BOC Gases) pass over it) to a temperature of 80-90°C for 2 h to facilitate reaction. Successful reaction was indicated by the production of a pale yellow solution which was then filtered from the unreacted Te solid. An IR spectrum of the pale yellow solution in DMF or DMSO featured a peak at 2079 cm^{-1} due to $TeCN^-$ ion [41]. The solution was stored under OFN until required. The concentration of $TeCN^-$ produced was assumed to be 0.05 mol L^{-1}.

Electrolyte solutions for IR spectroelectrochemistry were prepared by adding solid tetrabutylammonium perchlorate (TBAP from Aldrich Chemical Co, > 97.0%) directly to the prepared ~0.05 mol L^{-1} $TeCN^-$ solution to a concentration of 0.1 mol L^{-1} where it functioned as an inert supporting electrolyte. In other IR spectroelectrochemistry experiments involving CN^- as ion as an electrolyte, 0.1 mol L^{-1} solutions in KCN were prepared containing also 0.1 mol L^{-1} TBAP.

The thin layer spectroelectrochemical cell, windows, specular reflectance unit and electrodes (working, reference and secondary) used in this study were as described and illustrated as per chapter 3. Due to the configuration of the cell, the signals detected were solution species existing in the thin layer between the IR transparent window and the working electrode. The working electrode consisted of a 7 mm diameter polycrystalline Ni, Cu or Au foil electrode as described previous chapters. The electrochemical and spectroscopic instrumentation including the liquid-N_2 cooled detectors used to carry out the cyclic voltammetry and the IR spectroscopy of the systems were all as described in chapter 3. The spectral acquisition technique for SNIFTIRS which involved single potential alteration has also been described earlier. Generally background spectra were acquired at -900 mV (AgCl/Ag) and all sample spectra were acquired at 4 cm^{-1} resolution for 100 scans. As done in the chapter 3, current-potential data from the systems were collected at the same time as the IR data by averaging over the starting current in the cell at the beginning of an IR acquisition and the final current (after several minutes of acquisition) at the end of the scan to generate effectively what could be regarded as "slow" "single sweep" voltammograms.

Model solutions in the case of the Ni and Cu systems were also prepared to confirm the existence of species which were proposed to have formed during electrochemical polarisation at anodic potentials. These consisted of preparations of mixtures of partially pre-dried metal salts (e.g. $CuCl_2.2H_2O$ and $Ni(NO_3)_2.6H_2O$) codissolved in DMSO only with $TeCN^-$ or CN^- in certain metal ion:$TeCN^-$ or metal ion:CN^- mole ratios ranging from 1:1 to 1:8. Drying of the $Ni(NO_3)_2.6H_2O$ at 50°C in an oven only partially removed the water from these compounds [139] which was proven by an IR spectrum of the compound after drying. However the $CuCl_2.2H_2O$ could be rendered into the anhydrous form (brown in colour) by oven drying. These model solutions were sampled by FTIR in conventional transmission mode using a Press-Lok™ cell via procedures and instrumentation/ accessories as described in chapter 3.

Computational calculations were also carried out in order to predict what the ν(CN) stretching frequencies of hypothetical, electrogenrated Ni-DMSO-TeCN, Ni-DMF-TeCN, Au-DMSO-TeCN, Au-DMF-TeCN, Cu-DMSO-TeCN and Cu-DMF-TeCN complexes would be. For this purpose, density functional theory

(DFT) calculations using the B3LYP function were completed using Gaussian 09. The complexes for which ν(CN) stretching frequencies were calculated were as follows: $[Ni(DMSO \text{ or } DMF)_5(TeCN)]^+$,$[Ni(DMSO \text{ or } DMF)_4(TeCN)_2]$, [Au(DMSO or DMF)(TeCN)], and $Cu(DMSO \text{ or } DMF)_3(TeCN)$. To calculate the frequencies of these complexes, a mixed basis set approach was implemented to provide the best compromise between cost of calculation and accuracy. The 6-31+G(d) basis set was used for the H, C, O and S atoms of the DMSO/DMF ligands whereas the aug-cc-pVTZ (augmented correlation-consistent-polarised valence-only triple zeta) basis set was used for the C and N atoms of $TeCN^-$. For Te, Ni, Cu and Au, the aug-cc-pVTZ basis set and effective core potential were used. Geometry optimizations and frequency calculations were run with the integral equation formalism polarizable continuum model (IEFPCM) which is the implicit solvation model for both the DMSO and DMF complexes, respectively. No imaginary frequencies were calculated indicating that all structures were true minima. The calculated CN-stretching frequencies of the complexes were scaled to account for anharmonicity and deficiencies in the utilised theoretical model. The scaling factors were determined from comparison of the experimental and calculated ν(CN) stretching frequency of uncomplexed $TeCN^-$ ion which was obtained via the same theoretical approach as the complexes.

7.3 Results and Discussion

7.3.1 Cyclic voltammograms and single sweep voltammograms.

Figure 7.1(a)-(f) shows the cyclic voltammograms of nickel, copper and gold electrodes in $TeCN^-$/TBAP/DMSO (a)-(c) respectively and in $TeCN^-$/TBAP/DMF (d)-(f). The CVs show very different shapes across samples, e.g. between Ni/$TeCN^-$, Cu/$TeCN^-$ and Au/$TeCN^-$. Figure 7.2(a) to (f) show the "single sweep voltammograms" for the systems which represent current-voltage plots for the systems obtained during the in situ IR spectral acquisitions. In general, the CVs recorded are approximately similar and characteristic in their overall shape for each metal in DMSO (Figure 7.1(a) to (c)) or DMF (Figure 7.1(d) to (f)). The same may be said for the single sweep voltammograms (Figure 7.2(a) to (f)) except in the case of Cu/DMSO/TBAP/$TeCN^-$ and Cu/DMF/TBAP/$TeCN^-$ which are different to each other in shape. The cell currents for the Ni and Au systems as observed in both the CVs and the single sweep voltammograms were similar in

magnitude to each other whereas the CVs and single sweep voltammograms of the Cu systems exhibited higher currents, the significance of which will be discussed when in situ IR results are described (see later). In general for all systems studied, the thin layer cell currents started from low or small negative values in all CVs recorded and increased significantly in magnitude as the potential was adjusted > 0 mV(AgCl/Ag) where the electrode was being anodically polarised. In all cases after doing CV experiments or IR experiments (see later), a black deposit was observed on the electrodes for each metal. This signified decomposition of the $TeCN^-$ ion was likely to be occurring to form elemental Te [41] and CN^- ion. The significance of this was that the CVs and single sweep voltammograms could be the result of the interaction of the decomposition products of $TeCN^-$ rather than of the ion itself with the electrodes. It was also evident especially in the case of the Au electrode that various features in the CV could be observed due to electrochemical events that may arise from oxidation of Au or electroactive species present. The return sweep of these are featureless/unremarkable suggesting that the processes giving rise to the features on the forward sweep are irreversible (see Figure 7.1(c) and Figure 7.1(f)). As suggested earlier, the features observed may be due to the formation of Au cyano complexes (from cyanide present in the thin layer which was either unreacted and present in the original electrolyte solution or which corresponded to cyanide which has been released via decomposition of $TeCN^-$ during the anodic polarisation process). In situ IR data (see later) suggest the latter possibility. Indeed, in a study by Kunimatsu et al. [7], who reported polarisation modulated Fourier transform infrared reflection absorption (PM-FTIRRAS) spectra of Au electrodes in aqueous 0.1 mol L^{-1} KCN and K_2SO_4, a CV indicated that the increase in current from -0.1 V(AgCl/Ag) to -0.7 V(AgCl/Ag) is due to the oxidation of Au to $[Au(CN)_2)]^-$ although their reported CV was simply a monotonically increasing profile as opposed to the more complex shaped CVs illustrated in Figure 7.1(c).

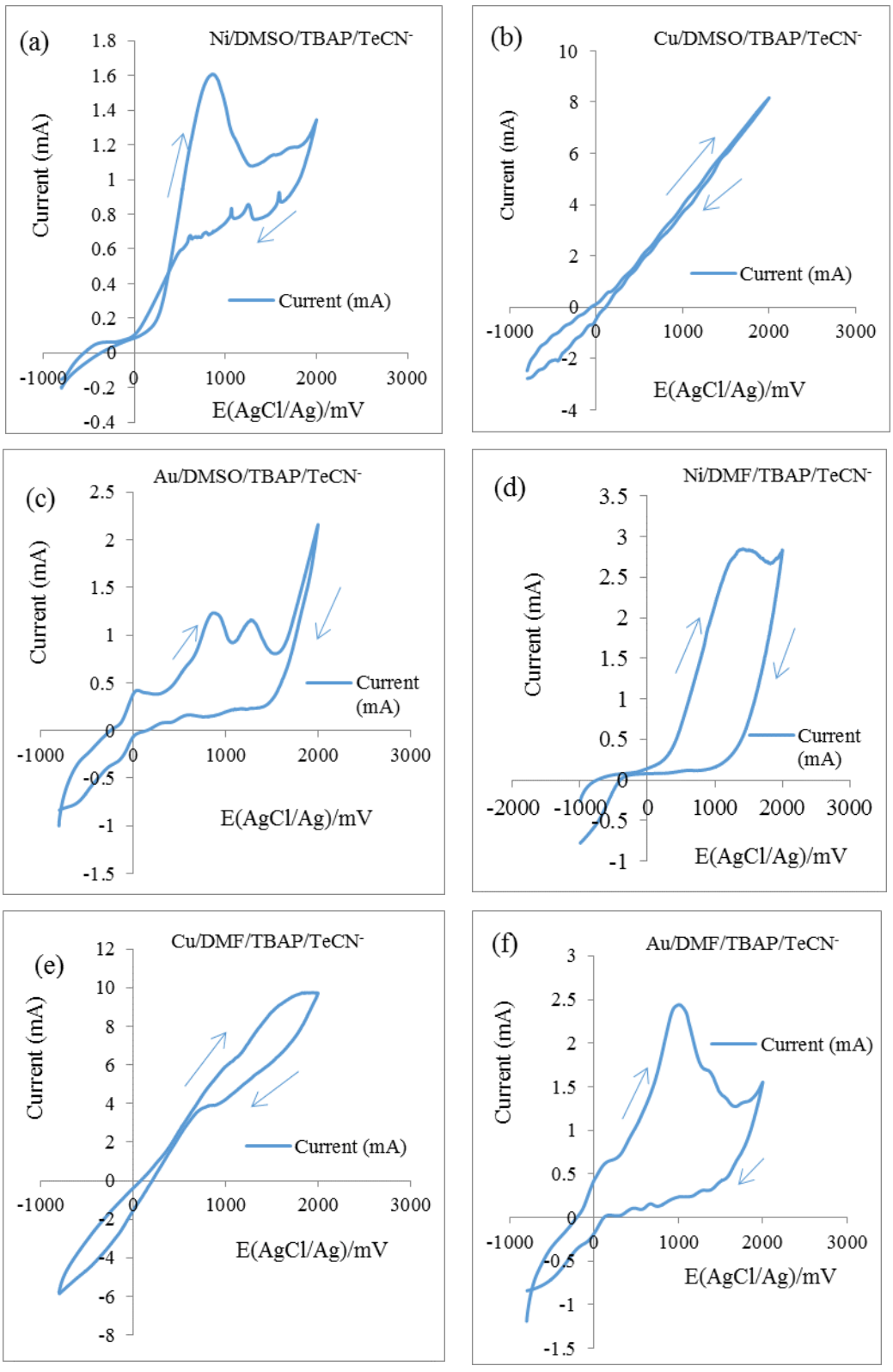

Figure 7.1: Cyclic voltammograms of the nickel, copper and gold electrodes in DMSO and DMF solvents containing tellurocyanate ions and 0.1 mol L^{-1} TBAP (sweep rate = 20 mV/s): (a) Ni electrode and ~0.05 mol L^{-1} $TeCN^-$ in DMSO, (b) Cu electrode and ~0.05 mol L^{-1} $TeCN^-$ in DMSO, (c) Au electrode and ~0.05 mol L^{-1} $TeCN^-$ in DMSO, (d) Ni electrode and ~0.05 mol L^{-1} $TeCN^-$ in DMF, (e) Cu electrode and ~0.05 mol L^{-1} $TeCN^-$ in DMF and (f) Au electrode and ~0.05 mol L^{-1} $TeCN^-$ in DMF. Arrows show the path actually traced upon conducting the sweep of potentials.

As for the features observed in the other systems studied, i.e. Ni and Cu, it is evident that the decomposition products of the tellurocyanate ion and their interaction with the electrodes in question are responsible for these and that other metal cyano complexes and electro oxidation products of cyanide may be responsible for the overall shape of the CV. In addition, especially at the higher applied anodic potentials (> +1.5 V(AgCl/Ag), there will be some contribution to the observed current-voltage curves from oxidation of the solvent, DMSO or DMF [140]. The different appearance of the CV traces compared to the single sweep voltammograms is related to the fact that CVs are acquired at a faster sweep rate relative to the single sweep voltammograms of the same systems which are averages of the observed current when the electrode was adjusted to a certain potential for IR spectral acquisition and hence represent a far slower "sweep" rate for the system under study. Such observations were made in earlier chapters.

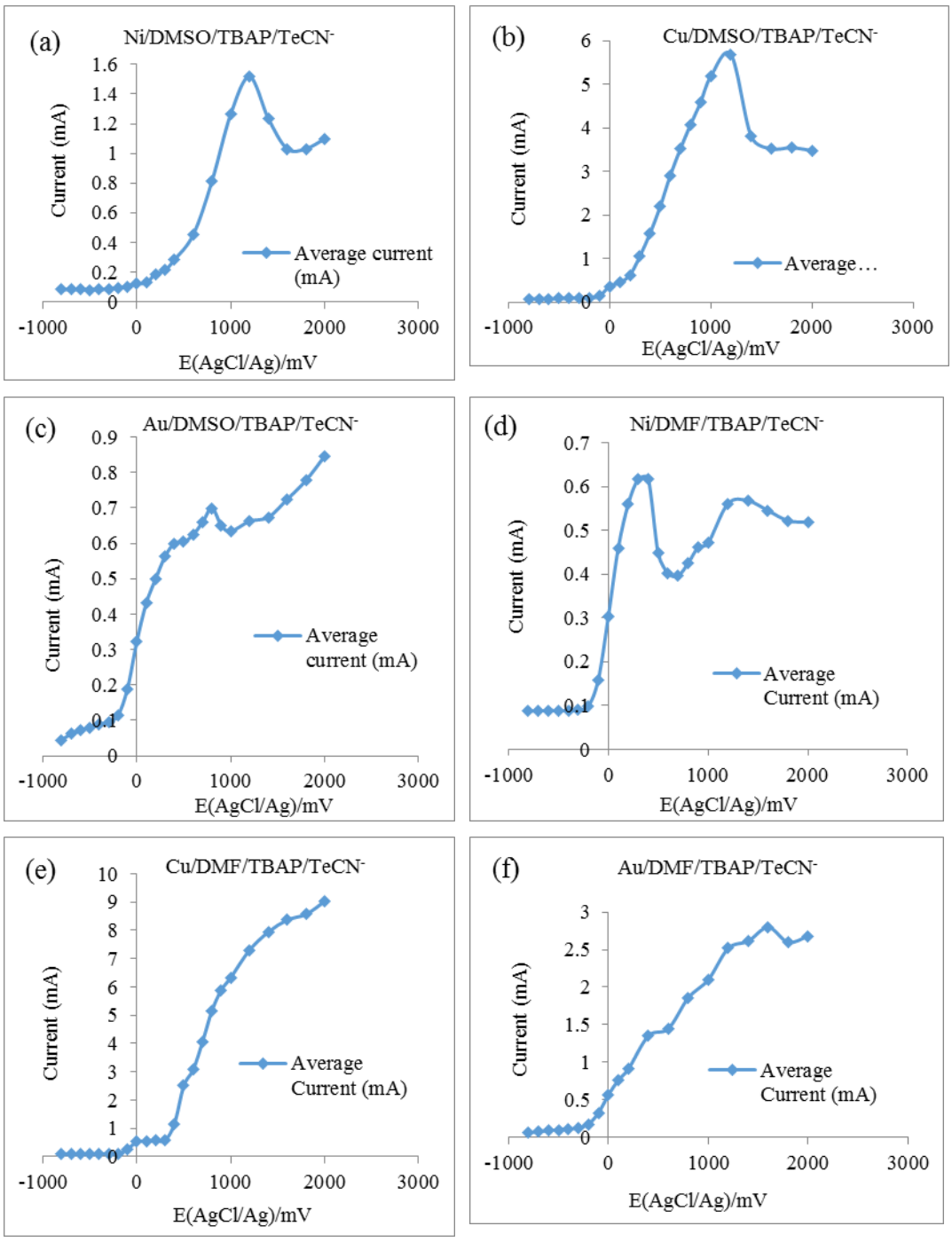

Figure 7.2: Single sweep voltammograms acquired of the nickel, copper and gold electrodes during a SNIFTIRS experiment in DMSO and DMF solvents containing tellurocyanate ions and 0.1 mol L^{-1} TBAP: Data were obtained from calculating the average current at the beginning and end of the spectral acquisition period for each applied potential at which SNIFTIRS spectra were acquired. (a) Ni electrode and ~0.05 mol L^{-1} $TeCN^-$ in DMSO, (b) Cu electrode and ~0.05 mol L^{-1} $TeCN^-$ in DMSO, (c) Au electrode and ~0.05 mol L^{-1} $TeCN^-$ in DMSO, (d) Ni electrode and ~0.05 mol L^{-1} $TeCN^-$ in DMF, (e) Cu electrode and ~0.05 mol L^{-1} $TeCN^-$ in DMF and (f) Au electrode and ~0.05 mol L^{-1} $TeCN^-$ in DMF.

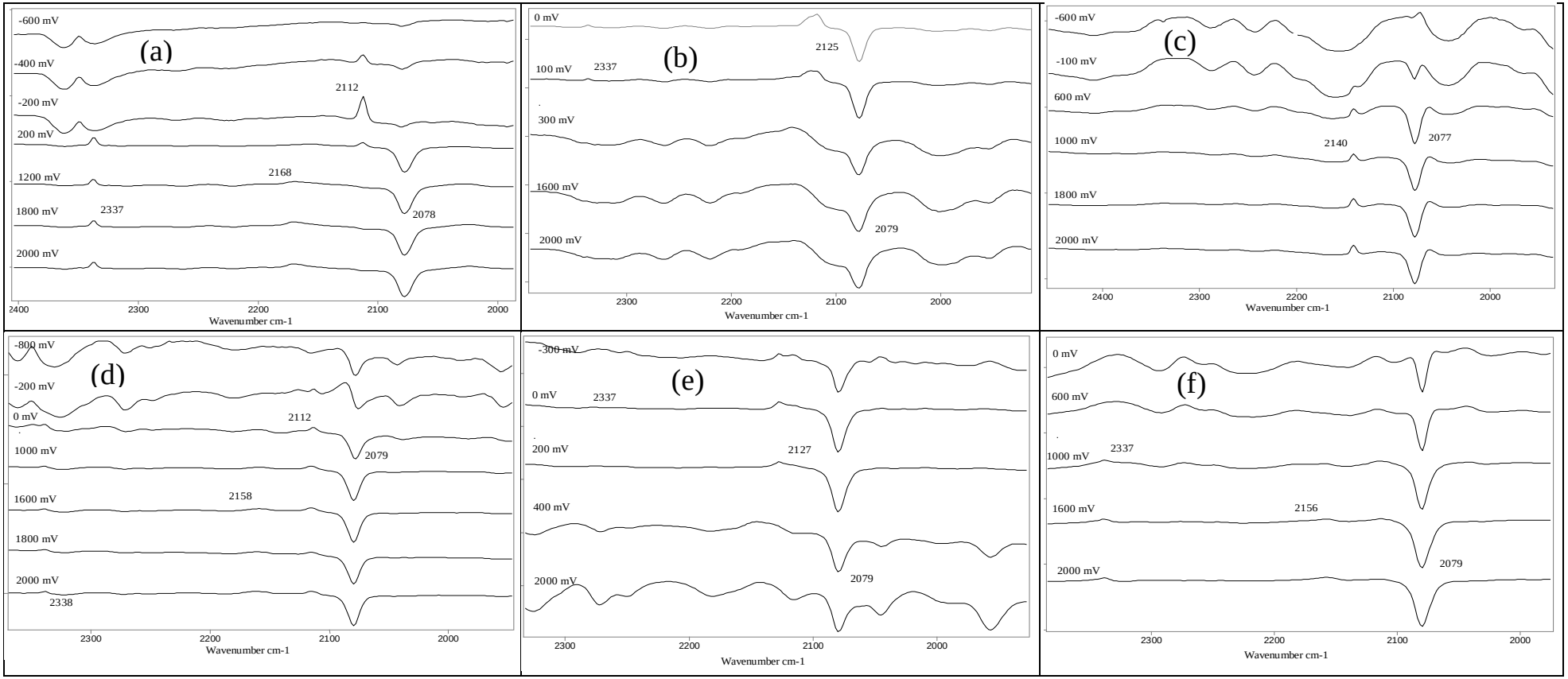

Figure 7.3: Series of SNIFTIRS spectra of the nickel, copper and gold electrodes as a function of applied potential in DMSO and DMF solvents containing tellurocyanate ions and 0.1 mol L^{-1} TBAP. (a) Ni electrode and ~0.05 mol L^{-1} $TeCN^-$ in DMSO, (b) Cu electrode and ~0.05 mol L^{-1} $TeCN^-$ in DMSO, (c) Au electrode and ~0.05 mol L^{-1} $TeCN^-$ in DMSO, (d) Ni electrode and ~0.05 mol L^{-1} $TeCN^-$ in DMF, (e) Cu electrode and ~0.05 mol L^{-1} $TeCN^-$ in DMF and (f) Au electrode and ~0.05 mol L^{-1} $TeCN^-$ in DMF.

Figure 7.3(a) to (f) represent the in situ IR spectra of the nickel, copper and gold electrodes when anodically polarised in the presence of tellurocyanate ion. Table 7.1 summarises the FTIR data from all 6 electrochemical systems studied. The most dominant feature in these spectra relates to the peak attributable to the free tellurocyanate ion at 2078-2079 cm^{-1} which is always present as a *negative* going peak in spectra which becomes a very dominant feature at applied anodic potentials > 0 mV(AgCl/Ag). The observation of a negative going peak indicates that there was more tellurocyanate ion in the original background spectrum acquired at -900 mV(AgCl/Ag) than at the applied potential at which each in situ IR absorbance spectrum was acquired. This and the observation of blackened electrodes (see earlier) in each system are strong evidence that the tellurocyanate ion is decomposing in the thin layer cell when subjected to electrode polarisation especially in the regions where the metal electrodes are being oxidised. This can be further proven when observing the spectral intensity trends as a function of applied potential for each system studied as illustrated in Figure 7.4(a) to (f). These clearly show that the intensity of the free $TeCN^-$ peak decreases negligibly in regions of negative applied potentials (-800 to 0 mV(AgCl/Ag)) with the exception of copper electrodes which are more reactive relative to the other electrodes, but then shows a very sharp decline to negative intensities after 0 mV(AgCl/Ag) as anodic dissolution processes begin to occur on the electrodes. For copper this is evidently occurring at a more negative electrode potential (> -500 mV (AgCl/Ag) due to its being less noble. Hence it is proposed that the formation of oxidised species on the respective electrodes is catalysing the decomposition of the tellurocyanate ion into elemental tellurium and cyanide ion. Certainly in the case of the Au/$TeCN^-$ systems (Figure 7.4(c) and Figure 7.4(f), where the formation of oxidised Au species occurs at more highly anodic potentials, it is evident that the decline in intensity of the peak due to tellurocyanate ion is relatively less steep than what is observed in other systems where less noble metals are involved such as Cu and Ni where oxidation processes occur at less positive potentials.

In the spectra illustrated in Figure 7.3(a) to (f), other weaker features can be observed. For example in the Ni/DMSO/$TeCN^-$ system, a weak peak at 2112 cm^{-1} is evident. In trying to determine if this represents a peak due to complexation of Ni(II) by $TeCN^-$ ion, theoretical calculations performed using Gaussian 09 were

undertaken to predict the ν(CN) stretching frequency of a putative Ni-DMSO-TeCN complex ion. In general for a mono isotellurocyanato-Ni(II) complex ion, such as $[Ni(DMSO)_5TeCN]^+$, ν(CN) was calculated to be 2104 cm^{-1} which, although similar in number to the peak observed, is not believed to be due to this complex. Instead, it is believed to be the peak due to the species formed from the interaction of the *cyanide* ion (from the electrochemically induced breakdown of tellurocyanate ion), with Ni(II) ions formed by anodic dissolution, with the species being identified as $[Ni(CN)_4]^{2-}$ ion in DMSO. This was later proven from model solution work involving the addition of CN^- ions to DMSO solutions of Ni^{2+}. Also, in earlier in situ IR studies involving anodic dissolution of Ni in *aqueous* alkaline cyanide solutions, Mucalo et.al. reported this peak to occur at 2124 cm^{-1} [36]. The observation of the $[Ni(CN)_4]^{2-}$ species thus proves that the tellurocyanate ion has decomposed to form free cyanide ion in the thin layer. A weak peak at 2112 cm^{-1} is also observed in the Ni/DMF/$TeCN^-$ system but to a lesser extent. Likewise in the Cu/DMSO/$TeCN^-$ and Cu/DMF/$TeCN^-$ systems, weak, broad-appearing peaks are observed at 2125-2127 cm^{-1} which are presumed to be due to $[Cu(CN)_2]^-$ [34]. It is unlikely to be a putative $[Cu(DMSO)_3TeCN]$ complex as the DFT calculations find such a complex would have a ν(CN) of 2080 cm^{-1} which is distant from the observed IR stretching frequency.

Table 7.1: FTIR data from in situ IR spectroelectrochemical studies of the Ni/$TeCN^-$, Cu/$TeCN^-$ and Au/$TeCN^-$ systems electrochemically polarised in 0.1 mol L^{-1} TBAP in DMSO or DMF solvents.

System studied	ν(CN) of free $TeCN^-$ ion cm^{-1}	ν(CN)[1] of Ni(II)/CN^- complex ion cm^{-1}	ν(CN)[1] of Cu(I)/CN^- complex ion cm^{-1}	ν(CN) of solid NCO^- (cyanate) species cm^{-1}	ν(CN)[1] of Au(I) /CN^- complex ion cm^{-1}	ν(CO) of CO_2 dissolved in solvent cm^{-1}	Colour of cell solution after SNIFTIRS experiment
Ni/DMF/$TeCN^-$	2078	2112		2158		2338	colourless
Cu /DMF/$TeCN^-$	2079		2127			2337	gold yellow
Au /DMF/$TeCN^-$	2079				2160	2337	colourless
Ni /DMSO/$TeCN^-$	2079	2112		2165		2337	colourless
Cu /DMSO/$TeCN^-$	2079		2125			2337	gold yellow
Au /DMSO/$TeCN^-$	2077				2140	nd	colorless

[1] Note that the $TeCN^-$ ion decomposed in the experiment so that ν(CN) stretching frequencies refer to complexes of the respective metal ions Ni(II), Cu(I) and Au(I) ions with cyanide rather than with $TeCN^-$.

nd = not detected

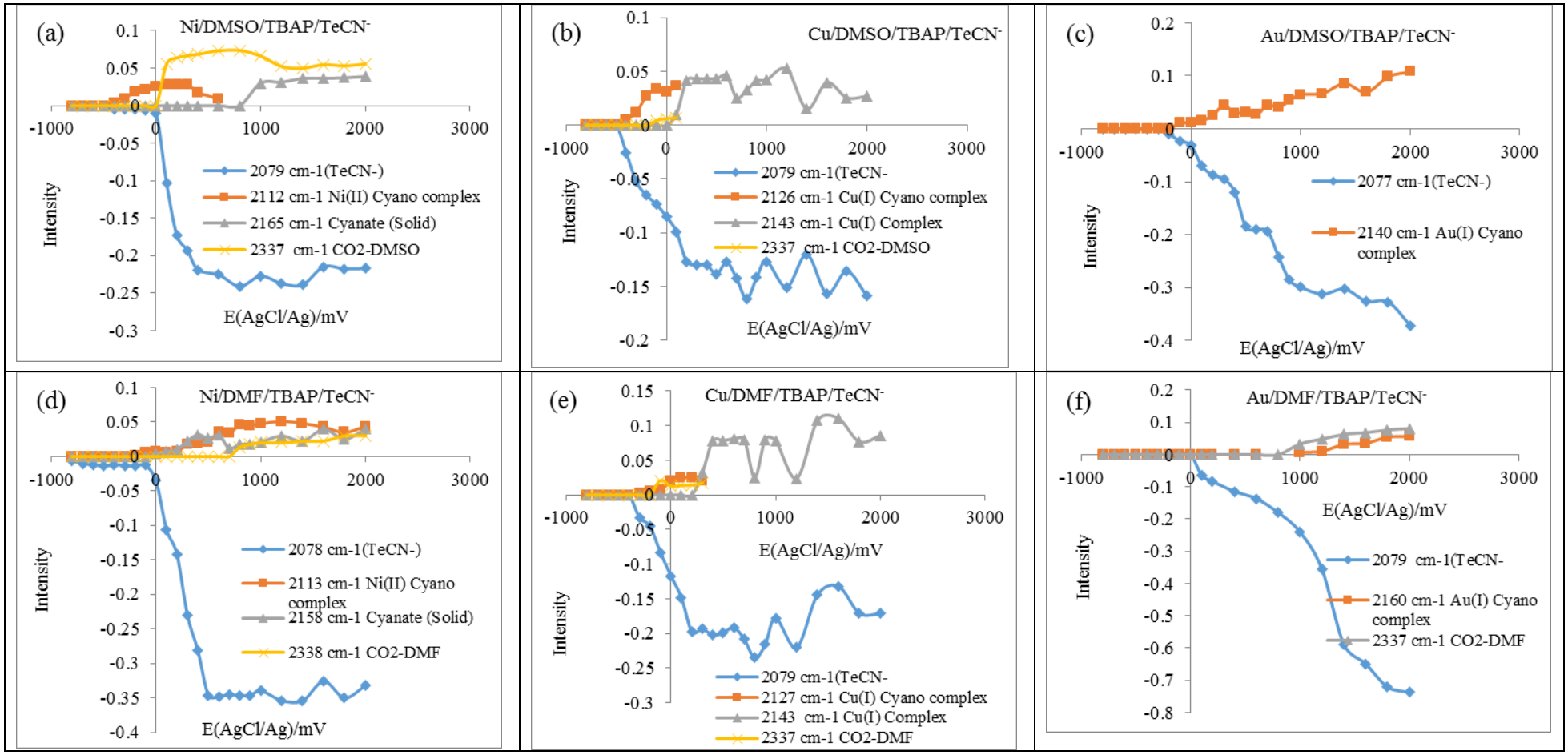

Figure 7.4: Plots of the intensity changes of the various molecular species generated in the thin layer during electrochemical polarisation and observed in the SNIFTIRS spectra as a function of applied potential in the nickel, copper and gold electrodes as a function of applied potential in DMSO and DMF solvents containing tellurocyanate ions and 0.1 mol L^{-1} TBAP. (a) Ni electrode and ~0.05 mol L^{-1} $TeCN^-$ in DMSO, (b) Cu electrode and ~0.05 mol L^{-1} $TeCN^-$ in DMSO, (c) Au electrode and ~0.05 mol L^{-1} $TeCN^-$ in DMSO, (d) Ni electrode and ~0.05 mol L^{-1} $TeCN^-$ in DMF, (e) Cu electrode and ~0.05 mol L^{-1} $TeCN^-$ in DMF and (f) Au electrode and ~0.05 mol L^{-1} $TeCN^-$ in DMF.

Model solution IR data for the Cu/CN^- system in DMSO have provided strong evidence that this peak is in fact due to the Cu(I) species, $[Cu(CN)_2]^-$ (see later). In the $Au/DMSO/TeCN^-$ system, a weak peak is observed at 2140 cm^{-1}. Given the ν(CN) stretching frequency of a putative Au(DMSO)TeCN complex was calculated to be 2101 cm^{-1}, it is obvious that such a complex is not the one giving rise to the observed vibrational spectrum. Instead it is more plausible that it is due to the $[Au(CN)_2]^-$ ion [7] which would have formed from the electrogenerated Au(I) ion interacting with cyanide ion obtained from the electrochemically induced decomposition of $TeCN^-$. In the $Au/TeCN^-/DMF$ electrochemical system, however, no peaks at 2140 cm^{-1} attributable to the $[Au(CN)_2]^-$ species were observed.

The explanation for this would be that decomposition of the $TeCN^-$ ion has coated the Au electrode in a black layer of elemental Te which has blocked the surface and inhibited further reactions on it as a function of applied potential. This is supported by physical observations of a black coating on the Au electrode after electrochemical polarisation experiments.

An additional feature observed in in situ IR spectra is the appearance of a weak peak at 2337-2338 cm^{-1} which can be assigned on the basis of working in chapter 3 to dissolved CO_2 in the DMSO or DMF solvent. This peak was at its most intense only in the $Ni/DMSO/TeCN^-$ system. CO_2-associated peaks were weak or non-existent in the other electrochemical systems studied. This CO_2 is eleectrogenerated and has arisen from oxidation of either the DMSO solvent or, from the liberated cyanide via decomposition of $TeCN^-$ at the electrodes.

7.3.2 IR data from the model solutions prepared from mixing Ni(II) and Cu(II) salts with tellurocyanate solutions prepared in DMSO

The in situ IR spectroelectrochemical data required verification of the species present by the preparation of model solutions of $TeCN^-$ with Ni(II) and Cu(II) salts.

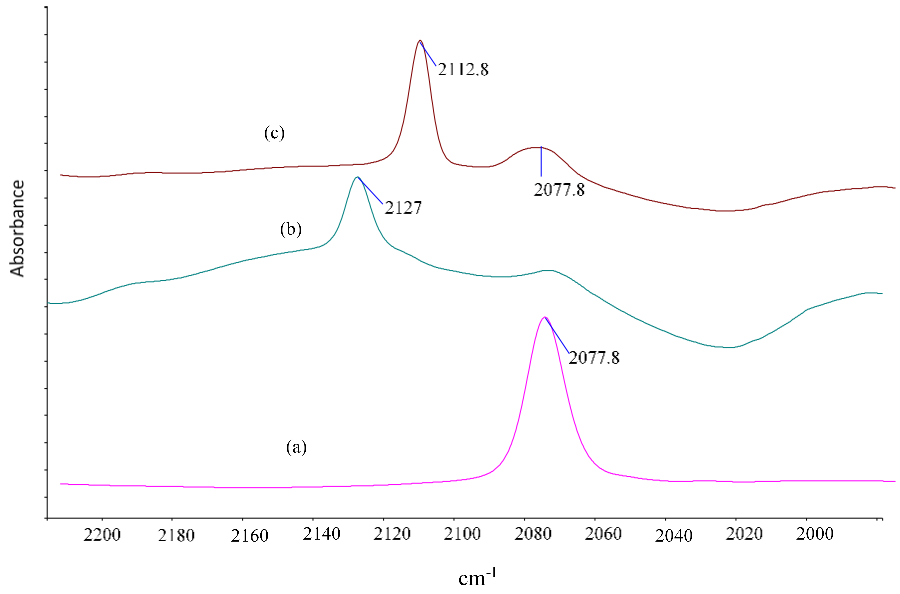

Figure 7.5: IR transmission spectra for (a) the pale yellow solution of tellurocyanate ion generated in DMSO from reaction of the 1:1 mole ratio mixture of finely ground elemental Te and KCN, (b) 1:2 mole ratio model solution prepared from mixing partially dehydrated $CuCl_2$ (0.025 mol L^{-1}) and $TeCN^-$ (~0.05 mol L^{-1}) in DMSO (solution observed to deposit black solid), and (c) 1:2 mole ratio model solution prepared from mixing partially dehydrated $Ni(NO_3)_2$ (0.025 mol L^{-1}) and $TeCN^-$ (~0.05 mol L^{-1}) in DMSO (solution observed to deposit black solid).

The model solution methodology was used in earlier chapters for confirming electrochemically generated species. Figure 7.5 illustrates the model solution spectra for Ni(II) and Cu(II) ions interacting with the tellurocyanate solution generated in DMSO. Figure 7.5(a) is the IR spectrum of the free tellurocyanate ion when it is prepared from the reaction of elemental tellurium with potassium cyanide. The intense peak at 2078 cm^{-1} is due to the ν(CN) stretching frequency of the $TeCN^-$ ion [41]. Figure 7.5(b) and Figure 7.5(c) represent the spectra obtained from mixtures of tellurocyanate and Cu(II) and Ni(II) salts respectively in the mole ratio metal ion (Cu(II) or Ni(II)) : $TeCN^-$ ion of 1:2 . Table 7.2 summarises model solution IR data. However when mixing the two solutions of metal salt and free tellurocyanate ion in DMSO, an immediate reaction was observed in the form of a black solid that deposited in the reaction container. This was an indication that the $TeCN^-$ ion is very unstable in the presence of Ni(II) and Cu(II) ions and that they have caused the decomposition of the $TeCN^-$ ion into black finely divided elemental Te and free cyanide ion [41]. This result is not too surprising as Austad et al. [41] have commented that the $TeCN^-$ ion is unstable in the presence of highly polarising ions, a fact which has prevented its being crystallised as a solid when even potassium ion has been used as the counter ion.

Table 7.2: FTIR data from IR studies of DMSO model solutions of $Ni(NO_3)_2$ and $CuCl_2$ and potassium cyanide salts prepared with different mole ratios.

Model solution studied and mole ratio of $Ni(NO_3)_2$ or ($CuCl_2$): KCN prepared in DMSO	ν(CN) of free NCO^- ion or cyanate-containing complex ion species cm^{-1}	ν(CN) of Ni(II) and Cu(I)/CN^- complex ion species cm^{-1}	ν(CO) of CO_2 dissolved in solvent cm^{-1}	Observed colour of model solution preparations
DMSO				
$Ni(NO_3)_2$/ KCN 1:1		2112[1]	nd	colourless
$Ni(NO_3)_2$/ KCN 1:2		2112	nd	colourless
$Ni(NO_3)_2$/ KCN 1:4		2112	nd	colourless
$Ni(NO_3)_2$/ KCN 1:8		2112	nd	colourless
$CuCl_2$/ KCN 1:1	2224[2] (s), 2200[3] (sh)	2127[4]	2337	gold yellow
$CuCl_2$/ KCN 1:2	2224	2127	2337	gold yellow
$CuCl_2$/ KCN 1:4	2136[5], 2146[5] (sh)	2085[6]	nd	orange brown
$CuCl_2$/ KCN 1:8	2136[5], 2147[5] (sh)	2085	nd	orange brown

nd = not detected, s= strong, sh=shoulder

[1] $[Ni(CN)_4]^{2-}$, [2] $[Cu(NCO)_2]^-$, [3] $[Cu(NCO)_4]^{2-}$, [4] $[Cu(CN)_2]^-$, [5] free cyanate ion, $[NCO]^-$, [6] $[Cu(CN)_3]^{2-}$,

This observation would also explain the trends in the intensity of the peak attributable to the $TeCN^-$ ion as anodic polarisation is carried out on the Ni and Cu electrodes (see Figure 7.4) where it is observed to dramatically decrease in the region where oxidised species of Ni and Cu are expected to form. The IR spectra of the decomposed solutions (Figure 7.5(b) and 7.5(c)) feature two weak peaks at 2127 cm^{-1} and 2112.8 cm^{-1} respectively for the Cu(II)/$TeCN^-$ and Ni(II)/$TeCN^-$ model solutions and these can be assigned on the basis of similar observations (for the Cu/CN^- system from chapter 5) to be due to $Cu(CN)_2^-$ ion (*ca.* 2127 cm^{-1}) and the $[Ni(CN)_4]^{2-}$ ion (*ca.* 2112 cm^{-1}). These assignments were experimentally proven by recording FTIR transmission spectra of model solutions of Ni(II) and KCN prepared in DMSO using various Ni(II):KCN and Cu(II):KCN mole ratios which varied from 1:1 to 1:8 (see Table 7.2 for FTIR data). In all the Ni/KCN model solutions examined by transmission FTIR, a peak at 2112 cm^{-1} was observed which is evidence that this must be the $[Ni(CN)_4]^{2-}$ complex ion in this solvent.

In contrast, for the Cu/KCN/DMSO model solutions (see Figure 7.6(a) to (d)), 3 peaks at *ca.* 2127.5 cm^{-1}, *ca.* 2224 cm^{-1} (with a shoulder at *ca*. 2200 cm^{-1}, and 2337 cm^{-1} were observed in the transmission IR spectra of the 1:1 and 1:2 mole ratio (Cu^{2+}:CN^-) solutions in DMSO. For solutions with Cu^{2+}:CN^- mole ratios of

1:4 and 1:8, the peak at *ca.* 2127.5 cm^{-1} reduced dramatically in intensity or disappeared. The 2337 cm^{-1} peak also disappeared completely in the 1:4 and 1:8 mole ratio solutions. Peaks appearing in place of these were observed at 2145/2137 and 2084 cm^{-1}. The assignments for all of these species are given in Table 7.2 some of which are based on assignments made by Lee et al. [34] from an IR spectroelectrochemical study of the Cu/CN^- system in aqueous electrolyte media. These peaks, as observed in Figure 7.6, show that a redox reaction between Cu^{2+} and CN^- has occurred. This reaction has been studied before in aqueous media [141-143] and was found to produce Cu(I) species in solution. However the earlier aqueous solvent-based studies focussed on UV detection of the copper(I) species generated and reported no IR data.

In the present study of these model solutions, IR spectral evidence has led to the detection of a peak at 2337 cm^{-1} attributable to CO_2 which shows the fate of the cyanide ion from this redox reaction, i.e. that it oxidises to CO_2. In the 1:1 mole ratio Cu^{2+}:CN^- model solution, the detection of the broad peak at 2224 cm^{-1} is attributable most likely to the $[Cu(NCO)_2]^-$ species based on related work from chapter 5.

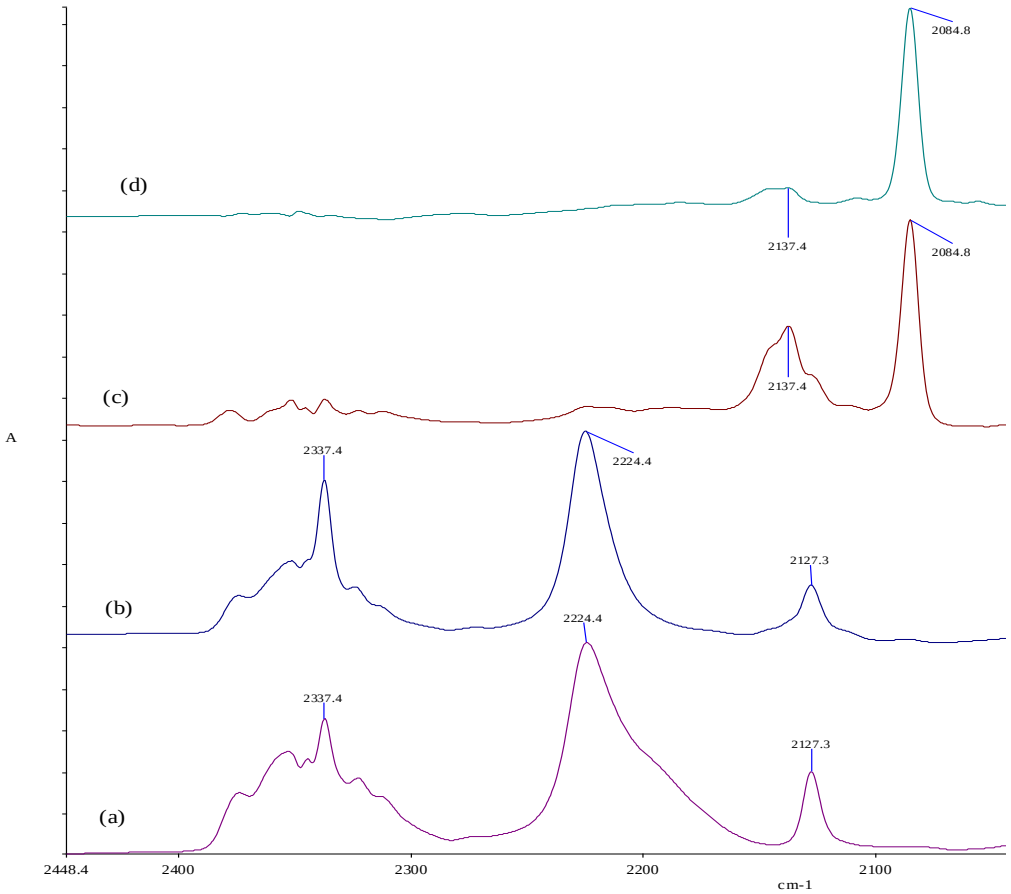

Figure 7.6: IR transmission spectra for (a) the 1:1 mole ratio model solution for Cu^{2+}: KCN in DMSO prepared from mixing partially dehydrated $CuCl_2$ (0.025 mol L^{-1}) and KCN (0.025 mol L^{-1}) in DMSO (solution), (b) 1:2 mole ratio model for Cu^{2+}: KCN in DMSO, (c) 1:4 mole ratio model solution prepared for for Cu^{2+}: KCN in DMSO and (d) 1:8 mole ratio model for Cu^{2+}: KCN in DMSO.

The broadening of the 2224 cm^{-1} peak at lower cm^{-1} values (i.e *ca.* 2200 cm^{-1}*)* is due to a Cu(II) cyanate species [96] which is proof that Cu^{2+} and Cu^{+} coexist in the solution at this point. It is speculated that the isocyanato complex ion, $[Cu(I)(NCO)_2]^-$ could be an intermediate species that precedes CO_2 formation. This is supported by the observation in the model solutions (with a Cu^{2+}:CN^- mole ratio of 1:4 and 1:8) that the 2224 cm^{-1} band is either weakly or not observed at all. Reaction generated CO_2 at 2337 cm^{-1} is also not observed. The reason could be the formation of the higher order Cu(I) cyano complex which is observed the relative concentrations of cyanide and $[Cu^{2+}]$ ion in the model solutions change. This species known as $([Cu(CN)_3]^{2-}$ can be assigned to the peak at 2084 cm^{-1} and is formed at the expense of the peaks at 2224 cm^{-1} and 2128 cm^{-1}. This agrees with the studies conducted earlier in aqueous solution [141-143] although Duke et al. [141] states that cyanogen ($(CN)_2$) is produced as an oxidation product. Katagiri et al. and Parkash et al. [142, 143] also state this in their work, also done in aqueous media. No apparent gaseous species were observed in the presently

studied Cu/CN^- model solution systems in DMSO upon preparation. Cyanogen is a very reactive molecule and could break down to form cyanate ion. It is known to be unstable in the presence of metal salts [144]. Carley et al. [145] have noted that cyanogen can be oxidised to NCO^- ions on a polycrystalline copper surface through adsorption and dissociation at 300 K to form adsorbed CN species which then react with oxygen under preadsorption and coadsorption conditions to give surface cyanate species, -NCO. This may then explain the presence of cyanate species in this model solution system studied.

As mentioned earlier, CO_2 formation is not observed in spectra from the 1:8 mole ratio Cu^{2+}:CN^- solutions and instead, free cyanate (attributed to the 2145/2137 cm^{-1} peak) accumulates in the solution (see Figure 7.6(c) and (d)).

In conclusion, the model solutions, though proving the identity of the ~2125 and 2085 cm^{-1} species in the Cu/KCN/DMSO electrochemical system illustrated in Figure 7.8(b), reveal the inherent complexity in the chemistry of these systems as revealed by the inherent redox chemistry. The observation of Cu(I) cyano and cyanato complex ion species in the Cu/KCN/DMSO model solutions may reflect the higher stability of the Cu(I) oxidation state in these non-aqueous polar aprotic solvents [146].

Gold/tellurocyanate model solutions were not generated for the purpose of this study. In the (decomposed) model solutions involving Ni(II) or Cu(II) with tellurocyanate ion, it was observed that the peak at 2079 cm^{-1} due to free tellurocyanate ion was absent indicating complete decomposition of the species (via interactions with the strongly polarising Ni(II) and Cu(II) anions. It hence was anticipated on the basis of these results that mixing of tellurocyanate ion with Au(III) would lead to similar instability and chemical complexity and hence was not attempted.

7.3.3 In situ IR spectroelectrochemical study of the interaction of Ni, Cu and Au electrodes in the presence of cyanide ion in DMSO.

As it has been shown that the electrochemical systems involving tellurocyanate ions lead to decomposition of the tellurocyanate ion into elemental tellurium and

free cyanide ion, it is hypothesised that the CVs and in situ IR spectroelectrochemical spectra plus associated data obtained for Ni/$TeCN^-$, Cu/$TeCN^-$ and Au/$TeCN^-$ systems are in fact representative of the interaction of the metal electrode with CN^- ion than with $TeCN^-$ ion itself. To prove this, it was decided to study the IR spectroelectrochemistry of CN^- dissolved in DMSO and DMF at Ni, Cu and Au electrodes. Figure 7.7 to Figure 7.9 summarise the data (CVs, in situ IR spectra and intensity trends for IR-detected species as a function of applied potential) from these experiments. Figure. S.15 in Appendix 8 illustrates the single sweep voltammograms for these systems obtained during the IR spectroelectrochemical experiments.

In general, due to the insolubility of KCN in DMF, only IR spectroelectrochemical studies conducted in DMSO were carried out for comparison with the corresponding data obtained for Ni/DMSO/$TeCN^-$, Cu/DMSO/$TeCN^-$ and Au/DMSO/$TeCN^-$ systems discussed earlier. Figure 7.7(a) to (c) illustrate the CVs for the Ni, Cu and Au systems. When compared to Figure 7.1(a) to (c) (see earlier), there are some similarities in the CV although the closest similarities are to be seen when comparing the CVs for the Cu/$TeCN^-$ and Cu/CN^- systems. Also the currents observed between the Cu/$TeCN^-$ and Cu/CN^- systems are of similar magnitude suggesting on the basis of cell current alone that these systems may be more reactive given the lower nobility of Cu electrochemically. When comparing the CVs for the Ni/$TeCN^-$ and Ni/CN^- systems (Figure 7.1(a) and Figure 7.7(a), the Ni/$TeCN^-$ system has an overall larger current compared to the Ni/CN^- system in spite of having half (or possibly less) of the concentration of the electroactive $TeCN^-$ ion present. This was reasoned to be due to the decomposition of the $TeCN^-$ ion to Te and CN^-. The CVs obtained from the interaction of the Au electrode with the $TeCN^-$ or CN^- solution appear different from each other.

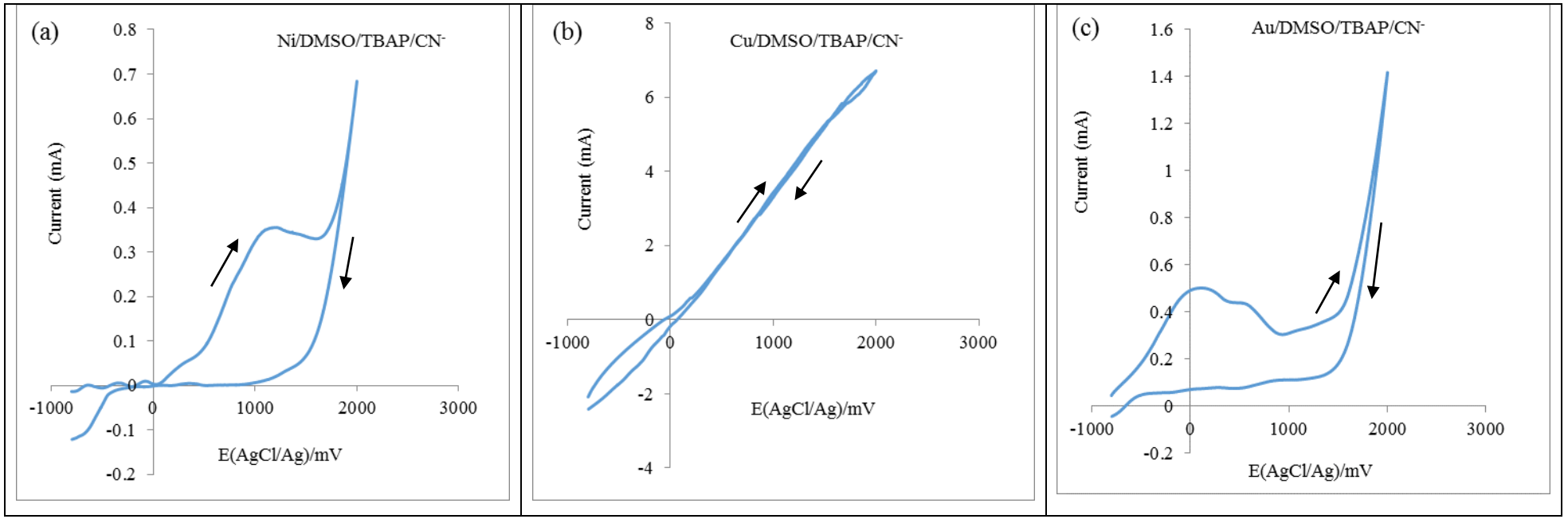

Figure 7.7: Cyclic voltammograms of the nickel, copper and gold electrodes in DMSO solvents containing cyanide ions and 0.1 mol L^{-1} TBAP (sweep rate = 20 mV/s): (a) Ni electrode and 0.05 mol L^{-1} CN^- in DMSO, (b) Cu electrode and 0.05 mol L^{-1} CN^- in DMSO, (c) Au electrode and 0.05 mol L^{-1} CN^- in DMSO.

Figure 7.8(a) to (c) illustrate both the in situ IR spectra as a function of applied potential of Ni, Cu and Au electrodes in 0.1 mol L^{-1} KCN solution in DMSO only. Table 7.3 summarises all the spectroscopic data from Figure 7.8, (b) and (c). Figure 7.9(a) to (c) represent the intensity of the peaks observed in each system as a function of applied potential. For the spectroscopic and (single sweep CV, see Figure. S.15 in Appendix 8)) electrochemical data obtained from the Ni/0.1 mol L^{-1} KCN/DMSO system (Figure 7.8(a) and Figure. S.15(a) in Appendix 8), no features of interest are observed until -500 mV(AgCl/Ag) where a weak peak at 2112 cm^{-1} is observed. This has been assigned to the ν(CN) stretching frequency of $[Ni(CN)_4]^{2-}$ in DMSO.

The intensity of this peak increases from -500 mV(AgCl/Ag) and is maximised at *ca.* +100 mV(AgCl/Ag) before decreasing to zero at +1500 mV(AgCl/Ag). This feature has been observed before in earlier in situ IR studies of a Ni electrode [36] in an aqueous alkaline KCN electrolyte where a higher frequency peak (due to solvatochromatic shifts) at 2124 cm^{-1} was observed and assigned to $[Ni(CN)_4]^{2-}$ (aq). The formation of this ion in the present system in DMSO electrolyte is evidence that Ni is being oxidised to Ni(II) at a relatively cathodic value of the applied potential which is supported by the observation of a small positive feature in the single sweep voltammogram of the Ni/KCN/DMSO system in Figure S.15(a) in Appendix 8.

Table 7.3: FTIR data from in situ IR spectroelectrochemical studies of Ni/CN^-, Cu/CN^- and Au/CN^- systems electrochemically polarised in 0.1 mol L^{-1} TBAP in DMSO solvents (nd= not detected)

System studied	ν(CN) of free CN^- ion cm^{-1}	ν(CN) of Ni(II)/CN^- complex ion species cm^{-1}	ν(CN) of solid NCO^- (cyanate) species cm^{-1}	ν(CN) of Cu(I)/CN^- complex ion species cm^{-1}	ν(CN) of Au(I)/CN^- complex ion species cm^{-1}	ν(CO) of CO_2 dissolved in solvent cm^{-1}	Colour of cell solution after SNIFTIRS experiment
Ni/DMSO/CN^-	nd	2112[1]	2168			2337	colourless
Cu /DMSO/CN^-	nd			2085[2], 2125[3]		2337	gold-yellow
Au /DMSO/CN^-	2054				2140[4]	2337	colourless

[1] $[Ni(CN)_4]^{2-}$, [2] $[Cu(CN)_3]^{2-}$, [3] $[Cu(CN)_2]^-$, [4] $[Au(CN)_2]^-$

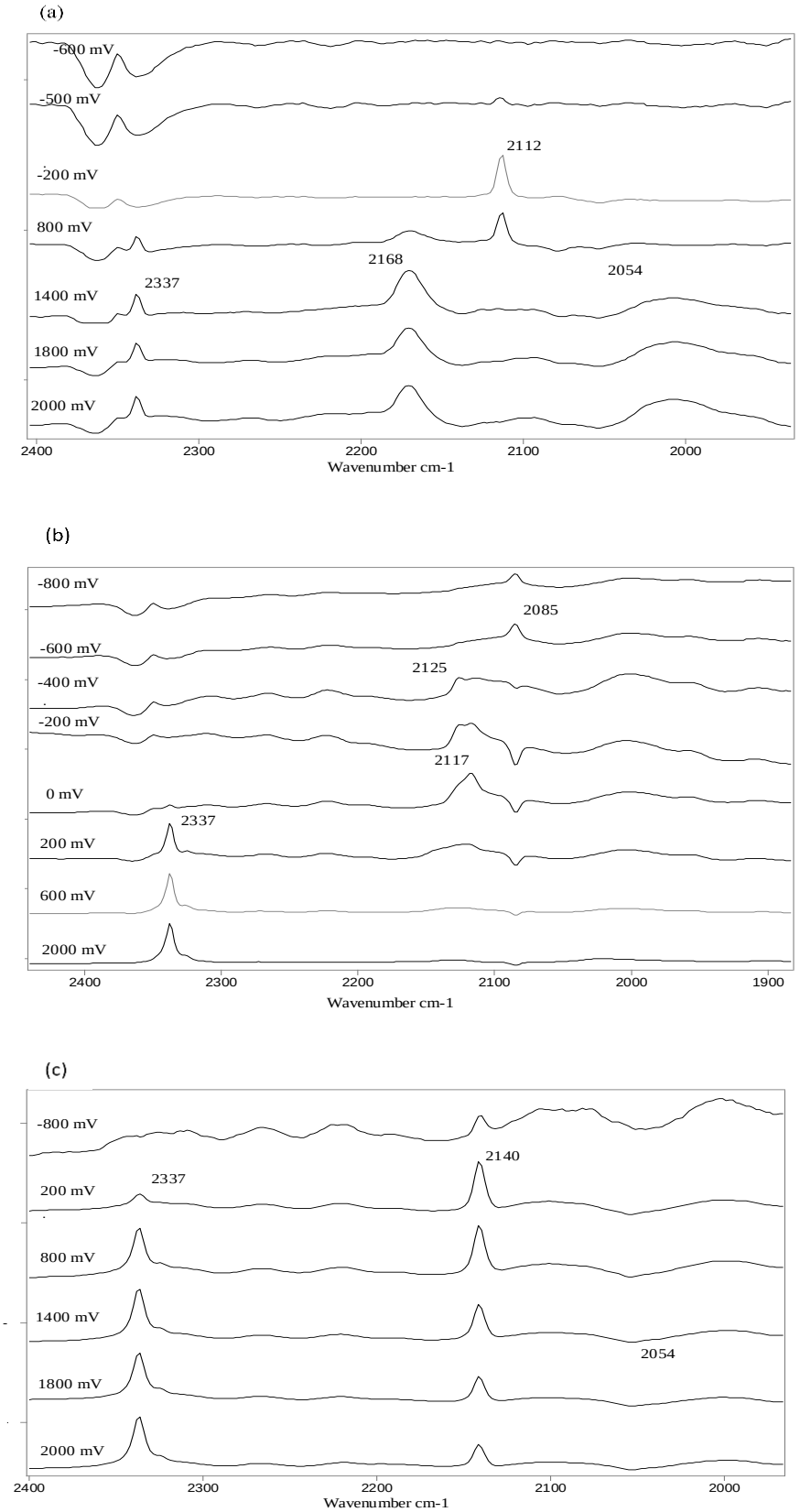

Figure 7.8: Series of SNIFTIRS spectra of the nickel, copper and gold electrodes as a function of applied potential in DMSO solvents containing cyanide ion and 0.1 mol L^{-1} TBAP. (a) Ni electrode and 0.05 mol L^{-1} CN^- in DMSO, (b) Cu electrode and 0.05 mol L^{-1} CN^- in DMSO, (c) Au electrode and 0.05 mol L^{-1} CN^- in DMSO.

This feature is like a similar feature observed in the single sweep voltammogram of the aqueous solvent Ni/KCN system [36] which confirms that the stability associated with the formation of the $[Ni(CN)_4]^{2-}$ ion is most likely the driving force for the oxidation of Ni to Ni(II) at cathodic potentials. In contrast to chapter 3 of the anodic polarisation of Ni in the presence of NCO^- ion in DMSO, no peak due to the blue-coloured $[Ni(NCO)_4]^{2-}$ complex ion was observed in IR spectra of the system for applied $E < +200$ mV(AgCl/Ag) hence the nickel electrode is more noble in these systems compared to what it is in cyanide containing electrolytes.

In relation to the Ni/$TeCN^-$/DMSO and Ni/$TeCN^-$/DMF in situ IR spectra discussed earlier (see Figure 7.3(a) and Figure 7.3(d)), the weak peak observed at 2112 cm^{-1} in these spectra are obviously the same species as observed in Figure 7.8(a) which proves that $TeCN^-$ has decomposed to form CN^- which has then interacted with Ni(II) species formed off the Ni electrode. The weakness or sometimes complete absence of the peak in the Ni/$TeCN^-$/DMSO or DMF systems may be an indirect indicator of the elemental Te deposited from decomposition of the $TeCN^-$ ion blocking the Ni electrode and hence inhibiting any surface reactions as a function of applied potential.

In Figure 7.8(a) additional features were observed in the in situ IR spectra of the Ni/KCN/DMSO system at 2168 cm^{-1} and 2337 cm^{-1}. In addition, a very weak negative going peak was observed at 2054 cm^{-1}. The weak negative going peak at 2054 cm^{-1} is assigned to KCN dissolved in DMSO which was confirmed from dissolving some KCN salt in DMSO and running a conventional transmission IR spectrum of the solution. The explanation for the negative intensity is due to the fact that the CN^- ion is being actively consumed and signifies that there is more peak signal due to solution CN^- in the background spectrum than in the spectrum acquired at more anodic potentials. The weakness of this peak makes this feature difficult to observe in spectra. The broad peak at 2168 cm^{-1} is attributable to a *solid* cyanate salt, KOCN that may be forming on the electrode in the thin layer. It is not believed to be due to dissolved cyanate ion in DMSO because in earlier studies the ν(CN) stretching frequency of dissolved cyanate ion in DMSO was observed as a lower, 2 component frequency peak at 2145/2136 cm^{-1}. The weak peak at 2337 cm^{-1} is due to CO_2 (solvated in DMSO) which has formed at the

electrode this feature having been observed in chapter 3 Ni/KOCN/DMSO or DMF systems. Inspection of Figure 7.9(a) suggests that the solid cyanate salt and the CO_2 are formed at the expense of the $[Ni(CN)_4]^{2-}$ ion as the intensity due to this complex ion drops as the intensity due to the cyanate salt and the solvated CO_2 in DMSO peaks increase in intensity.

Figure 7.8(b) represents the in situ IR spectra of the Cu/0.1 mol L^{-1} KCN/DMSO system. At very cathodic applied potentials, a weak peak is observed at 2085 cm^{-1}. This peak has been assigned to a species which had been discussed in a PM-FTIRRAS study of an aqueous Cu/CN^- solution interphase study reported by Lee et al. [34] where a 2093 cm^{-1} peak appearing at applied E values as negative as -1300 mV(AgCl/Ag) was observed. This peak was attributed by Lee et al. [34] to the Cu(I) species $[Cu(CN)_3]^{2-}$. In DMSO solvent in the present study, the solvatochromatic shift expected for this complex ion would mean that a peak at 2085 cm^{-1} could be attributable to this species. The peak at 2085 cm^{-1} is observed until -400 mV(AgCl/Ag) where it disappears and becomes negative in intensity. This is proof that the ion was formed at very cathodic potentials and hence existed in the background spectrum of this system recorded at -900 mV(AgCl/Ag). Inspection of the single beam spectrum recorded as the background for the Cu/KCN/DMSO system confirmed the observation of a peak at 2085 cm^{-1} being present. The observation of a Cu(I) complex is not surprising as this was observed by Lee et al. [34] and it has also been stated that mixtures of Cu(II) and CN^- in water lead to the formation of copper cyano complexes from eighth-order reactions, i.e. second order in Cu(II) and sixth order in cyanide [147]. In Figure 7.8(b), another complex-shaped weak peak which varied from 2117-2125 cm^{-1} was observed from -400 mV(AgCl/Ag) onwards which effectively "replaced" the peak at 2085 cm^{-1} due to $[Cu(CN)_3]^{2-}$. This complex peak was attributed on the basis of a similar observed peak also from Lee et al.'s study [34] to the species $[Cu(CN)_2]^-$. This species remained in spectra recorded up to +2000 mV(AgCl/Ag).

In relation to the Cu/$TeCN^-$/DMSO and Cu/$TeCN^-$/DMF in situ IR spectra discussed earlier (see Figure 7.3(b) and Figure 7.3(e)), the weak peak observed at 2125-2127 cm^{-1} in these spectra are obviously the same species $[Cu(CN)_2]^{2-}$ as observed in Figure 7.8(b) which also proves in the case of the Cu electrode systems that $TeCN^-$ has decomposed to form Te and CN^- which has then

interacted with the Cu electrode. However in common with Ni, the weakness or sometimes complete absence of the peak in the Cu/$TeCN^-$/DMSO or DMF systems is further proof that the elemental Te deposited from decomposition of the $TeCN^-$ ion was blocking the Cu electrode and hence inhibiting surface reactions as a function of applied potential.

Further evidence for this blocking by Te was seen most dramatically when comparing the level of CO_2 formation in the Cu/$TeCN^-$/DMSO and Cu/KCN/DMSO systems as discussed below.

The peak at 2337 cm^{-1} in Figure 7.8(b) is attributable to CO_2 dissolved in the DMSO solvent as observed in the other metal electrode systems discussed. It is a dominant feature in the in situ IR spectra recorded at potentials > 0 mV (AgCl/Ag) in the Cu/KCN/DMSO system. In contrast, in the Cu/$TeCN^-$/DMSO system (Figure 7.3(b)), CO_2 formation is not occurring given the fact that a peak at 2337 cm^{-1} is not detected at any applied potentials. This is further evidence that the elemental Te from the decomposition of $TeCN^-$ is blocking surface sites on the Cu electrode.

It is also interesting to compare the in situ IR spectra of the Cu/KCN/DMSO system and the Ni/KCN/DMSO system in which the observed intensity of the CO_2 peak at 2337 cm^{-1} is low. In Figure 7.9(b), in contrast, the importance of the CO_2 peak in the Cu/KCN/DMSO system is evident as the intensity of the peak increases sharply above E= 0 mV(AgCl/Ag) which appears to indicate that the CN^- oxidation to CO_2 is being electrocatalysed at the Cu electrode. In contrast, the intensities of other spectral features discussed for this system namely the 2085 and 2125 cm^{-1} peaks are low in value or negative and appear constant as a function of applied potential except for the 2085 cm^{-1} peak due to $[Cu(CN)_3]^{2-}$ which shows a small maximum in intensity at -500 mV(AgCl/Ag). In the Ni/KCN/DMSO system, the level of CO_2 observed in in situ FTIR spectra is comparatively low. In this system, hence solid, possibly potassium cyanate is instead observed to accumulate in the thin layer cell with only a small conversion to CO_2. The Cu/KCN/DMSO system is more catalytically active to converting CN^- to CO_2. This is interesting because in aqueous electrochemical systems involving Cu and cyanide, the destruction of cyanide is thought [147] to be catalysed by a heterogeneous reaction which involves the species $[Cu(CN)_3]^{2-}$ and $[Cu(CN)_4]^{3-}$. This reaction

could be technologically important for managing cyanide waste waters in the gold mining industry. Most studies have involved aqueous solvent based electrochemical systems and the present study has shown how Cu can be catalytic towards CN^- oxidation in a non-aqueous system, namely DMSO.

Figure 7.8(c) represents the series of in situ IR spectra for the Au/KCN/DMSO system. In all spectra observed (from -800 to 2000 mV(AgCl/Ag), a peak at 2140 cm^{-1} is present. This peak can be assigned to the Au(I) cyano complex, $[Au(CN)_2]^-$.

In relation to the Au/$TeCN^-$/DMSO and Au/$TeCN^-$/DMF in situ IR spectra discussed earlier (see Figure 7.3(c) and Figure 7.3(f)), the weak peak observed at 2140 cm^{-1} (and only in the Au/$TeCN^-$/DMSO series of spectra) is the same species as observed in Figure 7.8(c) which also proves in the case of the Au electrode systems that $TeCN^-$ has also decomposed on the electrode to form Te and CN^- which has then interacted with electrogenerated Au(I) species from the Au electrode to form the $[Au(CN)_2]^-$ complex ion. However in common with Ni and Cu electrodes, the weakness or complete absence of the 2140 cm^{-1} peak in the Au/$TeCN^-$/DMSO or DMF systems is proof of the blocking of the electrode surface by the deposited Te from breakdown of the $TeCN^-$ ion. In addition this blocking effect was further demonstrated by the fact that no CO_2 peak at 2337 cm^{-1} is observed in the Au/$TeCN^-$/DMSO or DMF systems. This is in stark contrast to the spectra acquired from the Au/KCN/DMSO systems to be discussed below.

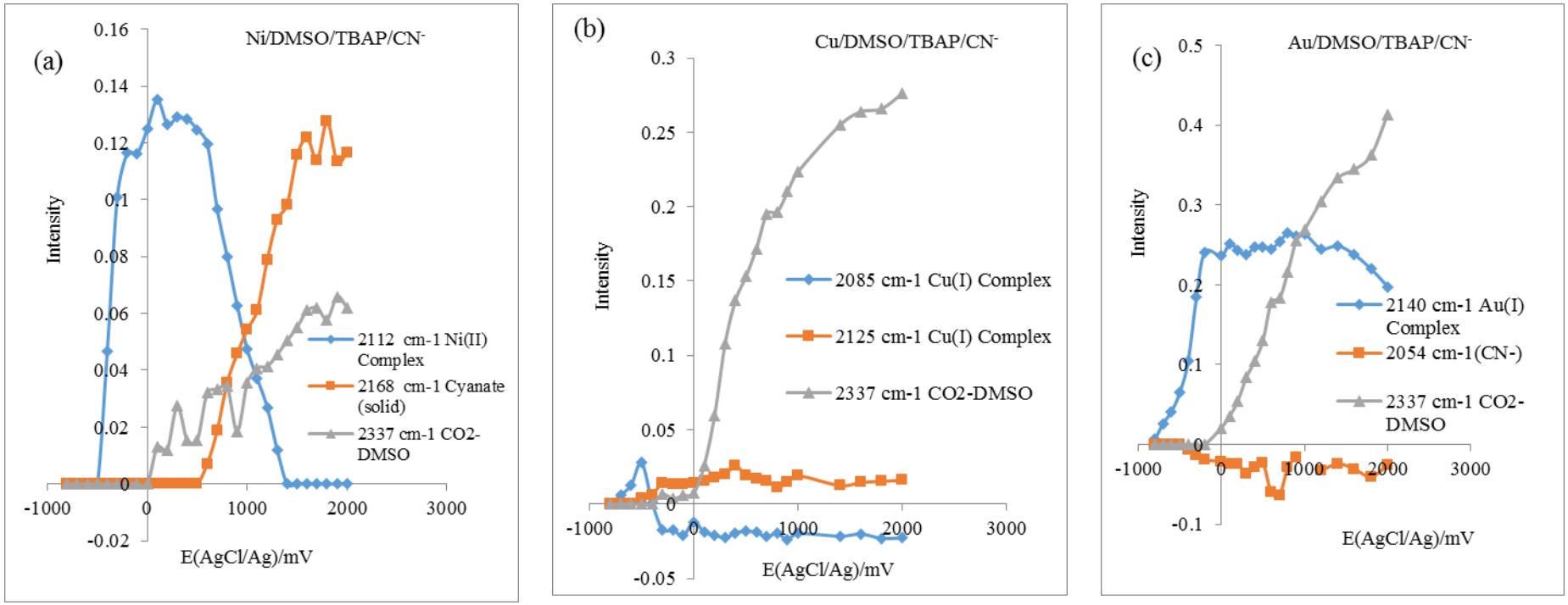

Figure 7.9: Plots of the intensity changes of the various molecular species generated in the thin layer during electrochemical polarisation and detected in the SNIFTIRS spectra as a function of applied potential at the nickel, copper and gold electrodes as a function of applied potential in DMSO solvents containing cyanide ions and 0.1 mol L^{-1} TBAP. (a) Ni electrode and 0.05 mol L^{-1} CN^- in DMSO, (b) Cu electrode and 0.05 mol L^{-1} CN^- in DMSO, (c) Au electrode and 0.05 mol L^{-1} CN^- in DMSO.

Figure 7.9(c) shows the intensity trends of IR spectra in the Au/KCN/DMSO system. In common with Cu/KCN/DMSO, the Au electrode appears to be catalytic with respect to the electro-oxidation of CN^- to CO_2. In terms of the $[Au(CN)_2]^-$ ion, the intensity of the peak due to this ion increases from -800 mV(AgCl/Ag) to a maximum at *ca.* -200 mV(AgCl/Ag) and then levels off in spectra acquired at applied potentials above -200 mV(AgCl/Ag). Interestingly, the intensity of the peak attributed to CO_2 dissolved in DMSO (at 2337 cm^{-1}) begins to also increase steadily and monotonically from -200 mV(AgCl/Ag) to +2000 mV(AgCl/Ag). This indicates that the $[Au(CN)_2]^-$ is probably providing the source of cyanide for oxidising to CO_2 in this system, with the level of $[Au(CN)_2]^-$ remaining constant (see Figure 7.9(c)) throughout all applied potentials above -200 mV(AgCl/Ag). In the case of the CN^- oxidation to CO_2 in Cu/KCN/DMSO systems, it is likely that the low and constant level of $[Cu(CN)_2]^-$ is providing the source of soluble CN^- for oxidation to CO_2.

In this study, first time IR spectroelectrochemical investigate of the anodic dissolution of Ni, Cu, and Au in DMSO and DMF solutions of the unstable $TeCN^-$ ion have convincingly shown that the $TeCN^-$ ion is unstable in anodically polarised electrochemical cell. The observed speciation of products in these electrochemical cells is reflective of the interaction of the metal electrode with *cyanide* ions rather than tellurocyanate ions although on electrodes that are stained by deposited tellurium from the decomposition of $TeCN^-$. These observations were supported by running the IR spectra of model solutions prepared from mixing together Cu(II) and CN^- as well as $TeCN^-$ ions. Further, model solutions of the Ni and Cu salts with cyanide which were used to prove metal-cyano complex ion speciation in the in situ IR spectra, overall proved that these species existed but also showed other interesting redox chemistry indicating the reactivity of these systems, for example the interaction of Cu(II) and cyanate ion.

Chapter 8

Conclusion

This study has concentrated on the IR spectroelectrochemical characterisation of nickel, copper and gold electrodes in non-aqueous solutions (DMF and DMSO) of pseudohalide (i.e. CN^-, NCO^-, NCS^-, $NCSe^-$ and the unstable $TeCN^-$) ions as a function of applied potential. It was found that these electrodes anodically dissolved in these solvents to form Ni^{2+}, Cu^+/Cu^{2+} and Au^+ complex ions formed by coordination to pseudohalide ions and solvent molecules. Model solutions prepared have generally provided convincing evidence to support assignments made from the in situ IR spectra.

8.1 Ni/pseudohalide systems

In general, it showed that nickel undergoes irreversible anodic dissolution in the cyanate, thiocyanate and selenocyanate systems studied to form complex ion species involving both the respective pseudohalide ion and solvent at relatively high values of the applied potential > +500 mV (AgCl/Ag). In cyanate solutions, nickel dissolves to produce a solution species characterised by an IR peak at 2200 cm^{-1} which has been assigned to a blue-coloured Ni(II) cyanate complex which is highly likely to be $[Ni(NCO)_4]^{2-}$. In contrast, when the nickel electrode anodically dissolves in thiocyanate-containing or selenocyanate-containing solutions, species giving IR peaks at 2094 cm^{-1} can be assigned to an approximately octahedral Ni(II) thiocyanate/solvent or selenocyanate/solvent complex ion with a suggested formula of $[Ni(NCS)(solvent)_5]^+$ or $[Ni(NCSe)(solvent)_5]^+$ These conclusions were largely supported by model solution IR data and previous literature. Other peaks of interest observed in SNIFTIRS spectra of these systems were those of the free pseudohalide ion which gave negative-going features in spectra at anodic potentials due to its consumption in electrochemical processes. An insoluble nickel-oxide/cyanate film (possibly due to an interrelated cyanate ion in a nickel hydroxide film) was detected in the Ni/NCO^- systems at highly anodic potentials with contemporaneous detection of solvent-dissolved-CO_2 at 2337-2339 cm^{-1} arising from oxidation of the solvent or pseudohalide ion. CO_2 peaks were also observed in the Ni/NCS^- and $Ni/NCSe^-$ systems but to a lesser extent than in the Ni/NCO^- systems.

In addition to this work there has also been interesting research on using alternative techniques to study directly the electrogenerated products from these systems by using X-ray absorption near edge spectroscopy (XANES) and Extended X-ray Absorption Fine Structure Spectroscopy (EXAFS). These have been applied to the Ni and Cu electrode systems studied.

In general, it is obvious that the EXAFS results indicate that Ni/cyanate complexes are being detected in the model solutions prepared as well as in the electrochemically generated Ni/cyanate system sample. It was important to include multiple scattering paths in the EXAFS fitting for the linear NCX^- ligand. The results support the accepted view that the Ni^{2+} ion in these complex ion species bonds to the pseudohalide ion via the nitrogen atom, given the failure of EXAFS models constructed to describe realistic bonding models involving Se or S directly bonded to Ni^{2+}.

It can also be confirmed that in the case of the Ni/cyanate/DMSO system studied that the model solution prepared to mimic the electrochemically generated solution after anodic polarisation of Ni in DMSO/KOCN is a realistic representation of the species being generated (based on the XANES/EXAFS spectra presented).

EXAFS/XANES is also able to produce evidence of what the coordination environment is in the species being detected. However, it is important to note that all of the analyses reported represent an average snapshot of species existing in the frozen solution systems being investigated. Hence when the results of the coordination numbers of the Ni/pseudohalide species being "detected" are analysed, it is necessary to account for this when making interpretations about specific complex ion species and the coordination environment around the Ni^{2+} ion.

For instance in the case of the model solutions involving Ni^{2+}/NCS^- or $Ni^{2+}/NCSe^-$, the "coordination numbers" extracted for the Ni/pseudohalide species detected are 4.8 (~5) DMSO molecules and 0.9 (~1) NCS^- ion bonded to one Ni^{2+} ion and 4.2 (~4) DMSO molecules and 1.9 (~2) $NCSe^-$ ions bonded to one Ni^{2+} ion. Overall these results confirm that the bonding in these Ni^{2+} complexes for these

particular pseudohalide ligands are octahedral as suggested in in situ IR spectroelectroscopy results. The difference in the relative coordination numbers of Ni^{2+} and $SCN^-/SeCN^-$ in the multiple scattering entries for the table are not regarded as being statistically significant in light of the large errors in N. It is believed that because of the relative concentrations used in making the model solutions and what is also actually used in the IR spectroelectrochemical experiments that the stoichiometry of the Ni-thiocyanate and selenocyanate complex ions that have been detected are mono or dipseudohalide complexes with the remainder of the attached ligands being coordinated solvent molecules (DMSO). Pilaczyk [79] has indicated in studies investigating the dissolution of $Ni(SCN)_2$ in DMSO that the charge-neutral dithiocyanate complex of Ni(II) forms but that this complex cannot be detected or distinguished when observing UV/Vis spectra. They have stated through conductivity measurements that the monothiocyanate complex ion of Ni(II) must also exist in such solutions. The EXAFS/XANES technique will only see an average of the (frozen) solution environment and this may also have some influence on the N numbers determined for DMSO and NCX^-. In chapter 3 it was suggested that on the basis of model solution IR data that a monopseudohalide complex was more likely to form, in this system i.e. $[Ni(DMSO)_5(NCX)]^+$ (X=S, Se). The alternative species (to this terminally bonded complex) that could be considered to exist in solution is a bridging complex such as $(DMSO)_4Ni(NCS)_2Ni(DMSO)_4$. According to Nelson et al. [148] the CN stretches of bridged metal thiocyanate complexes (i.e. M-NCS-M) occur over a wider range of values and tend toward higher numbers than are observed in terminal M-NCS complexes. The possibility of a bridged complex was considered in EXAFS calculations but cursory processing of data in the present study using this bridging M-NCS-M model did not yield any changes in the overall results obtained from when the original models (assuming terminal bonding) were used, and also resulted in too many free parameters to yield a statistically meaningful result. Hence for both the Ni-thiocyanate *and* Ni-selenocyanate systems, it is believed that the stoichiometry of the system is at least a *monopseudohalide Ni(II) ion*, though it is plausible that dipseudohalide ion substitutions may also be possible (though no change to IR frequencies of coordinated thiocyanate or selenocyanate reflect this in the model solution IR data) with the remainder being coordinated solvent molecules. This was made most obvious at least in the thiocyanate system's case from the colour of solutions

where the Ni(II) thiocyanate complex ion present in model solutions produced a green colour while colours of the tetrahedral tetrathiocyanatonickelate(II) species or salts are blue [100, 149], as is the case for solids containing the dithiocyanatonickelate(II) complex [150].

In the case of the Ni/cyanate systems, the EXAFS/XANES data have given a distinctly different result for overall coordination numbers to Ni of ligands. In general (see Table 4.3 at chapter 4), an average coordination of 5 is observed for Ni. Although 5-coordinate Ni(II) complexes are possible [151], what is believed to be the situation here is that the EXAFS/XANES measurement depicts an average environment in which tetrahedral Ni(II) cyanate complexes (i.e. $[Ni(NCO)_4]^{2-}$, responsible for the blue colour in these solutions, are mixed with other Ni(II) species which have an octahedral environment, e.g. $[Ni(DMSO)_6]^{2+}$ [79]. Hence there is a mixture of 4 and 6 coordinate species present in both the electrochemically generated solution and the model solution so that the EXAFS/XANES method effectively is sensing on average a 5-coordinate species based on the calculated N numbers. This also accounts for the different features observed for Ni-NCO XANES compared to the other, octahedrally co-ordinated, Ni-NCS and Ni-NCSe samples and standards. It is strongly believed that the "6 coordinate" species is $[Ni(DMSO)_6]^{2+}$ because the N values for DMSO in the "average" 5 coordinate complex are weighted toward the DMSO ligand.

8.2 Cu/pseudohalide systems

Chapter 5 is an IR spectroelectrochemical and XANES study of the Cu/pseudohalide electrochemical system. XANES has been pivotal in these studies for understanding the Cu speciation resulting in the electrochemical systems involving pseudohalides in non-aqueous, polar aprotic solvents. XANES showed what the dominant redox states were for Cu in these electrochemical systems. In all six Cu/pseudohalide ion systems examined by IR spectroelectrochemicaly, the presence of Cu(I) species is shown to be important. In the Cu/thiocyanate electrochemical system and to a lesser extent the Cu/selenocyanate electrochemical system, there is evidence (provided mostly by XANES and (for thiocyanate systems) colours of solutions) that Cu(I) and Cu(II) species are electrogenerated upon anodic dissolution and end up in the cell

solution after the IR experiment as complex ion species. This has been supported by XANES data which definitively show the presence of Cu(I) species in the electrochemically generated solutions in all systems but also a mixture of Cu(I) and Cu(II) in the Cu/NCS^- and Cu/$NCSe^-$ systems. Model solutions prepared have generally provided convincing evidence to support assignments made from the in situ IR spectra. Though the XANES work is concentrated on DMSO-containing systems, it is assumed that given the similarity of the electrochemistry of the Cu/DMSO/pseudohalide ion systems to the DMF solvent-based systems, the electrochemistry in the DMF-based solvent systems would be largely very similar in terms of speciation produced.

8.3 Au/pseudohalide systems

SNIFTIRS studies have shown that Au electrodes undergo anodic dissolution in DMSO and DMF solutions of pseudohalide ions to form the corresponding diisocyanato-, dithiocyanato- and diselenocyanatoaurate(I) complex ion species. These are the main species formed as well as CO_2 which is detected for electrodes polarised in the presence of NCS^- and NCO^- only. Electrochemically the onset of formation of these complex ions is mostly above +500 mV(AgCl/Ag) in all systems studied.

The Au(I) species observed in the SNIFTIRS spectra of the Au electrodes polarised in the presence of thiocyanate and seleonocyanate ions (i.e. $[Au(SCN)_2]^-$ and $[Au(SeCN)_2]^-$ were confirmed by independently synthesising them in DMSO model solutions made from combining known mole ratios of the Au(III) salt, $KAuBr_4$ and the relevant pseudohalide salt (NaSCN and KSeCN) and utilising some fortuitous redox chemistry leading to the formation of Au(I) from Au(III). The independent synthesis and proof of the $[Au(NCO)_2]^-$ ion, on the other hand, was accomplished by adding excess cyanate ions to the preformed mixture of $KAuBr_4$ and NaSCN (1:4 mole ratio) in order to generate this ion by displacement of thiocyanate ions from the already formed $[Au(SCN)_2]^-$ ions in the mixture. FTIR spectroscopy and electrospray ionisation mass spectrometry were used to confirm the presence of the $[Au(NCO)_2]^-$, $[Au(SCN)_2]^-$ and $[Au(SeCN)_2]^-$ species and additionally showed that Au-cyano complexes had also formed in the model solutions as a result of side reactions involving the pseudohalide ions.

8.4 $TeCN^-$ systems

In Chapter 7, IR spectroelectrochemical studies of the anodic dissolution of Ni, Cu and Au in DMSO and DMF solutions of the unstable $TeCN^-$ ion were studied for the first time. These have conclusively shown that the $TeCN^-$ ion is unstable in anodically polarised electrochemical cells. This was also conclusively proven by theoretical calculations where a putative metal–isotellurocyanato complex was modelled and its theoretical CN stretching frequency was calculated. It was also found that the electrochemical decomposition region for $TeCN^-$ ion is earlier potentiometrically speaking on Cu electrodes compared to Ni and Au electrodes. The observed speciation of products in these electrochemical cells is reflective of the interaction of the metal electrode with *cyanide* (originating from the breakdown of $TeCN^-$ ion) ions rather than tellurocyanate ions albeit on electrodes that are fouled by the deposited tellurium from the decomposition of $TeCN^-$. These observations were supported by running the IR spectra of model solutions prepared from mixing together Cu(II) and CN^- as well as $TeCN^-$ ions. Generally, the $TeCN^-$ ions are unstable in these model solutions due to the polarizing effect of the metal counter ions generated via anodic polarization. Model solutions of the Ni and Cu salts with cyanide which were used to prove the existence of metal-cyano complex ion speciation in the in situ IR spectra. Overall this proved that these species existed but also showed other interesting redox chemistry indicating the reactivity of these systems, for example the interaction of Cu(II) and cyanate ion which led to spectrum such as $[Cu(CN)_2]^-$, $[Cu(CN)_3]^{2-}$, NCO^- and CO_2.

Overall, the IR spectroelectochemistry has indicated through different speciation and where it starts occurring on these electrodes the difference in reactivity between Ni, Cu and Au. It has also shown the dramatic surface blocking effect of the decomposition of $TeCN^-$ to elemental (black) Te and CN^- on these electrodes which is believed to inhibit electrochemical reaction.

In general, this study has given useful information on systems which have not been characterised specifically by IR spectroelectrochemical techniques. Further studies relating to this area should involve investigating the system at different metal electrodes (i.e. Rhenium, Vanadium, Magnesium, Niobium and Tantalam) which have not studied before in IR spectroeletrochemical techniques. Using different IR beam angle at the electrode surface should also be attempted in order

to obtain information on surface adsorbed species at the electrode/electrolyte interface.

References

[1] P. Zanello, Inorganic Electrochemistry Theory, Practice and Application, The Royal Society of Chemistry, Cambridge, 2003.

[2] A.J. Bard, L.R. Faulkner, Electrochemical Methods Fundamentals and ApplicationSecond edition ed., John Wiley & Sons, New York, 2001.

[3] J.O. Bockris, N. Bonciocat, F. Gutmann, An Introduction to Electrochemical Science, Wykeham publications (London) Ltd., London and Winchester, 1974.

[4] J.O. Bockris, D.M. Drazic, Electro-Chemical Science, Taylor & Francis Ltd, London, 1972.

[5] S.P. Kounaves, in: F.A. Settle, (Eds.) Hand book of Instrumental Techniques for Analytical Chemistry, Prentice Hall PTR, New Jersey, 1997.

[6] P.T. Kissinger, W.R. Heineman, J. Chem. Educ. 60 (1983) 702-706.

[7] K. Kunimatsu, H. Seki, W.G. Golden, J.G. Gordon, M.R. Philpott, Langmuir 4 (1988) 337-341.

[8] B. Beden, C. Lamy, in: R.J. Gale, (Eds.) Spectroelectrochemistry Theory and Practice, Plenum Press, New York, 1988, pp. 189-262.

[9] C. Korzeniewski, B.S. Pons, Prog. Anal. Spectrosc. 10 (1987).

[10] C. Korzeniewski, M.W. Sevrson, Specrochem Acta 51A (1995) 499.

[11] K. Ashley, Talanta 38 (1991) 1209-1218.

[12] R.G. Greenler, J. Chem. Phys. 44 (1966).

[13] A. Bewick, K. Kunimatsu, Surf. Sci. 101 (1980) 131-138.

[14] A. Bewick, K. Kunimatsu, B. Stanley Pons, Electrochim. Acta 25 (1980) 465-468.

[15] J.K. Foley, S. Pons, Anal. Chem. 57 (1985) 945 A-956 A.

[16] K. Ashley, S. Pons, Chem. Rev. 88 (1988) 673-695.

[17] H. Neugebauer, G. Nauer, A. Neckel, G. Tourillon, F. Garnier, P. Lange, J. Phys. Chem. 88 (1984).

[18] A. Bewick, K. Kunimatsu, B.S. Pons, J.W. Russell, J. Electroanal. Chem. 160 (1984) 47-61.

[19] L.S. Kau, D.J. Spira-solomon, J.E. Penner-Hahn, K.O. Hodgson, E.I. Solomon, J. Am. Chem. Soc. 109 (1987) 6433-6442.

[20] M. Newville, Fundamentals of XAFS, Technical Report, Consortium for Advanced Radiation Sources, University of Chicago, Chicago, IL, 2004. 40p.

[21] S.A. Hofstadler, R. Bakhtiar, R.D. Smith, J. Chem. Soc. 73 (1996).

[22] K.A. Rubinson, J.F. Rubinson, in: (Eds.) Contemporary Instrumental Analysis, Prentice-Hall, Inc., New Jersey, 2000, pp. 514.

[23] W. Henderson, J.S. McIndoe, in: (Eds.) Mass Spectrometry of Inorganic, Coordination and Organometallic Compounds, John Wiley & Sons, Ltd, 2005, pp. 127-173.

[24] H.B. Mark, B.S. Pons, Anal. Chem. 38 (1966) 119.

[25] D. Tallant, D.H. Evans, Anal. Chem. 41 (1969) 835.

[26] M. Fleischmann, P.J. Hendra, A.J. McQuillan, J. Chem. Soc. Chem. Commun 80 (1973).

[27] S. Pons, A. Bewick, Nav. Res. Rev. 37 (1985) 33-41.

[28] W.G. Golden, D. Saperstein, M.W. Sevrson, J. Overend, J. Catal. 71 (1981) 395.

[29] W.G. Golden, K. Kunimatsu, H. Seki, J. Phys. Chem. 88 (1984) 1275-1277.

[30] D.K. Lambert, Solid State Commum. 51 (1984) 297.

[31] K. Kunimatsu, H. Seki, W.G. Golden, J.G. Gordon, Surf. Sci. 158 (1985) 596-608.

[32] K. Nakamoto, Infrared and Raman Spectra of Inorganic and Coordination Compounds5th edition ed., John Wiley & Sons, Inc., New York, 1997.

[33] K. Kunimatsu, H. Seki, W.G. Golden, Chem. Phys. Lett. 108 (1984) 195-199.

[34] K.A.B. Lee, K. Kunimatsu, J.G. Gordon, W.G. Golden, H. Seki, J. Electrochem. Soc. 134 (1987) 1676-1678.

[35] F. Kitamura, M. Takahashi, M. Ito, Chem. Phys. Lett. 130 (1986) 181-184.

[36] M.R. Mucalo, R.P. Cooney, G.A. Wright, J. Chem. Soc. Faraday Trans. 86 (1990) 1083-1086.

[37] M.R. Mucalo, Q. Li, J. Colloid Interface Sci. 269 (2004) 370-380.

[38] R.A. Bailey, L.S. Kozak, T.W. Michelsen, W.N. Mills, Coord. Chem. Rev. 6 (1971) 407-445.

[39] A.H. Norbury, in: H.J. Emeleus, A.G. Sharpe, (Eds.) Advances in Inorganic Chemistry and Radiochemistry, Academic Press, Inc (London) Ltd., New York, 1975, pp. 231-386.

[40] T. Yamaguchi, K. Yamamoto, H. Ohtaki, Bull. Chem. Soc. Jpn. 58 (1985) 3235.

[41] T. Austad, J. Songstad, Acta. Chem. Scand. 25 (1971) 331-333.

[42] D.S. Corrigan, P. Geo, L.H. Leung, M.J. Weaver, Langmuir 2 (1986) 744-752.

[43] D. Parry, J.M. Harris, Langmuir 6 (1990) 209-217.

[44] D.S. Corrigan, M.J. Weaver, Langmuir 4 (1988) 599-606.

[45] M. Bron, R. Holze, Electrochim. Acta. 45 (1999) 1121-1126.

[46] M. Bron, R. Holze, J. Electroanal. Chem. 385 (1995) 105-113.

[47] M. Bron, R. Holze, J. Anal. Chem. 361 (1998) 694-696.

[48] F. Kitamura, M. Takahashi, M. Ito, Chem. Phys. Lett. 136 (1987) 62-66.

[49] P.A. Kilmartin, G.A. Wright, J. Chem. Soc. Faraday Trans. 91 (1995) 4403-4411.

[50] P.A. Kilmartin, G.A. Wright, Aus. J. Chem. 50 (1997) 321-327.

[51] M.E. Martins, C. Castellano, A.J. Calandra, A.J. Arvia, J. Electroanal. Chem. 81 (1977) 191-300.

[52] M.E. Martins, C. Castellano, A.J. Calandra, A.J. Arvia, J. Electroanal. Chem. 92 (1978) 45-53.

[53] A.W. Downs, Chem. Comm. (1968) 1290-1291.

[54] H.K. Spencer, M.V. Lakshmikantham, M.P. Cava, J. Am. Chem. Soc. 99 (1977) 1470-1473.

[55] R.M. Souto, F. Ricci, L. Spyrkowicz, J.L. Rodriguez, E. Pastor, J. Phys. Chem. C 115 (2011) 3671.

[56] A.B. Delgado, D. Posadas, A.J. Arvia, Electrochim. Acta 21 (1976) 385-393.

[57] F. Bellucci, G. Capobianco, A. Deganello, A. Glisenti, T. Monetta, G. Moretti, in: P.L. Bonora, F. Deflorian, (Eds.) Electrochemical Methods in Corrosion Research Vl, Pts 1 and 2, Transtec Publications, Zurich-Uetikon, 1998, pp. 1311-1320.

[58] N.P. Abrashkina, T.R. Agladze, G.S. Raskin, Prot. Met. 13 (1977) 565-569.

[59] L. Ercolano, T. Monetta, F. Bellucci, Corros. Sci. 35 (1993) 161-167.

[60] J. Banas, B. Stypula, K. Banas, J. Swiatowska-Mrowiecka, M. Starowicz, U. Lelek-Borkowska, J. Solid State Electrochem. 13 (2009) 1669-1679.

[61] F. Bellucci, C.A. Farina, G. Faita, Electrochim. Acta 26 (1981) 731-733.

[62] A. Vaskevich, F. Sinapi, Z. Mekhalif, J. Delhalle, I. Rubinstein, J. Electroanal. chem. 152 (2005) C744-C750.

[63] A.M. Vecchio-Sadus, J. Appl. Electrochem. 23 (1993) 401-416.

[64] M. Pilarczyk, W. Grzybkowski, L. Klinszporn, Bull. Pol. Acad. Sci. Chem. 35 (1987) 559-567.

[65] K.P. Sarma, R.K. Poddar, Transition Met. Chem. 9 (1984) 135-138.

[66] Detectors for Fourier Transform Spectroscopy. Thermo Scientific Application Note 50808, https://fscimage.fishersci.com/images/ D10942~.pdf (accessed 2 September 2014).

[67] S.F. Mason, J Chem. Soc. (1959) 1263-1268.

[68] J.P. Fackler Jr, G.E. Dolbear, D. Coucouvanis, J. Inorg. Nucl. Chem. 26 (1964) 2035-2037.

[69] B. Mavis, M. Akinc, Chem. Mater. 18 (2006) 5317.

[70] Wikipedia: Solvent, http://en.wikipedia.org/wiki/Solvent (accessed February 2013).

[71] D. Aurbach, Y. Gofer, in: D. Aurbach, (Eds.) Nonaqueous Electrochemistry, Marcel Dekker, New York, 1999, pp. 137-212.

[72] J. McMurry, in: (Eds.) Organic Chemistry, 8th ed. Brooks/Cole, Cengage Learning, Canada, 2012, pp. 871-872.

[73] L.Y. Cho, J.M. Madurro, J.R. Romero, J. Catal. 186 (1999) 31-35.

[74] Y. Inada, S. Founahashi, Anal. Sci. 13 (1997) 373-377.

[75] J.M. Charnock, D. Collison, C.D. Garner, E.J.L. McInnes, J.F.W. Mosselmans, J. Phys. IV 7 (1997) C2-657-C2-658.

[76] B. Ingham, N.B. Illy, M.F. Toney, M.L. Howdyshell, M.P. Ryan, J. Phys. Chem. C 112 (2008) 14863-14866.

[77] B. Ingham, M. Ko, G. Kear, P. Kappen, N. Laycock, J.A. Kimpton, D.E. Williams, Corros. Sci. 52 (2010) 3052-3061.

[78] J. Yeo, M.H. Cheah, M.I. Bondin, S.P. Best, Aust. J. Chem. 65 (2012) 241-253.

[79] M. Pilarczyk, W. Grzybkowski, L. Klinszporn, J. Chem. Soc. Faraday Trans. 1 85 (1989) 3395-3402.

[80] F.A. Cotton, G. Wilkinson, Advanced Inorganic Chemistry: A Comprehensive Text4th , completely rev. from the original literature. ed., Wiley, New York, 1980.

[81] Y. Inada, H. Hayashi, K. Sugimoto, S. Funahashi, J. Phys. Chem. A 103 (1999) 1401-1406.

[82] B. Ingham, N. Gaston, K. Fahy, X.Y. Chin, C.J. Dotzler, E. Rees, G. Haslam, Z.H. Barber, G.T. Burstein, M.P. Ryan, J. Phys. Chem. C 116 (2012) 6159-6165.

[83] J. Krakowiak, D. Lundberg, I. Persson, Inorg. Chem. 51 (2012) 9598-9609.

[84] F.F. Xia, D. Zeng, H.B. Yi, C. Fang, J. Phys. Chem. A 117 (2013) 8468-8476.

[85] B. Ravel, M. Newville, J. Synchrotron Rad 12 (2005) 537.

[86] M. Newville, J. Synchrotron Rad 8 (2001) 322.

[87] G.J. Colpas, M.J. Maroney, C. Bagyinka, M. Kumar, W.S. Willis, S.L. Suib, N. Baidya, P.K. Mascharak, Inorg. Chem. 30 (1991) 920.

[88] M.G. Kim, J. Cho, J. Mater. Chem. 18 (2008) 5880.

[89] E. Montargès-Pelletier, V. Chardot, G. Echevarria, L.J. Michot, A. Bauer, J.L. Morel, Phytochem 69 (2008) 1695.

[90] T.J. Strathmann, S.C.B. Myneni, Geochim. Cosmochim. Acta 68 (2004) 3441.

[91] R.S. Goncalves, A.M.S. Lucho, J. Braz. Chem. Soc. 11 (2000) 486-490.

[92] R.S. Vakhidov, Russ. J. Electrochem. 30 (1994) 1165-1166.

[93] G.A. Bowmaker, P.A. Kilmartin, G.A. Wright, J. Solid State Electrochem. 3 (1999) 163-171.

[94] G.A. Bowmaker, D.A. Rogers, J.Chem. Soc. (1982) 1873-1876.

[95] M.D. Benari, G.T. Hefter, A.J. Parker, Hydrometallurgy 10 (1983) 367-389.

[96] D. Forster, D.M.L. Goodgame, J. Chem. Soc. (1965) 262-267.

[97] C.A. Melendres, G.A. Bowmaker, J.M. Leger, B. Beden, Nucl. Instrum. Methods Phys. Res., Sect. B 133 (1997) 109-113.

[98] A. Ray, G.M. Rosair, R. Rajeev, R.B. Sunoj, E. Rentschler, S. Mitra, Dalton Trans. (2009) 9510-9519.

[99] J.L. Burmeister, T.P. O'Sullivan, Inorg. Chem. Acta 3 (1969) 479-486.

[100] D. Forster, D.M.L. Goodgame, Inorg. Chem. 4 (1965) 823-829.

[101] J. Rannou, M. Chabanel, Inorg. Chem. 24 (1985) 2319-2320.

[102] D.A. Skoog, D.M. West, F.J. Holler, Fundamentals of Analytical Chemistry7th ed., Saunders College Publishing, USA, 1995.

[103] L.M. Kul'berg, A.K. Gorlinskii, Russ. J. Gen. Chem 9 (1939) 1707-1709.

[104] J.H. Clark, C.W. Jones, Inorg. Chim. Acta. 179 (1991) 41-45.

[105] M. Kabesova, J. Kohout, J. Gazo, Inorg. Chem. Acta 31 (1978) L435-L436.

[106] S.K. Tobia, E.R. Souaya, W.G. Hanna, Polyhedron 4 (1985) 425-428.

[107] C.J. Burchell, P. Kilian, A.M.Z. Slawin, J.D. Woollins, Inorg. Chem. 45 (2006) 710-716.

[108] A. Solangi, A.M. Bond, I. Burgar, A.F. Hollenkamp, M.D. Horne, T. Ruther, C. Zhao, J. Phys. Chem. B 115 (2011) 6843-6852.

[109] A. Manceau, D. Gallup, Environ. Sci.Technol. 31 (1997) 968-976.

[110] D.L. Smith, V.L. Saunders, Acta. Cryst. B37 (1981) 1807-1812.

[111] E.E. Aynsley, N.N. Greenwood, M.J. Sprague, J. Chem. Soc. (1964) 699-704.

[112] F. Cataldo, Polyhedron 19 (2000) 681-688.

[113] T. Krogulee, Pol. J. Chem, 69 (1995) 746-755.

[114] J. Kohout, M. Hvastijova, J. Gazo, Coord. Chem. Rev. 27 (1978) 141-172.

[115] F.E. Huggins, G.P. Huffman, J.D. Robertson, J. Hazard. Mater. 74 (2000) 1-23.

[116] P. Frank, M. Benfatto, B. Hedman, K.O. Hodgson, Inorg. Chem. 51 (2012) 2086-2096.

[117] J.S. McEwen, T. Anggara, W.F. Schneider, V.F. Kispersky, J.T. Miller, W.N. Delgass, F.H. Ribeiro, Catalysis Today 184 (2012) 129-144.

[118] J.L. Gardea-Torresdey, J.R. Peralta-Videa, G. de la Rosa, J.G. Parsons, Coord. Chem. Rev. 249 (2005) 1797-1810.

[119] E.I. Solomon, C.B. Bell III, in: A. Bakac, (Eds.) Physical Inorganic Chemistry: Principles, Methods, and Models, John Wiley & Sons, Hoboken NJ, 2010, pp. 1-38.

[120] C. Pyun, S. Park, J. Electrochem. Soc. 133 (1986) 2024-2030.

[121] C.A. Melendres, G.A. Bowmaker, K.A.B. Lee, B. Beden, J. Electroanal. Chem. 449 (1998) 215-218.

[122] M.D. Adams, M.W. Johns, in: H. Schmidbaur, (Eds.) Gold Progress in Chemistry- Biochemistry and Technology, John Wiley & Sons, 1999.

[123] R. Kissner, J. Electroanal. Chem. 385 (1995) 71-75.

[124] C.-H. Zhen, S.-G. Sun, C.-J. Fan, S.-P. Chen, B.-W. Mao, Y.-J. Fan, Electrochim. Acta 49 (2004) 1249-1255.

[125] T. Dickinson, A.F. Povey, M.A. Sherwood, J. Chem. Soc., Faraday Trans. 1 71 (1975) 298-311.

[126] W. Beck, W.P. Fehlhammer, P. Poellmann, H. Schaechl, Chem. Ber. 102 (1969) 176-187.

[127] J.B. Melpolder, J.L. Burmeister, Inorg. Chem. 11 (1972) 911-913.

[128] W.R. Mason, H.B. Gray, Inorg. Chem. 7 (1968) 55-58.

[129] N. de Stefano, J.L. Burmeister, Inorg. Chem. 10 (1971) 998-1003.

[130] T. Guo, L. Li, V. Cammarata, A. Illies, J. Phys. Chem. B 109 (2005) 7821-7825.

[131] A.C. Reeder, H.E. Spencer, J. Imag. Sci. 31 (1987) 126-129.

[132] O. Topel, I. Persson, E. Avsar, J. Mol. Liq. 143 (2008) 89-94.

[133] M. Rawashdeh-Omary, M. Omary, H.H. Patterson, J. Am. Chem. Soc. 122 (2000) 10371-10380.

[134] J. Emsley, The ElementsSecond ed., Clarendon press- Oxford, 1991.

[135] O.H. Ellestad, P. Klaeboe, J. Songstad, Acta Chem. Scand., 26 (1972) 1724-1726.

[136] A.Z. Al-Rubaie, in: M.A. Cato, (Eds.) New Developments in Organometalic Chemistry Research, Nova Science, New York, 2004, pp. 191-213.

[137] P. Klaeboe, C.J. Nielsen, J. Songstad, Acta Chem. Scand. A 31 (1977) 884-886.

[138] G. Cauquis, G. Pierre, B. Soc. Chim. Fr. (1972) 1225-1228.

[139] W.M. Keely, H.W. Maynor, J. Chem. Eng. Data 8 (1963) 297-300.

[140] P. Krtil, L. Kavan, I. Hoskovcová, K. Kratochvilová, J. Appl. Electrochem. 26 (1996) 523-527.

[141] F.R. Duke, W.G. Courtney, J. Phys. Chem. 56 (1952) 19-21.

[142] A. Katagiri, S. Yoshimura, S. Yoshizawa, Inorg. Chem. 20 (1981) 4143-4147.

[143] R. Parkash, J. Zyka, Microchem. J. 17 (1972) 309-317.

[144] T.K. Brotherton, J.W. Lynn, Chem. Rev. 59 (1959) 841-883.

[145] A.F. Carley, M. Chinn, C.R. Parkinson, Surf. Sci. 537 (2003) 64-74.

[146] S. Ahrland, K. Nilsson, B. Tagesson, Acta. Chem. Scand. A37 (1983) 193-201.

[147] J.H. Baxendale, D.T. Westcott, J. Chem. Soc. (1959) 2347-2351.

[148] S.M. Nelson, T.M. Shepherd, J. Inorg. Nucl. Chem. 27 (1965) 2123-2125.

[149] D. Forster, D.M.L. Goodgame, J. Inorg. Nucl. Chem. 26 (1964) 2035.

[150] A.W. Downs, B.A. Gotz, A.E. McCarthy, Inorg. Nucl. Chem. letters 11 (1974) 365-366.

[151] M.D. Santana, A.A. Lozano, G. Garcia, G. Lopez, J. Perez, Dalton Trans. (2005) 104-109.

Appendix 1

Table S.1: Parameters used to fit the NiO powder standard ('Sample 1'), shown in Figure 4.2 and (Figure S.1 in Appendix 1).

# parameters	6
Independent points	27.6
k-range	2-13
R-range	1-5
k-weights used	1, 2, 3
Reduced χ^2	750
ΔE_0 [eV]	-0.97 ± 0.57
amp (S_0^2)	0.78 ± 0.07
ss1a (σ^2 for first single scattering path, Ni-O)	0.0036 ± 0.0019
ss1 (σ^2 for subsequent single scattering paths)	0.0029 ± 0.0005
ss (σ^2 for multiple scattering paths)	0.0035 ± 0.0005
scale (for each path, $\Delta r = r*scale$)	0.0020 ± 0.0010

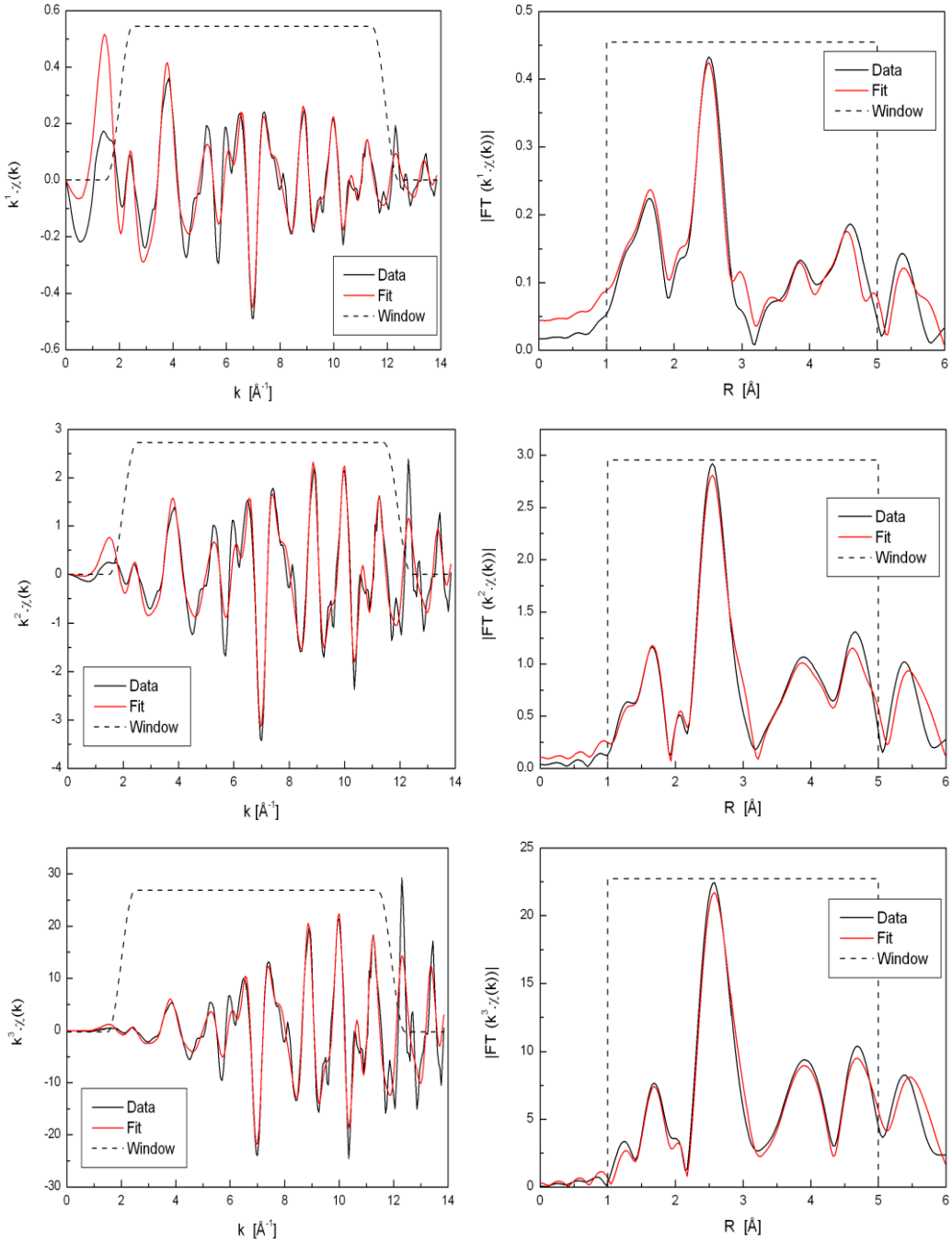

Figure S.1: NiO powder standard ('Sample 1') EXAFS data (black lines) and fits (red lines) in k-space (left) and R-space (right) for various k-weightings: k^1 (top), k^2 (middle), k^3 (bottom). The data ranges used for fitting are shown by the window functions (black dashed lines).

Appendix 2

Table S.2: Parameters used to fit the Ni^{2+} in H_2O standard ('Sample 2'), shown in Figure 4.3 and (Figure S.2 in Appendix 2).

# parameters	7
Independent points	24.7
k-range	2-11.85
R-range	1-5
k-weights used	1, 2, 3
Reduced χ^2	58
ΔE_0 [eV]	-2.17 ± 0.37
amp (S_0^2), 1st path	4.00 ± 0.15
r, 1st path	2.054 ± 0.004
ss, 1st path	0.0023 ± 0.0006
amp (S_0^2), 2nd path	5.75 ± 1.59
r, 2nd path	4.070 ± 0.026
ss, 2nd path	0.023 ± 0.011

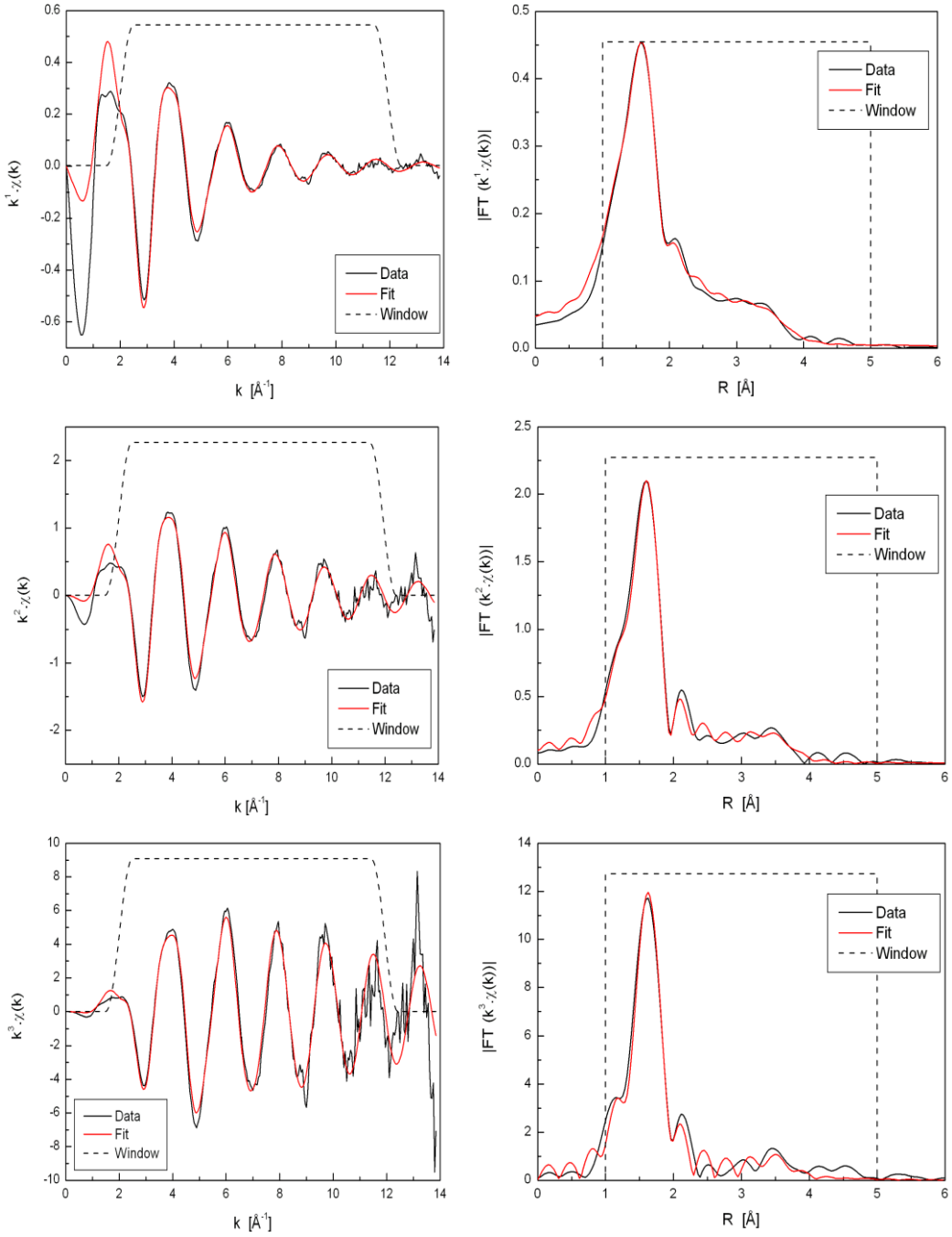

Figure S.2: $Ni(NO_3)_2$ in H_2O ('Sample 2') EXAFS data (black lines) and fits (red lines) in k-space (left) and R-space (right) for various k-weightings: k^1 (top), k^2 (middle), k^3 (bottom). The data ranges used for fitting are shown by the window functions (black dashed lines).

Appendix 3

Table S.3: Parameters used to fit the Ni^{2+} in DMSO standard ('Sample 3'), shown in Figure 4.4 and (Figure S.3 in Appendix 3).

# parameters	9
Independent points	18.7
k-range	2-11.9
R-range	1-4
k-weights used	1, 2, 3
Reduced χ^2	62
ΔE_0 [eV]	-4.72 ± 0.53
amp (S_0^2), O path	4.16 ± 0.20
r, O path	2.051 ± 0.006
ss, all paths	0.0041 ± 0.0009
amp (S_0^2), S path	2.14 ± 0.28
r, S path	3.162 ± 0.011
amp (S_0^2), C paths	4.89 ± 0.66
r, C_1 path	3.932 ± 0.026
r, C_2 path	4.151 ± 0.027

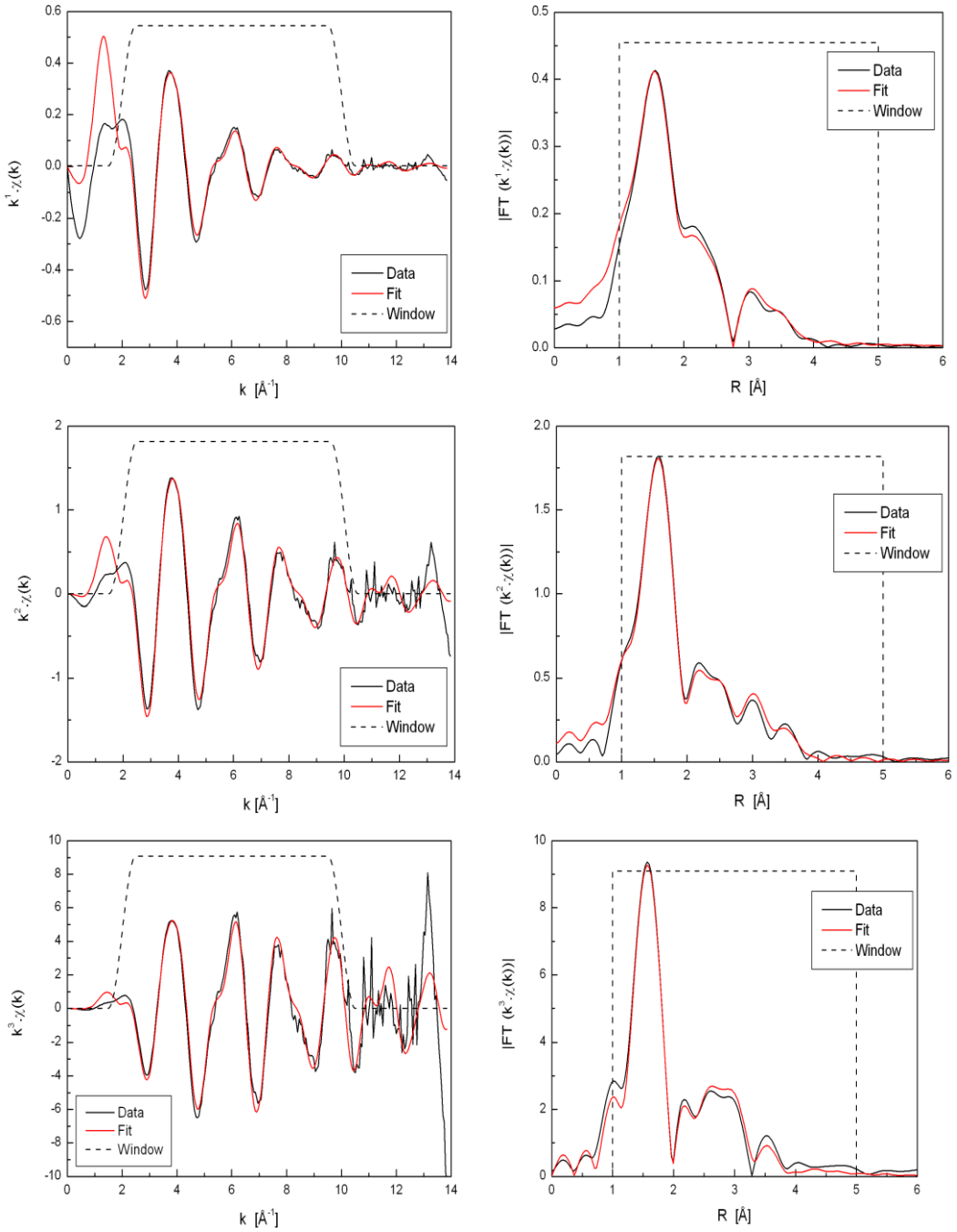

Figure S.3: $Ni(NO_3)_2$ in DMSO ('Sample 3') EXAFS data (black lines) and fits (red lines) in k-space (left) and R-space (right) for various k-weightings: k^1 (top), k^2 (middle), k^3 (bottom). The data ranges used for fitting are shown by the window functions (black dashed lines).

Appendix 4

Table S.4: Parameters used in single-scattering fits for NCX^- coordinated to a Ni(II) centre (X=O, S, and Se), shown in Figures S4-S7.

Parameter	X = O	X = S	X = Se	echem X = O
Reduced χ^2	126	232	252.7	34.44
ΔE_0 (all paths)	-5.6 ± 1.3	-6.2 ± 1.2	-5.6 ± 2.2	-6.9 ± 1.5
σ^2 (DMSO paths)	0.006 ± 0.006	0.003 ± 0.002	0.003 ± 0.003	0.006 ± 0.010
σ^2 (NCX^- paths)	0.003 ± 0.019	0.001 ± 0.008	0.008 ± 0.009	0.001 ± 0.015
scale (DMSO)[a]	0.65 ± 0.24	0.64 ± 0.11	0.61 ± 0.18	0.60 ± 0.26
amp_S (DMSO)	1.69 ± 1.01	2.19 ± 0.44	1.58 ± 1.17	1.62 ± 1.31
amp (NCX^-)	0.95 ± 1.13	1.25 ± 0.74	1.58 ± 1.17	0.82 ± 0.92
r_O (DMSO)	2.047 ± 0.127	2.014 ± 0.017	2.041 ± 0.041	2.042 ± 0.066
r_S (DMSO)	3.147 ± 0.024	3.132 ± 0.016	3.134 ± 0.023	3.118 ± 0.025
r_C1 (DMSO)	3.939 ± 0.056	3.927 ± 0.046	3.955 ± 0.065	3.963 ± 0.059
r_C2 (DMSO)	4.163 ± 0.073	4.102 ± 0.058	4.127 ± 0.092	4.152 ± 0.082
r_N (NCX^-)	2.073 ± 0.352	2.155 ± 0.048	2.098 ± 0.181	2.033 ± 0.156
r_C (NCX^-)	2.735 ± 0.093	2.709 ± 0.041	2.817 ± 0.097	2.693 ± 0.098
r_X (NCX^-)	4.438 ± 0.112	4.632 ± 0.045	4.848 ± 0.061	4.431 ± 0.109

[a] For the DMSO paths, amp(O) = scale*4.14, amp(C) = scale*4.61.

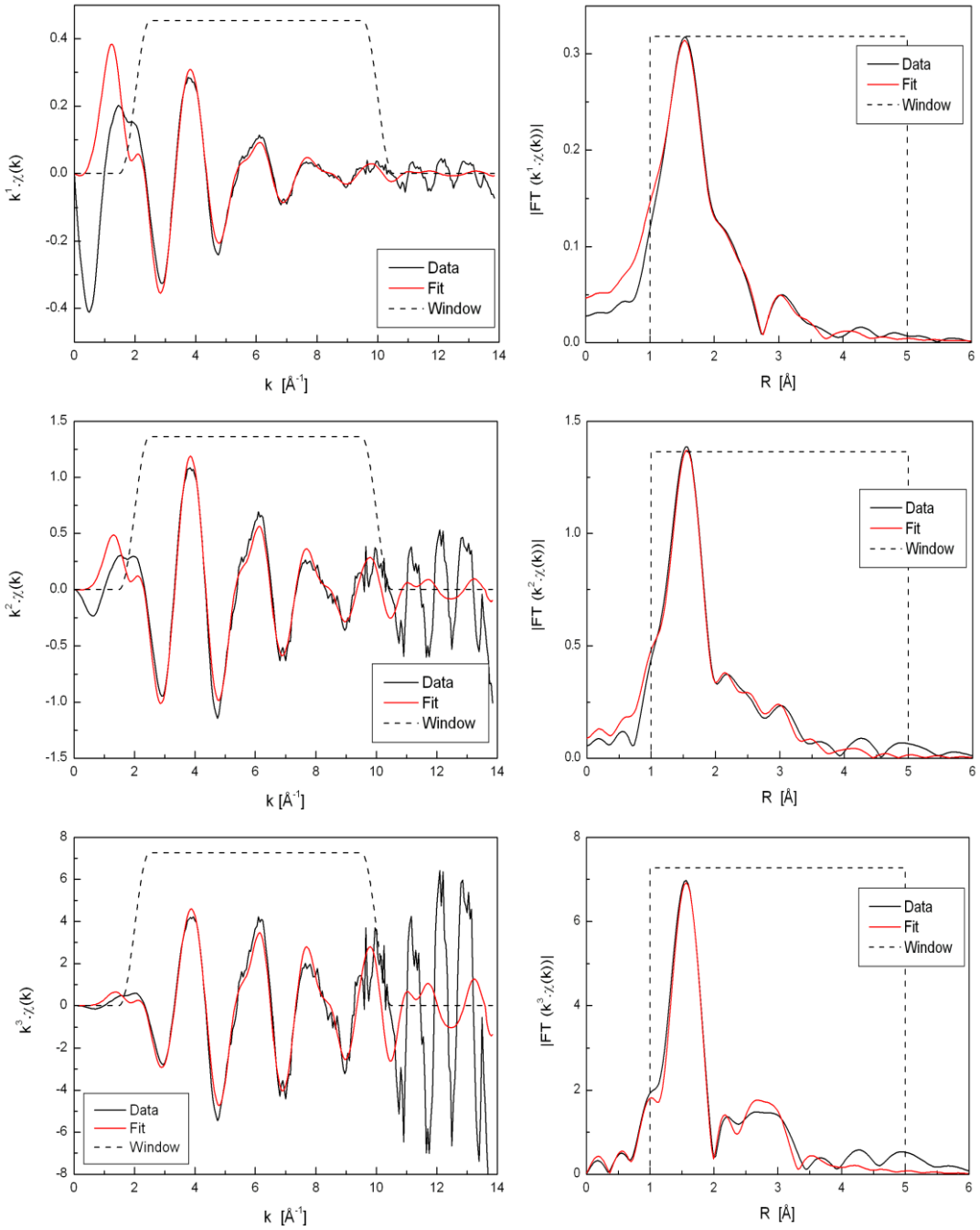

Figure S.4: Ni-NCO 2:1 KOCN:Ni^{2+} mole ratio model solution in DMSO ('Sample 4'), fitted using a single shell model. EXAFS data (black lines) and fits (red lines) in k-space (left) and R-space (right) for various k-weightings: k^1 (top), k^2 (middle), k^3 (bottom). The data ranges used for fitting are shown by the window functions (black dashed lines).

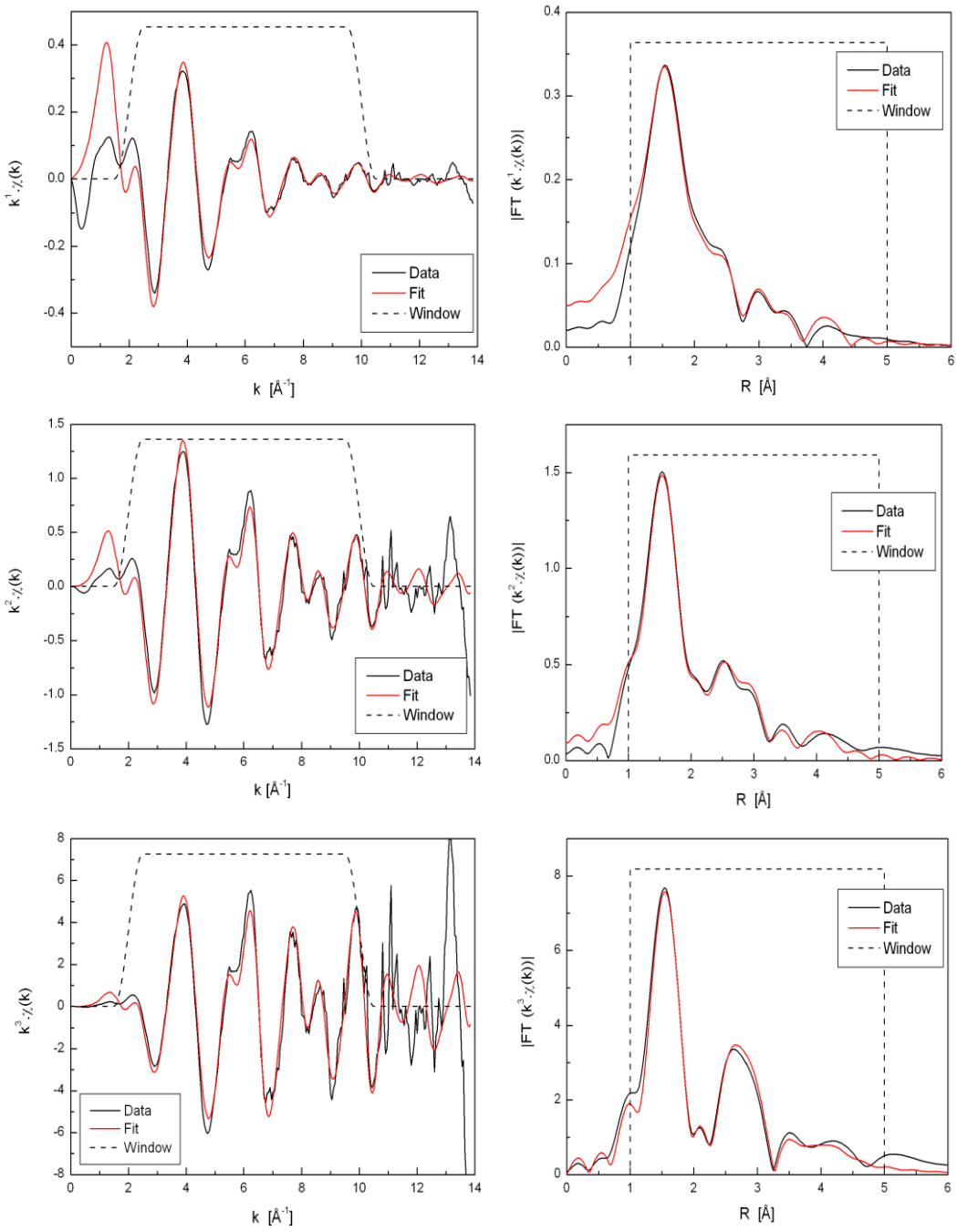

Figure S.5: Ni-NCS 2:1 KSCN:Ni^{2+} mole ratio model solution in DMSO ('Sample 5'), fitted using a single shell model. EXAFS data (black lines) and fits (red lines) in k-space (left) and R-space (right) for various k-weightings: k^1 (top), k^2 (middle), k^3 (bottom). The data ranges used for fitting are shown by the window functions (black dashed lines).

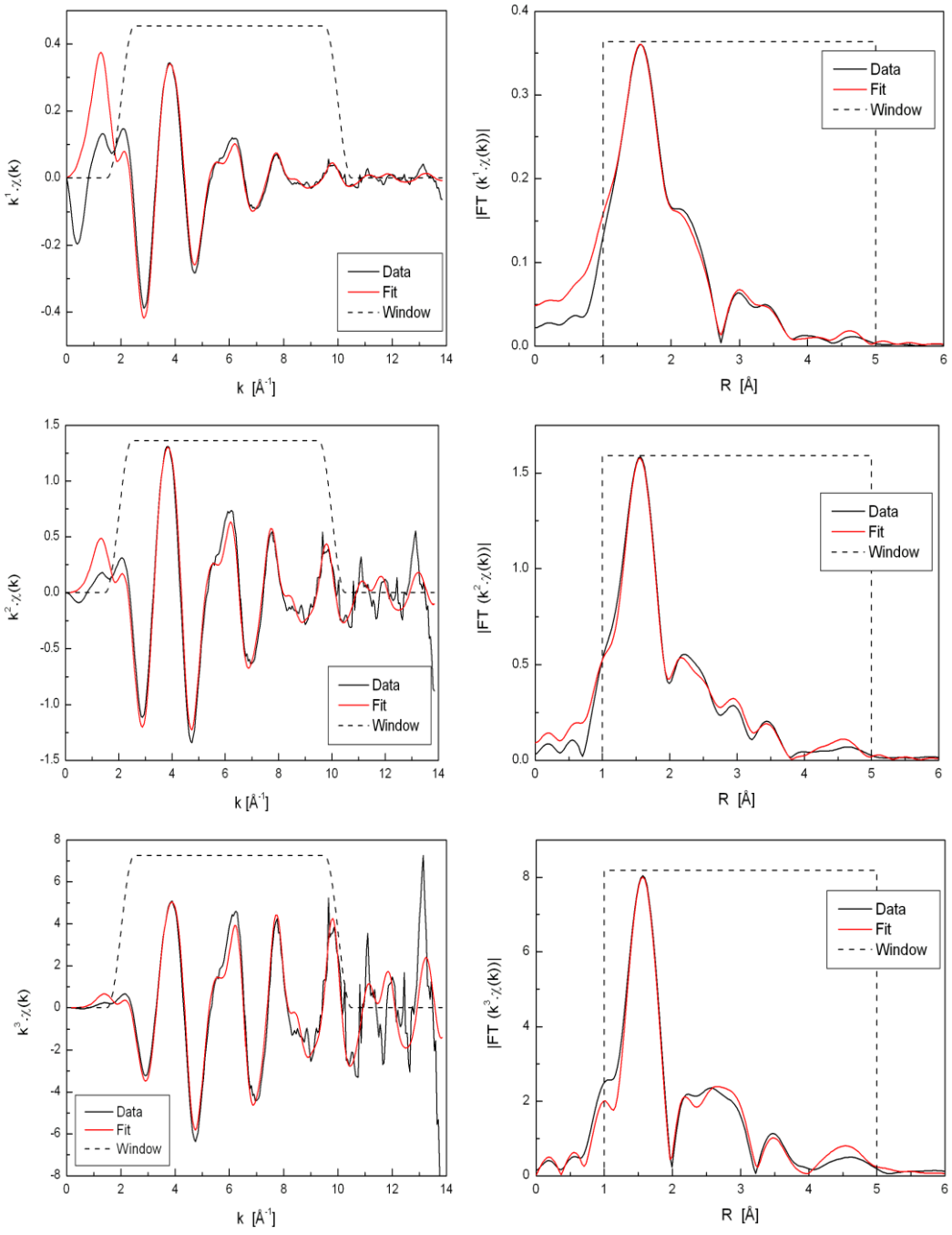

Figure S.6: Ni-NCSe 2:1 KSeCN:Ni^{2+} mole ratio model solution in DMSO ('Sample 6'), fitted using a single shell model. EXAFS data (black lines) and fits (red lines) in k-space (left) and R-space (right) for various k-weightings: k^1 (top), k^2 (middle), k^3 (bottom). The data ranges used for fitting are shown by the window functions (black dashed lines).

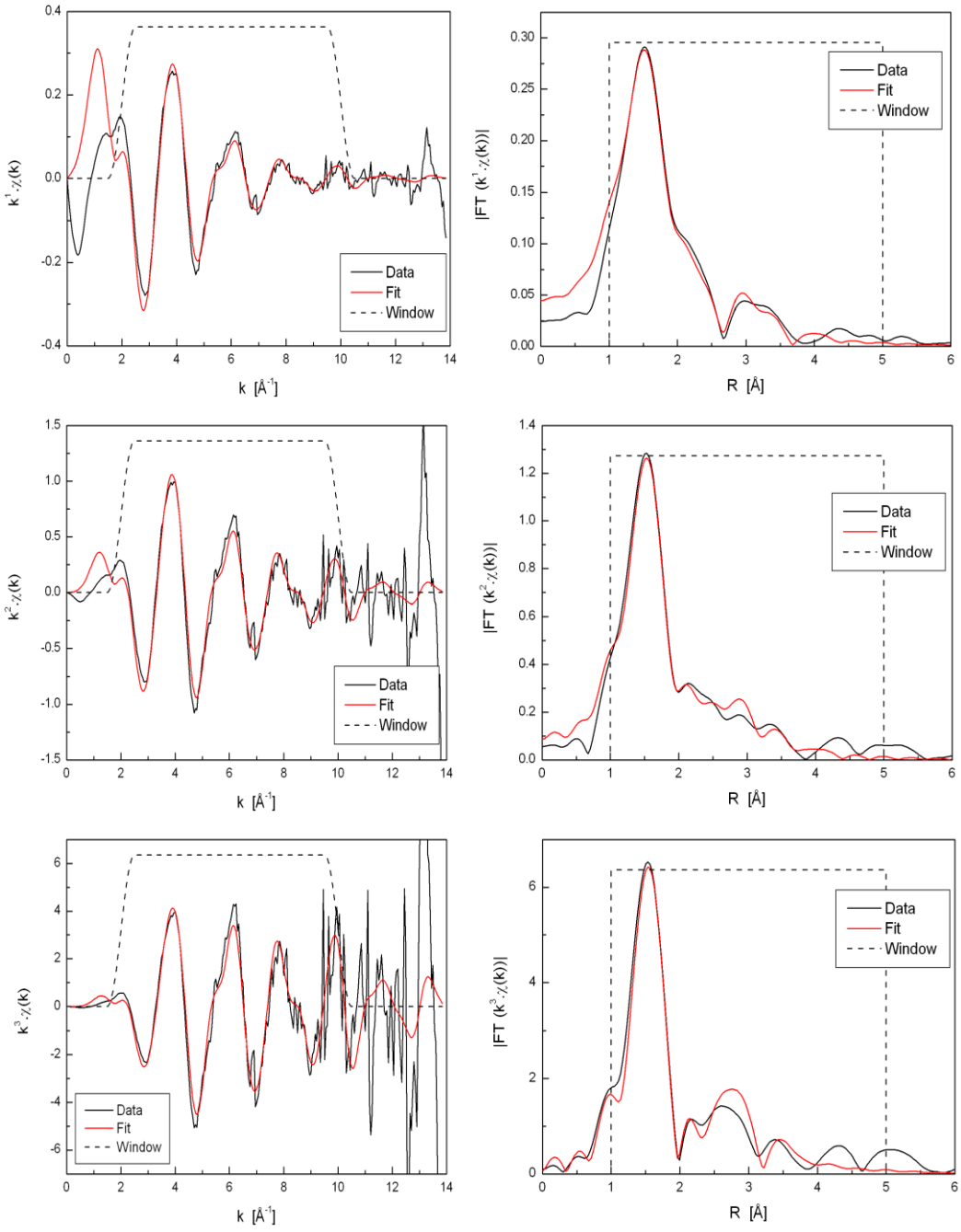

Figure S.7: Ni-NCO electrochemically generated solution in DMSO ('Sample 7'), fitted using a single shell model. EXAFS data (black lines) and fits (red lines) in k-space (left) and R-space (right) for various k-weightings: k^1 (top), k^2 (middle), k^3 (bottom). The data ranges used for fitting are shown by the window functions (black dashed lines).

Appendix 5

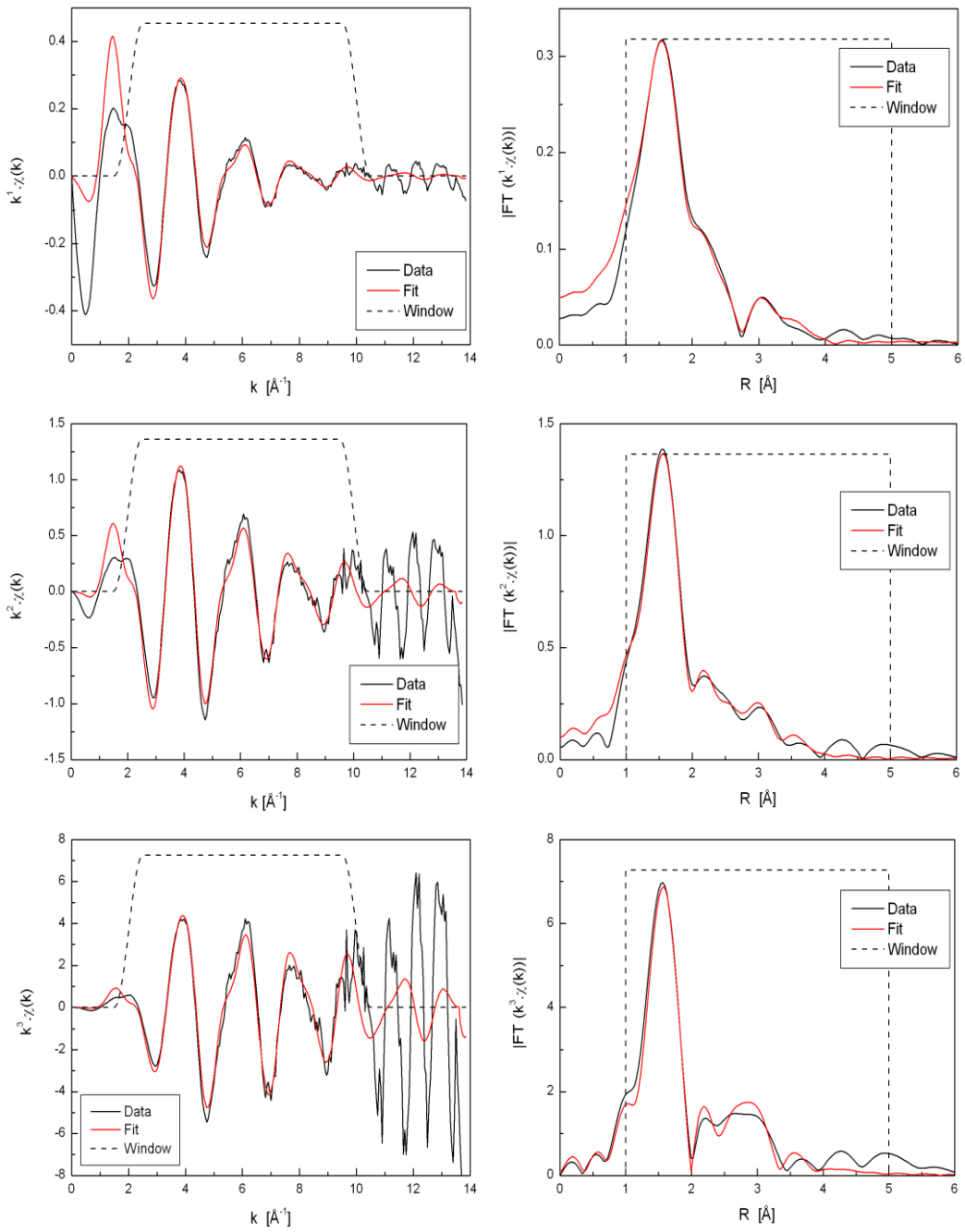

Figure S.8: Ni-NCO 2:1 KOCN:Ni^{2+} mole ratio model solution in DMSO ('Sample 4'), fitted using a single shell model for DMSO and a multiple-scattering model for OCN. EXAFS data (black lines) and fits (red lines) in k-space (left) and R-space (right) for various k-weightings: k^1 (top), k^2 (middle), k^3 (bottom). The data ranges used for fitting are shown by the window functions (black dashed lines).

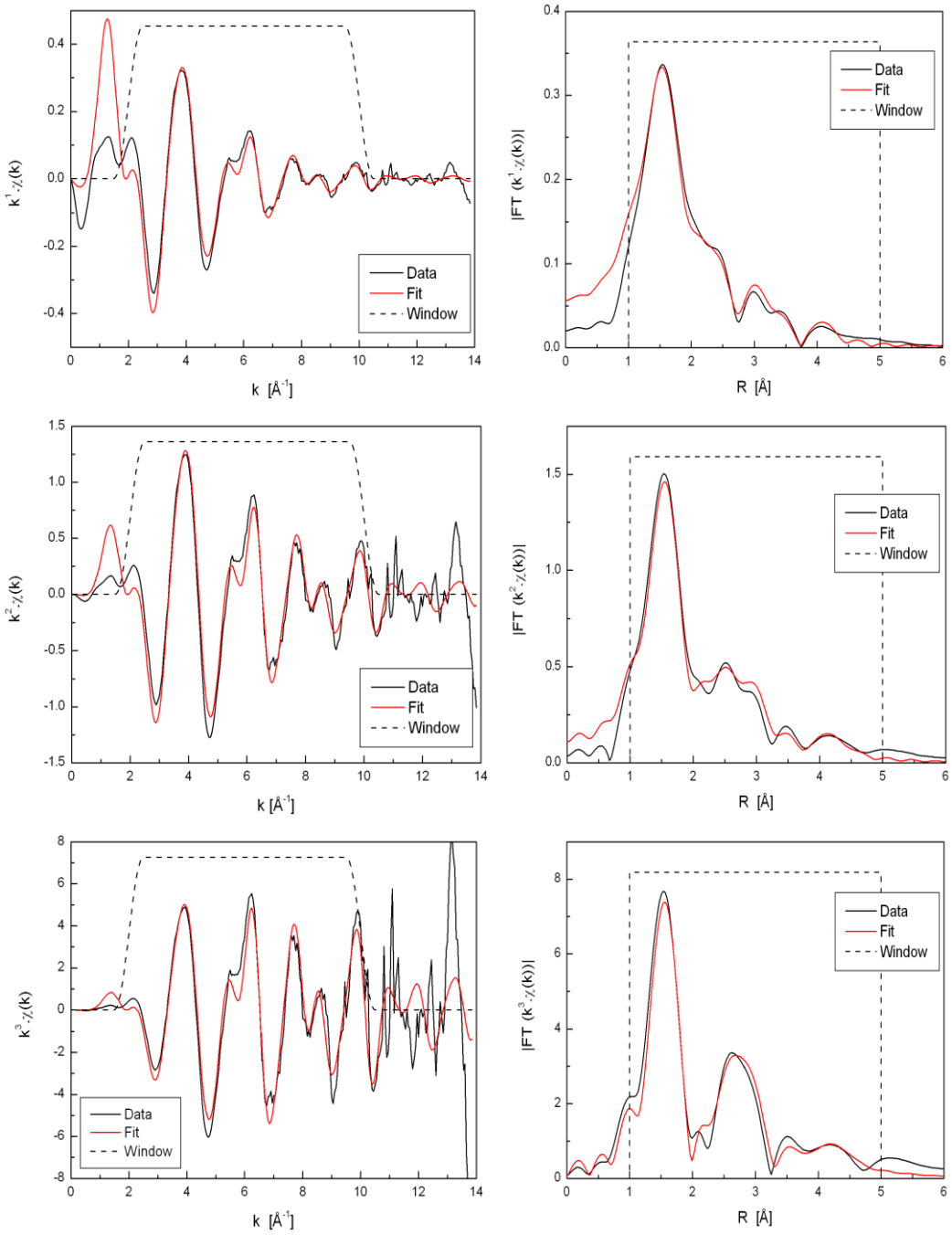

Figure S.9: Ni-NCS 2:1 KSCN:Ni^{2+} mole ratio model solution in DMSO ('Sample 5'), fitted using a single shell model for DMSO and a multiple-scattering model for SCN. EXAFS data (black lines) and fits (red lines) in k-space (left) and R-space (right) for various k-weightings: k^1 (top), k^2 (middle), k^3 (bottom). The data ranges used for fitting are shown by the window functions (black dashed lines).

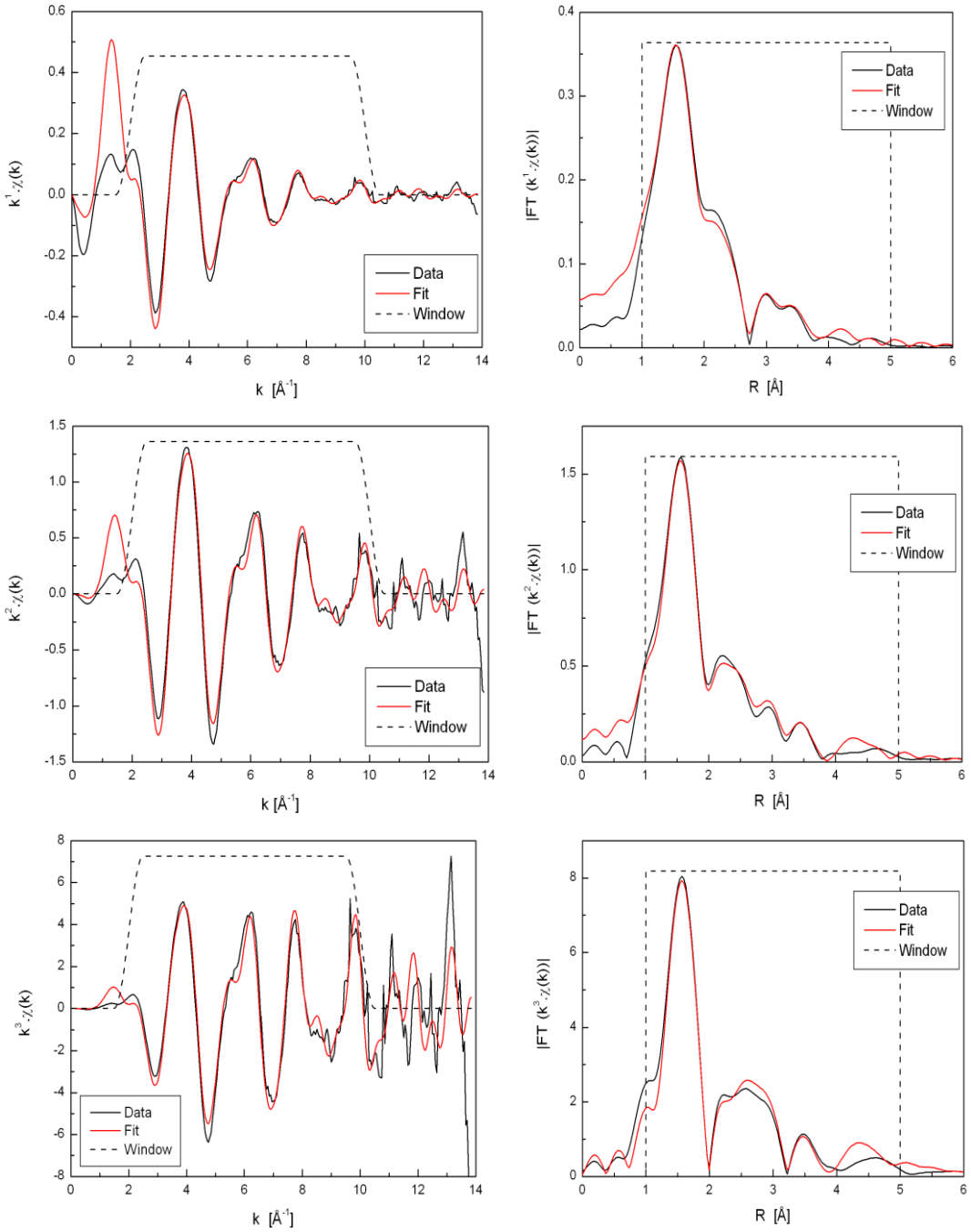

Figure S.10: Ni-NCSe 2:1 KSeCN:Ni^{2+} mole ratio model solution in DMSO ('Sample 6'), fitted using a single shell model for DMSO and a multiple-scattering model for SeCN. EXAFS data (black lines) and fits (red lines) in k-space (left) and R-space (right) for various k-weightings: k^1 (top), k^2 (middle), k^3 (bottom). The data ranges used for fitting are shown by the window functions (black dashed lines).

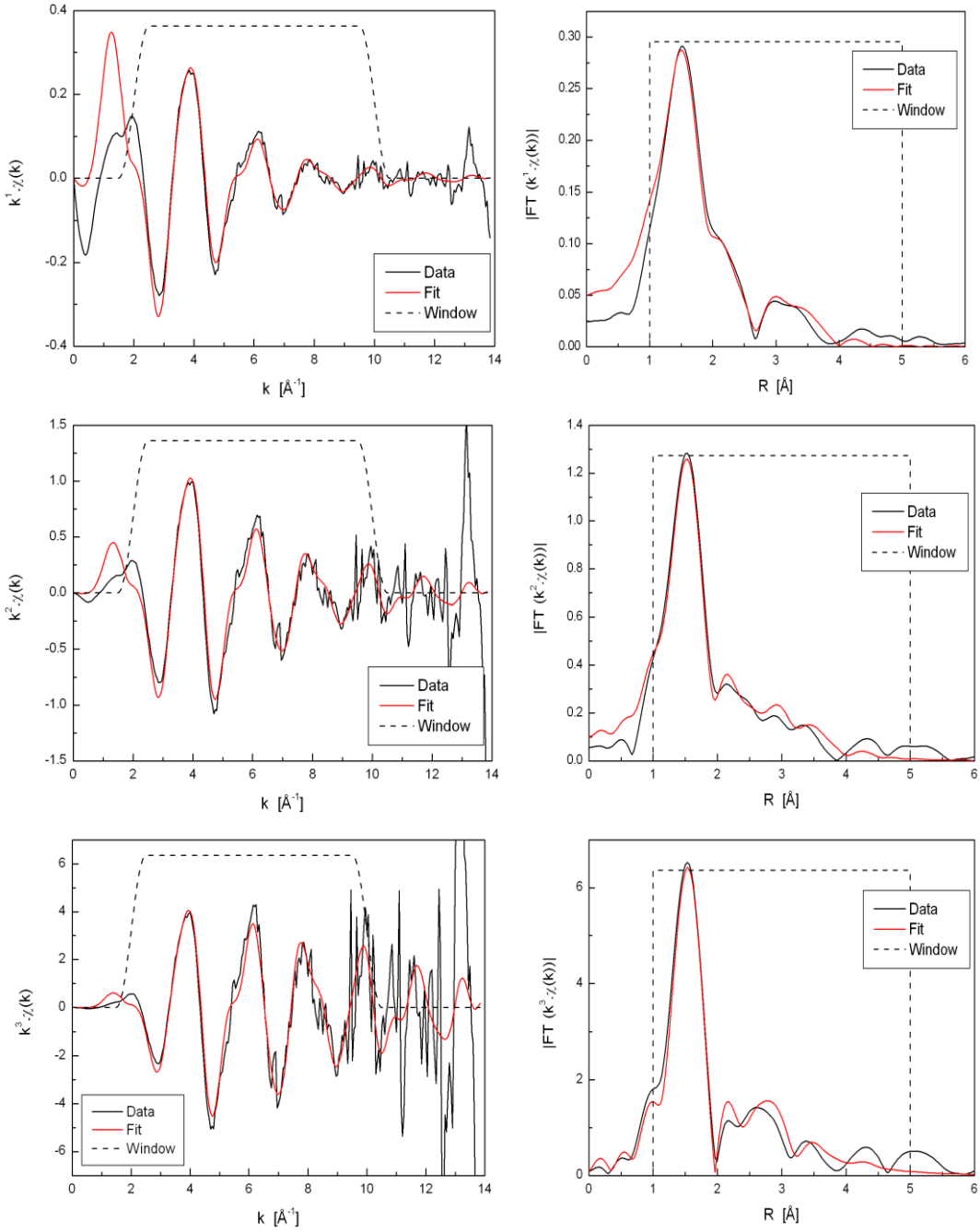

Figure S.11: Ni-NCO electrochemically generated solution in DMSO ('Sample 7'), fitted using a single shell model for DMSO and a multiple-scattering model for OCN. EXAFS data (black lines) and fits (red lines) in k-space (left) and R-space (right) for various k-weightings: k^1 (top), k^2 (middle), k^3 (bottom). The data ranges used for fitting are shown by the window functions (black dashed lines).

Appendix 6

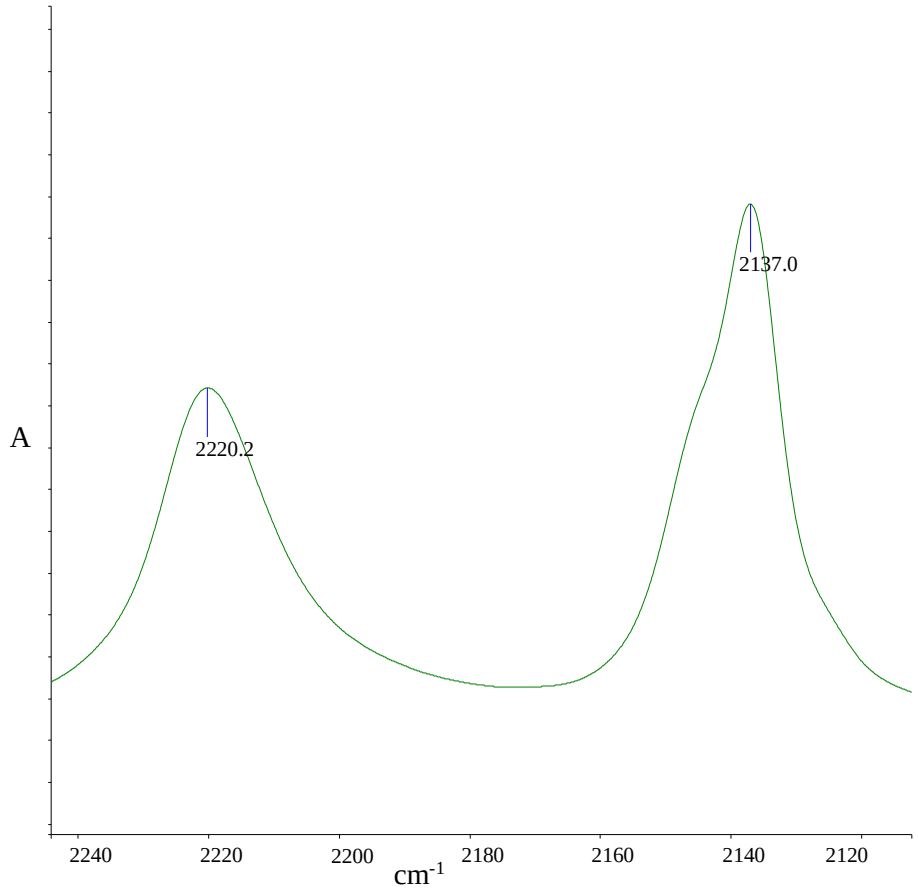

Figure S.12: IR transmission spectrum of the electrochemically generated cell solution from the Cu/NCO^-/DMSO system. The solution was produced after polarising the Cu electrode at - 800 mV(AgCl/Ag) for one hour, extracting of solution from the cell and recording the IR transmission spectrum.

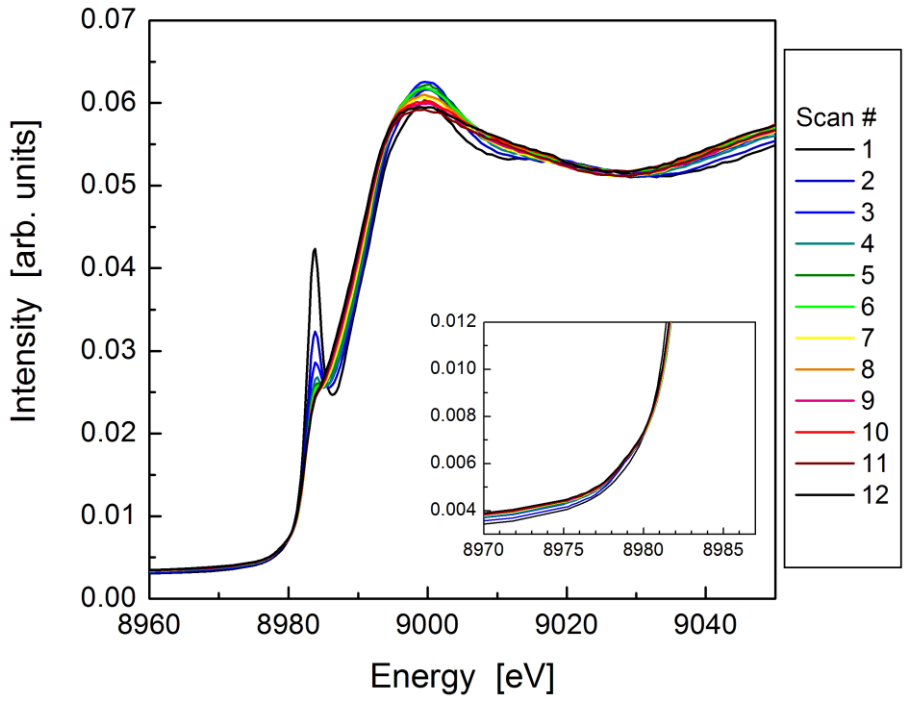

Figure S.13: XANES spectra of the electrochemically generated cell solution sample from the Cu/NCO^-/DMSO system, collected in rapid succession for 12 scans. Each scan took approximately 7 minutes. The inset shows the pre-edge region.

Appendix 7

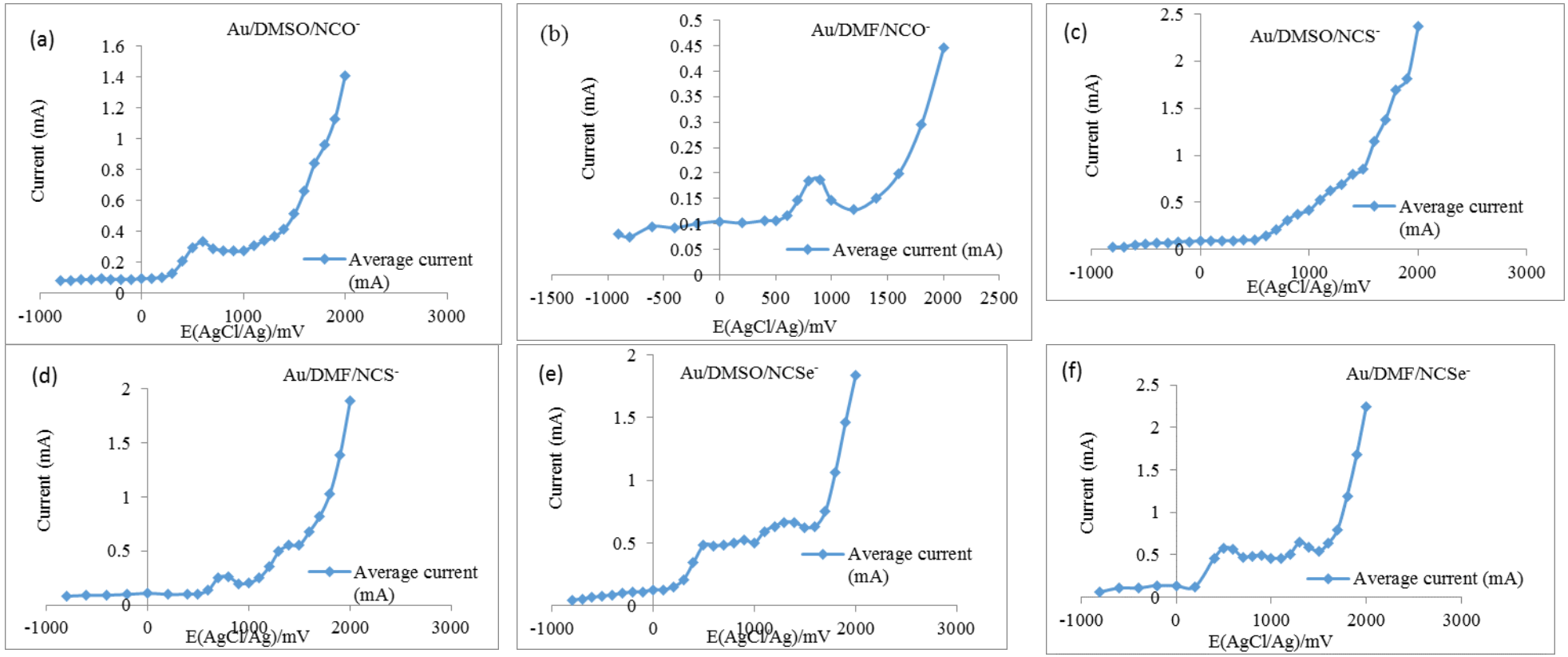

Figure S.14: Single sweep voltammograms acquired of the gold electrodes during a SNIFTIRS experiment in DMSO and DMF solvents containing pseudohalide ions and 0.1 mol L^{-1} TBAP: Data were obtained from calculating the average current at the beginning and end of the spectral acquisition period for each applied potential at which SNIFTIRS spectra were acquired. (a) Au electrode and 0.025 mol L^{-1} $KOCN^-$ in DMSO, (b) Au electrode and 0.025 mol L^{-1} KOCN in DMF, (c) Au electrode and 0.05 mol L^{-1} NaSCN in DMSO, (d) Au electrode and 0.05 mol L^{-1} NaSCN in DMF, (e) Au electrode and 0.05 mol L^{-1} KSeCN in DMSO, (f) Au electrode and 0.05 mol L^{-1} KSeCN in DMF.

Appendix 8

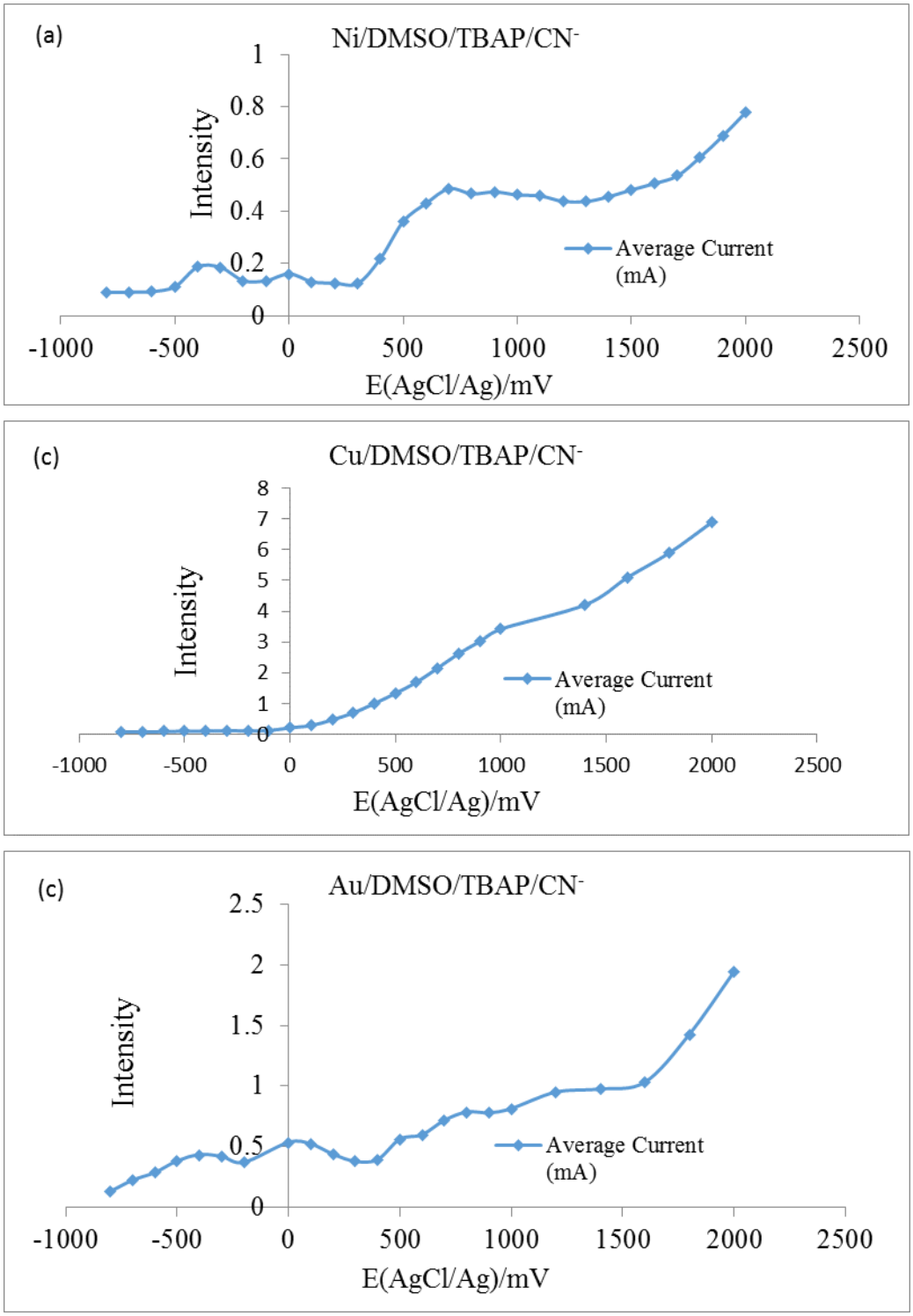

Figure S.15: Single sweep voltammograms acquired of the nickel, copper and gold electrodes during a SNIFTIRS experiment in DMSO solvents containing cyanate ions and 0.1 mol L^{-1} TBAP: Data were obtained from calculating the average current at the beginning and end of the spectral acquisition period for each applied potential at which SNIFTIRS spectra were acquired. (a) Ni electrode and 0.025 mol L^{-1} CN^- in DMSO, (b) Cu electrode and 0.025 mol L^{-1} CN^- in DMSO, (c) Au electrode and 0.025 mol L^{-1} CN^- in DMSO.

List of publications

- **A fundamental IR spectroelectrochemical study of the anodic polarisation of nickel, copper and gold electrodes in the presence of the unstable tellurocyanate ion in DMF and DMSO**

  Kethsiri H.K.L. Alwis, Michael R. Mucalo and Joseph R. Lane

  RCS Advances **DOI: 10.1039/C4RA15609A**

- **An X-ray absorption spectroscopy investigate the coordination environment of electrogenerated Ni(II)-pseudohalide complexes arising from the anodic polarization of Ni electrodes in DMSO solutions of NCO^-, NCS^- and $NCSe^-$ ions.**

  Kethsiri H.K.L. Alwis, Bridget Ingham, Michael R. Mucalo, Peter Kappen and Chris Glover

  RSC Advances **DOI: 10.1039/C4RA14940H**

- **Anodically polarised copper electrodes in DMSO and DMF solutions of pseudohalide ions: A combined IR spectroelectrochemical and XANES study.**

  Kethsiri H.K.L. Alwis, Bridget Ingham, Michael R. Mucalo and Peter Kappen.

  Journal of The Electrochemical Society-2015 **DOI: 10.1149/2.0321507jes**

- **In situ IR Study of the Anodic Polarisation of Gold Electrodes in Polar Aprotic Solvents - DMSO and DMF Solutions of Cyanate, Thiocyanate and Selenocyanate ions**

  L.K.H. K. Alwis, Michael R. Mucalo

  Journal of The Electrochemical Society-2014 **DOI: 10.1149/2.0441412jes**

- **Anodically polarised nickel electrodes in DMSO or DMF solutions of pseudohalide ions: IR spectroelectrochemical studies**

  L.K.H. K. Alwis, Michael R. Mucalo, and Bridget Ingham

  Journal of The Electrochemical Society-2013 **DOI: 10.1149/2.010311jes**

Under review **In situ IR studies on the electro-oxidation of cyanide on Ni, Cu and Au electrodes electrically polarised in dimethyl sulfoxide (DMSO) electrolyte media.**
L.K.H. K. Alwis and Michael R. Mucalo, Electrocatalysis

Conferences

2013

A combined IR specroelectrochemical and EXAFS/XANES study of the speciation from Ni electrodes anodically polarized in cyanate- thiocyanate- and selenocyanate- containing solutions of dimethylformamide (DMF) and dimethyl sulfoxide (DMSO). M.R.Mucalo, Kethsiri Alwis L.H.K, and Bridget Ingham Australian Synchrotron user meeting 2013 (oral)

2013

A combined IR spectroelectrochemical and EXAFS/XANES study of the speciation from Ni electrodes anodically polarized in cyanate-, thiocyanate- and selenocyanate-ontaining solutions of dimethyl formamide (DMF) and dimethyl sulfoxide (DMSO), M.R. Mucalo, K.H.K. Alwis, & B. Ingham, 19th Australia/New Zealand Electrochemistry Symposium (19ANZES), Melbourne, Australia 2013 (oral)

2011

Electrochemistry in non-aqueous corrosion system monitored in situ by FTIR-Spectroscopy, L.K.H. K. Alwis, Michael R. Mucalo and Merilyn Manley-Harris, New Zealand Institute of Chemistry Conference, University of Waikato (poster)